Modelling barrier function of the villous and follicle-associated epithelium in 3D

Thesis submitted in accordance with the requirements of the University of Liverpool for the degree of Doctor in Philosophy

By

Louise Miranda Thompson

February 2019

DECLARATION

I hereby declare that this thesis is a presentation of my original work. Wherever contributions of others are involved, every effort has been made to indicate this clearly, with due reference to the literature.

The work was performed under the joint guidance of Professor Barry J Campbell and Dr Carrie A Duckworth, both from the Institute of Translational Medicine at the University of Liverpool.

ACKNOWLEDGEMENTS

My first thanks go to the Wellcome Trust for their funding, without which this project would not have been possible. Thanks also to the Physiological Society for funding parts of the project.

Thank you to my supervisors, Professor Barry Campbell and Dr Carrie Duckworth, for their continual support over the last 3.5 years. Despite being incredibly busy with work and family lives, you have always made time when I needed it and made sure the important things got done. I have really valued your pragmatism when things did not initially go to plan but also your unfailing encouragement and confidence in me.

Thank you to Alison Beckett for her excellent training and support in electron microscopy and to Dr Jeff Barclay for the kind use of his equipment throughout the project. My gratitude also goes to the inimitable Dr Matoula Papoutsopoulou for all her help with cloning.

A huge thank you to everyone in the Gastroenterology Research Unit, past and present. In particular, thank you to Dr Kate Lloyd, who has been an amazing friend and mentor. To Stephanie French, thank you for keeping me sane with laughs and tea and regular sessions on the squash court. Thank you to Dave Berry for putting up with me and for the words 'what do you need to get you through today?' ('I just need PBS!'). To pick on just a few others: Dr Alessandra Frau, thank you for your advice; Brad Meehan and Stephanie James, thanks for not letting me get carried away in my first year. You have all made working in Gastro a pleasure.

Moving across the country to a city where I initially knew no one was not always easy. I am enormously grateful to my family and friends (old and new), who have encouraged me, inspired me and provided a sympathetic ear or a weekend away on their sofa whenever I needed one. Special thanks to Mum and Dad for their constant support (including traipsing my life all over the country) and to Jamie for the weekends exploring Durham and Liverpool – the hours on the train were always worth it. Last but not least, thank you to my incredible flatmate, Mary, with whom I feel so lucky to have shared all the ups and downs of the last 4 years – we made it.

ABSTRACT

The intestinal epithelium acts as a barrier that excludes external molecules from the tissues beneath. Defects in this barrier function are increasingly associated with pathological states, including inflammatory bowel disease, irritable bowel syndrome, coeliac disease, obesity and food allergies. Understanding of epithelial biology and barrier function has been limited by a lack of physiologically representative in vitro models. Identification of intestinal epithelial stem cells and recent methodological advances have allowed intestinal stem cells to be cultured so that they proliferate, differentiate and self-assemble to mimic in vivo tissue architecture, forming a continuous epithelium around a hollow central lumen, known as an enteroid.

The initial aim of this study was to evaluate the extent to which mouse small intestinal enteroids simulate their parent tissue. The second intention was to investigate whether this system can be used to model barrier function of both villous epithelium and specialised areas of epithelium overlying gut-associated lymphoid tissues, where antigen sampling occurs due to the presence of rare phagocytic M cells.

Enteroids were shown to contain all major epithelial cell lineages and to retain region-specific differences in the distribution of cell types that are observed in vivo. An assay based on leakage of a fluorescent was developed to allow investigation of epithelial barrier function in 3D enteroids. Peptide fragments of dietary gliadin were used to probe the ability of enteroids to model barrier function, since they are involved in the pathogenesis of coeliac disease and have been linked to increased epithelial permeability. A peptide spanning α-gliadin amino acids 56-68 induced rapid, dose-dependent luminal fluid secretion via activation of an apical chloride channel, the cystic fibrosis transmembrane regulator. In contrast, a second peptide had no effect on fluid secretion.

Regarding modelling the follicle-associated epithelium, it was confirmed that M cell differentiation is stimulated by treatment of enteroids with the cytokine RANKL. Alternative pathway NF-κB signalling was required, as M cell-associated gene expression was not upregulated in RelB- or NF-κB2-deficient enteroids. As previously suggested, co-culture with B cells also appeared to promote M cell differentiation, although their presence was insufficient to induce mature M cells. Finally, plasmid constructs were generated to express a fluorescently labelled bacterial surface adhesion molecule for microinjection into the enteroid lumen. As a tool, this will allow modelling of bacterial adhesion to, and translocation by, enterocytes and M cells.

This work supports a growing body of evidence showing that enteroids accurately reproduce in vitro many characteristics of the small intestinal epithelium. It is demonstrated that enteroids can be used to model barrier function, fluid secretion and the role of epithelium-intrinsic factors in differentiation of a rare cell lineage. Further assay developments will likely result in more widespread use of enteroids for various applications, including basic research, therapeutic screening and drug development.

ABBREVIATIONS USED

AUC	Area under the curve
ANOVA	Analysis of variance
cAMP	Cyclic adenosine triphosphate
CFTR	Cystic fibrosis transmembrane regulator
CFTR-inh-172	Cystic fibrosis transmembrane regulator inhibitor 172
CgA	Chromogranin A
DCLK1	Doublecortin like kinase 1
ddH_2O	Double distilled water
DMEM	Dulbecco's modified Eagle's medium
DMSO	Dimethylsulfoxide
EDTA	Ethylenediaminetetraacetic acid
EGF	Epidermal growth factor
EGTA	Ethylene glycol-bis(2-aminoethylether)-N,N,N',N'-tetraacetic acid
FAE	Follicle associated epithelium
FD4	Fluorescein isothiocyanate-conjugated 4 kDa dextran
GALT	Gut-associated lymphoid tissue
GP2	Glycoprotein 2
GST	Glutathione S-transferase
IBD	Inflammatory bowel disease
IBS	Irritable bowel syndrome
IgA	Immunoglobulin A
IKK	IκB kinase

IPTG	Isopropyl β-D-1-thiogalactopyranoside
LB	Lysogeny broth
LPS	Lipopolysaccharide
Lyz	Lysozyme
MAPK	Mitogen-activated protein kinase
M cell	Microfold cell
NCWS/NCGS	Non-coeliac wheat sensitivity/non-coeliac gluten sensitivity
NF-κB	Nuclear factor κB
NIK	NF-κB-inducing kinase
PB	Phosphate buffer
PBS	Phosphate buffered saline
PCR	Polymerase chain reaction
RANK	Receptor activator of nuclear factor κB
RANKL	Receptor activator of nuclear factor κB ligand
SD	Standard deviation
SEM	Standard error of the mean
sIgA	secretory immunoglobulin A
TBS/TBST	Tris buffered saline/Tris buffered saline + 0.1% Tween-20
TEER	Transepithelial resistance
TEM	Transmission electron microscopy
TFF3	Trefoil factor 3
TG2	Tissue transglutaminase 2
TNF	Tumour necrosis factor

UEA-1	*Ulex europeaus* agglutinin 1
ZO-1	Zonula occludens-1

CONTENTS

Chapter 2 – Methods

Chapter 3 – Location-specific characteristics of enteroids derived from murine proximal or distal small intestine

LIST OF FIGURES

LIST OF TABLES

Chapter 1

Introduction, Hypothesis and Aims

1.1 Structure of small intestinal epithelium and regional differences along the small intestine

1.1.1 Anatomy of the small intestine

The gastrointestinal tract overall and small intestine in particular are largely anatomically and physiologically similar in both humans and mice, making mice a good model for many aspects of human intestinal biology (Nguyen *et al.*, 2015; Hugenholtz and de Vos, 2018). The small intestine begins after the pyloric sphincter and ends with the start of the large intestine or colon. In humans, the small intestine is approximately 8 m in length, while in mice it is around 30 cm long (Bowcutt, 2014); this translates to a size relative to total body weight of 10 cm per kilogram in humans compared to 1500 cm per kilogram in mice (Hugenholtz and de Vos, 2018). From proximal to distal, the small intestine is divided into three regions: duodenum, jejunum and ileum.

The small intestinal wall consists of different functional layers. The outer layer is the serosa. Inside this is the muscularis, consisting of two smooth muscle layers, which are responsible for the shape, tone and peristaltic movement of the gut. Within this is the submucosal layer containing stromal elements, such as connective tissue, blood vessels and immune cells. Finally, innermost layer is the mucosa, which is smooth in mice but forms circular folds in humans (Hugenholtz and de Vos, 2018). The mucosa contains the lamina propria and a single layer of columnar epithelial cells makes up its luminal surface.

The intestinal epithelium contains the same epithelial cell types in humans and mice. These fulfil various specialised roles, including nutrient and water absorption and secretion of hormones, enzymes and anti-microbial molecules. The epithelium adopts an intensely folded architecture, with invaginated crypts and protruding, finger-like villi. This is similar in humans and mice, although the villi in mice tend to be taller and their shapes vary slightly along the length of the small intestine (Nguyen *et al.*, 2015; Hugenholtz and de Vos, 2018). The crypts and villi form distinct microenvironments, with most absorption taking place in the villus epithelium while secretion occurs mainly in the crypts. Villi serve to increase the surface area available for absorption of nutrients, fluid and electrolytes. Overlying the epithelium is a mucus layer made up of highly glycosylated mucins secreted by specialised cells within the epithelium. The key secreted mucin in the intestine is mucin 2 (encoded by *MUC2*/*Muc2*) (Pelaseyed *et al.*, 2014). Unlike in the colon, the mucus layer is thinner and discontinuous in the small intestine (Johansson *et al.*, 2011; Ermund *et al.*, 2013).

1.1.2 Intestinal stem cells and epithelial renewal

In the adult small intestine, leucine rich repeat containing G protein coupled receptor 5 $(Lgr5)^+$ intestinal epithelial stem cells are found at the crypt bases (Sato *et al.*, 2009), where they give rise to all the intestinal epithelial cell lineages: absorptive enterocytes, Paneth cells and goblet cells (**Figure 1.1**). The stem cell niche at the crypt base is maintained by factors produced by Paneth cells, which flank the $Lgr5^+$ stem cells (Sato *et al.*, 2011) and other cells, such as myofibroblasts (Lahar *et al.*, 2011). In addition, there is a second compartment of cells located at the +4 position of the crypt, which may or may not express Lgr5, along with other markers of quiescent stem cells, including Bmi1, mTert and Hopx (Potten *et al.*, 2002; Clevers, 2013). These are committed to the secretory cell lineage but are able to act as a reserve stem cell population, generating daughters of all lineages following intestinal injury (Buczacki *et al.*, 2013). Except for Paneth cells, which migrate downwards to the crypt base (Clevers and Bevins, 2013), daughter cells migrate upwards from the crypt base along the crypt-villus axis. The majority of the rest of the crypt consists of rapidly proliferating progenitor cells known as transit-amplifying cells. Transit-amplifying cells divide 4-5 times as they move up towards the crypt shoulder, before becoming terminally differentiated. The turnover period of the epithelium is around 5 days. The oldest epithelial cells undergo apoptosis and are shed from the villus tip (Bullen *et al.*, 2006; van der Flier and Clevers, 2009).

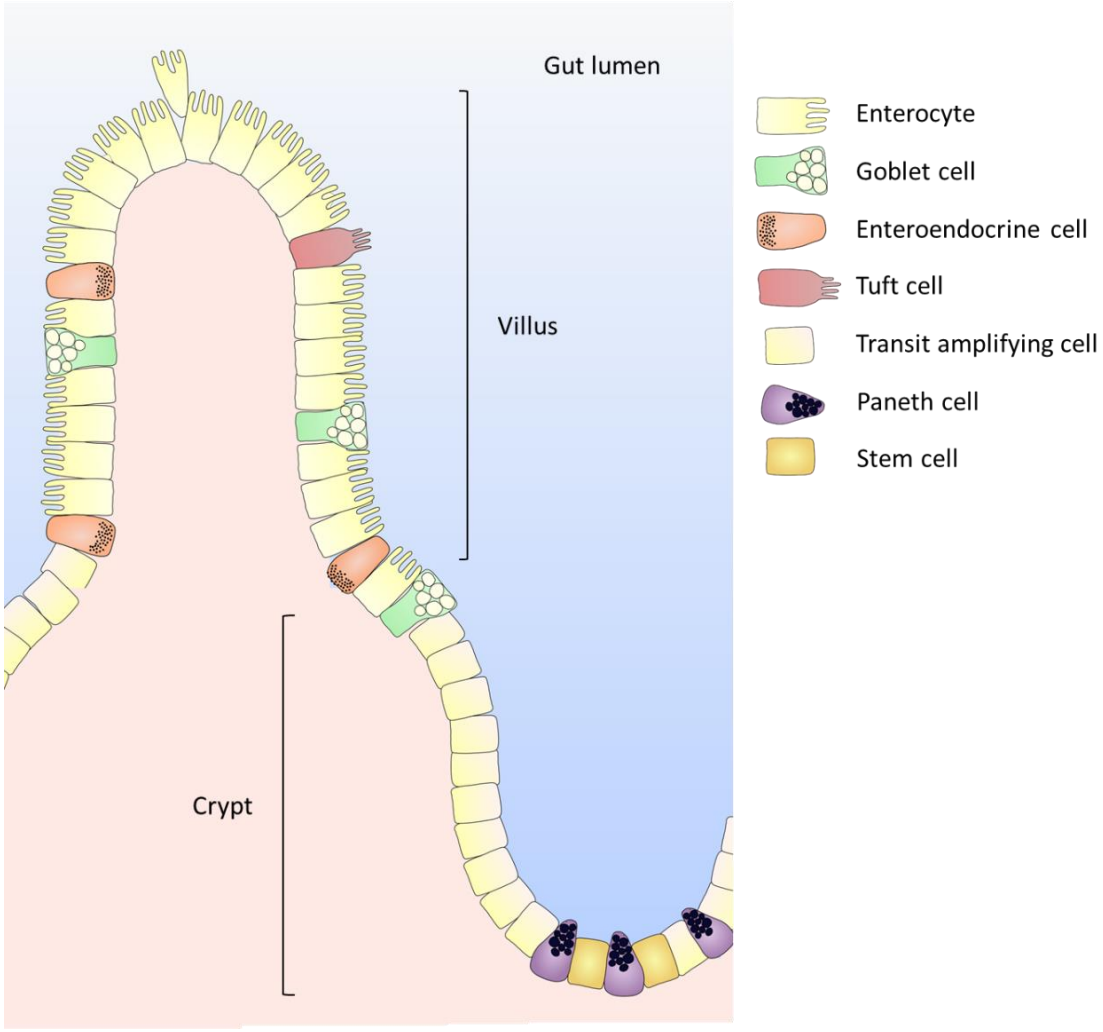

Figure 1.1. A crypt-villus axis within the small intestinal epithelium. The luminal surface of the small intestine is covered with small finger-like projections interspersed with invaginated crypts. Stem cells reside at the base of the crypts, where they divide to produce daughter cells. As they differentiate, cells move upwards towards the villus tip, creating a zone of dividing and differentiating cells known as 'transit amplifying cells'. Cells on the villus are fully committed to one of the epithelial lineages, the major types of which are absorptive enterocytes, mucus-secreting goblet cells, enteroendocrine cells and tuft cells. Paneth cells, the fifth major lineage, migrate down to the crypt base where they produce niche factors that maintain the stem cells. The whole epithelium turns over approximately every 5-6 days, with cells undergoing apoptosis and being shed into the lumen from the villus tip. Figure adapted from (Crosnier, Stamataki and Lewis, 2006).

1.1.3 Intestinal epithelial cell types

The intestinal epithelium comprises four major cell lineages that are derived from $Lgr5^+$ crypt base stem cells. The same epithelial cell types are present in both human and mouse small intestine (Nguyen *et al.*, 2015). Absorptive enterocytes are the most abundant of these and

are responsible for the uptake of nutrients from the small intestinal lumen. Although once thought to be purely devoted to absorption, the intestinal epithelium is also now known to have various important secretory roles. The major secretory cell types found in the epithelium are Paneth cells, goblet cells and enteroendocrine cells. As discussed previously, Paneth cells secrete factors such as Wingless-type MMTV integration site (Wnt) proteins, epidermal growth factor (EGF) and Notch ligands, which are crucial for the maintenance of $Lgr5^+$ stem cells. Ablation of Paneth cells *in vivo* in mice, either by mutation of growth factor-independent 1 transcription repressor (*Gfi1)* or expression of diphtheria toxin A under the Paneth cell-specific cryptdin 2 promoter, causes loss of intestinal stem cells (Sato *et al.*, 2011). Paneth cells also have a role in innate immunity by secreting anti-microbial molecules, such as lysozyme, defensins and cryptdins, into the intestinal lumen. Goblet cells secrete mucins to make up the mucus layer that physically excludes many microbes from contacting and translocating across the epithelium (Birchenough *et al.*, 2015). The final major secretory lineage is enteroendocrine cells, which express sensory receptors that allow them to monitor the composition of the gut contents, particularly nutrient and chemical substances (Worthington *et al.,* 2017). They respond to this by secretion of hormones, such as serotonin, cholecystokinin, gastric inhibitor polypeptide, ghrelin and glucagon-like peptide 1 (Gunawardene *et al.*, 2011; Furness *et al.*, 2013; Worthington *et al.,* 2017). Other epithelial cell types that are very rare in the intestine include tuft cells and microfold (M) cells, which are found throughout the crypt-villus axis and in the follicle-associated epithelium, respectively. Tuft cells play a role in immunity against parasitic infections (Gerbe and Jay, 2016), while phagocytic M cells are involved in induction of immune responses via antigen sampling of the luminal contents (Mabbott *et al.*, 2013).

1.1.4 Intestinal epithelial cell differentiation

The differentiation of intestinal epithelial stem cells into these separate lineages is determined by a complex interplay between cell signalling pathways (**Figure 1.2**). Wnt signalling is crucial for the maintenance of $Lgr5^+$ stem cells at the crypt base (Crosnier, Stamataki and Lewis, 2006) as evidenced by the fact that mice lacking lymphoid enhancer factor/T cell factor (TCF), which complexes with β-catenin and translocates to the nucleus to activate Wnt target genes, results in loss of intestinal stem cells (Korinek *et al.*, 1998). A gradient of Wnt signalling is thought to exist from the base of the crypt, where Wnt ligands are produced by Paneth cells and are therefore at their highest concentration, to the top of the crypt where they are weakly expressed (Sato *et al.*, 2011). As progenitor cells are pushed upwards along the crypt-villus axis they escape this region of high Wnt signalling and undergo

differentiation. Allocation of cells to either the absorptive or secretory lineages at this point is controlled by Notch signalling, which normally maintains the stem cell compartment (Riccio *et al.*, 2008; Pellegrinet *et al.*, 2011; VanDussen *et al.*, 2012). Notch promotes expression of hairy and enhancer of split-1 (Hes) family of basic helix-loop-helix (bHLH) transcription factors, such as Hes1, which represses atonal bHLH transcription factor 1 (Atoh1, also known as Math1). Atoh1 expression is required for commitment to the secretory lineage (Yang, 2001; VanDussen and Samuelson, 2010). As a result, experimental inhibition of Notch signalling causes goblet cell hyperplasia with concurrent decline in numbers of absorptive enterocytes (Milano *et al.*, 2004; van Es *et al.*, 2005; Kazanjian *et al.*, 2010), while enhancement of normal Notch signalling results in loss of secretory lineages (Fre *et al.*, 2005; Stanger *et al.*, 2005). Progenitors that experience high Notch signalling and repress Atoh1 commit to the absorptive lineage. Various other genes, including *Ptk6*, have been found to influence enterocyte differentiation but these do not appear to be specific for the absorptive lineage alone (Haegebarth *et al.*, 2006).

Following commitment to a secretory lineage, further signals regulate differentiation of progenitors into the distinct secretory cell types. Gfi1 activity has been proposed to be the switch controlling allocation of a common secretory progenitor to either Paneth/goblet cell or enteroendocrine cell lineages. This model is based on a report that the small intestine of *Gfi1*$^{-/-}$ mice contains Atoh1^{+} cells but no mature Paneth cells and fewer goblet cells, while showing parallel increases in the enteroendocrine cell population (Shroyer *et al.*, 2005). In support of a common secretory Atoh1^{+} precursor, experimental expression of neurogenin 3 (a member of another family of bHLH transcription factors) in the mouse intestine increases enteroendocrine cell numbers at the expense of goblet cells (López-Díaz *et al.*, 2007).

The precise pathways that govern these cell fate decisions are, however, far from completely understood. A later report found that *Gfi1* is normally expressed by Paneth and goblet cells but not by enteroendocrine cells (Bjerknes and Cheng, 2010). This second group confirmed reduced Paneth and goblet cells in an independent line of Gfi1-deficient mice but also identified 'mixed lineage' cells expressing neurogenin 3 – required for commitment to the enteroendocrine lineage (Jenny *et al.*, 2002) – and Paneth or goblet cell markers. To explain their observations, they propose an alternative model where Gfi1 mediates transcriptional repression of neurogenin 3 in Paneth and goblet cells, preventing them from becoming enteroendocrine cells. In *Gfi1* deficiency, this repression is lost and some Paneth and goblet cells express neurogenin 3 and undergo reprogramming to the enteroendocrine lineage. This model does not depend on the existence of a common secretory progenitor. Further

downstream of neurogenin 3, multiple factors have been identified that direct differentiation of cells into the various subsets of enteroendocrine cells.

Some evidence suggests the existence of a common goblet/Paneth cell precursor (Noah, Donahue and Shroyer, 2011). Abnormal cells with mixed goblet and Paneth cell characteristics were observed in mice following intestinal epithelium-specific deletion of liver kinase B1 (*Lkb1*), which is normally expressed strongly in Paneth and goblet cells (Shorning *et al.*, 2009). Furthermore, decreases in both goblet and Paneth cell differentiation have been described following loss of several other factors, including sex determining region Y box 9 (Sox9) (Bastide *et al.*, 2007) and sterile alpha motif pointed domain containing ets transcription factor (Spdef) (Gregorieff *et al.*, 2009; Noah *et al.*, 2010). Goblet cell differentiation also appears to depend strongly on Notch signalling, with experimental expression of Notch Intercellular Domain (NCID) resulting in expansion of the goblet cell population (Zecchini, 2005). In contrast, the Paneth cell lineage relies on Wnt/β-catenin signalling. Loss of either the Frizzled 5 receptor, through which Wnt signalling is transduced, or the pro-Wnt signalling Lgr4 disrupted Paneth cell maturation (van Es *et al.*, 2005; Mustata *et al.*, 2011). Since Paneth cells themselves secrete Wnt ligands, this may form a positive feedback loop to support further Paneth cell differentiation, as well as maintaining the columnar base stem cell population.

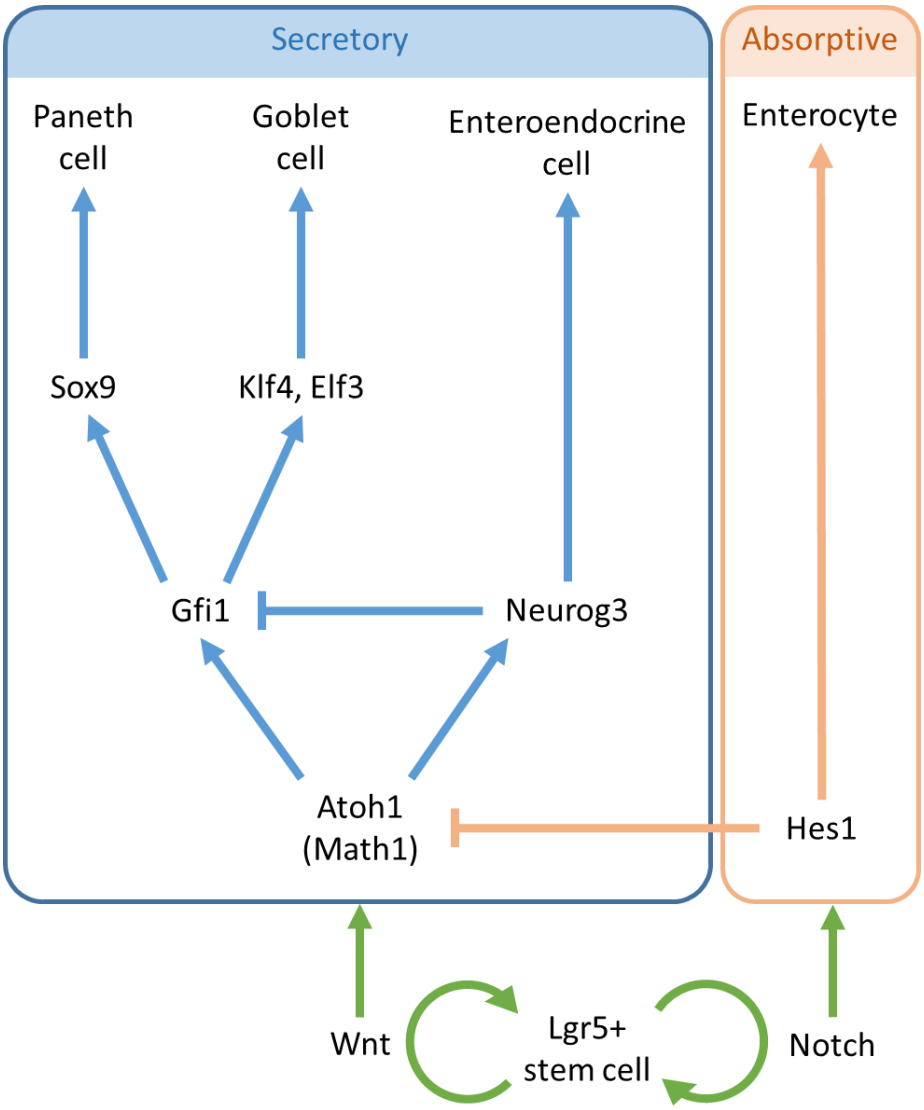

Figure 1.2. Factors regulating differentiation of intestinal epithelial cell lineages. Differentiating epithelial cells that are exposed to strong Notch signalling undergo upregulation of Hes1, which guides them to become enterocytes. Hes1 inhibits expression of Atoh1/Math1, which specifies the secretory lineage in response to high Wnt signalling. Gfi1 activity is important for Paneth and goblet cell development, whereas upregulation of neurogenin 3 results in suppression of Gfi1 and development into enteroendocrine cells. In cells dominated by Gfi1 activity, Sox9 is required for Paneth cell differentiation while Klf4 and Elf3 are expressed in developing goblet cells. Figure adapted from Van der Flier et al (van der Flier and Clevers, 2009).

1.1.5 Regional identity in the small intestine

In addition to the strictly regulated differentiation of the small intestinal epithelium along the crypt-villus axis, the characteristics of the small intestine also vary along its length, or cephalocaudal axis (Middendorp *et al.*, 2014). This includes regional variation in enterocyte

gene expression profiles and distribution of cell types. Several studies have demonstrated differential regional expression of certain nutrient transporters using array-based and RNA sequencing approaches (Mutch *et al.*, 2004; Anderle *et al.*, 2005; Comelli *et al.*, 2009; Middendorp *et al.*, 2014), which largely correspond to specialisation in terms of nutrient absorption. For example, both *Scl40a1* (encoding iron transporter ferroportin) and *Cybrd1* (encoding ferric reductase CYBRD1) are more strongly expressed in the duodenum, where the majority of iron absorption occurs (Anderle *et al.*, 2005; Middendorp *et al.*, 2014). In contrast, expression of the Na^+-dependent bile acid transporter (ASBT) is greater in the ileum than the jejunum, consistent with this being the major site of bile acid reabsorption (Anderle *et al.*, 2005; Middendorp *et al.*, 2014). One study described differences in expression of certain region-specific genes; for example, *Cybrd1* was expressed only in mouse duodenum, while its homologue in humans was expressed more highly in human ileum than duodenum (Middendorp *et al.*, 2014). Another study found similar expression of most transporters between human and mouse small intestine (Anderle *et al.*, 2005). Overall, these studies support the relevance of mouse as a model organism in this area.

GATA4, a zinc finger transcription factor, is believed to be important in conferring regional identity in the small intestine. In both mouse and humans, GATA4 is expressed strongly by enterocytes throughout the duodenum and jejunum but at much lower levels in the ileum (van Wering *et al.*, 2004; Bosse *et al.*, 2006). This differential expression is required for maintenance of duodenal and jejunal phenotypes as the epithelium in these regions acquired ileal characteristics in an inducible *Gata4*-knockout mouse model (Bosse *et al.*, 2006). Expression of transporters usually restricted to the ileum, such as *Slc10a2*, was observed in the jejunum of these mice and expression of jejunum-restricted transporter genes, such as fatty acid binding protein 1 (*Fabp1*), was greatly reduced. This indicates that GATA4 normally specifies regional identity by inhibiting expression of ileum-specific genes in the jejunum and duodenum. Location-specific function has been shown to be intrinsically programmed in adult intestinal epithelial stem cells. Region-specific expression profiles persist in long-term primary enteroid cultures derived from different small intestinal regions, even in the absence of any location-specific cues from stromal cells, luminal contents or microbiota (Middendorp *et al.*, 2014).

There are also differences in the cell type composition of the epithelium along the small intestine. Normally the abundance of goblet and Paneth cell populations increases from proximal to distal, likely reflecting the greater need for defence against the increasing presence of bacteria in the more distal regions of the small intestine (Bosse *et al.*, 2006;

Sekirov, Russell and Antunes, 2010). Goblet cells were increased in the jejunum of *Gata4*-knockout mice, suggesting that GATA4 has a role in determining region-specific cell type distribution as well as region-specific gene expression in enterocytes (Bosse *et al.*, 2006). Exactly how GATA4 exerts these effects, however, remains to be investigated.

1.2 Intestinal epithelial permeability

As discussed above, the intestinal epithelium is far from an inert barrier, having important roles in absorption of nutrients and water, secretion of mucus, hormones and antimicrobial peptides, and immune regulation. These roles are varied but movement of substances across the epithelium is key to many of them. Molecules and larger particles may cross the epithelium via several routes (**Figure 1.3**), which exhibit surprisingly dynamic regulation. There are two major routes across the epithelium: the paracellular and transcellular pathways.

1.2.1 Paracellular pathway

The paracellular route involves passage of particles between enterocytes. In addition to the adherens junctions and desmosomes that hold epithelial cells together to form a sheet, there are also tight junctions between cells that regulate the permeability of the paracellular pathway. Tight junctions are multi-protein complexes, consisting of membrane-spanning proteins like occludins and claudins, which interact with a network of cytoplasmic adaptor proteins, including zonulin and cingulin. These interact in turn with actin filaments and microtubules of the cytoskeleton (Zihni *et al.*, 2016). Tight junctions are not completely impermeable, instead selectively allowing passage of certain molecules based on size and charge (Shen *et al.*, 2011). Tight junctions are thought to have two pathways of permeability: a pore-dependent pathway and a leak pathway (Shen *et al.*, 2011; Zihni *et al.*, 2016). The first is thought to be mediated by pores formed by intramembrane protein strands and allows movement of ions and certain small uncharged molecules. The leak pathway appears to facilitate a slower flux of larger solutes up to 60 Å in diameter and has been proposed to occur with the gradual remodelling of the junction. Selectivity varies between tight junctions in different tissues; for example, tight junctions in the crypt regions of the small intestine are permeable to much larger particles than those in the villi. Although it was formerly thought that tight junctions were stable and mostly fixed, many signalling proteins have been identified that dynamically regulate these structures to alter epithelial permeability (Capaldo and Nusrat, 2009; Fasano, 2011).

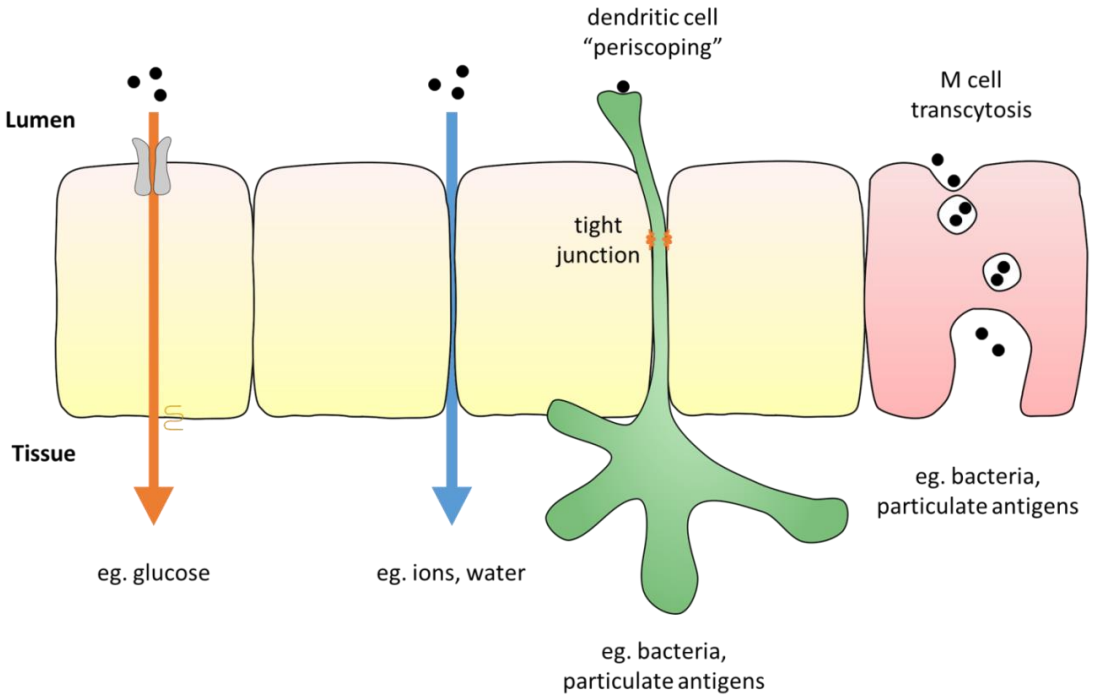

Figure 1.3. Paracellular and transcellular pathways of transport across the small intestinal epithelium from the lumen. Figure adapted from (Ménard, Cerf-Bensussan and Heyman, 2010).

1.2.2 Transcellular pathway

In contrast to the paracellular route, transcellular transport is where molecules move across cells. This is important in the small intestine as one of its key functions is nutrient absorption. As mentioned above, absorptive enterocytes express transporters that allow absorption of particular solutes. For example, expression of Na^+-glucose co-transporters facilitates uptake of glucose, which then exits the cell via glucose transporter 2 (GLUT2) at the basolateral membrane of the enterocyte to complete its passage across the epithelium. Aside from nutrient transport pathways, where molecules usually diffuse across the cytoplasm, other types of transepithelial paths also exist. Particles may be taken up at the luminal surface of the epithelium by endocytosis and moved across the cell in vesicles. This route is particularly relevant for the uptake of antigens, which is an important step in induction and regulation of some immune responses in the gut (Knoop, Miller and Newberry, 2013; Schulz and Pabst, 2013).

Several cell types are involved in antigen uptake across the intestinal epithelium. The classical example of this is microfold (M) cells, which are epithelial cells specialised for antigen uptake and translocation in a number of ways that will be described in more detail at a later point. Antigen sampling by M cells has been shown to be necessary for induction of some antigen-specific immune responses against pathogens (Mabbott *et al.*, 2013). In addition to M cells, certain dendritic cell subsets have been reported to extend protrusions between epithelial cells into the intestinal lumen and take up antigens (Rescigno *et al.*, 2001). These periscope-like processes have been described under steady-state conditions but increased in number in the presence of pathogenic bacteria (Niess *et al.*, 2005), possibly due to activation of Toll-like receptors on epithelial cells (Chieppa *et al.*, 2006). In addition, luminal dextran was shown to form plumes across the epithelium that co-localised with goblet cells markers under steady-state conditions in mice (McDole *et al.*, 2012). Dextran was also observed in $CD103^+$ lamina propria dendritic cells that associated closely with goblet cells at the basolateral surface. These so-called goblet cell-associated antigen passages represent a further route of transepithelial transport for low molecular weight particles.

1.2.3 Intestinal permeability in disease

There is evidence to suggest that altered intestinal permeability may contribute to a range of pathological states, including trauma-induced sepsis, inflammatory bowel disease, food allergies and metabolic disease (Ménard, Cerf-Bensussan and Heyman, 2010; Bischoff *et al.*, 2014). Abnormal permeability may occur acutely, for example in the case of trauma-induced sepsis, or chronically, as in inflammatory bowel disease. Several factors have been proposed to alter intestinal permeability, such as inflammation, degree of intestinal perfusion, infection and toxins, dietary factors and dysbiosis of the gut microbiota.

An acute increase in intestinal permeability is common in critically ill patients (Bischoff *et al.*, 2014). Here, altered permeability is demonstrated by elevation of markers such as fatty acid binding protein – which is released from damaged enterocytes – and bacterial components, such as lipopolysaccharide (LPS), in the blood plasma. The cause is thought to be hypoperfusion of the intestine and the consequences can be severe, including gut-derived sepsis. In contrast, patients with Crohn's disease are thought to have chronically altered intestinal permeability (Keita *et al.*, 2008; König *et al.*, 2016). Epithelial damage caused by ongoing inflammation and changes to epithelial tight junctions are thought to underpin this state; for example, tumour necrosis factor (TNF), characteristically elevated in Crohn's patients (Jones-Hall and Nakatsu, 2016), has been shown to increase epithelial permeability (Ma *et al.*, 2004). Increased epithelial permeability may also contribute to driving

inflammation by allowing greater access of immune-activating microbial components to the mucosa.

1.2.4 Coeliac disease – intestinal permeability gone wrong

Coeliac disease presents a unique example of the consequences of disrupted intestinal permeability and immune homeostasis. It is a multi-factorial disorder triggered by an abnormal adaptive immune response to dietary gluten. Most food antigens are thought to be fairly inert in the gut, either because they are rapidly digested and absorbed or because tolerance is developed against them (Ménard, Cerf-Bensussan and Heyman, 2010). Gluten contains gliadin proteins, which are broken down by digestive enzymes to form peptide fragments. These fragments are resistant to further digestion due to their high proline content so relatively large peptides (up to at least 33 amino acids) persist to interact with the mucosa (Shan, 2002). In certain genetically susceptible individuals, these gliadin-derived peptides initiate a chronic inflammatory response in the small intestine. In most populations, the prevalence of coeliac disease is 1 in 100-200 (Schuppan and Zimmer, 2013). The most commonly recognised symptoms are due to this small intestinal enteropathy and include diarrhoea, constipation, malnutrition and abdominal pain (Schuppan, Junker and Barisani, 2009); however, coeliac disease can also manifest as extra-intestinal symptoms, such as dermatitis hepatiformis and neuropathy (Leffler, Green and Fasano, 2015).

The sequence of pathological events that initiates coeliac disease is not fully understood. It is known that gliadin peptides somehow access the lamina propria, where they are modified by tissue transglutaminase (TG2), a ubiquitous enzyme that deamidates glutamine residues to form negatively charged glutamic acid (Di Sabatino *et al.*, 2012). The modified peptides are ideal ligands for HLA-DQ2 and -DQ8 molecules on antigen-presenting cells. In this context they are recognised by certain $CD4^+$ T cells, which become activated and drive an inflammatory response resulting in huge accumulation of intraepithelial lymphocytes, villus atrophy and crypt hyperplasia (Ciccocioppo *et al.*, 2005; De Re *et al.*, 2013). The HLA-DQ2/8 alleles and exposure to dietary gluten are therefore the largest risk factors for coeliac disease; however, given that 30-40% of the population carry HLA-DQ2/8 and only a fraction develop the condition, additional factors are clearly also important (Schuppan *et al.*, 2009; McAllister *et al.,* 2018).

Significant evidence suggests a role for abnormal intestinal permeability in the pathogenesis of coeliac disease (Heyman *et al.*, 2012; Schumann *et al.*, 2017). Genome-wide association studies have identified many genes that contribute to disease predisposition; the majority

with known functions are involved in regulating adaptive immunity but a number are also implicated in controlling intestinal barrier function (Schuppan *et al.*, 2009; Schumann *et al.*, 2017). Furthermore, there are many reports of increased intestinal permeability in coeliac patients and even their unaffected first-degree relatives (van Elburg *et al.*, 1993; Schumann *et al.*, 2017). This suggests that a defect in intestinal permeability may exist prior to development of coeliac disease and could contribute to its initiation by facilitating exposure of immune cells to gliadin peptides, or by interfering with normal intestinal immune homeostasis. Certain gliadin-derived peptides have also been reported to have various direct effects on the intestinal epithelium; these effects are not dependent on the presence of coeliac disease so could cause enhanced intestinal permeability in all individuals following gluten ingestion (Ciccocioppo *et al.,* 2005; De Re *et al.*, 2013).

1.2.5 Non-coeliac gluten/wheat sensitivity and irritable bowel syndrome

In addition to its role in coeliac disease, gluten has also been implicated in the pathophysiology of non-coeliac gluten sensitivity or wheat sensitivity (NCGS or NCWS) and in some cases of irritable bowel syndrome (IBS) (Aziz *et al.* , 2015). There is considerable overlap between the two conditions; both are associated with a range of symptoms, commonly including diarrhoea, abdominal pain and bloating (Schuppan *et al.*, 2015; Catassi *et al.*, 2017). Extraintestinal symptoms, such as skin rashes, foggy mind and fatigue, may also be reported. Importantly, patients with both conditions are serologically negative for coeliac disease and typically do not exhibit gluten allergy or signs of overt intestinal inflammation (Aziz *et al.*, 2015). NCWS in particular has been associated with some controversy because of the lack of a clear underlying pathological process or diagnostic test and the difficulty in performing robust clinical trials (Pinto-Sánchez and Verdú, 2016; Casella *et al.*, 2018). Adherence to a gluten-free diet is difficult to monitor and the popularity of gluten-free diets has increased dramatically among individuals who are not necessarily gluten-sensitive but perceive it to be healthier (Aziz *et al.,* 2015).

A link between gluten and certain cases of IBS or NCWS was suggested by a recent clinical trial, in which patients with IBS who managed their symptoms with a gluten-free diet reported worsened symptom control following introduction of dietary gluten, compared to those who consumed a placebo (Biesiekierski *et al.*, 2011). In contrast, other studies have implicated non-gluten components of wheat, such as amylase/trypsin inhibitors, and fermentable oligosaccharides, disaccharides, monosaccharides and polyols (FODMAPs) in non-coeliac gluten-related diseases (Junker *et al.*, 2012; Biesiekierski *et al.*, 2013). Altered intestinal permeability has been associated with both NCWS and gluten-sensitive IBS. One

study reported a greater increase in intestinal permeability in biopsies of patients with both coeliac disease and NCWS compared to non-coeliac controls following exposure to gliadin (Hollon *et al.*, 2015). Another study found enhanced small intestinal epithelial permeability in patients with diarrhoea-predominant IBS (IBS-D) following a gluten-containing diet compared to those consuming a gluten-free diet (Vazquez-Roque *et al.*, 2013).

1.3 Mucosal immunity in the GI tract

By surface area, the intestinal epithelium constitutes the largest external surface of the human body. It is continually exposed to foreign antigens that are ingested in the form of food and microbial contamination. The gastrointestinal tract is also intimately colonised by the commensal microbiota. As a result, intestinal immunity is a balance between protecting from pathogens and keeping the microbiota in check, while also maintaining oral tolerance to prevent excessive inflammation in response to harmless dietary antigens. The intestine contains gut-associated lymphoid tissues (GALT), which constitute the major foci of immune activity. In the small intestine, these mostly take the form of Peyer's patches – distinct regions of the mucosa that are specialised for immune function in a number of ways. Development of GALT largely occurs postnatally in response to signals from microbes, as demonstrated by the incomplete maturation of GALT in mice raised under germ-free conditions (Round and Mazmanian, 2009). The major tactic of intestinal immunity is immune exclusion, where foreign particles are barred from coming into contact with the epithelium (Strugnell and Wijburg, 2010; Mantis, Rol and Corthésy, 2011). Several components contribute to this effect, including the mucus layer, epithelium and gut-associated lymphoid tissues.

1.3.1 Role of the mucus layer

The mucus layer forms a barrier that prevents the contents of the small intestine lumen from contacting the epithelium. It consists mainly of highly glycosylated mucin proteins, which are produced and secreted by goblet cells. The most abundant mucin in the small intestine is MUC2, which oligomerises to form a gel. In the colon, bacteria are physically excluded by a denser inner mucus layer but the single mucus layer in the small intestine is discontinuous and penetrated to some degree by bacteria (Pelaseyed *et al.*, 2014; Johansson and Hansson, 2016). These are mostly found at the level of the villus tips, with few apparently able to penetrate down to the tops of the crypts (Ermund *et al.*, 2013). In addition to acting as a physical barrier, the mucus also retains anti-microbial peptides and antibodies, maintaining

higher concentrations of them in the vicinity of the epithelium (Johansson and Hansson, 2016).

1.3.2 Function and induction of IgA

A huge volume of antibodies, mostly in the form of secretory immunoglobulin A (sIgA), is secreted into the intestinal lumen under homeostatic conditions, playing a crucial role in immune exclusion. Humans deficient in sIgA are frequently more prone to gastrointestinal and respiratory infections (Strugnell and Wijburg, 2010). IgA is produced by plasma cells, mostly in the lamina propria of the intestine. From here it is taken up by enterocytes via the polymeric immunoglobulin receptor (pIgAR), expressed on their basolateral surface. In complex with pIgAR, IgA is transcytosed by the epithelial cells and released into the intestinal lumen along with the secretory component.

Once in the lumen, sIgA exerts protective effects against bacterial pathogens. IgA-mediated protection is mediated in part by direct binding to toxins or virulence factors, effectively neutralising them (Strugnell and Wijburg, 2010). For example, one IgA molecule directed against *Shigella flexneri* lipopolysaccharide was found to inhibit the type 3 secretion system required by this pathogen for invasion of epithelial cells (Forbes *et al.*, 2011). Additional mechanisms of 'immune exclusion' have also been proposed, referring to physical interference of sIgA with bacterial-mucosal interactions, possibly by agglutinating the bacteria as in strain-typing (Mantis, Rol and Corthésy, 2011). Recently, Slack and colleagues showed that IgA enchains dividing bacterial daughter cells to generate clumps of rapidly dividing bacteria that are efficiently cleared (Moor *et al.*, 2017).

IgA responses are thought to be mainly initiated in gut-associated lymphoid follicles. In the small intestine, most lymphoid follicles are found as Peyer's patches – domed areas where a follicle in the submucosa is covered by specialised follicle-associated epithelium (FAE; **Figure 1.4**). Peyer's patches are most abundant in the ileum but may also be found in the jejunum and duodenum. They vary in size and number between individuals. In addition to containing M cells, the FAE has additional characteristics that aid its role as a site of immune induction, including a much thinner overlying mucus layer as the FAE contains very few goblet cells.

Initiation of an IgA response depends on antigen sampling. The FAE is thought to be a site of antigen sampling because it contains M cells, which transcytose luminal antigens and transfer them to antigen-presenting cells with which they are in close contact with at their basolateral surface. The antigen-presenting cells, including dendritic cells and B cells, migrate to the perifollicular areas of the lymphoid follicles where they interact with helper T cells (Mesin,

Sollid and Niro, 2012). B cells in the germinal centres that express cognate Ig receptors then become activated by the combination of signals from antigen-presenting cells and activated helper T cells. Activated B cells undergo immunoglobulin class switching, somatic hypermutation and affinity maturation and differentiate into plasma cells that secrete IgA with high antigen affinity. The importance of IgA to mucosal immunity is demonstrated by mice deficient in activation-induced cytidine deaminase, which lack IgA-secreting plasma cells. These mice exhibit defects in regulation of the gut microbiota, with 100-fold expansion of anaerobic bacteria in the small intestine and B cell hyperplasia (Fagarasan, 2002).

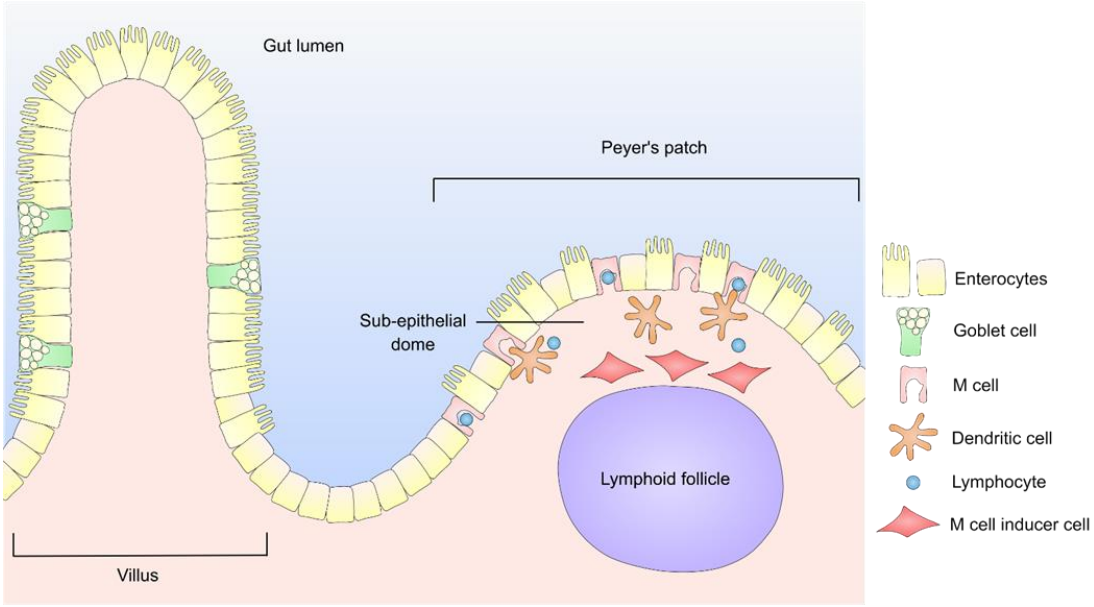

Figure 1.4. Peyer's patch structure comparison of follicle-associated epithelium to villus epithelium. Peyer's patches are found most commonly in the terminal ileum of the small intestine and appear as domes in comparison to the surrounding villi. They consist of a lymphoid follicle beneath the mucosa, covered by the specialised follicle-associated epithelium. In the sub-epithelial dome area, mesenchymal M cell inducer cells express RANKL, which acts on the epithelium to stimulate M cell differentiation. For this reason, M cells are largely restricted to the follicle-associated epithelium. Unlike villus enterocytes, M cells lack defined apical microvilli and have large basolateral pockets in which dendritic cells and lymphocytes are found. Fewer mucus-secreting goblet cells in the FAE results in a thinner or completely absent mucus layer compared to that over the villus epithelium. Figure adapted from (Ohno, 2016).

1.4. M cells

1.4.1. M cell morphology

M cells are the key component of the FAE that make it a site of luminal antigen sampling and immune induction. They are a rare subset of intestinal epithelial cells, with reports of their frequency varying between 5-10% of cells within the FAE (Miller, 2007; Mabbott *et al.*, 2013; Ohno, 2016). Aside from the FAE, M cells are also found in the epithelium overlying colonic lymphoid follicles. Whether there is any lineage relationship between M cells in the small and large intestines has not been investigate, although at the ultrastructural level they appear to be similar (Jacob *et al.*, 1987).

M cells were first described in the 1970s due to their distinct morphology and ability to take up particles. Using an electron microscope, it is noticeable that murine M cells have stunted,

irregular microvilli, while human M cells have microfolds, on their apical surface (Miller, 2007). They possess large invaginated pockets in their basolateral membrane, in which immune cells like B cells and dendritic cells have been observed to reside (Miller, 2007). Such pockets are thought to facilitate close interactions between M cells and these antigen-presenting cells in order to enable more rapid transfer of particles and antigens.

1.4.2. M cell development

Our knowledge of the factors guiding M cell differentiation has increased over the last three decades but many aspects of this process still remain to be understood. A major point of controversy has been whether M cells are specified as crypt progenitor cells, which then migrate from the crypts to the dome of Peyer's patches, or whether they develop from differentiated enterocytes within the epithelium overlying a Peyer's patch. In support of the first theory, it was reported in rabbit caecal patches that the pattern of glycosylation of M cells varied from the base of the dome to its top (Gebert and Posselt, 1997). M cells with similar glycosylation patterns were observed in clusters arranged like spokes radiating from the top of the dome and it was suggested that each spoke represented M cells derived from a common precursor cell in an associated crypt. More recently, it was demonstrated that M cells are derived from $Lgr5^+$ crypt stem cells, along with the other major epithelial cell lineages (de Lau *et al.*, 2012).

1.4.2.1. Role of RANKL in M cell differentiation

In a key study, Knoop *et al* demonstrated comprehensively that the TNF superfamily cytokine, receptor activator of NF-κB ligand (RANKL), is crucial for M cell differentiation. In *Rankl*$^{-/-}$ mice, Peyer's patch M cells are almost completely absent and exhibit reduced uptake of nanoparticles (Knoop *et al.*, 2009). Interestingly, the number of remaining M cells in *Rankl*$^{-/-}$ mice was greatest in the most distal Peyer's patches and decreased in those located more proximally in the small intestine. This deficiency was largely rescued by injection of recombinant murine RANKL, with increased M cell numbers in Peyer's patches and ectopic M cells appearing on the villi. These RANKL-induced M cells were able to take up both latex beads and fixed enteric bacteria, including *Salmonella enterica* serovar Typhimurium and *Yersinia enterocolitica*. *Rankl*$^{-/-}$ mice also have a number of another abnormalities, such as lack of teeth and lymph nodes (Kong *et al.*, 1999). It could therefore be argued that the reduction in M cells in *Rankl*$^{-/-}$ mice might be an indirect result of the lack of RANKL, caused by other defects present throughout development; however, the authors also showed that adult wild-type mice treated with a neutralising RANKL antibody recapitulated the loss of M cells described in *Rankl*$^{-/-}$ mice. The concentration of IgA present

in the faeces of *Rankl*$^{-/-}$ mice was consistently lower than that of wild-type mice, suggesting that they have defective induction or production of IgA. RANKL also reportedly promotes differentiation of M cells found in the epithelium overlying nasopharynx-associated lymphoid tissues (Mutoh *et al.*, 2016), indicating that it may be a feature common to many mucosae.

RANKL – also referred to as TNF-related activation-induced cytokine (TRANCE) and TNFSF11 – is a 316-amino acid type II homotrimeric transmembrane protein that undergoes proteolytic cleavage of its ectodomain to produce a secreted form. RANKL was initially described by two groups in 1997 as regulating T cell and dendritic cell function (Anderson *et al.*, 1997; Wong *et al.*, 1997). Around the same time, RANKL was also found to be the key stimulator of osteoclast differentiation expressed by osteoblasts and stromal cells (Nakagawa *et al.*, 1998). The receptor for RANKL is receptor activator of NF-κB (RANK), which is expressed on the surface of osteoclast progenitors, many immune cells, and on both apical and basolateral surfaces of epithelial cells throughout the small intestinal epithelium (Knoop *et al.*, 2009). In addition, RANKL also binds to a soluble decoy receptor known as osteroprotegerin (Nagy and Penninger, 2015).

The source of the RANKL responsible for M cell differentiation in the FAE was long thought to be mesenchymal cells in the sub-epithelial dome as they have been shown to express RANKL (Taylor *et al.*, 2007; Knoop *et al.*, 2009). This has recently been confirmed and the cells have been termed microfold cell inducer cells (Nagashima *et al.*, 2017). RANKL is highly expressed by podoplanin^{+}MadCAM-1^{-} sub-epithelial mesenchymal cells that directly contact the FAE. In two independent mouse models in which RANKL is knocked out specifically in mesenchymal cells (*Tnfsf11*$^{fl/\Delta}$; *Twist2*-Cre and *Tnfsf11*$^{fl/\Delta}$ *Col6a1*-Cre mice), expression of RANKL by podoplanin^{+}MadCAM-1^{-} cells is dramatically reduced, with concurrent reductions in expression of *Ccl20*, *Spib* and glycoprotein 2 (*Gp2)* in the FAE and in numbers of GP2^{+} M cells in the FAE observed by immunostaining and scanning electron microscopy (Nagashima *et al.*, 2017; Nagashima *et al.*, 2017). In contrast, mice with a haematopoietic cell-specific deletion of RANKL have apparently normal M cells (Nagashima *et al.*, 2017). Interestingly, mice expressing truncated RANKL, which lacks the cleavage sites required for release of its soluble form but is still expressed on the cell membrane, showed normal expression of M cell markers in the FAE, indicating that soluble RANKL may not be necessary for M cell differentiation (Nagashima *et al.*, 2017).

Binding of RANKL to its receptor, RANK, results in receptor oligomerisation and recruitment of adaptor molecules to sites within the cytoplasmic region of RANK. TNF receptor-associated factors (TRAFs) are particularly important in this context, with TRAF-2, -5 and -6 all able to bind to RANK (Boyce and Xing, 2007). Of these, TRAF-6 is thought to be the principle driver of RANKL-induced osteoclast differentiation as only *Traf6*$^{-/-}$ mice are deficient in osteoclasts and exhibit osteopetrosis (abnormally dense bones). A recent study has confirmed that TRAF-6 is crucial for M cell differentiation driven by RANKL; this process is blocked when *Traf6* is deleted in the intestinal epithelial cells of mice (Kanaya *et al.*, 2018). Recruitment of TRAFs activates further intracellular signalling, including activation of NF-κB, c-Src and mitogen-activated protein kinase (MAPK) pathways. This means that the RANKL-RANK interaction has a variety of consequences, including regulation of gene expression. Activation of NF-κB results in its translocation to the nucleus, while MAPK activation causes nuclear translocation of transcription factors c-Fos and c-Jun. These pathways are important for the role of RANKL in osteoclast differentiation, since mice lacking both of the NF-κB subunits, p50 and p52, or c-Fos also exhibit osteopetrosis (Nagy and Penninger, 2015). Intestinal epithelium-specific deletion of *Traf6* resulted in impaired nuclear translocation of NF-κB complexes (Kanaya *et al.*, 2018).

The precise signalling cascades that drive M cell differentiation downstream of RANKL remain largely unclear. The transcription factor SpiB is required for RANKL-stimulated M cell differentiation (de Lau *et al.*, 2012). This is demonstrated by evidence showing that SpiB is specifically expressed in M cells and that *Spib*$^{-/-}$ mice lack M cells. Reconstitution of *Spib*$^{-/-}$ mice with wild-type bone marrow did not restore the M cell population, indicating that the defect is not due to the absence of SpiB expression in the immune cells of the lymphoid follicle (de Lau *et al.*, 2012; Sato *et al.*, 2013). SpiB expression is increased in intestinal epithelial cells following RANKL stimulation and subsequently regulates expression of other M cell-associated genes; for example, expression of M cell marker GP2 is markedly reduced in *Spib*$^{-/-}$ mice (Sato *et al.*, 2013). As such, SpiB has been described as the master transcription factor of the M cell lineage. It appears, however, that not all genes reported to be specific to M cells are controlled by SpiB. Gene expression analysis of the FAE of wild-type versus *Spib*$^{-/-}$ mice showed that expression of *Gp2* and uromodulin *(Umod)* was reduced whereas expression of MARCKS-like 1 (*Marcksl1)*, fucosyltransferase 1 (*Fut1)* and peptidoglycan recognition protein 1 *(Pglyrp1)* were unchanged (Sato *et al.*, 2013). GP2^{+} M cells detected by immunostaining were almost entirely absent in the FAE of *Spib*$^{-/-}$ mice, while a small number of cells remained that stained positively using alternative M cell

identifiers, NKM 16-2-4 (an anti-M cell antibody recognising a (1,2)-fucose-containing cell surface carbohydrate moiety (Nochi *et al.*, 2007)) and wheat germ agglutinin (WGA) (Sato *et al.*, 2013). Clevers and colleagues have suggested that a small proportion of M cells may develop independently of SpiB (Sato *et al.*, 2013).

1.4.2.2. Role of B cells in M cell differentiation

Given that M cells are found in the FAE but not usually in the surrounding villus epithelium, it is reasonable to hypothesise that immune cells in the lymphoid follicle may have a role in triggering M cell differentiation. Support for this theory initially came from a study reporting that Caco-2 cells, a human intestinal cell line, could be converted to an M cell-like phenotype by co-culturing them with lymphocytes isolated from Peyer's patches of BALB/c mice in a Transwell system (Kernéis *et al.*, 1997). The Caco-2 cell monolayers lost the apical expression of villin that is typical of differentiated enterocytes and developed disorganised apical microvilli rather than the classical brush border. Unlike control monolayers, those cultured with the lymphocytes were able to translocate fluorescently tagged latex beads, suggesting that they had taken on an M cell-like phenotype, both morphologically and functionally. Co-culture of Caco-2 cells with Raji B cells – a human B cell lymphoma line (Karpova *et al.*, 2005) – also induced an M cell-like phenotype in the epithelial cells, suggesting that B cells were the main driver of M cell differentiation (Gullberg *et al.*, 2000; des Rieux *et al.*, 2007).

The factors secreted by Peyer's patch B cells and Raji B cells that are responsible for stimulating M cell differentiation remain largely unknown. Gene expression analysis of Raji B cells that either induced or did not induce particle transport in Caco-2 monolayers revealed that genes associated with monolayer conversion include tumour necrosis factor (TNF) family cytokines (including TNF-α and lymphotoxin (LT)-β), growth factors of the transforming growth factor (TGF)-β family, the chemokine RANTES, and interferon-regulatory factor IRF-1 (Gullberg, 2005). Others found that TNF and LTβ receptor agonists induce expression of certain genes associated with the FAE, such as *Gp2* and chemokine (C-C motif) ligand 20 (*Ccl20*), in primary rat small intestinal IEC-6 cells and Caco-2 cells (Wang *et al.*, 2009). None of these factors alone, however, reproduce the same induction of particle transport as Raji B cells (Gullberg, 2005).

In spite of this, the role of B cells in M cell differentiation is further supported by evidence that mice lacking B cells due to ablation of genes encoding the immunoglobulin genes had fewer Peyer's patches and fewer cells with microfold morphology as assessed by scanning

electron microscopy (Golovkina *et al.*, 1999). Mice deficient in either αβ or γδ T cells had normal Peyer's patches. The authors also reported that *Rag1*$^{-/-}$ mice, which lack both mature B and T cells, showed the most severe reduction in Peyer's patch numbers; however, another study reported that *Rag1*$^{-/-}$ mice have normal numbers of M cells within the FAE, although the Peyer's patches in these animals were smaller than in wild-types and lacked follicles (Debard *et al.*, 2001). This contradicts the claim that B cells are required for M cell differentiation. Furthermore, a population of CCR6^{hi}CD11c^{int} B cells found in the sub-epithelial dome of the mouse Peyer's patch promote M cell differentiation (Ebisawa *et al.*, 2011). This study, as well as others, have demonstrated that M cells are depleted in CCR6-deficient mice, indicating that the interaction between CCR6 and its chemokine ligand CCL20 may be crucial for M cell formation (Lügering *et al.*, 2005; Westphal *et al.*, 2008). Accordingly, CCR6^{hi}CD11c^{int} B cells are also depleted in CCR6-deficient mice, while transfer of these cells to CCR6-deficient mice rescues the lost M cells (Ebisawa *et al.*, 2011). More generally, B cells are already known to be involved in the development of secondary lymphoid organs by providing TNF and lymphotoxin required for maturation and retention of follicular dendritic cells (Aguzzi, Kranich and Krautler, 2014).

1.4.2.3. Role of NF-κB signalling in M cell differentiation

RANKL is a potent activator of NF-κB signalling, which is known to regulate intestinal inflammation and RANKL-induced osteoclast differentiation. The NF-κB pathway is therefore also likely to be involved in M cell differentiation. NF-κB signalling is mediated by transcription factors formed of dimers between different combinations of NF-κB subunits. It is broadly divided into the classical and alternative pathways, which are defined by the subunits involved and the mechanisms of activation. The classical pathway requires degradation of IκB inhibitors by IκB kinases (IKK), releasing NF-κB1 (p50)-RelA dimers to translocate into the nucleus and regulate gene expression (Sun, 2011). In contrast, the alternative pathway involves processing by NF-κB-inducing kinase (NIK) of p100 to NF-κB2 (p52) to form transcriptionally active NF-κB2-RelB dimers. The complexity of this system is further increased by the existence of a fifth subunit, c-Rel, and the ability of most subunits to form both homo- and heterodimers.

RANKL stimulates both classical and alternative NF-κB pathways (Sun, 2011). Furthermore, analysis of transcription factor binding site motifs in the promoters of genes found to be expressed specifically in the FAE identified a number with NF-κB binding motifs (Kobayashi *et al.*, 2012). These data suggest NF-κB-mediated gene regulation may be important for M cell differentiation.

The relative roles of different NF-κB signalling pathways in M cell development have been investigated to some extent using knockout mouse models. Normal Peyer's patches and M cells are found in c-Rel-deficient mice, indicating that c-Rel is not essential for M cell differentiation (Sehgal *et al.*, 2017). In contrast, Peyer's patches are absent in mice deficient in NF-κB2, RelB (Yilmaz, 2003) or RelA (Alcamo *et al.*, 2002), and in *aly/aly* mice that express dysfunctional NIK (Shinkura *et al.*, 1999); this may be due to disruption of LT-β signalling via the alternative NF-κB pathway, which is crucial for the development of secondary lymphoid tissues (Karrer *et al.*, 2000; Yilmaz, 2003). Whether any M cells can still be detected in these mice was not investigated, but in the absence of Peyer's patches it is unlikely. This makes it difficult to assess the importance of these individual subunits in M cell differentiation. To get around this, one group injected alymphoplasia (*aly/aly*) mice with RANKL; they observed no formation of ectopic M cells as seen in wild-type mice, suggesting that NIK-dependent alternative NF-κB signalling is necessary for M cell differentiation itself (Kimura *et al.*, 2015). Primary small intestinal cultures established from *aly/aly* mice also do not undergo M cell differentiation when treated with exogenous RANKL (Wood *et al.*, 2016).

The importance of alternative pathway NF-κB signalling in M cell differentiation has been confirmed during the course of the current study by the finding that both M cell differentiation and nuclear translocation of RelB are compromised in the FAE of mice carrying an epithelium-specific deletion of *Traf6* (Kanaya *et al.*, 2018). In contrast, RelB predominantly localised to the nuclei of FAE cells in wild type mice. Furthermore, treatment with RANKL rapidly upregulated expression of alternative pathway subunits, *Relb* and *Nfkb2*. The role of alternative pathway NF-κB signalling in M cell differentiation is further supported by experiments performed in murine thymic epithelial cells suggesting that *Spib* is a target gene of RANKL-NIK-RelB signalling (Akiyama *et al.*, 2014). Finally, TNF-α – a known activator of the alternative pathway – enhances the effect of RANKL on M cell differentiation, possibly by increasing the availability of RelB and NF-κB2 subunits in enterocytes by causing their rapid induction (Wood *et al.*, 2016).

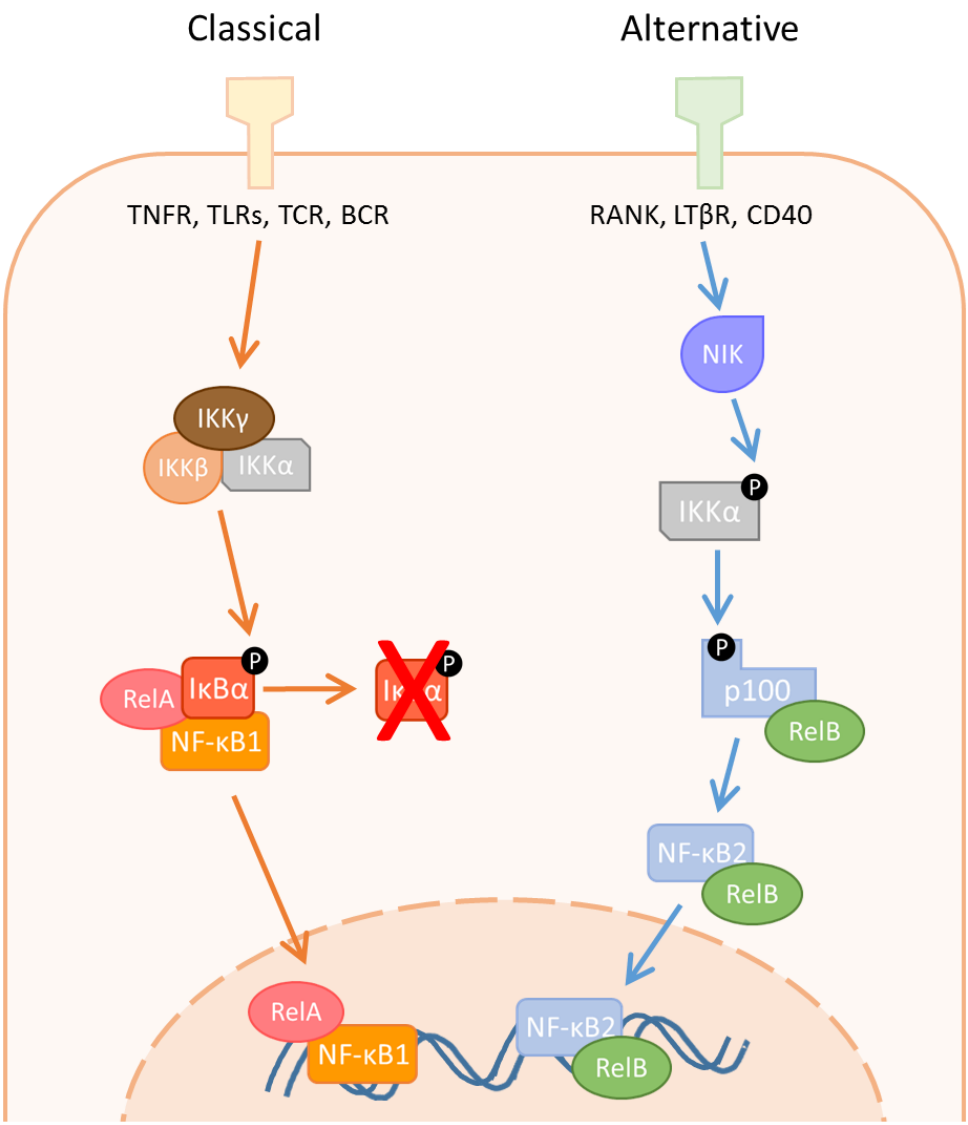

Figure 1.5. Major events in the classical and alternative pathways of NF-κB signalling. The classical NF-κB pathway is activated by signalling via cell surface receptors including the TNF receptor (TNFR), TLRs, T cell (TCR) and B cell receptors (BCR). Through the activities of kinases such as RIP and TAK, the IKK complex (IKKα, β and γ) is activated and in turn causes the ubiquitin-dependent degradation of IκBα. Freed from its inhibition, the RelA-NF-κB1 (also known as RelA-p50) complex translocates to the nucleus where it regulates gene transcription. Alternative NF-κB signalling is switched on in response to activation of a different set of receptors, including RANK and LT-β. The result is stabilisation of NIK, allowing it to activate IKKα by phosphorylation. IKKα in turn phosphorylates p100, which is processed by cleavage of ankyrin repeats, which are then degraded to leave NF-κB2 (also known as p52). RelB-NF-κB2 complexes are then able to enter the nucleus. This schematic is greatly simplified and does not show other possible subunit complexes, which include homodimers and heterodimers with an additional subunit, c-Rel. Figure adapted from (Sun, 2011) and (Taniguchi and Karin, 2018).

1.4.2.4. Induction of M cell differentiation by microbial signals

In addition to signals from the underlying tissue, exposure to certain microbes has also been reported to stimulate M cell differentiation. Mahajan and colleagues described trans-differentiation of enterocytes within the FAE of mice into M cells in response to wild type *S.* Typhimurium (Tahoun *et al.*, 2012). This response was found to be dependent on the *S.* Typhimurium type III effector protein, SopB, as it did not occur with a *ΔsopB* strain. The authors found that a similar effect was also observed in bovine rectal epithelial cells derived from crypts neighbouring lymphoid follicles. Here, the effect was found to require SopB-stimulated autocrine RANKL signalling and Wnt/β-catenin signalling-driven epithelial-mesenchymal transition. Another group reported that cholera toxin is also capable of inducing trans-differentiation of FAE enterocytes into M cells (Wang *et al.*, 2011). Since enteropathic bacteria have been shown to specifically target M cells for invasion (Miller, 2007), it is speculated that such mechanisms allow them to boost M cell numbers and increase their own chances of host colonisation.

1.4.3. M cell markers

Results from efforts to identify specific cellular markers of M cells have been mixed and often contradictory (Casteleyn *et al.*, 2013). This is largely due to the rarity of M cells *in vivo* and the challenge of isolating them. For some time, *Ulex europaeus* agglutinin-1 (UEA-1) – a lectin that selectively binds α(1,2)-fucose cell surface moieties – was the best available tool for defining M cells (Clark *et al.*, 1993). The utility of UEA-1 as a marker is significantly limited, however, by the fact that it also binds goblet cells and is only specific for murine M cells (Ohno and Hase, 2010). As technologies advanced, two studies attempted to identify an M cell transcriptional profile by using DNA microarrays to compare gene expression in intestinal epithelial cells from FAE and villus regions (Hase *et al.*, 2005; Terahara *et al.*, 2008). These studies identified a number of genes whose expression was upregulated specifically in FAE, including genes encoding chemokines, such as CCL9 and CCL20, and others encoding proteins involved in immune defence. The latter include peptidoglycan recognition protein 2 and mannose receptor C type 1, which are involved elsewhere in pathogen recognition. A comprehensive list of putative M cell markers may be found in **Table 1.1**. Encouragingly, both studies confirmed elevated expression of some genes previously described as having M cell-specific expression. A major limitation of these studies is that M cells only make up a small portion of cells within the FAE, so the starting material still contained a mixed population of M cells and non-M cells.

Importantly, these studies identified GP2 as an M cell-specific marker. M cell-specific expression of GP2 was confirmed by *in situ* hybridisation and immunostaining and it was later shown to have functional significance by acting as an uptake receptor for *S.* Typhimurium fimbrial adhesion molecule, FimH (Hase *et al.*, 2009). GP2 is an integral membrane protein that localises to the apical surface of the M cell plasma membrane by a glycosylphosphatidylinositol linkage (Ohno and Hase, 2010). Notably, GP2 is expressed by both mouse and human M cells (Hase *et al.*, 2009). GP2 has since become the standard M cell marker; however, evidence suggests that it may only be expressed on more mature M cells. For instance, GP2 expression was only found to peak on day 3 after exogenous RANKL stimulation (Kanaya *et al.*, 2012). Cells that exhibited the classical M cell morphology and expressed other M cell-specific markers but not GP2 have also been identified; these GP2-low cells showed much reduced uptake of latex beads compared to GP2-high cells (Kimura *et al.*, 2015). The lack of robust markers uniquely expressed by M cells and the lack of understanding about how expression of putative markers changes throughout M cell differentiation has been a major obstacle for progress in this area.

Table 1.1. Putative M cell markers.

Marker	***Species***	***Additional details***	***Citation***
SpiB	Mouse, human	M cell lineage master transcription factor	(de Lau *et al.*, 2012; Kanaya *et al.*, 2012; Rouch *et al.*, 2016)
GP2	Mouse, human	Involved in uptake of $FimH^+$ bacteria	(Hase *et al.*, 2009; Kim *et al.*, 2010)
α(1,2)-fucose (recognised by UEA-1)	Mouse	UEA-1 also recognises mouse goblet cells and Paneth cells	(Clark *et al.*, 1993)
α(1,2)-fucose (recognised by NKM 16-2-4 antibody)	Mouse	Also appears to recognise mouse Paneth cells in experiments performed by our group	(Nochi *et al.*, 2007)
MARCKS-related protein	Mouse	SpiB-independent expression	(Terahara *et al.*, 2008; Kanaya *et al.*, 2012; Wood *et al.*, 2016)
Annexin V	Mouse	SpiB-independent expression	(Verbrugghe *et al.*, 2006; Wood *et al.*, 2016)
Uromodulin	Mouse		(Sato *et al.*, 2013)
CCL9	Mouse	Involved in recruitment of $CD11b^+$ dendritic cells to the sub-epithelial dome region; SpiB-dependent expression	(Terahara *et al.*, 2008; Kanaya *et al.*, 2012)
M-Sec or TNFaip2	Mouse	SpiB-dependent expression	(Hase *et al.*, 2009; Wood *et al.*, 2016)
Sgne-1	Mouse	SpiB-dependent expression	(Hase *et al.*, 2005; Kanaya *et al.*, 2012)
Siglec-F	Mouse		(Rochereau *et al.*, 2013; Gicheva *et al.*, 2016)
Clusterin	Human	Also expressed by enteroendocrine cells in the villus epithelium. Highly expressed in mouse FAE but M cell-specific expression not confirmed	(Verbrugghe *et al.*, 2006, 2008)
Cellular prion protein (PrP^C)	Mouse	Also highly expressed in chicken bursa of Fabricius, which contains a high density of M cells	(Nakato *et al.*, 2012)
Cyclophilin A	Cow		(Hondo *et al.*, 2016)
Sialyl Lewis A	Human	Anti-sialyl Lewis A monoclonal antibodies also strongly stained goblet cell mucins	(Giannasca *et al.*, 1999)

1.4.4. M cell function

1.4.4.1. Antigen uptake

In comparison to absorptive enterocytes, M cells have enhanced phagocytic and transcytotic capacities. This allows them to function as immune surveillance posts, sampling antigens from the intestinal lumen and transport them to the lamina propria, where they can interact with immune cells. The importance of antigen sampling by M cells for initiation of IgA responses against luminal bacteria is demonstrated in mice carrying an intestinal epithelium-specific deletion of RANK, meaning that they lack M cells (Rios *et al.*, 2016). Compared to wild type littermates, the Peyer's patches of these mice display impaired particle uptake and reduced numbers of lamina propria IgA-secreting plasma cells. They also had lower faecal sIgA concentrations and displayed impaired IgA responses, both following oral immunisation with ferritin and following conventionalisation when previously germ-free.

Despite this evidence of the importance of M cells in induction of mucosal immune responses, the cellular mechanisms responsible for antigen uptake by M cells remain unclear. Certain M cell surface molecules have been shown to act as uptake receptors for particular bacteria; for example, GP2 interacting with FimH expressed by *S.* Typhimurium and *Escherichia coli* (Hase *et al.*, 2009). Other bacterial molecules have been reported to mediate preferential targeting of Peyer's patches but whether they interact specifically with M cells, and the molecular identities of their target receptors, are unknown. These include the long polar fimbriae of *S.* Typhimurium (Baumler *et al.,* 1996) and adherent-invasive *E. coli* (Chassaing *et al.*, 2011), and GipA (Vazeille *et al.*, 2016). On the other hand, certain M cell molecules have been implicated as uptake receptors but their bacterial interaction partners have not been confirmed; for example, cellular prion protein is reported to be responsible for uptake of *Brucella abortus*, possibly via an interaction with bacterial surface-expressed heat shock protein 60 (Nakato *et al.*, 2012). Overall, these data support the hypothesis that antigen sampling by M cells occurs via specific receptor-mediated endocytosis, in contrast to earlier proposals that sampling occurs non-specifically, such as by pinocytosis. Despite this, latex beads are used in many studies to model uptake and translocation of particulate antigens, raising the question of how this process is mediated and whether it accurately recapitulates M cell translocation of bacterial antigens.

1.4.4.2. Transcytosis of antigens

Several studies have suggested that M cells transcytose various antigens, including non-opsonised and sIgA-bound antigens, by different pathways. Evidence for reverse transcytosis of sIgA-bound antigens comes from studies showing selective binding, uptake and transport of sIgA by rabbit, mouse and human M cells (Mantis *et al.*, 2002). Reverse sIgA transcytosis could facilitate delivery of many different antigens to the GALT. Rochereau *et al* provided evidence that Dectin-1 acts as a receptor for sIgA, with Siglec-5 also playing an important role (Rochereau *et al.*, 2013).

The mechanisms of apical to basolateral antigen transcytosis by M cells have been minimally characterised. Antigens are presumed to be transcytosed via the vesicular system (Rios *et al.*, 2016); several studies have observed vesicle-bound antigens within M cells, including *Mycobacterium tuberculosis* (Nair *et al.*, 2016), labelled protein tracers (Neutra *et al.*, 1987) and *E. coli* (Roberts *et al.*, 2010). Translocation to underlying dendritic cells has been reported to occur in as little as 10 minutes after addition of bacteria to the lumen (Sakhon *et al.*, 2015). To date, the only available studies investigating the molecular regulation of transcytosis have been conducted in cell line models of the FAE. Using the Caco-2 human carcinoma cell line, one study found that expression of constitutively active SRC family tyrosine kinase, haematopoietic cell kinase (HCK) increased the rate of transcytosis of polystyrene microspheres, while expression of a dominant negative form blocked transcytosis (Asai and Morrison, 2013). In addition, the authors found that HCK expression is regulated by SpiB and that forced expression of SpiB or a related transcription factor, EHF, was sufficient to enhance transcytosis. The lack of progress in identifying regulators of M cell transcytosis is largely due to the difficulty in obtaining sufficient quantities of M cells to conduct rigorous biochemical studies.

An alternative proposed mechanism of antigen transport across the FAE is the extension of dendrites via M cell-specific pores into the intestinal lumen by Peyer's patch dendritic cells (Lelouard *et al.*, 2012). Such extensions were observed in both mouse and rabbit Peyer's patches and involved recruitment of epithelial cellular adhesion molecule and junctional adhesion molecule A to the pore-forming membrane of the M cell. Imaging suggested that the dendritic cells were capable of phagocytosing microspheres and live *S.* Typhimurium from the luminal surface of the epithelium, before withdrawing into the sub-epithelial dome. Previously, studies have demonstrated dendritic cells extending periscope-like tendrils between cells of the villus intestinal epithelium to sample luminal antigens

(Rescigno *et al.*, 2001). This report highlights another route of antigen translocation in which M cells may be involved.

1.4.4.3. Basolateral antigen handling and interaction with Peyer's patch immune cells

M cells are in close contact with immune cells, some even residing within the deep pocket formed within the M cell basolateral surface (Mabbott *et al.*, 2013). This spatial arrangement is proposed to facilitate efficient transfer of translocated antigens between M cells and antigen-presenting cells; however, little is known about these processes. Ohno and colleagues showed that CXCL16 is expressed highly in the FAE compared to the villus epithelium and that its receptor, CXCR6/Bonzo, is upregulated on the surface of certain $CD4^+$ T cells in the Peyer's patch (Hase *et al.*, 2006). Their findings suggest that CXCL16 promotes migration of activated T cells to the sub-epithelial dome. The uncleaved form of CXCL16 also acts as a cell adhesion molecule, raising the possibility that it may contribute both to immune cell homing to the vicinity of M cells and their direct interaction with M cells.

Recently, microvesicles have been described that are shed by M cells into the sub-epithelial space (Sakhon *et al.*, 2015). In this study in mice, microvesicle release occurred constitutively and independently of particle translocation. Microvesicles were rapidly taken up by dendritic cells, where they frequently co-localised with transcytosed bacteria supplied to the intestinal lumen. The number and size of microvesicles appeared to be regulated by the type of bacteria supplied and by pro-inflammatory signals such as TLR2 activation. The authors speculate that transcytosed bacteria are released from M cells inside the microvesicles, suggesting a possible pathway by which antigens may be delivered to antigen presenting cells.

1.4.5. Role of M cells in disease

1.4.5.1. Targeting of M cells by enteropathogens

The same adaptations that enable M cells to perform their primary role of immune surveillance also make them vulnerable to targeting by enteropathogens seeking to invade the intestinal epithelium (Miller, 2007). The reduced or absent mucus layer covering the FAE allows close contact between luminal microbes and M cells. As discussed above, M cells also express molecules on their apical surfaces that act as receptors for bacterial antigens; for example, GP2, which interacts with bacterial fimbrial adhesion H (FimH), a component of type I pili (Hase *et al.*, 2009). Finally, the transcytotic ability of M cells means that they

are specialised for transporting intact particles and even whole bacteria across the epithelium.

The importance of M cells in the initiation of infection is demonstrated by the fact that infection with several enteric pathogens is impaired in M cell-deficient mice. In CCR6-deficient mice, which have reduced M cell numbers, infection with *Y. enterocolitica* was blocked (Westphal *et al.*, 2008). Additionally, infection with mouse mammary tumour virus was greatly reduced in mice lacking M cells as a result of the absence of B cells (Golovkina *et al.*, 1999). An *in vitro* study in a cell line model indicated that the fungal pathogen *Candida albicans* selectively invades M cells (Albac *et al.*, 2016). Interestingly, prion infection is also blocked in the absence of M cells and enhanced when M cell numbers are inflated (Donaldson *et al.*, 2012, 2016). A number of other pathogenic agents have also been reported to preferentially infect Peyer's patches rather than villus epithelium, including *Listeria monocytogenes* (Chiba *et al.*, 2011), *Mycobacterium avium* subspecies *paratuberculosis* (Ponnusamy *et al.*, 2013) and *S.* Typhimurium (Clark *et al.*, 1994; Baumler, Tsolis and Heffron, 1996). Elsewhere, a lack of M cells in the airways was shown to prevent disseminated *M. tuberculosis* infection, suggesting that exploitation of M cells as a route of entry may be common to all mucosal surfaces (Nair *et al.*, 2016).

As described previously, *S.* Typhimurium is also able to stimulate enterocytes in crypts in the vicinity of lymphoid follicles to adopt an M cell-like phenotype (Tahoun *et al.*, 2012). Bacterial effector protein SopB was shown to be responsible for the increase in M cell numbers by inducing expression of both RANK and RANKL and driving Wnt/β-catenin signalling. SopB is a phosphoinositide phosphatase that is injected into host cells via a type III secretion system and regulates many cellular pathways. Although the authors do not demonstrate that this process contributes to increased infectivity of *S.* Typhimurium, this is likely given the evidence for its selective invasion of M cells. M cell differentiation is therefore a further pathway exploited by pathogens to promote their own invasion.

1.4.5.2. Involvement of M cells in inflammatory conditions

There is some evidence suggesting a role for M cells in inflammatory intestinal conditions, such as inflammatory bowel disease. Firstly, the initial lesions observed in the development of Crohn's disease tend to occur in the FAE overlying lymphoid follicles (Gullberg and Söderholm, 2006). An increase in M cell numbers in the colon has also been recorded in mouse models of colitis triggered by both dextran sodium sulphate and *Citrobacter rodentium* (Bennett *et al.*, 2016). It is notable that certain cytokines that promote M cell

differentiation, such as TNF-α and LT-β, are also drivers of inflammation. Although it had no effect alone on M cell differentiation, TNF-α was found to enhance M cell differentiation stimulated by RANKL (Wood *et al.,* 2016). Many patients with inflammatory bowel disease (IBD) have elevated TNF-α and anti-TNF-α antibodies are commonplace in IBD treatment (Jones-Hall and Nakatsu, 2016). These data indicate a close relationship between M cells and inflammation. It is unclear, however, whether expansion of the M cell population in response to inflammatory signals promotes resolution by enhancing immune regulation, or whether more M cells allowing bacteria greater access to the mucosa could sustain and exacerbate inflammation. In support of the latter, increased translocation of both non-pathogenic and adherent-invasive *E. coli* has been observed in the mucosa of Crohn's patients (Keita *et al.*, 2008).

1.4.5.3. Targeting M cells for oral vaccine development

Vaccination can offer a highly effective method of disease prevention. Most currently used vaccines are given parentally; however, development of successful oral vaccines is desirable for ease of administration and induction of protective immune responses at the mucosal surfaces, the initiation sites of most infections (Kim and Jang, 2014). Development of oral vaccines has been hampered by the challenge of efficient delivery of antigens to the GALT and requirement for an adjuvant that can overcome the tendency to develop tolerance to orally encountered antigens. M cells are of interest to this field because it is thought that their transcytotic ability could be exploited to aid antigen delivery. As a result, efforts have been made to combine vaccines with M cell ligands, including UEA-1 (Du *et al.*, 2018) and the antigen-binding region of anti-GP2 (Shima *et al.*, 2014). These conjugates showed increased efficacy compared to the same molecules lacking the M cell-targeting regions. Improved characterisation of M cell-specific markers and function is driving further efforts in this area.

1.4.6. *In vitro* models for studying M cells

1.4.6.1. Cell line models

Progress in understanding of M cell biology has been severely limited by the challenging nature of studying native M cells *in vivo* in humans or animal models. In response, efforts have been made to develop suitable *in vitro* models. The first of these was described over two decades ago by Kernéis *et al*, who cultured the human colonic carcinoma Caco-2 cell line on the lower surface of Transwell inserts with primary murine Peyer's patch B cells in the upper chamber of the insert (Kernéis *et al.*, 1997). Although derived from a colorectal

adenocarcinoma, Caco-2 cells adopt a phenotype more similar to that of small intestinal enterocytes when grown beyond confluence, forming a polarised monolayer with apical microvilli, tight junctions and expression of brush border enzymes (Sambuy *et al.*, 2005). This configuration allows the B cells to move through the pores of the Transwell filter and make direct contact with the Caco-2 cells. The authors observed a number of M cell-like phenotypic changes in the co-cultured Caco-2 cells, including redistribution of villin from the apical surface, irregular microvilli and increased translocation of both latex beads and live *Vibrio cholerae*. Further characterisation of this model also found reduced expression of alkaline phosphatase and increased apical α5β1 integrin on co-cultured Caco-2 cells (Tyrer *et al.*, 2002).

The model developed by Kernéis *et al* was later modified to avoid the need for access to primary lymphocytes by using the human Burkitt's lymphoma Raji B cell line instead (Gullberg *et al.*, 2000). In this version, the Raji B lymphoid cells and Caco-2 cells were physically separated by culturing the Caco-2 cells on the upper surface of the Transwell insert and placing the Raji cells in the lower chamber. This separation allowed the model to be used to study genes expressed specifically in the M-like cells (Lo *et al.*, 2004). The authors again observed cells with disorganised microvilli and demonstrated downregulation of alkaline phosphatase and increased transcytosis of inert particles. M cell conversion was reportedly enhanced in a variation on this model, where inserts were inverted following seeding and adherence of Caco-2 cells to allow direct contact between epithelial cells and Raji B cells (des Rieux *et al.*, 2007; Ahmad *et al.*, 2017). The use of a Caco-2 sub-clone, C2BBe1 cells, has also been reported to increase the efficiency of M cell conversion (Masuda *et al.,* 2011).

A major advantage of these Transwell-based systems is the ease of investigating translocation across the epithelium due to the separated apical and basolateral compartments. This has been exploited to characterise factors that regulate particle transcytosis by M cells, including physical properties of the particles (des Rieux *et al.*, 2005), cellular and bacterial receptors (Tyrer *et al.*, 2006; Tahoun *et al.*, 2011), and dietary components (Roberts *et al.*, 2010, 2013). More recently, the model has been adapted to use murine (Gonzalez-Hernandez *et al.*, 2013) and bovine (Miyazawa *et al.*, 2010) intestinal epithelial cell lines and to include mucus-secreting, goblet cell-differentiated HT-29-MTX cells (Lesuffleur *et al.*, 1990), to more accurately reflect *in vivo* conditions (Schimpel *et al.*, 2014; Araújo *et al.*, 2016).

While the Caco-2/B cell co-culture system presents several advantages, its usefulness has been limited by variability and doubts over its physiological relevance. A comparison of gene expression in Caco-2 cells cultured with and without Raji cells revealed that co-culture alters expression of around 100 genes; however, on validation of co-localisation with UEA^+ M cells in murine and human FAE, most of the genes investigated did not show M cell-specific expression, although some were expressed throughout the FAE but not in villus epithelium (Lo *et al.*, 2004). Notably, several important M cell-associated genes, including *Spib*, *Gp2*, *Tnfaip2* (encoding TNFaip2 or M-Sec), *Ccl9* (encoding CCL9), *Marcksl1* (encoding MRP) and *Prnp* (encoding prion protein), have been found by microarray expression profiling not to be upregulated in co-cultured Caco-2 cells (Mabbott *et al.*, 2013). Together, these data suggest that the transcriptome of Caco-2 cells in the co-culture model does not fully recapitulate that of Peyer's patch M cells, although they do recapitulate certain phenotypic and functional characteristics of the FAE.

1.4.6.2. Enteroid model

Around the time of the discovery that RANKL is necessary and sufficient to induce M cell differentiation in mice (Knoop *et al.*, 2009), a novel method of culturing primary intestinal stem cells was described (Sato *et al.*, 2009). This followed from the discovery that leucine-rich-repeat-containing G-protein-coupled receptor 5 $(Lgr5)^+$ cells located at the base of small intestinal crypts were the stem cells that populated the intestinal epithelium and gave rise to all epithelial lineages (Barker *et al.*, 2007). To generate these cultures, intestinal crypts containing $Lgr5^+$ intestinal epithelial stem cells are isolated from primary tissue and suspended in a 3D matrix with a cocktail of specific factors that mimic the stem cell niche. Proliferation of the stem cells generates a spheroid with a polarised epithelium surrounding a hollow lumen that is equivalent to the intestinal lumen (Sato *et al.*, 2009). Daughter cells undergo differentiation into all the major epithelial cell lineages and the activity of stem cells forms crypt regions with stem cells and Paneth cells at their base. As *in vivo*, cells are shed from the villus regions into the enteroid lumen. *The* technique has since been extended to different regions of the gastrointestinal tract and other organs, including stomach (Barker *et al.*, 2010), colon (Sato, Stange, *et al.*, 2011), liver (Huch *et al.*, 2015) and brain (Lancaster *et al.*, 2013).

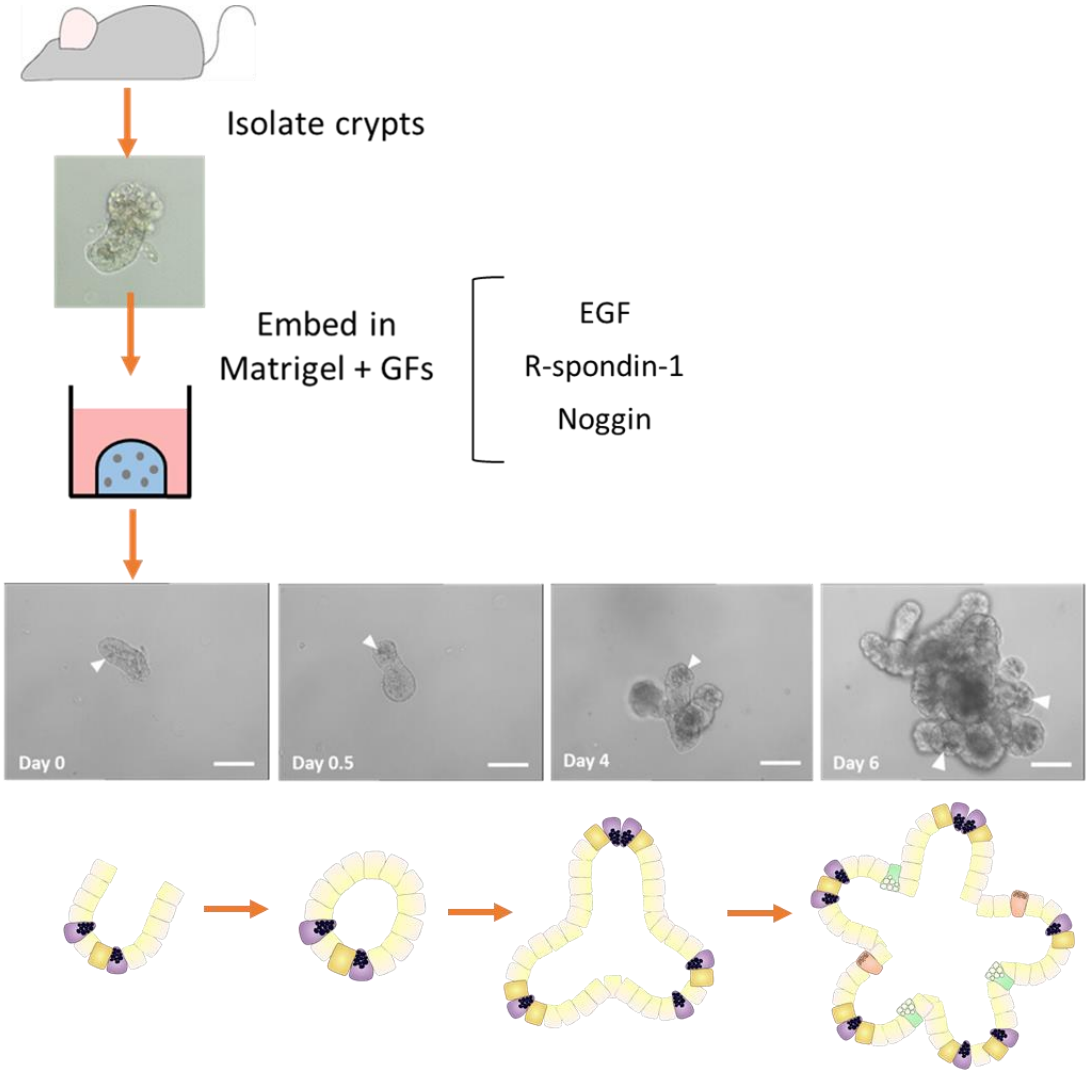

Figure 1.6. Establishment and growth of enteroid cultures from mouse small intestine. Crypts are isolated from mouse small intestine and embedded in Matrigel matrix, which is subsequently overlaid with media supplemented with EGF, R-spondin-1 and Noggin to mimic the stem cell niche. Bright field and cartoon images show growth of a single stem cell-containing crypt into a 3D enteroid. Soon after seeding, the crypt mouth closes to form a continuous epithelium around a central lumen. Over a matter of days, the proliferative activity of stem cells causes buds to form and cells differentiate into all major epithelial lineages, including Paneth, goblet and enteroendocrine cells. Accumulation of dead cells in the lumen makes it appear dark. Scale bars represent 100 µm.

It was soon confirmed that application of RANKL in this system induced differentiation of M cells, which are otherwise absent from the enteroids (de Lau *et al.*, 2012; Rios *et al.*, 2016). The gene expression profile of M cells induced by RANKL in enteroids showed upregulation of 164 genes in common with *in vivo* Peyer's patch M cells. Genes that showed the greatest upregulation in both include *Spib*, *Gp2*, *Ccl9*, *Anxa5*, *Umod*, *Prnp*, *Ccl20* and *Siglec5*. Other genes previously identified as M cell-associated – *Marcksl1* and *Tnfaip2* – were also upregulated in RANKL-treated enteroids (Wood, Rios and Williams, 2016). RANKL also increased the number of UEA-binding cells and induced uptake of beads (de Lau *et al.*, 2012). These data indicate that the M cells in the enteroid model closely resemble Peyer's patch M cells. Since these initial studies in enteroids derived from mice, generation of M cells in a RANKL-dependent manner has also been demonstrated in human-derived enteroids grown both as 3D cultures and as 2D monolayers (Rouch *et al.*, 2016). Again, M cells induced by RANKL in human enteroids showed increased expression of *Spib* and *Gp2* and enhanced uptake of beads and *S.* Typhimurium.

Although relatively novel, the enteroid M cell model has already proved a useful tool for identifying factors that regulate M cell differentiation. Evidence from human-derived enteroids suggested that Wnt signalling primes epithelial cells for M cell differentiation, since a low dose of Wnt3a also increased expression of *Spib* and *Gp2*, although the increase was much smaller than with RANKL treatment (Rouch *et al.*, 2016). In murine enteroids, TNF-α was shown to promote M cell differentiation by synergising with RANKL to induce NF-κB subunits, RelB and NF-κB2 (Wood, Rios and Williams, 2016). So far, no studies have utilised the 3D enteroid model to investigate bacterial-M cell interactions. This is an exciting goal as the 3D structure of the enteroids mimics the tissue architecture of crypts and villi found *in vivo*, making them a highly physiological model. Unfortunately, this increased complexity also means that the luminal compartment is only accessible by microinjection, which is technically challenging and not amenable to high throughput approaches.

Table 1.2. Models used to study M cells.

	Transwell co-culture	***Enteroid***	***2D enteroid***	***M cell-dense mouse model***
In vivo/ in vitro	*In vitro*	*In vitro*	*In vitro*	*In vivo*
Species	Human	Mouse or human	Human	Mouse
Epithelial component	Caco-2 cell line	Primary enterocytes derived from intestinal epithelial stem cells	Primary enterocytes derived from intestinal epithelial stem cells	Intestinal epithelium *in vivo*
Stimulating factors	Undefined factors secreted by Raji cells	RANKL	RANKL	RANKL (via intraperitoneal injection)
M cell characteristics reproduced	Morphological features; transcytosis of beads, various bacteria and viruses	Expression of SpiB, GP2, MRP, annexin V, TNFaip2; uptake of beads; morphological features not assessed	Expression of SpiB, and GP2; uptake of beads and *S.* Typhimurium; morphological features not assessed	Morphological features; increased UEA-binding and expression of SpiB and GP2; uptake of beads and bacteria
Advantages	Ease of investigating transcytosis using Transwell system	Mimics 3D intestinal structure; allows isolation of epithelial compartment or addition of specific immune cells via co-culture; primary, untransformed cells; can be made from many species (including human)	Primary, untransformed cells; ease of investigating transcytosis using Transwell system; allows isolation of epithelial compartment	Most physiologically relevant; contains all epithelial, mesenchymal and immune compartments
Limitations	Dubious physiological relevance	Lumen only accessible by microinjection	No 3D structure	Species barrier if interested in human biology; highly complex
Citation	(Kernéis *et al.*, 1997; Gullberg *et al.*, 2000; des Rieux *et al.*, 2007)	(de Lau *et al.*, 2012; Rios *et al.*, 2016)	(Rouch *et al.*, 2016)	(Knoop *et al.*, 2009; Donaldson *et al.*, 2016)

1.5. Hypothesis

Enteroid cultures are a highly physiologically relevant model of the small intestinal epithelium, closely reproducing many structural and functional characteristics of the small intestinal epithelium *in vitro*. Enteroids may therefore be an informative system in which to investigate aspects of intestinal biology that have previously proved challenging to study, such as epithelial barrier function. With this in mind, development of this thesis has been driven by several hypotheses:

1. Given previous evidence that regional identity is intrinsically programmed in intestinal stem cells, enteroids derived from different segments of the small intestine may retain region-specific characteristics in culture.

2. Enteroids may be used to assay changes in epithelial permeability in response to various stimuli, including dietary components.

3. Since M cells have been shown to differentiate from intestinal stem cells in response to the cytokine, RANKL, enteroids represent a suitable model in which to expand the M cell population, enabling a reductionist approach to identifying epithelium-intrinsic and -extrinsic factors that regulate M cell differentiation and to characterising bacterial interactions with M cells.

1.6. Aims

1. To further evaluate the ability of 3D, adult mouse stem cell-derived enteroid cultures to accurately reproduce their tissue of origin, including region-specific characteristics of the small intestine.

2. To develop an assay to measure epithelial permeability in 3D enteroid cultures that can be used to evaluate potential effects of bacteria and dietary components on intestinal epithelial barrier function.

3. To further characterise the RANKL-induced M cell enteroid model by quantifying the effect of exogenous RANKL on non-M cell epithelial cell lineages.

4. To investigate the role of alternative pathway NF-κB signalling in RANKL-induced M cell differentiation in enteroids.

5. To develop an assay in which to investigate interactions of particles and bacteria with M cells in the enteroid model.

Chapter 2

Methods

2.1. Materials

Unless otherwise specified, all general chemical reagents were obtained from Sigma-Aldrich (Gillingham, UK). Plastics for mammalian cell culture were supplied by Corning (Amsterdam, The Netherlands). Transwell inserts were from Millipore Ltd (Watford, UK). Plastics used for solid agar and broth bacterial culture were from Greiner Bio-One (Gloucestershire, UK). Bacto™ agar, yeast extract and tryptone used in bacterial cultures were obtained from BD Biosciences (Oxford, UK). All materials used for transmission electron microscopy (TEM) were supplied by Agar Scientific (Stansted, UK) or TAAB Laboratories Equipment (Aldermaston, UK). Recombinant murine epidermal growth factor (EGF), Noggin and R-spondin-1 were obtained from Bio-techne (Abingdon, UK). Recombinant murine RANKL was obtained from BioLegend (London, UK).

2.2. Mice

Wild type C57BL/6 and BALB/c controls were obtained from Charles River (Margate, UK). Transgenic *Nfkb2*$^{-/-}$ mice maintained on a C57BL/6 background were kindly provided by Jorge Caamaño (University of Birmingham, UK) via Mark Pritchard (University of Liverpool, UK) (Caamaño *et al.*, 1998). *Relb*$^{-/-}$ mice were bred on a 129/B6 background and back-crossed onto a C57BL/6 background (Weih *et al.*, 1995). All mice were maintained under specific pathogen-free conditions in the Biomedical Services Unit at the University of Liverpool. Mice were maintained under UK Home Office licences in the Biomedical Services Unit at the University of Liverpool. Schedule 1 sacrifices were performed either by cervical dislocation or CO_2 inhalation.

2.3. Genotyping of enteroid cultures obtained from *Nfkb2*$^{-/-}$ and *Relb*$^{-/-}$ mice

Genomic DNA was extracted from *Nfkb2*$^{-/-}$ enteroid cultures by hot alkaline lysis. Samples were lysed in base solution (25 mM NaOH, 0.2 M EDTA, pH 12.0) for 30 minutes at 95°C. Lysates were neutralised with an equal volume of neutralising solution (40 mM Tris-HCl, pH 5.0). Polymerase chain reaction (PCR) was performed using GoTaq G2 Green 2X Master Mix (Promega, Southampton, UK) and primers specific for either the wild type or knockout alleles of the *Nfkb2* gene. Primer sequences are shown in **Table 2.1**. Wild type alleles are characterised by a 230-base pair (bp) amplicon, whereas *Nfkb2* null alleles give rise to a 120 bp product (**Figure 2.1**). PCR was performed using a Multigene Optimax thermal cycler (Labnet Internatinal, New Jersey, USA) with the cycling conditions as detailed in **Table 2.2**. PCR products were separated in a 1.5% w/v agarose gel (UltraPure agarose, Invitrogen, Loughborough, UK) in 1X Tris-acetate-EDTA (TAE) buffer containing 1X SYBR Safe DNA gel stain

(Invitrogen) at 100 V. Bands were visualised using a Universal Hood II transilluminator (BioRad, Watford, UK). 50 bp GeneRuler DNA ladder (Thermo Fisher Scientific, Loughborough, UK) was used to determine the product size.

Table 2.1. Sequences of primers used for *Nfkb2*$^{-/-}$ genotyping PCR.

Primer	***Sequence (5'-3')***
Common forward	GCCTGGATGGCATCCCCG
WT-specific reverse	GTTTGGGCTGTTCCACCA
Null-specific reverse	CCAGACTGCCTTGGGAAA

Table 2.2. Cycling conditions used for *Nfkb2*$^{-/-}$ genotyping PCR.

Temperature (°C)	***Time (s)***	***Cycles***
95	60	1
95	20	35
55	90	
72	60	
72	120	1

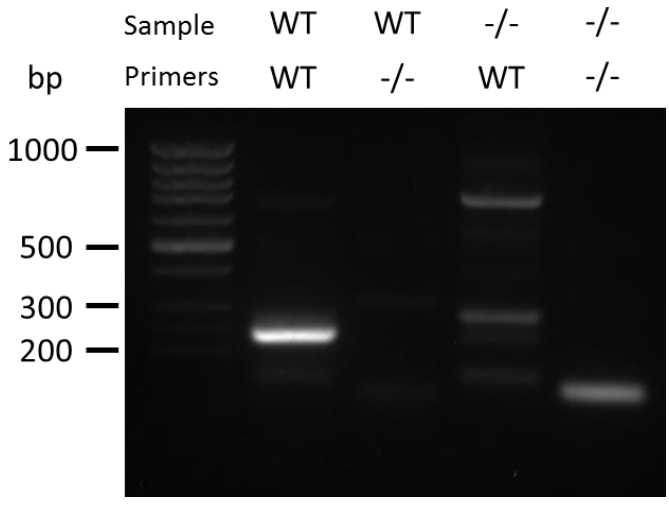

Figure 2.1. Representative image of *Nfkb2*$^{-/-}$ genotyping PCR products separated by gel electrophoresis in a 1.5% w/v agarose gel to validate genotype of *Nfkb2*$^{-/-}$ enteroids. Ladder is GeneRuler 50 bp DNA ladder (Thermo Fisher Scientific).

Relb transgenic mice were routinely genotyped for breeding purposes by Dr Katie Lloyd (University of Liverpool, UK). Genomic DNA was extracted from ear notches by incubating tissue in 20 µL DNAreleasy (Anachem, Leicester, UK) at 75°C for 5 minutes, followed by 96°C for 2 minutes. Two PCR reactions were performed per sample using ThermoPrime ReddyMix master mix (Thermo Fisher Scientific) with two primer sets: one specific for the wild type *Relb* gene, one specific for the *Relb*$^{-/-}$ locus. Primer sequences are shown in **Table 2.4.** The wild type gene gives rise to a product of 357 bp, while the null allele generates a product of 225 bp. Cycling conditions used for PCR are shown in **Table 2.4.** Gel electrophoresis of PCR products was performed as above for *Nfkb2*$^{-/-}$ genotyping. Only tissue from confirmed *Relb*$^{-/-}$ mice was used to establish enteroid cultures.

Table 2.3. Sequences of primers used for *Relb* genotyping PCR.

Primer	***Sequence (5'-3')***
WT-specific forward	GTGGTGCCCGGGAATAGGATTGCT
WT-specific reverse	CCATTTTGCTCTGGGTCTGTGTCT
Relb null-specific forward	CATCGACGAATACATTAAGGAGAACGG
Relb null-specific reverse	AAATGTGTCAGTTTCATAGCCTGAAGAACG

Table 2.4. Cycling conditions used for *Relb* genotyping PCR.

Temperature (°C)	***Time (s)***	***Cycles***
95	120	1
95	60	35
60	90	
72	60	
72	300	1

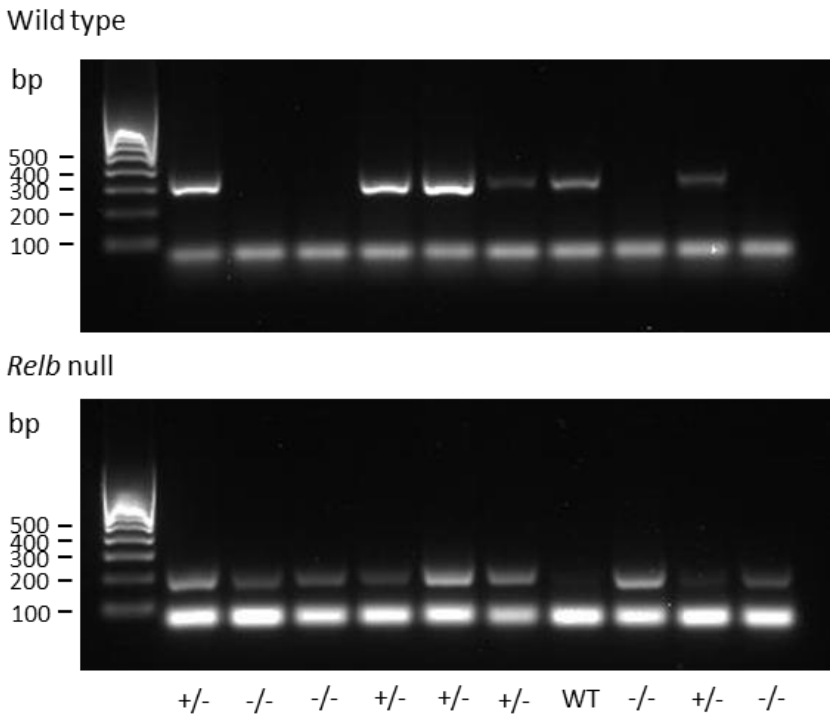

Figure 2.2. Representative image of *Relb* genotyping PCR products separated by gel electrophoresis in 1.5% w/v agarose gels. Upper gel shows products from PCR with primers for wild type *Relb*; lower gel shows products from PCR with primers for *Relb* null allele. Reactions for the same mouse are in matched lanes in each gel. Ladder is Hyperladder IV (100 bp, Bioline, London, UK). Labels beneath indicate genotype of each animal as shown by the two PCRs.

2.4. Enteroid culture

2.4.1. Crypt isolation

Enteroid cultures were derived from the following mouse strains: C57BL/6, BALB/c, *Nfkb2*$^{-/-}$ and *Relb*$^{-/-}$. To establish cultures, a 3-5 cm section of small intestine from either the proximal or distal region was flushed with ice cold phosphate buffered saline (PBS, pH 7.4) and opened longitudinally. The tissue was cut into approximately 1 cm lengths and washed by agitating with ice-cold PBS. Tissue was incubated in chelation buffer (2 mM ethylenediaminetetraacetic acid (EDTA)/PBS) on a rolling platform at 4°C for 30 minutes. Tissue was briefly agitated by hand to facilitate detachment of some villous material. Chelation buffer was removed and replaced with shaking buffer (43.3 mM sucrose, 59.4 mM sorbitol/PBS) and tissue was agitated by hand until crypts were released from the tissue. The solution was filtered using a 70 µm cell strainer on ice and the filter was washed with further ice-cold shaking buffer. The filtrate was centrifuged at 200 x *g* for 10 minutes at 4°C and

supernatant carefully removed. Pelleted crypts were re-suspended in ice-cold Matrigel (Corning), containing EGF, Noggin and R-spondin-1 (at final concentrations of 50 ng/mL, 100 ng/mL and 500 ng/mL, respectively; all R&D Systems, Abingdon, UK) and 50 µL of this suspension was plated per well in a 24-well plate. Matrigel was allowed to polymerise for at least 10 minutes at 37°C then 500 µL minigut media was added to cover the Matrigel domes. Minigut media consisted of phenol red-free Dulbecco's Modified Eagle Medium (DMEM)/F12 (Thermo Fisher Scientific) with 25 mM HEPES buffer, 4.5 mM L-glutamine, 1X N-2 supplement, 1X B-27 supplement and 100 µg/mL primocin (Invivogen, Toulouse, France). Media was replaced after 3-4 days with fresh minigut media supplemented with 50 ng/mL EGF, 100 ng/mL Noggin and 500 ng/mL R-spondin-1.

2.4.2. Maintenance of enteroid cultures

Media on enteroids was replaced every 3-4 days with fresh minigut medium supplemented with 50 ng/mL EGF, 100 ng/mL Noggin and 500 ng/mL R-spondin-1. Cultures were passaged every 7 days by removing medium and pipetting up and down with ice-cold PBS to break up Matrigel dome. Enteroids were mechanically disrupted by passing vigorously through a 27G needle and resuspended in fresh Matrigel supplemented with growth factors, as for initial establishment of cultures. The splitting ratio was 1:3-1:4. Matrigel was re-plated in pre-warmed 24-well plates, allowed to polymerise and overlaid with 500 µL minigut medium.

2.4.3. Cryopreservation and thawing

Matrigel was disrupted mechanically as for passaging by pipetting up and down with ice-cold PBS but was not passed through a syringe. Enteroids were centrifuged and resuspended in minigut medium supplemented with 10% v/v foetal bovine serum (FBS), 10% v/v dimethyl sulfoxide (DMSO). Cryovials were cooled gradually for 2 hours-overnight to -80°C in a Nalgene Mr Frosty freezing container, before being transferred to liquid nitrogen. To reinstate cultures stored in liquid nitrogen, frozen enteroids were thawed rapidly in a 37°C water bath, centrifuged for 30 seconds at 100 x *g,* washed once in cold, sterile PBS, and resuspended in Matrigel supplemented with growth factors, as described for initial establishment of cultures.

2.5. Culture of cell lines

2.5.1. Caco-2 cells

Caco-2 cells (ATCC HTB-37) were kindly provided by Dr Andrea Davies (University of Liverpool, UK). This is an adherent colonic epithelial cell line derived from a human colon carcinoma (Sambuy *et al.*, 2005). Once they have formed a confluent monolayer, Caco-2 cells undergo spontaneous differentiation and display many characteristics of polarised absorptive enterocytes typical of the small intestine, including a brush border. Caco-2 cells were maintained in high-glucose DMEM supplemented with 10% v/v FBS, 100 U/mL penicillin and 100 µg/mL streptomycin.

2.5.2. Raji B cells

Raji B cells (ATCC #CCL-86; Middlesex, UK) are a non-adherent human cell line derived from a Burkitt's lymphoma and are used as a model of human B lymphocytes. Cells were maintained in suspension culture in Roswell Park Memorial Institute-1640 (RPMI-1640, Thermo Fisher Scientific) medium supplemented with 10% v/v FBS, 100 U/mL penicillin, 100 µg/mL streptomycin and 4 mM L-glutamine. Cells were maintained at 37°C in a humidified atmosphere of 5% CO_2, 95% air. Cells were passaged every 3-4 days by removing two thirds of the cell suspension and replacing with fresh medium.

Since factors secreted by Raji B cells have been shown to convert Caco-2 cells to an M cell-like phenotype (Gullberg *et al.*, 2000), Raji B-conditioned medium was produced to investigate whether it would also convert epithelial cells in enteroids. For production of Raji B cell-conditioned medium, 3 x 10^5 cells/mL were seeded in DMEM supplemented with 10% FBS and 8 mM L-glutamine. After 5 days, cell suspension was centrifuged at 2000 x *g* for 5 minutes to remove cells and cell debris and culture medium was stored at -80°C. Control medium (without Raji B cells) was kept under identical conditions in parallel tissue culture flasks in the incubator and processed as above for conditioned medium.

2.6. Co-culture of enteroids and Raji B lymphocytes

Raji B cells were co-cultured with enteroids to assess whether B cells would induce conversion of intestinal epithelial cells to M cells. Raji B cells were not passaged during the 2 days prior to the experiment. Murine enteroids were passaged at day 7 and re-seeded in 50 µL Matrigel in a 24-well plate as per normal maintenance. Raji B cells were harvested by centrifugation (300 x *g*, 5 minutes) and resuspended in minigut medium at a density of 2 x 10^5 cells/mL. Once

polymerised, Matrigel droplets were overlaid with 0.5 mL Raji cell suspension so that each well contained ~1 x 10^5 cells. On day 3 of co-culture, Raji B cells were resuspended by gentle aspiration and removed, and replaced with fresh lymphocytes (again, 1 x 10^5 cells/well), or they were allowed to settle and only the culture medium was replaced. On day 6, culture medium and cells were removed and enteroids were harvested for RNA extraction to analyse expression of M cell-associated genes.

2.7. Immunohistochemical analysis of epithelial cell markers

2.7.1. Harvesting, fixation, paraffin-embedding and preparation of enteroid sections

Medium was removed and Matrigel domes were washed once with ice-cold, sterile PBS. Matrigel was dissociated by adding 0.4 mL of Cell Recovery Solution (Corning) over the dome and incubating on a shaking platform for 45 minutes at 4°C. Enteroids were fixed with 2% w/v PFA in PBS for 30 minutes at room temperature. Enteroids were isolated by allowing to settle or by centrifuging at 100 x *g* for 30 seconds. Supernatant was removed as far as possible and enteroids were re-suspended in 75-200 µL Richard-Allan Scientific HistoGel Specimen Processing Gel (Thermo Fisher Scientific), depending on number of enteroids. A pellet was made with the HistoGel and allowed to cool and set, before being placed into a Histosette II histology cassette (Simport Scientific, Quebec, Canada). Cassettes were stored in 70% v/v ethanol in H_2O for at least 2 hours. Samples were processed by dehydrating through a series of graded ethanol from 70-100%, then cleared by overnight incubation in xylene, followed by three incubations of 5 minutes in fresh xylene. Finally, infiltration of samples with paraffin wax was achieved by incubating for 2 and then 3 hours in wax at 60°C. Processed pellets were embedded in paraffin wax in peel-a-way embedding moulds (Simport Scientific) to make blocks. Sections of 4 µm were cut using an RM2255 microtome (Leica Microsystems, Milton Keynes, UK). Sections were placed onto glass slides pre-coated with 3-aminopropyltriethoxysilane (APES) and incubated in a dry oven at 37°C for at least 10 hours.

2.7.2. Fixation, embedding and preparation of mouse small intestine sections

Preparation of intestinal tissue blocks was performed by Dr Carrie Duckworth (University of Liverpool, UK) according to the gut bundling method (Williams *et al.*, 2016). Small intestine from C57BL/6 mice was removed immediately after sacrifice, flushed using a 23 G syringe with ice-cold PBS and incubated in formalin (3.75% w/v formaldehyde in PBS) for 24 hours at room temperature to fix. The small intestine was then divided into proximal, middle and

distal thirds and each was cut into approximately 1 cm lengths. Segments were arranged in parallel inside a loop of micropore tape and placed into histology cassettes. Samples were processed as described previously and paraffin-embedded so that cross-section of the lumen was parallel with the resulting block face. As above, 4 µm sections were cut using the RM2255 microtome, collected on slides pre-coated with APES and dried.

2.7.3. Immunohistochemical analysis of paraffin-embedded sections

Sections were deparaffinised in xylene and re-hydration was begun in 100% ethanol. Endogenous tissue peroxidase activity was blocked by placing sections in 3% hydrogen peroxide in methanol for 10 minutes. Rehydration of sections was completed through a graded series of alcohols from 100% to 70%. Antigen retrieval was then performed by heating sections in 10 mM sodium citrate buffer (pH 6) for 20 minutes. After cooling gradually over 20 minutes, sections were washed in Tris-buffered saline (TBS; 20 mM Tris, 150 mM NaCl, pH 7.4) containing 0.1% Tween-20 (TBST) and blocked with 2.5% v/v appropriate serum for 30 minutes at room temperature in a humidified chamber. Primary antibodies (diluted in 2.5% serum at titres described in **Table 2.5**) were applied overnight at 4°C or for 2 hours at room temperature. Sections were washed in TBST and detection of primary antibodies was performed using ImmPRESS horse radish peroxidase (HRP) polymer detection kit appropriate for the species of the primary antibody (Vector Laboratories, Peterborough, UK). The HRP-conjugated polymer reagent was applied for 30 minutes at room temperature. Following further washes in TBST, sections were incubated for approximately 6 minutes in the dark with a solution of 0.7 mg/mL 3,3'-diaminobenzidine (DAB), 2 mg/mL urea hydrogen peroxide, 60 mM Tris buffer. Sections were counterstained with haematoxylin, dehydrated, and mounted with distyrene-plasticiser-xylene (DPX) mountant (Sigma-Aldrich).

Table 2.5. Details of primary antibodies used for immunohistochemical analysis.

Target	***Antibody and supplier***	***Species & specificity***	***Titre***
Lysozyme (Lyz)	Dako, A0099	Rabbit anti-human/mouse	1:3500
Trefoil factor 3 (TFF3)	Santa Cruz, sc-18272	Goat anti-mouse polyclonal	1:500
Chromogranin A (CgA)	Abcam, ab15160	Rabbit anti-mouse/human	1:800
Active caspase 3	R&D Systems, AF835	Rabbit anti-human/mouse	1:800
DCLK1	Abcam, ab31704	Rabbit anti-mouse	1:500
SpiB	Bio-techne, AF7204	Sheep anti-mouse	1:25

2.8. Immunofluorescence staining of tight junction proteins in Caco-2 cell monolayers

Following fixation by incubating with 4% w/v methanol-free paraformaldehyde (PFA; TAAB Laboratories Equipment) in PBS for 10 minutes at room temperature, Caco-2 cells cultured on 13 mm glass coverslips were washed three times with PBS. Cell membranes were then permeabilised by incubating with 0.2% Tween-20, 0.5% Triton X-100 in PBS for 30 minutes at 4°C. Non-specific binding sites were blocked by incubating cells with 3% w/v bovine serum albumin in PBS for 1 hour at room temperature. Primary antibodies were applied to cell monolayers overnight at 4°C diluted in 1% w/v bovine serum albumin in PBS at the dilutions indicated in **Table 2.6**. Cells were washed three times with PBS and incubated with Hoechst-33342 diluted 1:5000 in PBS for 5 minutes at room temperature. After three further washes, coverslips were mounted on glass slides using mounting medium (4 mM Mowiol 4-88 with 2.5% 1,4-diazabicyclo[2.2.2]octane (DABCO)). Slides were examined and images captured using a Zeiss LSM 800 microscope and Zen Blue software. Identical laser power and gain settings were used for each sample.

Table 2.6. Details of primary antibodies used for immunofluorescence analysis.

Target	***Antibody and supplier***	***Species & specificity***	***Titre***
Zonula occludens 1 (ZO-1)	Thermo Fisher Scientific, 61-7300	Rabbit anti-human	1:50
Occludin	Abcam, ab31721	Rabbit anti-human	1:500

2.9. Quantitative RNA analysis

Medium was removed and Matrigel domes were washed once with ice-cold, sterile PBS. Since Matrigel is manufactured from mouse tumour cells, it is likely to contain RNA. As a result, it is essential that Matrigel is removed from enteroid samples as completely as possible prior to analysis. Matrigel was dissociated by adding 0.4 mL of Cell Recovery Solution over the dome and incubating on a shaking platform for 45 minutes at 4°C. Enteroids were isolated from this suspension by centrifuging at 200 x *g* for 10 minutes and removing supernatant. Enteroids were washed once in ice-cold PBS and centrifuged at 300 x *g* for 5 minutes at 4°C. PBS was removed as far as possible and RNA was either extracted immediately or enteroid pellets were

stored at -80°C. Enteroids were disrupted and cells lysed by resuspending in Buffer RLT and bead beating in a TissueLyser II at 30 Hz for 30 seconds with a 5 mm stainless steel bead, then rotating tubes and repeating (all Qiagen, Manchester, UK).

Total RNA was extracted using the RNeasy minikit and purified using the RNase-free DNase set (both Qiagen). Equal amounts of RNA from the same experiment (up to 1 µg) were reverse transcribed using the RT^2 First Strand kit (Qiagen) and cDNA was stored at -80°C.

Quantitative PCR (qPCR) was performed according to manufacturer's instructions using SYBR green I master (Roche, Welwyn Garden City, UK) and manufacturer-verified RT^2 primer assays for *Gapdh*, *Gp2*, *Spib* and *Tnfrsf11a* (Qiagen, details in **Table 2.7**) in a LightCycler 480 (Roche). Cycling conditions used are detailed in **Table 2.8**. Amplification of a single, specific amplicon was confirmed from melt curves. Where no threshold cycle (CT) value was detected consistently, an arbitrary value of 40 was assigned (McCall *et al.*, 2014). Due to consistent non-detection of certain gene products in control samples, data was analysed by the ΔCT method (Schmittgen and Livak, 2008) where the CT value of the gene of interest was normalised to that of the housekeeping gene, *Gapdh* and are expressed as $2^{-\Delta CT}$. *Gapdh* mRNA levels were unchanged in experimental samples compared to controls.

Table 2.7. Primers used for qPCR. †Reference position refers to a position contained within the sequence of the amplicon relative to the start of the relevant RefSeq sequence (as Qiagen do not make public exact primer sequences).

Gene name	***Full name***	***RefSeq Accession no.***	***Reference position†***	***Source***	***Catalogue no.***
Gapdh	Glyceraldehyde-3-phosphate dehydrogenase	NM_008084	478	Qiagen	PPM02946E
Spib	Spi-B transcription factor	NM_019866	635	Qiagen	PPM04709A
Gp2	Glycoprotein 2	NM_025989	1444	Qiagen	PPM29342A
Tnfrsf11a	TNF receptor superfamily, member 11a (Rank)	NM_009399	1353	Qiagen	PPM03749F

Table 2.8. Cycling conditions used for qPCR.

Step	*Number of cycles*	*Target temperature (°C)*	*Hold time (00:00:00)*	*Ramp rate (°C/s)*
Denaturation	1	95	00:10:00	4.4
Amplification	50	95	00:00:15	1
		60	00:01:00	1
Melt curve	1	60	00:00:15	4.4
		95	-	0.03

2.10. Assessment of epithelial permeability in enteroids using luminally microinjected fluorescent dextrans

To investigate permeability of the intestinal epithelium under several different conditions, an assay was established using enteroids, based on an experiment described previously to evaluate intestinal permeability in response to bacterial infection (Leslie *et al.*, 2015). Enteroids were seeded in Matrigel as described above on 13 mm glass coverslips in 24-well plate. On day 3-5 post-passage, coverslips were removed from wells. Only enteroids with an apparently undisrupted epithelium were selected for injection. Microinjection was performed using a Femtojet microinjector and Injectman micromanipulator (both Eppendorf, Stevenage, UK). A mixture containing 5 mg/mL 4 kDa fluorescein isothiocyanate-conjugated dextran (FD4, Sigma-Aldrich) and 1 mg/mL 10 kDa Alexa Fluor 594-conjugated dextran (Thermo Fisher Scientific) in H_2O was injected into the central lumen of 2-7 enteroids per well (**Figure 2.3**). Micropipettes used were made from borosilicate glass capillaries with a 1 mm outer diameter and 0.58 mm internal diameter (Harvard Apparatus, Edenbridge, UK) using a DMZ Universal electrode puller (Zeitz Instruments, Martiensried, Germany) with the settings detailed in **Table 2.9**. Matrigel domes were washed twice in warm PBS and returned to complete medium.

Microinjected enteroids were incubated at 37°C for 3.5 hours as luminal dextran levels were determined to stabilise by this time after a large initial decrease, presumably due to leakage from the puncture site (**Figure 2.4**). Enteroids were then imaged using a BX51 epifluorescence microscope (Olympus, Southend-on-Sea, UK). This was taken as time zero (t0) and the same enteroids were then imaged at hourly intervals, for up to 4 hours (t4). For each enteroid, bright field and red and green fluorescence images were collected. Exposure settings were adjusted for each enteroid at t0 and kept constant for all subsequent images of that enteroid. Analysis was performed using ImageJ 1.48v software (Schneider, Rasband and Eliceiri, 2012). Bright

field and fluorescence images were synchronised and the perimeter of each enteroid was defined from the bright field image for each time point. The mean pixel intensity within this area was measured and expressed as a percentage of the mean pixel intensity for that enteroid at t0.

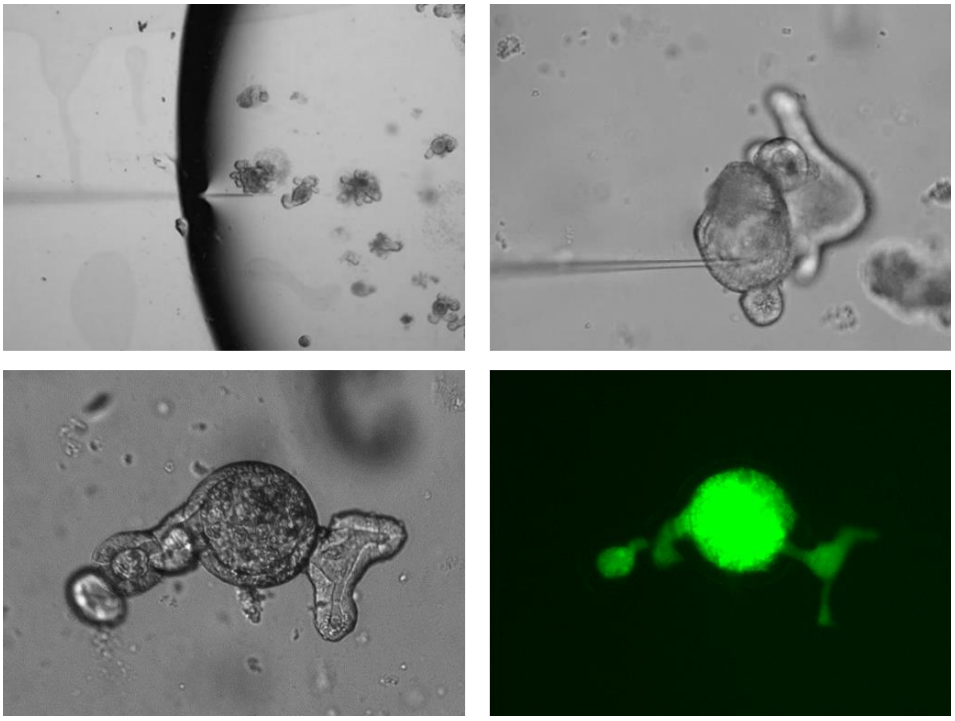

Figure 2.3. Microinjection of FD4 into enteroid lumen. Upper panel: bright field images showing enteroids within the Matrigel during microinjection. The microcapillary can be seen entering from the left. Lower panel: left image is a bright field image of an enteroid following luminal microinjection with FD4. Right image shows FD4 fluorescence inside the same enteroid.

Table 2.9. Settings used to pull microcapillaries for microinjection of enteroids.

Parameter	***Value***
Heat for glass softening, H	400
Preliminary pull, F(TH)	O3O
Distance threshold for elongation, s(TH)	O22
AD	12O

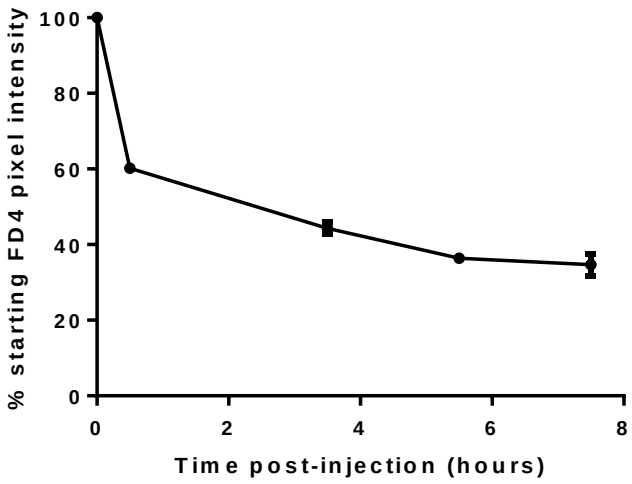

Figure 2.4. Quantification of loss of luminal fluorescence from enteroids following microinjection with FD4. N = 2, n = 3-4 enteroids per group. Error bars represent standard deviation (SD).

2.11. Analysis of enteroid swelling

Based on an assay previously used to investigate CFTR activity in enteroids (Dekkers *et al.*, 2013), the surface area of enteroids in bright field images was used to assess enteroid swelling. Enteroids were seeded in 25 µL Matrigel in 48-well plates and overlaid with 200 µL complete minigut medium. Experiments were performed on the second day post-seeding. Bright field images were collected of 5-8 enteroids per well prior to incubation with treatments and then at 0.5, 1, 2, 3 and 4 hours post-treatment. The cystic fibrosis transmembrane conductance regulator (CFTR) is expressed on the apical membrane of enterocytes and is the major regulator of intestinal fluid secretion. CFTR-mediated secretion of chloride ions results in movement of sodium ions and water into the intestinal lumen in response to the change in electrochemical and osmotic gradients (Saint-Criq and Gray, 2017). Forskolin has previously been shown to induce enteroid swelling by activating CFTR-dependent movement of fluid into the lumen (Dekkers *et al.*, 2013) and was therefore used as a positive control (5 µM, Sigma-Aldrich). CFTR-dependent swelling was blocked by pre-incubation of enteroids for 3 hours with 50 µM CFTR-inh-172 (Bio-techne), a selective CFTR inhibitor (Ma, Thiagarajah, *et al.*, 2002; Dekkers *et al.*, 2013). CFTR-inh-172 produces rapid, reversible and voltage-independent inhibition of Cl^- secretion via the CFTR and is known to prevent intestinal fluid secretion induced by cholera toxin (Ma, Thiagarajah, *et al.*, 2002). Enteroid perimeter was specified for each image and its area was determined using ImageJ software. Mean enteroid area at each

time point was normalised to mean enteroid area of that group at the first time point prior to treatment.

2.12. Transmission electron microscopy

2.12.1. Fixation and processing

2.12.1.1. Enteroids

All preparation of samples and imaging was carried out in the Biomedical Electron Microscopy Unit at the University of Liverpool, UK. Enteroids were harvested for transmission electron microscopy (TEM) on day 3 post-seeding, Matrigel was dissociated by incubation with Cell Recovery Solution for 45 minutes on ice with shaking. Enteroids were washed once with ice-cold PBS and fixed in 2.5% w/v glutaraldehyde in 0.1 M phosphate buffer (PB, 0.1 M Na_2HPO_4, 0.1 M $Na_2H_2PO_4$, pH 7.4) in a PELCO BioWave Pro+ Microwave Tissue Processing System (Ted Pella Inc., California, USA). The fixation programme was 20 Hg and 100 W for 1 minute on, 1 minute off, 1 minute on. Enteroids were then washed at least 3 times with 0.1 M PB and post-fixed and stained with reduced osmium (2% w/v OsO_4 in double distilled H_2O (ddH_2O) with 1.5% w/v potassium ferrocyanide) in the BioWave for 20 seconds on, 20 seconds off, 20 seconds on, 20 seconds off at 20 Hg and 100 W. All stains were filtered with a 0.22 µm syringe filter prior to use.

Incubation with the mordant 1% w/v thiocarbohydrazide in ddH_2O was performed for 5 minutes at room temperature. A second osmium staining was then performed with 2% w/v osmium in ddH_2O in the Biowave (20 Hg, 100 W, 20s on-20s off-20s on-20s off) before an overnight incubation at 4°C in aqueous 1% w/v uranyl acetate.

The following day, enteroids were stained with lead aspartate (0.02 M lead nitrate in 0.03 M aspartic acid in ddH_2O, pH 5.5) for 30 minutes at room temperature. Enteroids were dehydrated through a graded series of ethanol (70-100%) and then acetone (100%). Resin infiltration was performed in 1:1 mixture of 100% acetone and Epon 812 hard premixed resin kit (TAAB Laboratories Equipment) for 30 minutes, followed by two 30-minute infiltration steps in 100% hard resin. Finally, enteroids were embedded in hard resin in a flexible plastic dish and polymerised at 60°C in a dry oven for at least 48 hours.

2.12.1.2. Intestinal tissue

Intestinal tissue samples approximately 1 mm^3 in size were dissected from the proximal or distal ends of the small intestine of a C57BL/6 mouse. Samples were washed gently in ice-cold PBS and fixed temporarily in 4% w/v PFA and 2% w/v glutaraldehyde in 0.1 M PB, pH 7.4. As soon as possible, samples were transferred to 2.5% w/v glutaraldehyde in 0.1 M PB and fixed in the Biowave using the fixation programme. Samples were incubated in the fixative overnight at room temperature. After washing in 0.1 M PB, samples were stained with reduced 2% w/v OsO_4 in the Biowave and washed again. Samples were stained again with 2% w/v OsO_4 in ddH_2O in the Biowave, washed, and incubated overnight at 4°C in 1% w/v uranyl acetate in ddH_2O. The following day, samples were washed and sequentially dehydrated through a graded series of ethanol (70-100%) and then acetone (100%), each for 10 minutes. Resin infiltration was performed for 30 minutes each in 2:1, 1:1, 1:2, 1:3 solutions of acetone: medium resin. After two 30-minute incubations in 100% resin, samples were embedded in 100% resin and polymerised at 60°C in a dry oven for at least 48 hours.

2.12.2. Preparation of blocks and sectioning

Excess resin was trimmed away using a hacksaw and razor blade, then the blocks were mounted on a cryopin using super glue or epoxy resin. Block faces with dimensions of 350 x 350 µm were cut using a glass knife on an UC6 ultramicrotome (Leica Microsystems) and then 70-80 µm thick sections were cut using a diamond knife (Diatome, Switzerland). Sections were collected on copper grids (TAAB), which were prepared by coating with 0.3% w/v pioloform (polyvinyl butyral), and left to dry for at least 24 hours.

2.12.3. Post-staining of small intestinal tissue sections

To gain additional contrast, intestinal tissue sections prepared as described above were post-stained for 5 minutes at room temperature with 4% w/v uranyl acetate in ddH_2O, followed by washing in three separate baths of ddH_2O. Sections were then incubated for 5 minutes with Reynolds' lead citrate (TAAB), washed again, and dried at room temperature.

2.12.4. Transmission electron microscopy

Sections were imaged at 100-120 kV in a Tecnai G2 Spirit BioTWIN transmission electron microscope (FEI, Cambridge, UK) using analySIS 3.2 software (FEI) and Gatan Microscopy Suite software (Gatan, California, USA).

2.13. Statistical analysis

All statistical analyses were performed using Prism 6 (Version 6.01; GraphPad Software, Inc, California, USA). Data values in the text are expressed as mean ± standard error of the mean (SEM). N values refer to the number of independent experiments performed; n values refer to the number of replicates for individual experimental groups. Data sets exhibiting a normal distribution, as assessed using a Shapiro-Wilk normality test, were analysed using unpaired Student t-tests or one-way analysis of variance (ANOVA, to compare more than two sample groups) followed by multiple pairwise comparisons. Data that was not normally distributed were analysed using non-parametric tests, such as Mann-Whitney test. Spearman correlation coefficients were used to assess correlation between two measured variables. The threshold used to determine statistical significance was $p < 0.05$.

Chapter 3

Location-specific characteristics of enteroids derived from murine proximal or distal small intestine

3.1. Introduction

The small intestine is largely anatomically and physiologically similar in both humans and mice, making the mouse a good model for many aspects of human intestinal biology (Nguyen *et al.*, 2015; Hugenholtz and de Vos, 2018). In both species, the small intestine begins after the pyloric sphincter and ends at the ileocaecal junction. Along its cephalocaudal axis, the small intestine is divided into three regions – the duodenum, jejunum and ileum – which have distinct functions and must cope with different physiological challenges. Briefly, the duodenal epithelium produces digestive enzymes and bicarbonate, the latter of which contributes to neutralising the gastric chyme to support the former in breaking down macromolecular nutrients. Absorption of certain essential nutrients, such as the minerals iron and calcium, also begins in the duodenum. The majority of nutrient and water absorption occurs in the jejunum. Here, the epithelium expresses many brush border nutrient-specific transporters, such as the sodium-coupled glucose and neutral amino acid symporters (Bröer, 2008; Chen, Tuo and Dong, 2016). In the ileum, absorption of key fat- and water-soluble vitamins occurs (Reboul and Borel, 2011; Said, 2011) and bile salts are reabsorbed (Dawson and Karpen, 2015). As a result, the epithelium varies between these regions. Differences are observed in expression of enzymes (Bosse *et al.*, 2006) and transporters (Mutch *et al.*, 2004; Anderle *et al.*, 2005), size of villi, distribution of different epithelial cell types (Bosse *et al.*, 2006; Kim and Ho, 2010; Bevins and Salzman, 2011), and in the level of mucus secretion (Kim and Ho, 2010).

Regionalisation of the small intestine along the cephalocaudal axis is controlled by a few key transcription factors. The most important in this context are considered to be pancreatic and duodenal homeobox 1 (PDX1), GATA4 and GATA6.

PDX1 has been shown to be important in specifying the duodenum (Thompson, DeLaForest and Battle, 2018). PDX1 expression is required for expression of duodenum-specific genes, such as the enterocyte marker alkaline phosphatase 3 and proximal enteroendocrine cell marker, gastric inhibitory peptide (Chen *et al.*, 2009). Expression of PDX1 also represses genes that encode duodenal enzymes, such as lactase and sucrose isomaltase.

GATA4, in both mice and humans, is expressed by the epithelium of both duodenum and jejunum but not the ileum (Bosse *et al.*, 2006). The essential role of GATA4 in patterning the divide between jejunum and ileum is revealed by the fact that intestinal epithelium-specific deletion of *Gata4* during development results in a shift towards a more ileal phenotype

(Thompson, DeLaForest and Battle, 2018). In the *Gata4*-knockout jejunum, genes specific to jejunal enterocytes are repressed and ileal-specific genes, such as *Slc10a2* (encoding the apical sodium bile acid transporter, ABST), are enhanced (Bosse *et al.*, 2006; Battle *et al.*, 2008; Walker, Thompson and Battle, 2014). *Gata4*$^{-/-}$ mice demonstrate the importance of regionalisation in determining function, as they exhibit reduced absorption of fats. Reciprocally, experimental expression of GATA4 in the mouse ileum causes a shift towards a jejunal expression profile (Thompson *et al.*, 2017).

GATA6, a related transcription factor, is expressed along the whole length of the small intestinal epithelium and appears to be involved in determining small intestinal as opposed to colonic identity in these cells. Deletion of GATA6 in the intestinal epithelium causes the ileal epithelium to adopt a more colonic phenotype (Beuling *et al.*, 2011; Walker *et al.*, 2014), with impaired differentiation of Paneth and enteroendocrine cells (Beuling *et al.*, 2011). Similar consequences are only seen in the jejunum and duodenum if both GATA6 and GATA4 are deleted simultaneously (Beuling *et al.*, 2011). This suggests that GATA4 and GATA6 perform distinct roles in patterning the small intestinal epithelium, with GATA4 specifying the jejunal-ileal transition and GATA6 contributing to ileal identity, at least in part by repressing colon-specific genes.

Although these transcriptional regulators of regional specialisation along the small intestine have begun to be understood, it remained unclear how regional identity is specified in terms of intestinal epithelial stem cell biology (Middendorp *et al.*, 2014). One possibility is that stem cells receive locational signals from their local microenvironment, for example from neighbouring mesenchymal cells. Alternatively, regional identity might be intrinsically programmed in the stem cell. Evidence from enteroid models indicates that the latter is most likely true (Middendorp *et al.*, 2014; Kraiczy *et al.*, 2017). Enteroids are three dimensional (3D), *ex vivo* cultures of primary intestinal stem cells. This culture technique was first described by Clevers and colleagues (Sato *et al.*, 2009; Sato and Clevers, 2013) and has already seen huge uptake by researchers studying development and normal physiology of the small intestine, as well as intestinal disease and host-pathogen interactions (Bartfeld, 2016; Dedhia *et al.*, 2016; Fatehullah, Tan and Barker, 2016; Hill and Spence, 2016; In *et al.*, 2016; Dutta, Heo and Clevers, 2017). Enteroids may be established from adult intestinal stem cells and passaged for long term maintenance by regularly disrupting the structures and re-seeding the fragments. The stem cells are maintained by a cocktail of growth factors and proliferate to form a continuous epithelial monolayer that encloses a central lumen, with distinct crypt-like buds

forming with stem cells at their bases. Enteroids established in this way contain only epithelial cells, including all major intestinal epithelial lineages (Sato *et al.*, 2009).

A key study comparing the transcriptomes of murine enteroids established from duodenum, jejunum or ileum to their parent tissues showed that region-specific gene expression was largely retained *in vitro*, despite the absence of extrinsic locational cues from surrounding mesenchymal cells (Middendorp *et al.*, 2014). Intrinsic locational identity appears to be programmed epigenetically, as enteroids established from adult human ileum and colon exhibit stable, distinct patterns of DNA methylation, which are very similar to those of their parent tissues (Kraiczy *et al.*, 2017). These epigenetic modifications were found to regulate expression of region-specific genes, including *FABP6* and *MUC5B.* Methylation profiles of different segments within the small intestine have not been compared.

In this chapter, the terms 'proximal' and 'distal' are used to refer to the segments of the murine small intestine from which enteroid cultures were established. For proximal enteroids, the first 3-6 cm segment of intestine directly after the pyloric sphincter were used; this likely includes the duodenum but also jejunum, as the duodenum in mice is very short (Williams *et al.*, 2016). Distal enteroids were derived from a 3-6 cm section of small intestine up to, and directly adjacent to, the caecum.

3.2. Hypothesis

Enteroids derived from different regions of the mouse small intestine retain location-specific characteristics of their parent tissues in culture, despite the absence of extrinsic positional cues.

3.3. Aims

1. To assess whether enteroids derived from proximal and distal regions of mouse small intestine retain morphological differences in culture.

2. To compare the distribution of different epithelial cell types in proximal and distal murine small intestine and to assess whether differences in cell type distributions are maintained in enteroid cultures derived from these regions.

3. To assess for any differences in epithelial permeability of proximal and distal small intestine using the enteroid model.

3.4. Methods

Enteroid culture

Enteroids were established from proximal and distal regions of the small intestine of wild type C57BL/6 mice. The method used is described in detail in Section [Methods .4]. Briefly, a section of small intestine 3-6 cm long was taken from either directly after the pyloric sphincter (proximal) or directly before the caecum (distal). The tissue was washed and intestinal crypts were isolated by incubating with EGTA, followed by agitating vigorously. Crypts were embedded in Matrigel, which was allowed to set before being covered with culture medium. The essential growth factors, R-spondin 1, Noggin and EGF were supplied in the culture medium. Enteroids used for experiments were of passage 1-25.

Quantification of epithelial cell types by immunohistochemistry

For immunohistochemical analysis, enteroids were cultured for 6 days after passage. The Matrigel was then dissociated and the enteroids were fixed with paraformaldehyde and paraffin embedded. Sections were stained with antibodies against prominent markers of the different epithelial cell types present in the small intestine: trefoil factor 3 (TFF3; goblet cells) (Kim and Ho, 2010), lysozyme (Lyz; Paneth cells) (Sato, van Es, *et al.*, 2011), chromogranin A (CgA; enteroendocrine cells) (Engelstoft *et al.*, 2015) and doublecortin-like kinase 1 (DCLK1; tuft cells) (Middelhoff *et al.*, 2017). See Section [Methods .7] for a detailed description of this technique. Cell types were quantified as a percentage of the total cells per enteroid section. Sections of C57BL/6 mouse tissue from the same regions of the small intestine from which enteroids were derived were stained in parallel. In intestinal tissues, the number of each cell type was quantified as a percentage of the total number of cells observed in each crypt-villus axis.

Transmission electron microscopy (TEM)

Enteroids were harvested on day 3 post-passage. Matrigel was dissociated and enteroids were fixed and processed for TEM as detailed in Section 2.12.

Assessment of epithelial permeability in enteroids

Differences in the epithelial permeability of the proximal and distal small intestine were investigated by microinjecting FD4 into the lumen of enteroids derived from either region. Since enteroids vary in size, each enteroid was injected until it began to swell rather than with a fixed volume. The luminal fluorescence of injected enteroids was visualised using an epifluorescence microscope at hourly intervals following injection and bright field images were collected in parallel. To monitor loss of fluorescence from the lumen, the perimeter of each enteroid was specified using ImageJ software and the mean fluorescence intensity of pixels within this area was determined. To adjust for differences in starting fluorescence intensity within each microinjected enteroid (i.e. due to differences in volume of FD4 injected), the values for each enteroid were normalised against its starting value.

3.5. Results

3.5.1. Enteroids derived from proximal and distal small intestine exhibit similar patterns and rate of growth once established

Enteroid cultures established from crypts that were isolated from proximal and distal regions of the small intestine showed similar growth patterns (**Figure 3.1 A**). Both proximal and distal enteroids showed clear increases in size from day 3-7 post-passage (**Figure 3.1 B**). Enteroid area measured on days 5 and 7 was normalised to day 3 to negate any differences in the size of fragments generated during passage. During the course of the experiment, the observed areas of proximal enteroids varied between 0.005-0.180 mm^2, while distal enteroids were between 0.007-0.267 mm^2. Similar increases in size were observed for proximal and distal enteroids on days 5 and 7 post-seeding when normalised to enteroid size on day 3.

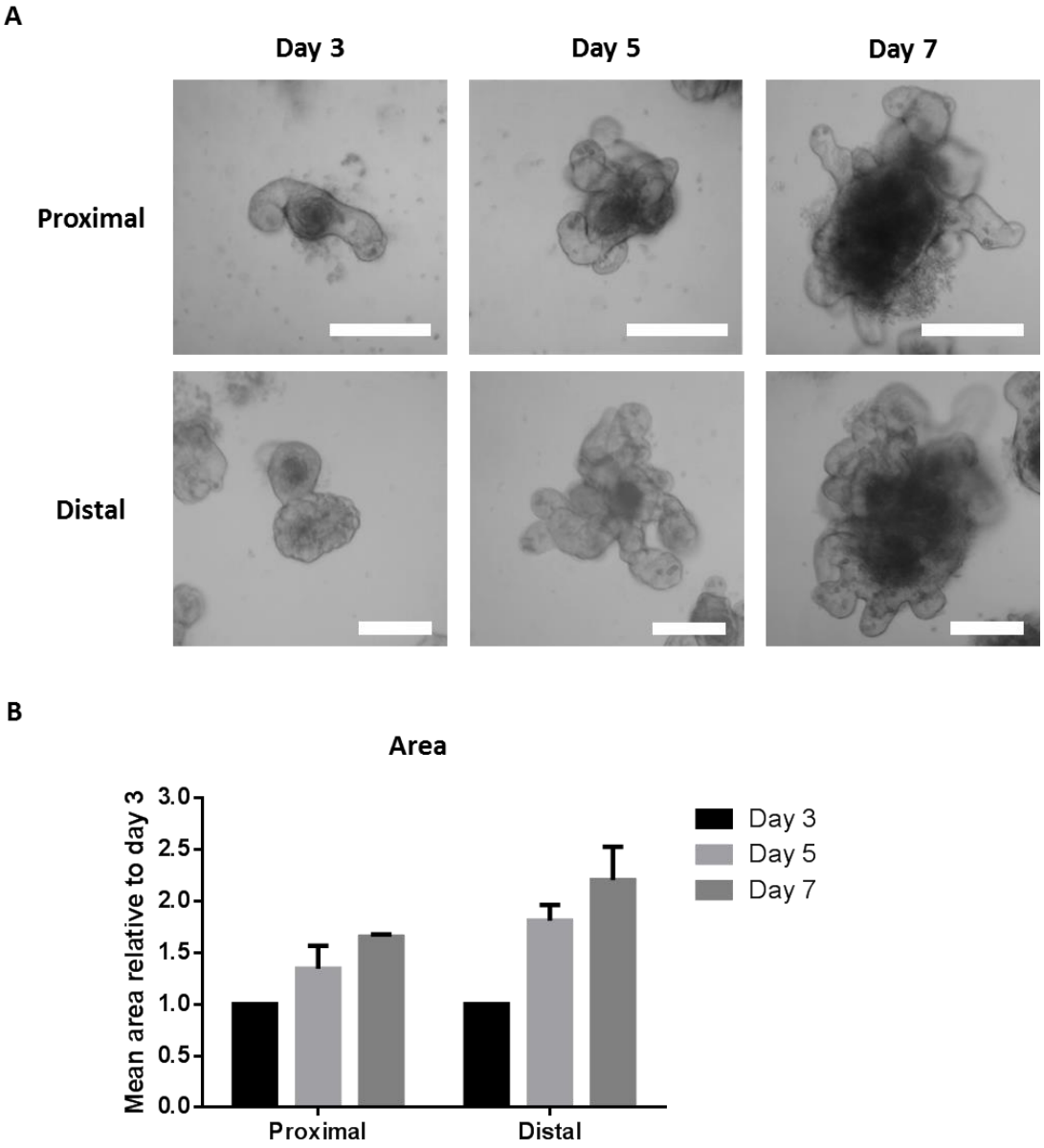

Figure 3.1. Growth of enteroids derived from proximal and distal small intestine. (A) Representative bright field images of enteroids established either from the proximal or distal region of the small intestine of a C57BL/6 mouse. Images captured on days 3, 5 and 7 post-seeding do not necessarily show the same enteroid at each time point. Scale bars represent 200 µm. **(B)** Quantification of mean area of proximal and distal enteroids at 3, 5 and 7 days post-seeding. Data are shown relative to mean area on day 3 to control for possible differences in size of fragments seeded. Across all time points, range of observed enteroid areas was 0.005-0.180 mm^2 (proximal) and 0.007-0.267 mm^2 (distal). For proximal cultures, N = 2 cultures established from different mice, n = 21-46 enteroids; for distal cultures, N = 3, n = 14-60. Error bars represent SEM.

3.5.2. Enteroids derived from proximal and distal small intestine exhibit location-specific morphological characteristics

Under normal conditions, it is apparent by light microscopy that enteroids derived from proximal and distal small intestinal tissue tend to have a different appearance (**Figure 3.2 A**). The morphological differences are difficult to quantify. Whereas the basolateral aspect of enteroids derived from proximal small intestine tends to have a smooth appearance, the basolateral aspect of the epithelium of distal enteroids has a more "raspberry-like" or ruffled appearance, particularly in the crypt bud regions. The difference in appearance is maintained over the course of many passages.

Efforts were made to quantify these morphological differences by evaluating enteroid circularity (a measure of how similar the overall enteroid shape is to a perfect circle, which would give a value of 1.0; **Figure 3.2 B**) and the number of buds per enteroid (**Figure 3.2 C**). Distal enteroids showed a trend towards higher mean circularity, indicating that they tend to be more round overall, but this did not reach significance. On day 3, the mean number of buds per enteroid was lower on in distal compared to proximal enteroids but by day 5 they were approximately equal.

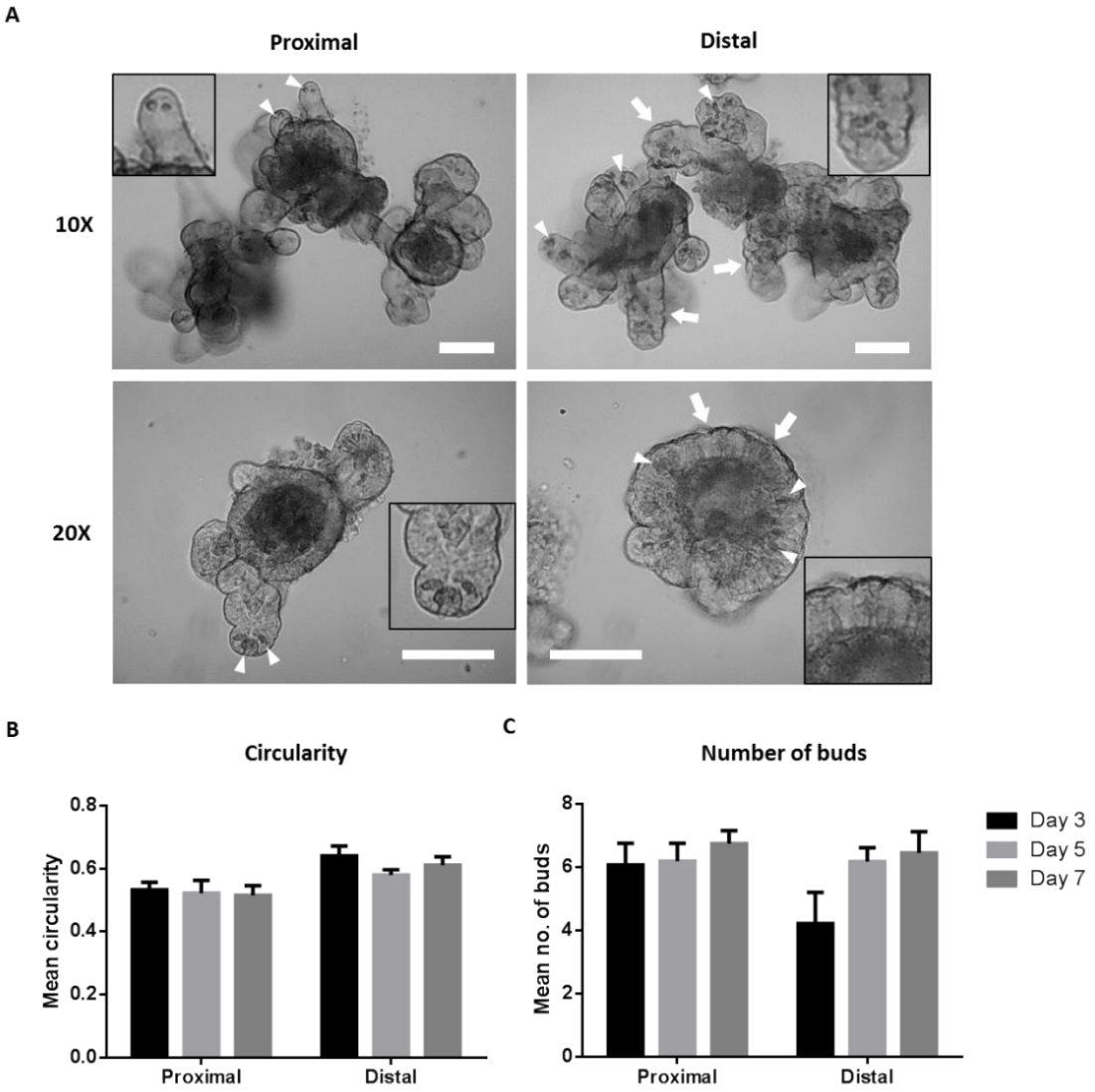

Figure 3.2. Location-specific morphological characteristics of enteroids. (A) Representative bright field images of enteroids derived from either proximal or distal small intestine of C57BL/6 mice. Full arrows indicate areas of where characteristic 'raspberry-like' appearance of basolateral aspect of epithelium of distal enteroids is noticeable. Arrow heads indicate Paneth cells. All scale bars represent 100 µm. Inset boxes show 2X (upper panel) or 1.7X (lower panel) magnified parts of the images. **(B)** Quantification of enteroid circularity from bright field images. For proximal enteroids, N = 2 independent enteroid cultures derived from different mice, n = 21-46 enteroids; for distal enteroids, N = 3, n = 13-60. **(C)** Mean number of buds per enteroid. For proximal enteroids, N = 2, n = 28-44; for distal enteroids, N = 3, n = 15-57. All error bars represent SEM.

To assess any differences in the ultrastructure of the epithelium, enteroids derived from the different regions of the small intestine were also analysed by transmission electron microscopy. Sections from throughout the enteroid were analysed, including within a crypt bud and from the villus region (**Figure 3.3 A**). In sections taken from towards the crypt base, enterocytes had short, irregular microvilli on their apical surface (**Figure 3.3 B**). In contrast, enterocytes in the villus regions exhibited long, regular microvilli that were very similar in appearance to those visualised on enterocytes in small intestinal tissue samples.

Paneth, goblet and enteroendocrine cells were identified by their characteristic features in enteroids derived from both regions (**Figure 3.4 A & B**). Paneth cells contain many large, densely staining cytoplasmic granules towards their apical surface. Goblet cells are named for their distinctive goblet-like shape and feature a large theca of mucus-containing vesicles towards their apical surface. Finally, enteroendocrine cells were identifiable by the small, darkly staining granules found basolateral to the cell nucleus.

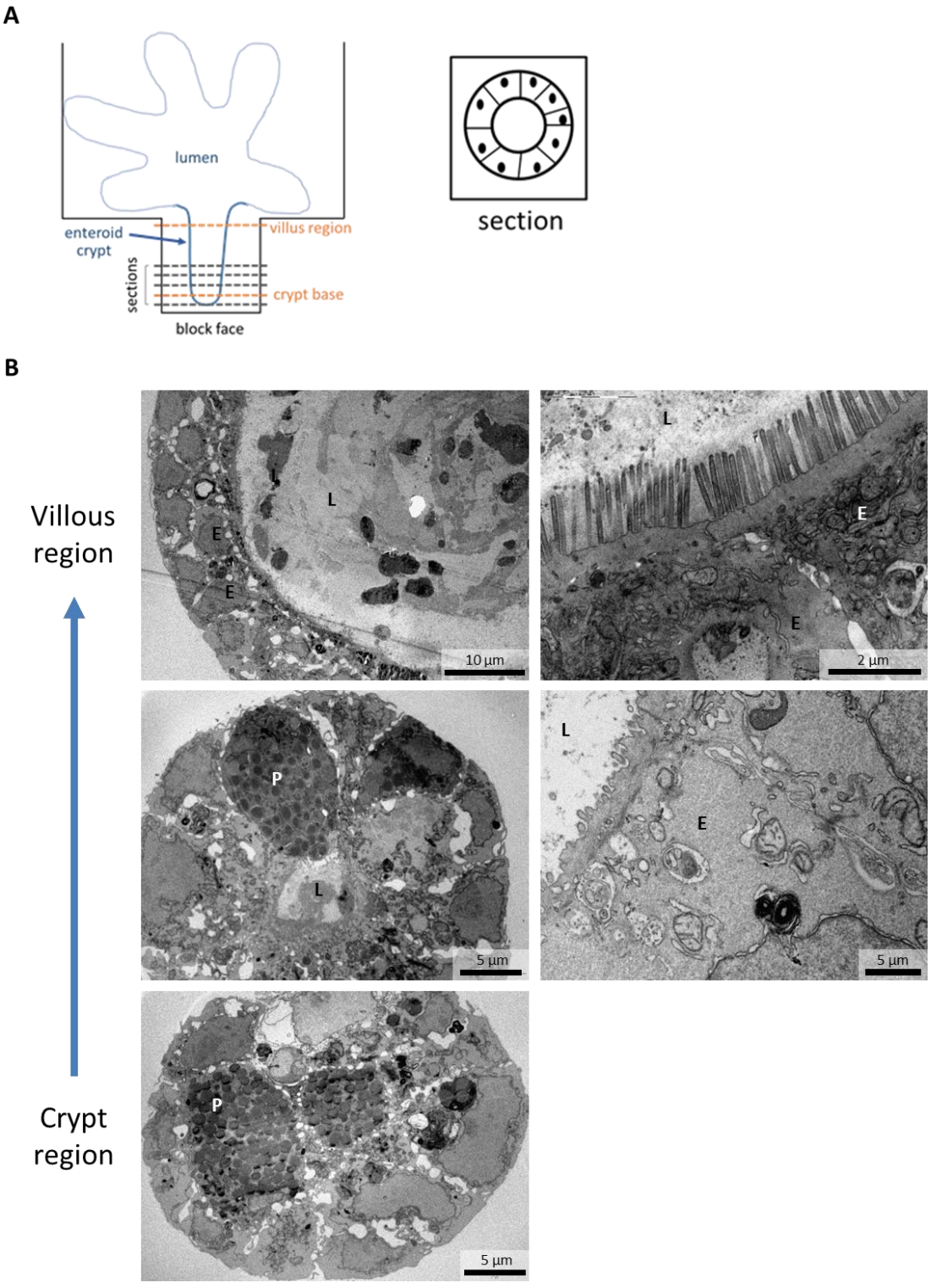

Figure 3.3. Analysis of murine enteroids by transmission electron microscopy. (A) Schematic showing the orientation of enteroids within the resin in relation to the block face from which sections are cut. Lower image schematic demonstrates the cross-sectional view of a crypt visible in sections. **(B)** TEM images demonstrating the different regions of an enteroid, moving from the crypt base up along the crypt-villus axis. L, lumen; E, enterocyte; P, Paneth cell.

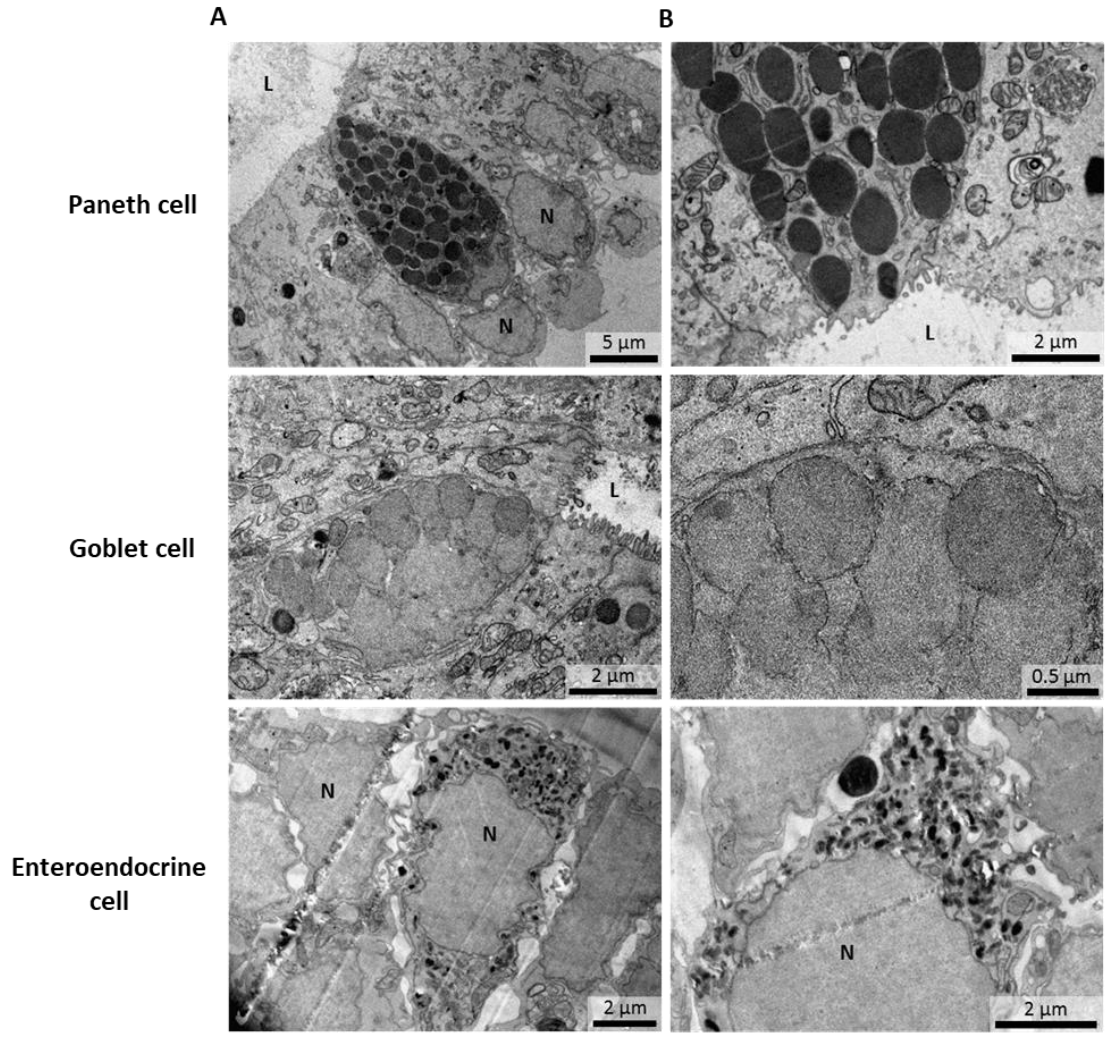

Figure 3.4. Identification by TEM of epithelial cell types in murine enteroids. TEM images of enteroids fixed on day 3 post-seeding an. Images show representative examples of the major intestinal epithelial cell types, Paneth cells, goblet cells and enteroendocrine cells. **(A)** Lower magnification and **(B)** higher magnification views of cell-specific morphology. L, lumen; N, nucleus.

In sections of tissue derived from proximal and distal small intestine, the luminal surface of enterocytes was found to be packed with long, regular microvilli (**Figure 3.5 A**). As expected, enterocytes were thin and columnar, with the nuclei located basally (**Figure 3.5 B**). This was closely mirrored by the epithelium of enteroids derived from both proximal and distal regions. Within crypt regions, the lumen was small in diameter and the apical surface of epithelial cells displayed short, irregular microvilli (**Figure 3.6 A & B**). In contrast, the lumen was expanded in the villus region and microvilli were long and regular, much more closely resembling those in the tissue (**Figure 3.6 C & D**).

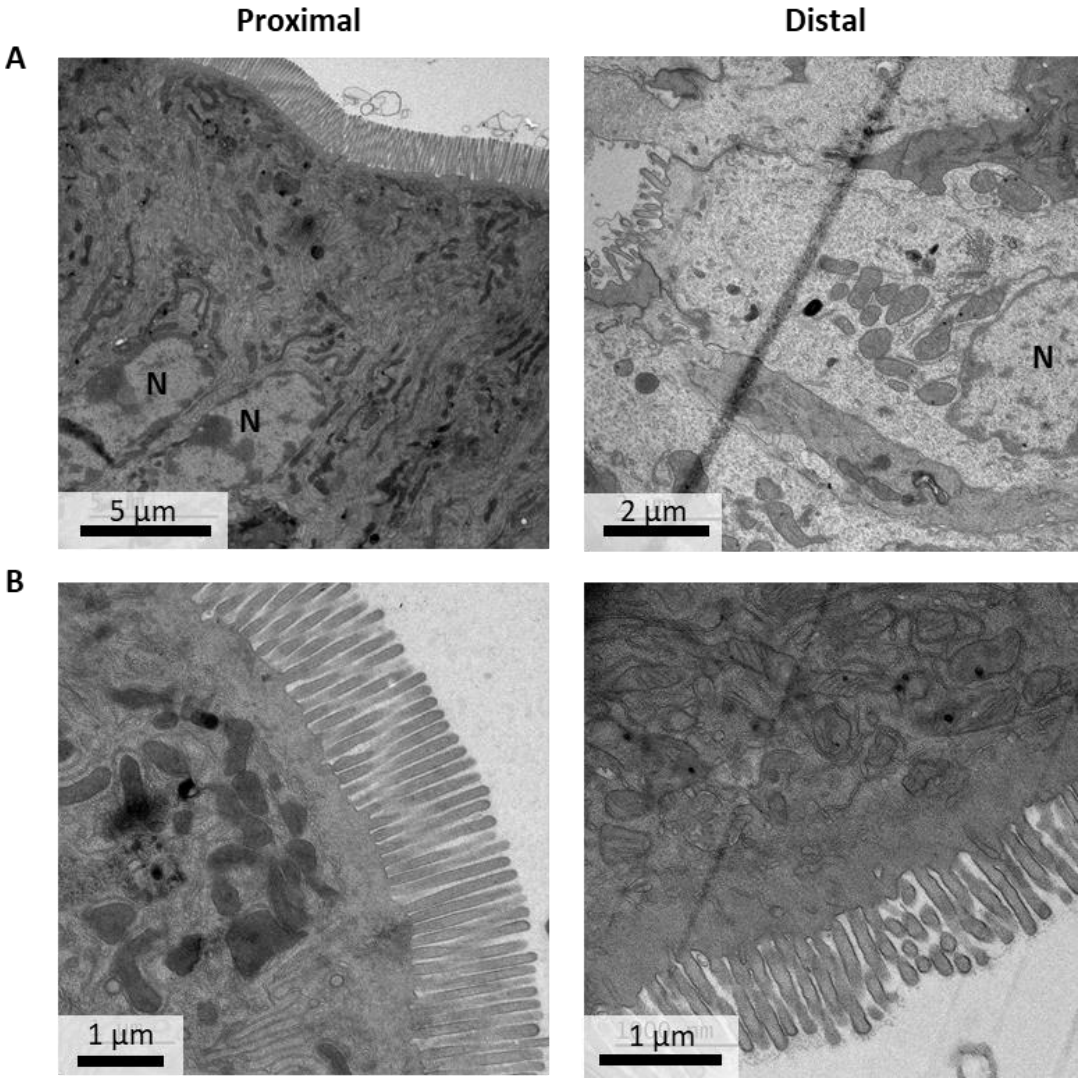

Figure 3.5. Ultrastructure of the murine small intestinal epithelium *in vivo*. Representative TEM images of **(A)** an overview of the epithelium and **(B)** the apical surface of enterocytes of proximal and distal small intestine from a C57BL/6 mouse. Microvilli are present on the apical surface. N, nucleus.

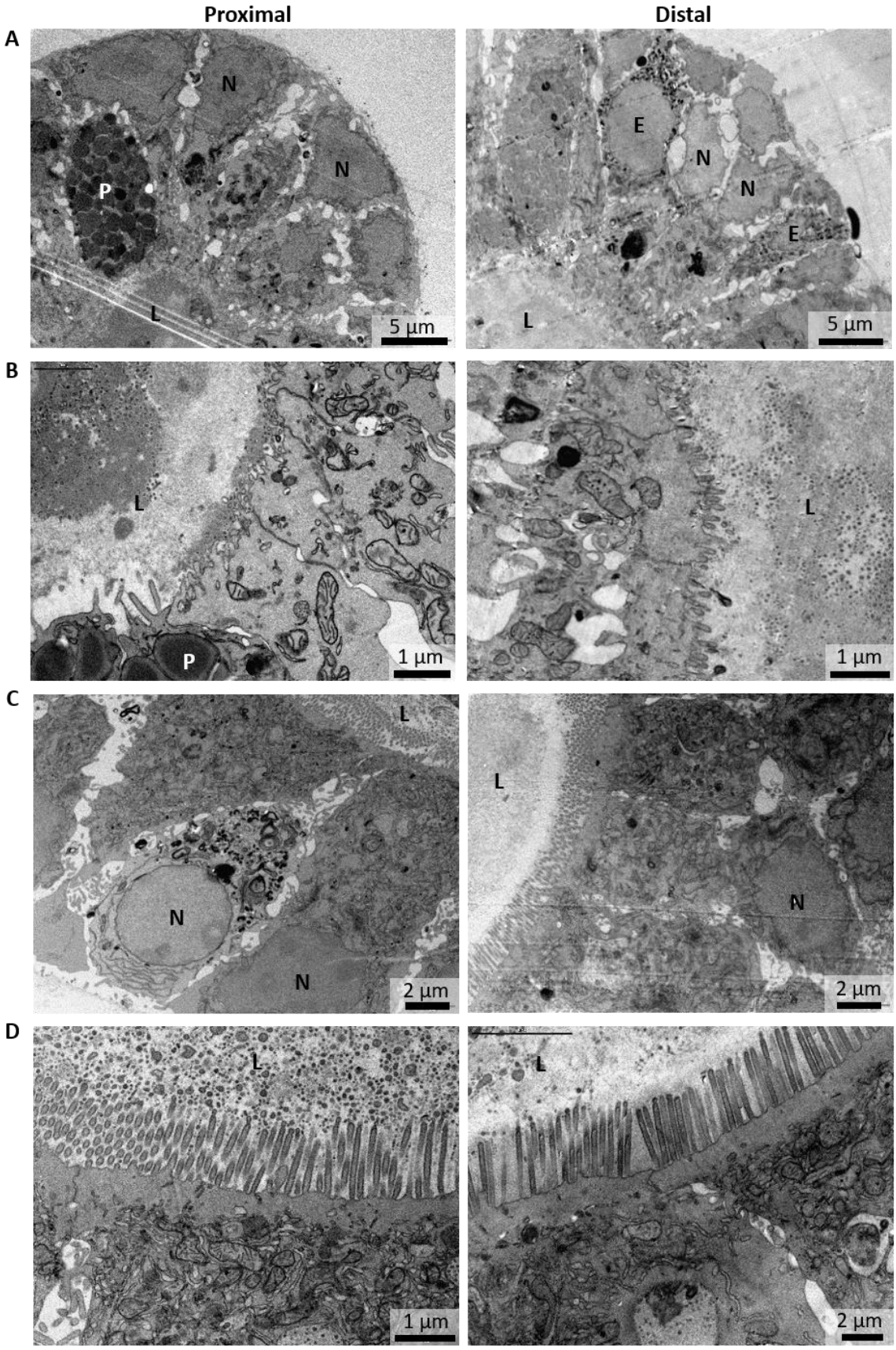
Proximal
Distal
A
N
N
P
L
5 µm
E
N
N
E
L
5 µm
B
L
P
1 µm
L
1 µm
C
L
N
N
2 µm
L
N
2 µm
D
L
1 µm
L
2 µm

Figure 3.6. Ultrastructure of the crypt and villous regions of enteroids derived from proximal and distal murine small intestine. (A & B) Representative TEM images of (A) an overview of the crypt epithelium and **(B)** the apical surface of crypt epithelial cells in an enteroid derived from either proximal or distal small intestine of a C57BL/6 mouse. Paneth cells are present in the images of the proximal enteroid and enteroendocrine cells are visible in the overview of the distal enteroid epithelium. (C & D) Representative TEM images of (C) an overview of the epithelium and **(B)** the apical surface of epithelial cells in the villous regoin of enteroids established from either proximal or distal small intestine of a C57BL/6 mouse. L, lumen; N, nucleus; P, Paneth cell; E, enteroendocrine cell.

3.5.3. Location-specific distribution of epithelial cell types in small intestinal tissue

It has been suggested that GATA4 alters cell fate specification as part of its role in regulating specialisation of the small intestine along the cephalocaudal axis (Bosse *et al.*, 2006), although this has not been comprehensively investigated. Immunohistochemical analysis was therefore performed on sections of tissue and enteroids derived from proximal and distal small intestine to compare the distribution of epithelial cell types. Tissue samples were derived from three different wild type C57BL/6 mice and enteroid samples were from cultures generated from three different mice. Cell types examined were Paneth, goblet, enteroendocrine and tuft cells, using the markers Lyz, TFF3, CgA and DCLK1, respectively. Individual cell types were quantified as a percentage of total cells per crypt-villus axis or per enteroid section.

As expected, Paneth cells were observed exclusively at the crypt bases in tissue sections and were frequently observed within the crypt buds of enteroids (**Figure 3.7 A**). The percentage of Paneth cells was significantly larger in distal compared to proximal small intestinal tissue by 2.9% ± 0.4% (mean ± SEM; $p < 0.01$; **Figure 3.7 B**). In enteroids, Paneth cells represented a larger proportion of total cells by 7.8% ± 3.9%, although this difference did not reach significance.

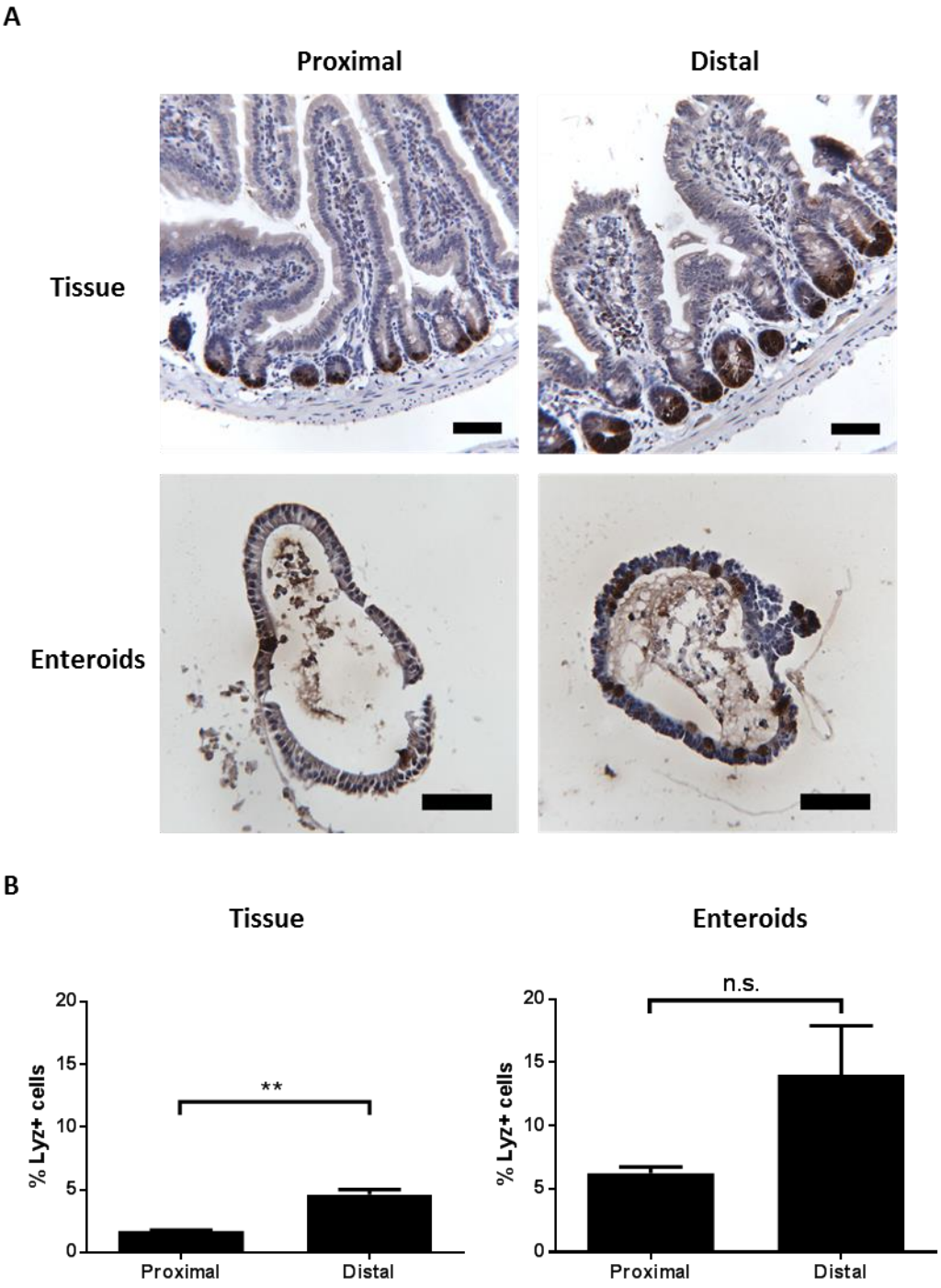

Figure 3.7. Quantification of Paneth cells in tissue and enteroids derived from proximal and distal mouse small intestine. (A) Representative images showing immunohistochemical staining of lysozyme (Lyz), an anti-microbial peptide stored in Paneth cell granules. Staining was performed on paraffin-embedded sections of tissue and enteroids derived from proximal and distal small intestine. Scale bars = 50 µm. **(B)** Quantification of number of Paneth cells per crypt-villus axis in intestinal tissue and per complete enteroid section. For intestinal tissue: N = 3, n = 30 crypt-villus axes. For enteroids: N = 3, n = 20-31 enteroid sections. Unpaired two-tailed t-test, **p < 0.01, n.s. non-significant. Error bars represent SEM.

Immunohistochemical staining revealed goblet cells distributed throughout the small intestinal epithelium in both tissue and enteroid sections (**Figure 3.8 A**). The percentage of goblet cells was significantly greater in both distal tissue and enteroids compared to their proximal equivalents, by 7.4% ± 0.7% and 6.3% ± 2.0% respectively ($p < 0.001$ and $p < 0.05$; **Figure 3.8 B**). The proportion of goblet cells in each region was closely matched between enteroids and their parent tissues. Goblet cells represented 14.2% ± 1.9% of cells in distal enteroids compared to 16.6% ± 0.6% in distal small intestine. In proximal samples, goblet cells represented 7.9% ± 0.3% of cells in enteroids compared to 9.2% ± 0.3% in proximal tissue.

Enteroendocrine cells were observed throughout the crypt and villous epithelium in both tissue and enteroids (**Figure 3.9 A**). In small intestinal tissue, enteroendocrine cells were significantly more abundant in the proximal compared to the distal region, by 0.4% ± 0.1% ($p < 0.05$; **Figure 3.9 B**). Although not statistically significant, the same trend was observed in enteroids derived from these tissues; enteroendocrine cells constituted 5.8% ± 0.6% of total cells in proximal enteroids and 4.5% ± 1.4% in distal enteroids.

Tuft cells were identified along the length of the crypt-villus axis in tissue from both proximal and distal small intestine (**Figure 3.10 A**). In enteroids, tuft cells again did not localise specifically to either crypt or villous regions. Tuft cells were the least abundant cell type; many enteroid sections did not contain any DCLK1-expressing cells. They appeared to be equally distributed in proximal and distal regions, representing 1.3% ± 0.3% of cells in proximal and only 0.6% ± 0.02% in distal small intestine (**Figure 3.10 B**). The percentage of tuft cells was 0.5% ± 0.1% in proximal enteroids and 0.8% ± 0.2% in distal enteroid cultures.

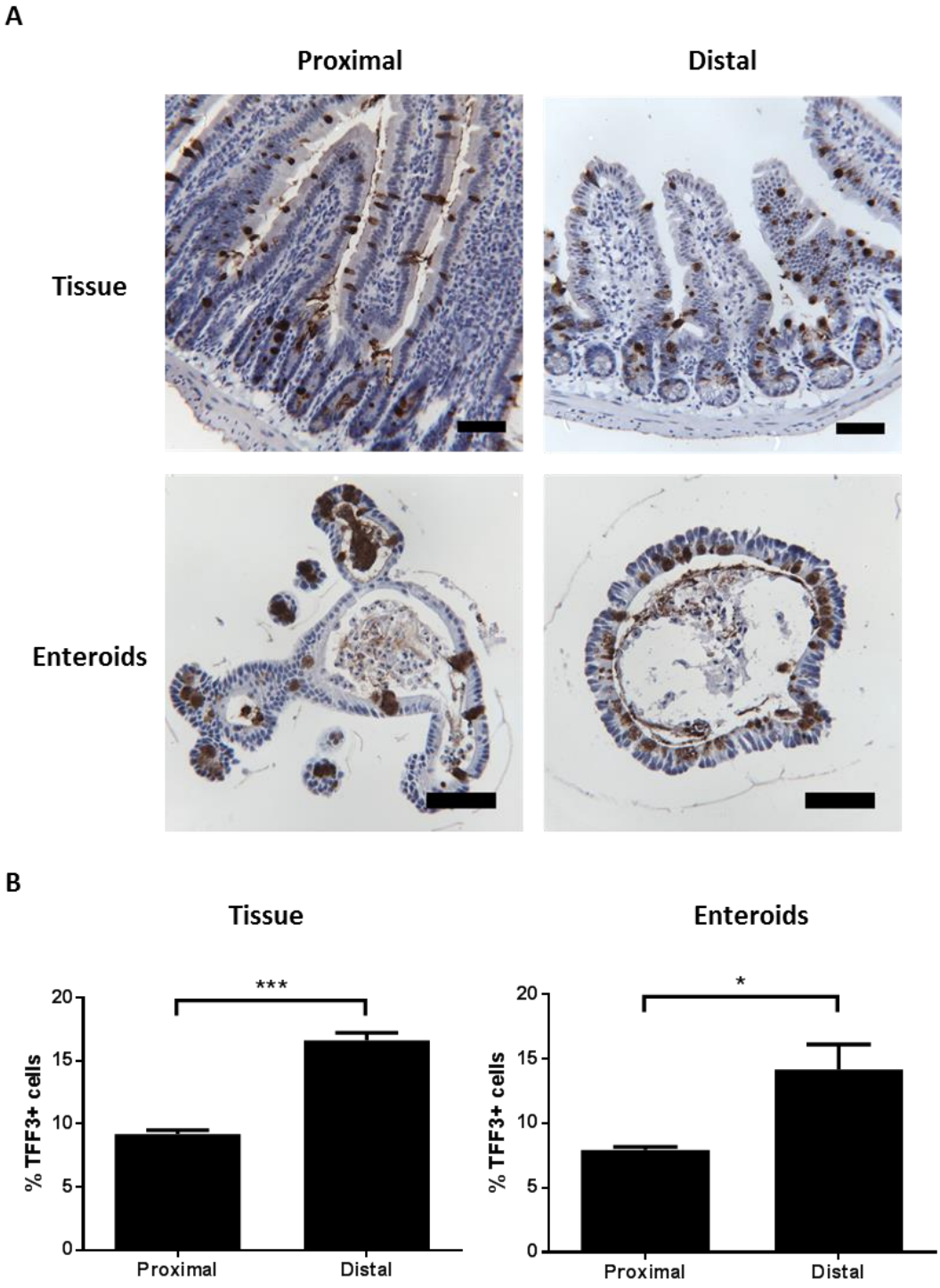

Figure 3.8. Quantification of goblet cells in tissue and enteroids derived from proximal and distal mouse small intestine. (A) Representative images showing immunohistochemical staining of goblet cell marker TFF3. Staining was performed on paraffin-embedded sections of tissue and enteroids derived from proximal and distal small intestine. Scale bars = 50 µm. **(B)** Quantification of number of goblet cells per crypt-villus axis in intestinal tissue and per complete enteroid section. For intestinal tissue: N = 3 mice, n = 30 crypt-villus axes. For enteroids: N = 3, n = 20-31 enteroid sections. Unpaired two-tailed t-test, ***p < 0.001, *p < 0.05. Error bars represent SEM.

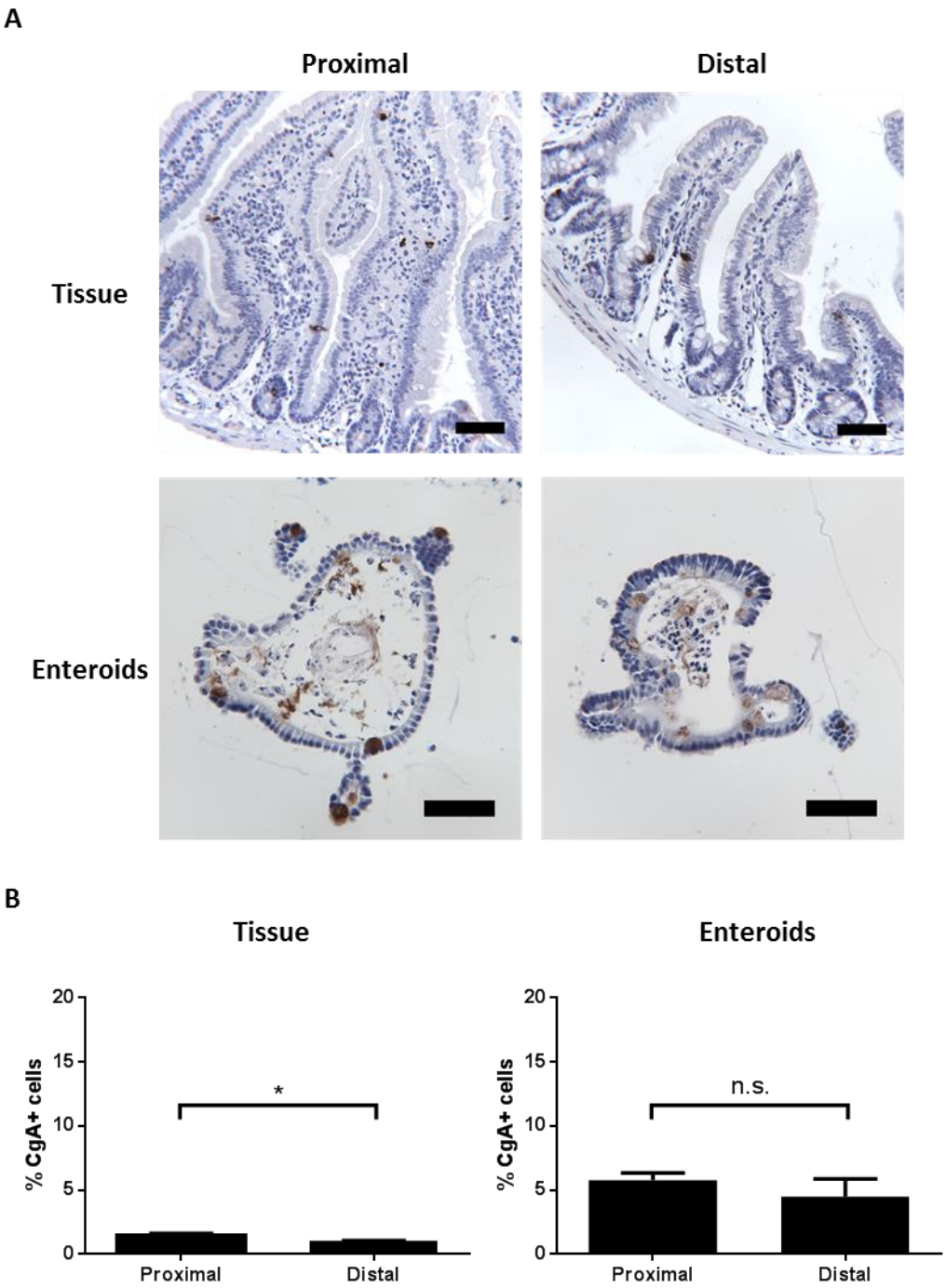

Figure 3.9. Quantification of enteroendocrine cells in tissue and enteroids derived from proximal and distal mouse small intestine. (A) Representative images showing immunohistochemical staining of CgA, a marker of enteroendocrine cells. Staining was performed on paraffin-embedded sections of tissue and enteroids derived from proximal and distal small intestine. Scale bars = 50 µm. **(B)** Quantification of number of enteroendocrine cells per crypt-villus axis in intestinal tissue and per complete enteroid section. For intestinal tissue: N = 3 mice, n = 30 crypt-villus axes. For enteroids: N = 3, n = 16-35 enteroid sections. Unpaired two-tailed t-test, *$p < 0.05$, n.s. non-significant. Error bars represent SEM. Y-axis scaled for comparison of Figures 3.7-10.

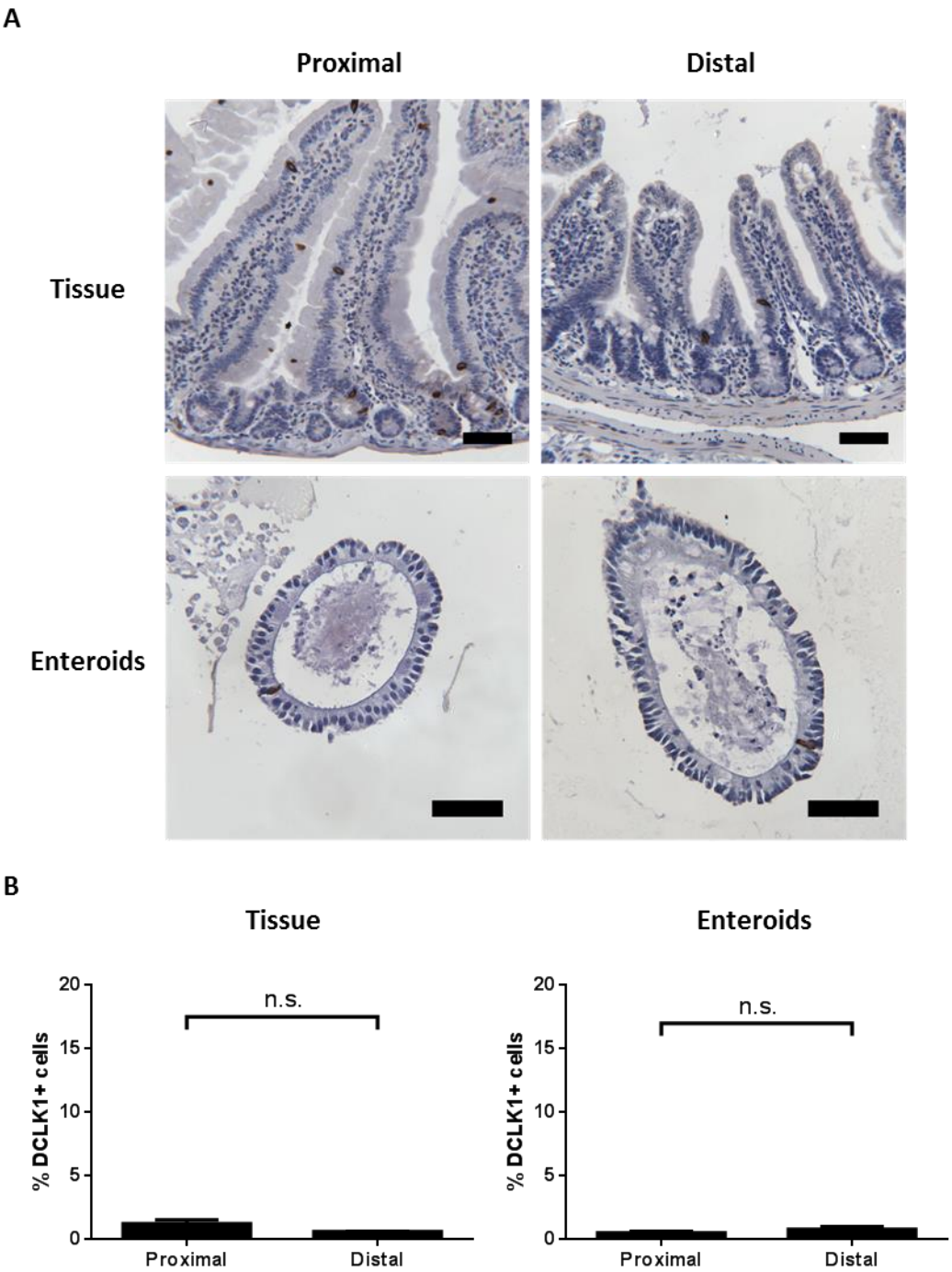

Figure 3.10. Quantification of tuft cells in tissue and enteroids derived from proximal and distal mouse small intestine. (A) Representative images showing immunohistochemical staining of tuft cell marker DCLK1. Staining was performed on paraffin-embedded sections of tissue and enteroids derived from proximal and distal small intestine. Scale bars = 50 µm. **(B)** Quantification of number of enteroendocrine cells per crypt-villus axis in intestinal tissue and per complete enteroid section. For intestinal tissue: N = 3 mice, n = 27-30 crypt-villus axes. For enteroids: N = 3, n = 23-36 enteroid sections. Unpaired two-tailed t-test, n.s. non-significant. Error bars represent SEM.

3.5.4. Relationship between enteroid size and frequency of different epithelial cell types

Certain cell types are found in specific regions of the intestinal epithelium; for example, Paneth cells migrate to the crypt base as they differentiate and are not generally found within the villus epithelium. Enteroids likely contain a proportionally larger crypt region than is found in intestinal tissue and this effect should be greater in smaller enteroids. As a result, it might be expected that there is a relationship between enteroid size and its percentage composition of certain cell types. Such a relationship might bias the quantification of cell types if one group of enteroids tended to be smaller or larger than the other. To test this, the percentage of each cell type was compared with the total number of cells within the enteroid section and the non-parametric Spearman's rank correlation coefficient was calculated (**Figure 3.11** and **Table 3.1**). Most comparisons, however, showed Spearman r_s values close to zero, which suggests that there is little correlation between enteroid size and its percentage of each cell type. The only exception to this was for goblet cells in distal enteroids, where the Spearman r_s value of -0.416, and a p value < 0.05 suggest a moderate, but significant, negative correlation that is not explained by random variation.

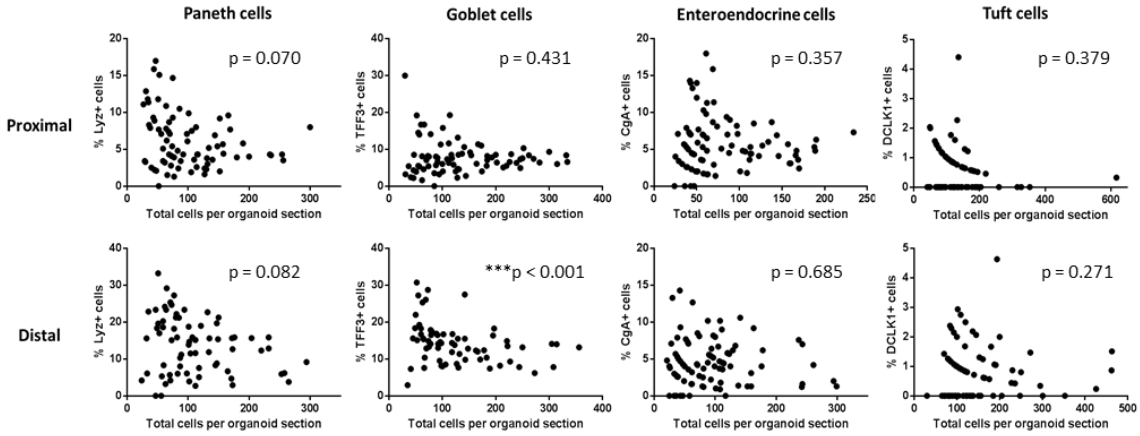

Figure 3.11. Relationship between enteroid size and frequency of different epithelial cell types. Comparison of the proportion of Paneth, goblet, enteroendocrine and tuft cells per enteroid section with the total number of cells in that section for enteroids derived from proximal and distal SI. Each dot represents one scored enteroid section (see Table 3.1 for the total numbers of sections scored for each sample, pooled from 3 independent experiments).

Table 3.1. Relationship between enteroid size and frequency of different epithelial cell types. Results from calculation of the non-parametric Spearman correlation coefficient (r_s) between the total cells per enteroid section with the percentage of each cell type present (as shown in Figure 3.8). N, total number of enteroid sections scored, pooled from 3 independent enteroid cultures.

	Paneth cells		***Goblet cells***		***Enteroendocrine cells***		***Tuft cells***	
	Proximal	***Distal***	***Proximal***	***Distal***	***Proximal***	***Distal***	***Proximal***	***Distal***
N (number of enteroid sections scored)	80	70	79	68	91	91	77	73
Spearman's r_s	-0.204	-0.209	0.090	-0.416	0.098	0.043	-0.102	0.131
95% confidence intervals	-0.411-0.023	-0.429-0.034	-0.141-0.311	-0.600	-0.117-0.303	-0.170-0.253	-0.325-0.132	-0.109-0.356
p value (two-tailed)	0.070	0.082	0.431	<0.001	0.357	0.685	0.379	0.271

3.5.5. Epithelial permeability of enteroids derived from proximal and distal small intestine

No difference was observed in the permeability of the epithelium of enteroids derived from proximal and distal regions of the small intestine (**Figure 3.12**). In untreated enteroids from both origins, a gradual decrease in the mean fluorescence intensity within the lumen was measured to a level approximately 80% of the starting fluorescence (100%). Both sets of enteroids responded similarly to treatment with 2 mM EGTA, showing significant, rapid reductions in mean luminal fluorescence intensity ($p < 0.05$; ANOVA). In both cases, this effect reached a plateau following a decrease of approximately 50% compared to the starting fluorescence.

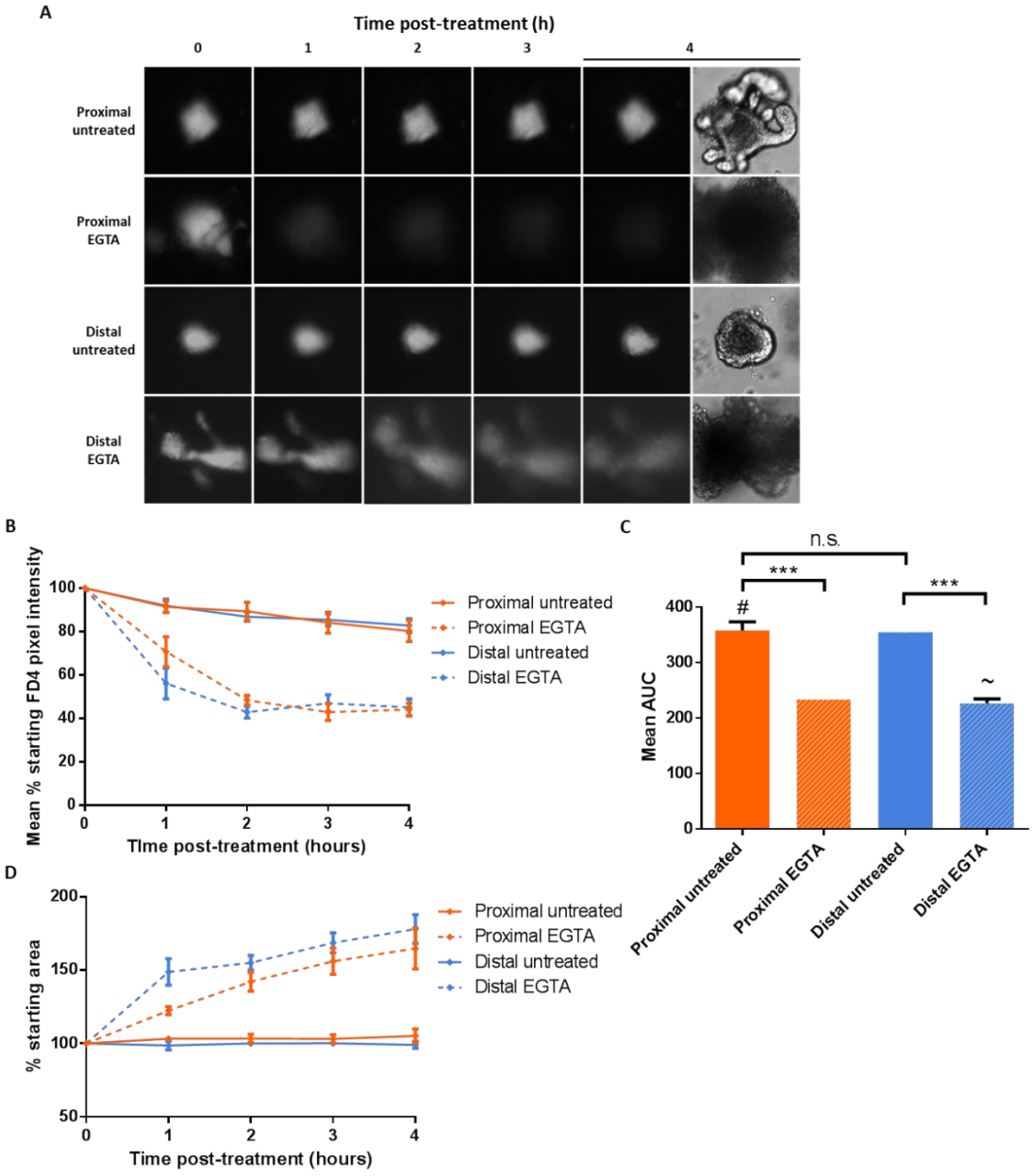

Figure 3.12. Epithelial permeability of enteroids derived from proximal and distal small intestine. (A) Representative fluorescence images of FD4-injected proximal and distal enteroids following treatment with 2 mM EGTA as indicated. Right-most panels show bright field images of enteroids 4 h post-treatment. **(B)** Quantification of the mean fluorescence intensity within the enteroid lumen at the indicated time points post-treatment. Mean intensity at each time point is shown relative to the starting mean intensity for each enteroid at 0 h (set to 100%). **(C)** Area under the curve analysis of the curves shown in (A). One-way ANOVA, ***p < 0.001, n.s. not significant, N = 4 (except groups marked #, where N = 5 and ~, where N = 3), n = 2-7 enteroids per group. **(D)** Quantification of changes in mean total enteroid area during the permeability assays. All error bars represent SEM.

3.6. Summary of results

1. Mouse enteroids derived from proximal and distal regions of the small intestine exhibit distinct gross morphologies but similar patterns of growth.

2. No differences were observed between the appearance of individual enterocytes nor the epithelium as a whole in enteroids derived from proximal and distal murine small intestine.

3. Mouse enteroids contain all the major epithelial cell types found *in vivo*. Although the absolute percentages of each cell type differ in some cases between tissue and enteroids, the pattern of differences between proximal and distal small intestinal tissue is maintained in enteroids derived from these regions.

4. Enteroids derived from proximal and distal small intestine display very similar levels of epithelial permeability.

3.7. Discussion

Enteroid cultures offer an exciting new model for investigating many aspects of the small intestine, from development to infection and ageing (Bartfeld, 2016; Dedhia *et al.*, 2016; Huch *et al.*, 2017; Hu *et al.*, 2018). The usefulness of this model has already been demonstrated in numerous recent studies. Thorough characterisation of this model system is therefore essential to understand the extent to which *in vitro* enteroids mimic conditions *in vivo*. The small intestine exhibits specialisation along its length to allow different regions to perform distinct functions. Tissue derived from the duodenum therefore exhibits different characteristics in terms of tissue architecture, but perhaps more importantly, in terms of gene expression and physiological function. Despite this, many publications currently do not specify from which region of the small intestine enteroids have been generated.

Here, we present evidence that regional specificity is retained in enteroid cultures. This is in support of a previous report that regional identity is encoded intrinsically in epithelial stem cells of the adult small intestine (Middendorp *et al.*, 2014). The authors demonstrated that location-specific transcriptomes were maintained in intestinal stem cells cultured as enteroids in the absence of tissue-derived cues. We find that enteroids derived from proximal and distal regions of the mouse small intestine show similar patterns of growth. At the ultrastructural

level, the cells in these cultures appear similar; however, we observe consistent differences in the gross morphology of these cultures. Importantly, we confirm that the distribution of differentiated epithelial cell lineages differs between proximal and distal tissue *in vivo* and that these differences are generally reflected in enteroids.

In our studies, we observe that the epithelium consistently has a different gross morphology when viewed by bright field microscopy, depending on whether enteroids are derived from proximal or distal small intestine. In distal enteroids, the epithelium frequently appears more bunched, giving the overall enteroid a raspberry-like appearance. The reason for this is unclear. As expected, we do not find notable variation in the ultrastructure of the epithelium in proximal and distal enteroids. It is therefore possible that the cause may be the different proportions of epithelial cell types found in proximal and distal enteroids.

The proportions of Paneth and goblet cells are shown here to be significantly larger in distal compared to proximal regions of the mouse small intestine *in vivo*. This is in support of previous reports that goblet cells become more abundant along the intestinal tract, correlating with increasing bacterial load towards the colon (Kim and Ho, 2010; Sekirov, Russell and Antunes, 2010). As the microbial density increases, there is a greater need for goblet cell-derived mucus to exclude them from the epithelium. These data also agree with previous findings that Paneth cell abundance increases from proximal to distal small intestine (Jones *et al*, 2018, in preparation,). Given that Paneth cells are major producers of antimicrobial peptides, it is possible that the observed increase in their numbers is also related to the rise in microbial content along the small intestine.

Our results indicate the same trends in enteroids derived from proximal and distal small intestinal tissue, with distal enteroids containing a greater proportion of goblet and Paneth cells. In distal enteroids, the distribution of Paneth cells also appeared to be less polarised, with Paneth cells found along the length of crypt buds rather than only at the crypt base. Since Paneth cells maintain the stem cell niche (Sato, van Es, *et al.*, 2011), this might indicate that stem cells in distal enteroids are also less restricted to the crypt base, which could contribute to the trend we observed of distal enteroids towards a more circular morphology.

We also find the trend for fewer enteroendocrine cells in both tissue and enteroids originating from the distal region. Any analysis of different cell types is dependent on the specificity of the markers used. Recent findings suggest that, while chromogranin A is expressed strongly in enterochromaffin cells, its expression is lower in other types that predominantly produce peptide hormones, such as gastric inhibitory peptide (Engelstoft *et al.*, 2015). This may have

resulted in an underestimate in our study of the true number of enteroendocrine cells. Current evidence indicates, however, that the markers used for the other cell lineages are robust and specific.

These findings indicate that, in addition to location-specific gene expression profiles, enteroids also maintain a location-specific composition of epithelial cell types. This is in agreement with previous reports that the abundance of goblet and Paneth cells towards the distal small intestine (Bosse *et al.*, 2006; Kim and Ho, 2010; Bevins and Salzman, 2011); however, it is not known how this is programmed. It seems likely the same factors that regulate other aspects of regional identity are involved. *Atoh1* is more highly expressed in mouse ileum than jejunum; this appears to be repressed by Gata4 since conditional mutation of *Gata4* increased *Atoh1* expression in jejunum (Bosse *et al.*, 2006). Since *Atoh1* specifies the secretory lineage (Yang *et al.*, 2001; see Section 1.1.4), this may represent a mechanism by which the Gata4 gradient regulates the increase in Paneth and goblet cells described in distal small intestine.

Alternatively, local microenvironment-derived signals in the different regions might drive immature epithelial cells towards particular lineages. Examples of this phenomenon have been described previously, including IL-13-stimulated expansion of the tuft cell population (von Moltke *et al.*, 2015) and RANKL expression by mesenchymal cells driving M cell differentiation in Peyer's patches (Nagashima, Sawa, Nitta, Tsutsumi, *et al.*, 2017). Enteroids only contain epithelial cells but a situation could be imagined where Wnt3a secretion by Paneth cells might promote further Paneth cell differentiation (van Es, Jay, *et al.*, 2005), so that enteroids derived from ileal crypts rich in Paneth cells due to other local signals go on to favour Paneth cell differentiation.

Although we find the same pattern of cell type distributions between enteroids and their parent tissues, the absolute percentages of these cell types in tissue and enteroids show some variation. For example, we find a markedly higher percentage of Paneth and enteroendocrine cells per enteroid compared to the number in a crypt-villus axis *in vivo*. This is likely due to overrepresentation of the crypt region in enteroids, although our analysis did not suggest a strong relationship between enteroid size and the proportion of most of the cell types we examined. Given that the graphs suggest that sections with more cells in total tend to have lower percentages of all the cell types, it is possible that there is a non-linear relationship between enteroid size and percentage of the different cell types that is not identified by the Spearman correlation coefficient. Middendorp and colleagues compared expression profiles of enteroid cultures to isolated crypts or villi and found that more of the genes known to be

specific to crypts were also expressed in enteroids from the same region, rather than those genes specifically expressed in villi (Middendorp *et al.*, 2014). The enteroids we used were harvested on day 7 post-seeding; enteroids cultured for longer may contain a larger villus region and more closely mimic the lower percentages of Paneth and enteroendocrine cells we observed in parallel tissue taken from the intestine. The percentages of goblet and tuft cells, in contrast, were very similar in both enteroids and intestinal tissue specimens.

Greater epithelial permeability has previously been reported in the distal compared to the proximal small intestine (Loehry and Parrish, 1970; Ross, Rubin and Deren, 1972; Collins *et al.*, 2017). This is based, however, on a variety of measurement techniques that may actually refer to different definitions of intestinal permeability. Most tests examine flux of a labelled molecule, for example a sugar or ion, across the epithelium, either *in vivo* or in explant tissue mounted in Ussing chambers; however, each test may describe a different property of the epithelium, since the pathways by which these different molecules cross the epithelium probably differ (Bischoff *et al.*, 2014). Here, we were interested in permeability or 'leakiness' of the epithelium to flux of a large molecule via the paracellular pathway. We observe no difference in permeability of the epithelium in proximal and distal enteroids to 4 kDa FITC-dextran. Most comparable to our data is a report of increasing FITC-dextran flux and transepithelial conductance in tissue from duodenum to ileum of BALB/c mice that received a sham ovariectomy prior to culture in Ussing chambers. The disparity with our observations may arise from differences in the protocols, with data from Ussing chamber experiments frequently found not to correlate with other permeability assays (Bischoff *et al.*, 2014).

An important consideration is that the maintenance of regional identity in enteroid cultures may be dependent on culture conditions. The only studies that have previously examined regional identity in enteroids used culture conditions very similar to our own for murine enteroids, including R-spondin, Noggin and EGF. Other protocols include Wnt through the use of conditioned media generated by L-WRN cells, which secrete R-spondin-3, Noggin and Wnt3a (Miyoshi and Stappenbeck, 2013). The use of commercial growth media, such as IntestiCult (STEMCELL Technologies, Cambridge, UK), for which the formulation is not publicly available, is also increasing. Altered growth factor concentrations may affect many aspects of enteroid cultures, including their cell type composition and maturity of differentiated cells. Indeed, addition of Wnt3a to murine enteroids results in spherical rather than budding enteroids, probably due to enhanced proliferation, and expression of differentiation markers, such as duodenum-specific *Sis* (encoding sucrose isomaltase) and ileum-specific *Slc10a2*, is decreased (Middendorp *et al.*, 2014). Regional patterns of *Gata4* expression were conserved after Wnt3a

treatment, however, suggesting that intrinsic regional programming was preserved (Middendorp *et al.*, 2014). Interestingly, intestinal organoids derived from induced pluripotent stem cells, another recently developed 3D intestinal model, contain both *GATA6*$^{+}$/*GATA4*$^{+}$ cells and *GATA6*$^{+}$/*GATA4*$^{-}$ cells, indicating that they contain a mixture of cells more similar to either duodenum or ileum (Spence *et al.*, 2011). The characterisation performed here may therefore not be applicable to enteroids cultured using alternative protocols.

Overall, the data presented here support a growing body of evidence demonstrating that enteroids are a highly physiologically representative model system. They suggest that the location within the small intestine from which murine enteroids are derived impacts on their physiology and function. The origin of tissue used for establishing enteroids should therefore be a consideration in experimental design as different regions may be more appropriate depending on the research question. Ideally, future publications should detail the regional origin of adult stem cell-derived enteroids as this information may be pertinent to the interpretation of results.

Chapter 4

Direct effects of gliadin-derived peptides on an enteroid model of the small intestinal epithelium

4.1. Introduction

Gliadin is the soluble protein component of gluten and is found in cereals including wheat, rye and barley (Wieser, 2007). Whereas most dietary proteins are rapidly broken down by proteases in the small intestine, gliadin is resistant to digestion because of its high proline content (Shan, 2002). As a result, relatively large fragments of gliadin survive digestion and are available to interact with the epithelium. Gliadin is pertinent to human health because it triggers coeliac disease in a subset of genetically susceptible individuals who carry HLA-DQ2 and/or HLA-DQ8 risk alleles (Meresse, Malamut and Cerf-Bensussan, 2012). This chronic condition causes gastrointestinal symptoms, including diarrhoea, constipation, malnutrition and abdominal pain due to bloating (Schuppan, Junker and Barisani, 2009), in addition to extra-intestinal symptoms and an increased risk of small bowel cancer and lymphoma (Leffler, Green and Fasano, 2015). Coeliac patients usually have elevated serum levels of anti-tissue transglutaminase 2 (TG2) and anti-endomysial autoantibodies, which are used as part of diagnosis; however, there are also patients who are serologically and histologically negative for coeliac disease but who report symptoms shortly after intake of gluten (Rej, Aziz and Sanders, 2019). This appears to represent a range of disorders, including non-coeliac wheat sensitivity/non-coeliac gluten sensitivity (NCWS/NCGS) and wheat-sensitive irritable bowel syndrome (IBS). There are several candidates, including gluten, for the causative dietary component in these conditions but their pathophysiology is still poorly understood.

The activities of gliadin-derived peptides in the small intestine are not yet fully understood. There is also no consensus on whether or how they access the small intestinal tissue. Based on available data, some researchers have suggested that there are two classes of gliadin peptides: ‘immunogenic’ and ‘cytotoxic’ peptides (Ciccocioppo, Di Sabatino and Corazza, 2005). The action of immunogenic peptides is the better understood and accepted. It is known that glutamine residues within gliadin peptides are modified by tissue transglutaminase 2 to become negatively charged glutamic acid (Di Sabatino *et al.*, 2012). This makes certain peptides preferential ligands for the HLA-DQ2 and -DQ8 molecules, which are expressed on antigen-presenting cells. The 33-mer fragment, which spans amino acids 56-88, and a subsection consisting of amino acids 56-68 (P56-68) are frequently described examples of ‘immunogenic’ peptides (Shan, 2002). T cells reactive to gliadin peptides in complex with these molecules have been detected in coeliac patients (Anderson *et al.*, 2000; Arentz-Hansen *et al.*, 2000; Camarca *et al.*, 2009). In this way, immunogenic gliadin peptides drive an inflammatory adaptive immune response that causes damage to the intestinal epithelium in the form of crypt hyperplasia and characteristic villus atrophy.

The role and mechanism of action of 'cytotoxic' gliadin peptides are less well-defined. The archetypal example of a cytotoxic peptide is the fragment spanning amino acids 31-43 (P31-43). Previous studies examining the actions of P31-43 on the intestinal epithelium have mostly been conducted using epithelial cell line models, with effects reported that include cytoskeletal rearrangement (Clemente *et al.*, 2003), increased secretion of cytokine IL-15 (Maiuri *et al.*, 2003), increased expression of tight junction regulator zonulin (Lammers *et al.*, 2008), and growth-promoting activities via interference with trafficking of epidermal growth factor receptor (EGFR) (Barone *et al.*, 2007, 2010, 2011). These reports indicate that gliadin P31-43 is capable of activating innate immune pathways in the epithelium, independently of adaptive immune activation.

Given that such cytotoxic activities are not dependent on the adaptive immune system, they would be equally relevant to individuals who do not carry coeliac HLA risk alleles. In recent years there has been growing interest from clinicians regarding NCWS/NCGS, which is characterised by intestinal symptoms similar to those seen in IBS and extra-intestinal symptoms that include headaches and fatigue (Volta *et al.*, 2015; Gibson, Skodje and Lundin, 2017). Furthermore, studies have estimated that one third of IBS patients may be gluten-sensitive, which could represent an overall prevalence of approximately 3% of the population (Catassi *et al.*, 2017).

No studies have previously been conducted to investigate the effect of gliadin-derived peptides in enteroids. In this context, enteroids offer several advantages. Firstly, the enteroid epithelium consists of a heterogeneous population of stem cells and differentiated intestinal epithelial cells, making it more complex and physiologically representative than 2D intestinal cell lines; secondly, enteroids offer the ability to study the epithelium in isolation from immune components; thirdly, the 3D structure of enteroids with an enclosed lumen equivalent to the gut lumen affords the opportunity to investigate paracellular and transcellular translocation across the epithelium, since the apical and basolateral compartments are separated and both are accessible (the former albeit via microinjection).

4.2. Hypothesis

Peptide fragments of α-gliadin will have direct effects on intestinal epithelial homeostasis.

4.3. Aim

To investigate whether peptide fragments of α-gliadin directly modulate the small intestinal epithelium in an enteroid model, including:

1. Perturbation of intestinal epithelial permeability

2. Alteration of intestinal epithelial cell viability and barrier integrity

4.4. Methods

Enteroid culture

All experiments in this chapter were performed using enteroids derived from the distal region of the small intestine. Enteroids were selected as an appropriate model because coeliac disease affects almost exclusively the small intestine.

Assessment of epithelial permeability in enteroids following incubation with gliadin peptides

Permeability of the enteroid epithelium following treatment with gliadin peptides was assayed using a fluorescent dye-based method based on a previously described method. A detailed description of the method may be found in Section 2.10. Briefly, a 4 kDa FITC-conjugated dextran (FD4) was microinjected into the lumen of enteroids suspended within a Matrigel matrix. Peptide fragments of α-gliadin were then added to the enteroid media. Two gliadin peptides (P31-43 and P56-68) were synthesised with N-terminal fluorenylmethyloxycarbonyl (Fmoc) protecting group by GenScript (New Jersey, USA) as previous findings from our research group had indicated that whole-gliadin peptic-tryptic digest contained unacceptably high levels of the endotoxin LPS (personal communication; Dr Carrie Duckworth, University of Liverpool, UK) that would have had confounding effects in planned experiments involving co-culture of enteroids with immune cells, known to be activated by LPS (Alexander and Rietschel, 2001). The sequences and sizes of synthesised gliadin peptides are described in **Table 4.1**. Fluorescence and bright field images were used to monitor the decreasing intensity of fluorescence remaining in the lumen over time.

Table 4.1. Details of the two peptide fragments of α-gliadin synthesised using Fmoc-based solid-phase chemistry.

Peptide	*Length*	*Amino acid (aa) sequence*	*Molecular weight*
P31-43	13 aa	Fmoc-LGQQQPFPPQQPY	1749.93
P56-68	13 aa	Fmoc-LQLQPFPQPQLPY	1791.06

Assessment of epithelial cell viability in response to gliadin peptides

Cell death by apoptosis was investigated by immunohistochemical staining with an antibody specific for the active form of the cysteine-aspartic acid protease, caspase 3. This antibody binds the p17 subunit of caspase 3, generated by proteolytic processing of an inactive precursor in cells undergoing apoptosis (Han *et al.*, 1997). Enteroids were fixed following 24 hours of treatment with 100 µg/mL gliadin P31-43 or P56-68. This time point was selected because others in our group had previously shown that significant apoptosis is induced in enteroids following 24 hours of treatment with another apoptotic stimulus, TNF-α (manuscript in preparation, Dr Carrie Duckworth). Paraffin-embedded sections of enteroids were analysed by immunohistochemical staining, a detailed protocol for which may be found in Section 2 .7.

Investigation of the effect of gliadin peptides on tight junction integrity

Since tight junctions are known to regulate epithelial permeability (Zihni *et al.*, 2016) and certain dietary components may regulate intestinal permeability (Ulluwishewa *et al.*, 2011), tight junction structure was investigated using immunofluorescence microscopy and TEM following exposure to gliadin peptides. Regulation of epithelial permeability can occur through redistribution of component proteins away from the tight junction, so localisation of key junctional proteins, occludin and ZO-1, was investigated using the Caco-2 cell line. This allowed for ease of observation of cell-cell junctions in cells spread out as 2D monolayers.

Caco-2 cells are a human colon carcinoma colonocyte cell line that undergo differentiation when cultured as a monolayer to adopt characteristics similar to those of small intestinal enterocytes (Sambuy *et al.*, 2005). Cells were seeded on sterile 13 mm glass coverslips in a 24-well plate at 2.5 x 10^5 cells per well and cultured to full differentiation for 15-18 days. Cells were incubated with 100 µg/mL gliadin P31-43 or P56-68, or equivalent volume of vehicle (0.2% DMSO) for 2 hours at 37°C. Monolayers were then washed twice with warm, sterile PBS and fixed with 4% w/v PFA in PBS for 10 minutes at room temperature. Localisation of occludin and ZO-1 was then examined by immunofluorescence staining as described in Section 2.8. TEM

was performed as described in Section 2.12 and used to examine the ultrastructure of cell-cell junctions in enteroids incubated for 2 hours with 100 µg/mL gliadin P31-43 or P56-68.

Assessment of enteroid swelling as a result of epithelial chloride secretion in response to gliadin peptides

Enteroid swelling was assessed using enteroid surface area – determined from bright field microscopy – as a surrogate measure for enteroid volume. This assay is described in detail in Section 2.11. On the second day post-seeding, enteroids were incubated with 25-100 µg/mL P56-68 or 100 µg/mL P31-43, in the presence or absence of CFTR inhibition by CFTR-inh-172, and monitored by bright field microscopy for up to 4 hours. Controls were treated with the highest concentration of vehicle (0.3% v/v DMSO).

For time-lapse videos, enteroids were seeded as above in a 48-well tissue culture plate. On day 2 or 3 post-seeding, enteroids were treated with vehicle control (DMSO), 100 µg/mL P31-43 or 100 µg/mL P56-68. Enteroids were observed for at least 12 hours post-treatment using a CytoSMART 2 in-incubator imaging system (CytoSMART Technologies, Eindhoven, The Netherlands). Images were collected at 5-minute intervals.

4.5. Results

4.5.1. Gliadin-derived peptide P56-68 appears to increase epithelial permeability in enteroids

4.5.1.1. Baseline epithelial permeability is similar in enteroids derived from wild type C57BL/6 and BALB/c mouse strains and transgenic *Nfkb2*$^{-/-}$ mice

Differences have been reported in the sensitivity of peritoneal macrophages isolated from C57BL/6 and BALB/c mouse strains to gliadin and its peptide fragments, with BALB/c mice showing lower responsiveness (Tucková *et al.*, 2002). *Nfkb2*$^{-/-}$ mice (on a C57BL/6 background) show reduced sensitivity to permeability-enhancing stimuli, such as LPS and TNF (Williams *et al.*, 2013). Epithelial permeability was therefore investigated in untreated enteroids derived from each of these three mouse strains to determine any intrinsic differences. In all three strains, the amount of FD4 within the lumen remained relatively constant over 4 hours, as observed by fluorescence imaging (**Figure 4.1 A**). No significant difference was identified between the areas under the curve (AUC) for enteroids generated from each strain, indicating that they exhibit similar rates of loss of luminal fluorescence intensity (**Figure 4.1 B**).

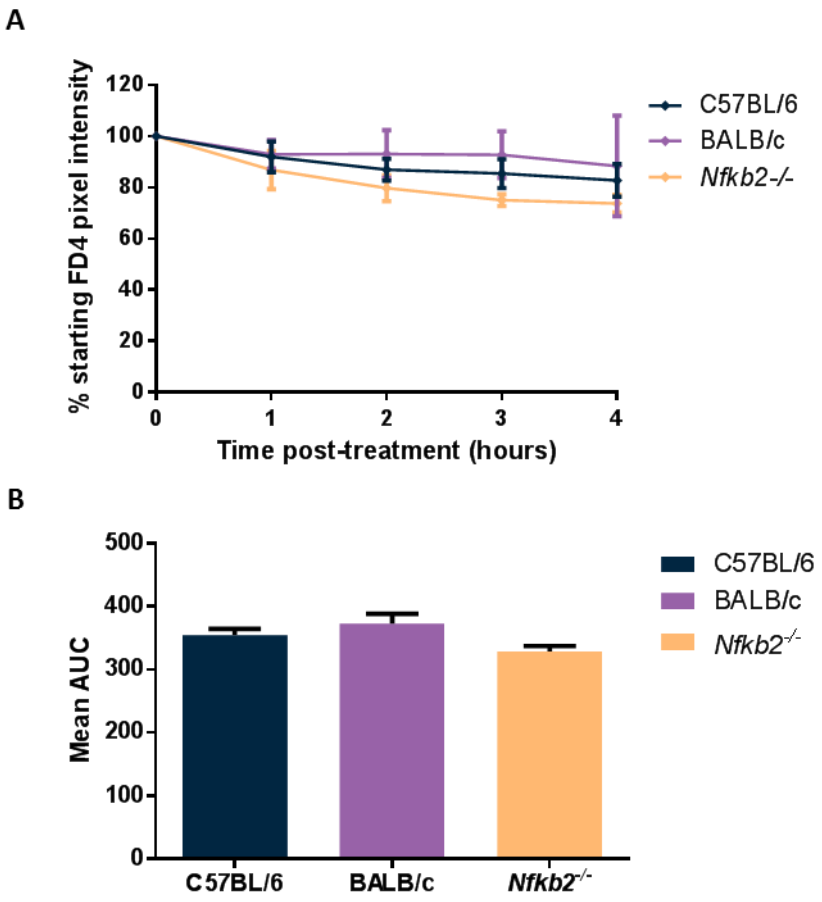

Figure 4.1. Enteroids derived from C57BL/6, BALB/c and *Nfkb2*$^{-/-}$ mouse strains display similar levels of epithelial permeability at baseline. (A) Comparison of the loss of fluorescence intensity from the lumen of untreated enteroids derived from C57BL/6, BALB/c and *Nfkb2*$^{-/-}$ mice. Error bars represent SEM. **(B)** AUC analysis of data series shown in (A). No significant differences were found as assessed by one-way ANOVA; N = 4, 5, 3 for C57BL/6, BALB/c and *Nfkb2*$^{-/-}$ respectively, n = 2-5 enteroids per group. All error bars represent SEM.

4.5.1.2. Gliadin-derived peptide P56-68 appears to increase epithelial permeability in BALB/c enteroids

Given that altered intestinal permeability has been reported in coeliac patients (Schumann *et al.*, 2017), the effect of the two 13-aa gliadin peptides, P31-43 and P56-68, on epithelial permeability was investigated in murine enteroids to ascertain whether each might affect permeability via a direct interaction with the epithelium. In BALB/c enteroids that were either untreated, treated with vehicle control (0.2% v/v DMSO), or treated with 100 µg/mL P31-43, the amount of FD4 within the lumen remained relatively constant over 4 hours, as observed by fluorescence imaging (**Figure 4.2 A & B**). No significant difference was determined between the AUC for enteroids treated with P31-43 compared to vehicle-treated control enteroids (**Figure 4.2 C**). As expected, treatment with 2 mM EGTA resulted in a rapid loss of fluorescence intensity from the lumen ($p < 0.001$ compared to untreated control; ANOVA, N = 6, n = 2-6 enteroids per group), likely due to its calcium chelating activity, which disrupts Ca^{2+}-dependant E-cadherin cell-cell interactions within tight junctions (Kim *et al.*, 2011). A significant decrease in AUC, indicating a greater rate of fluorescence loss, was also observed in enteroids treated with 100 µg/mL P56-68 compared to vehicle control ($p < 0.05$; ANOVA, N = 6, n = 2-6). Although the magnitude of the effect was slightly smaller, the time course of the effect was similar to that observed following treatment with 2 mM EGTA.

4.5.1.3. Gliadin-derived peptide P56-68 appears to increase epithelial permeability in wild type C57BL/6 enteroids

The effect of gliadin P56-68 does not appear to be strain-specific as similar results were observed in wild type C57BL/6 enteroids. C57BL/6 enteroids incubated with vehicle control (DMSO) or 100 µg/mL P31-43 showed little change in luminal fluorescence intensity over 4 hours post-treatment (**Figure 4.3 A & B**). Treatment with both 2 mM EGTA and 100 µg/mL P56-68 again caused significant loss of mean FITC fluorescence pixel intensity from the enteroids (**Figure 4.3 C**). This effect was rapid, with the greatest decrease occurring by 2 hours after treatment. After 2 hours, mean luminal pixel intensity stabilised. The magnitude of these changes was similar to those observed in BALB/c enteroids (**Figure 4.2**).

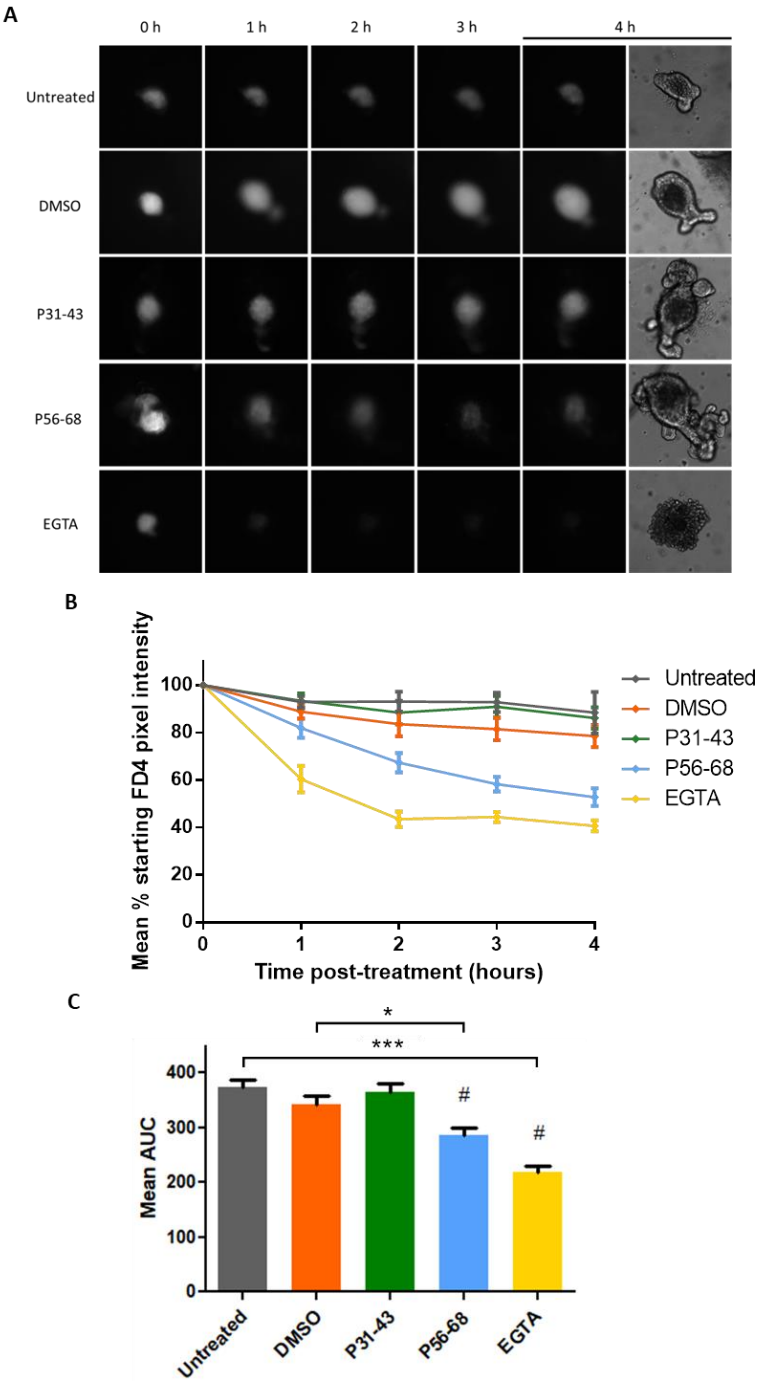

Figure 4.2. Gliadin-derived peptide P56-68 appears to increase epithelial permeability in BALB/c enteroids. (A) Representative images showing luminal FD4 fluorescence in enteroids derived from BALB/c mice at the indicated time points following treatment with vehicle control (0.2% v/v DMSO), 100 µg/mL gliadin P31-43 or P56-68, or 2 mM EGTA. The right-most panel shows corresponding bright field images of the enteroids 4 h post-treatment. **(B)** Quantification of the mean fluorescence intensity within the enteroid lumen at the indicated time points post-treatment. Intensity at each time point, for each enteroid, was measured relative to its intensity at 0 h (set to 100%). **(C)** Data shown in panel (B) calculated as mean area under the curve. Significant differences determined by one-way ANOVA; *p < 0.05, ***p < 0.001, N = 5 (except groups marked #, for which N = 6), n = 2-6 enteroids per group. All error bars represent SEM.

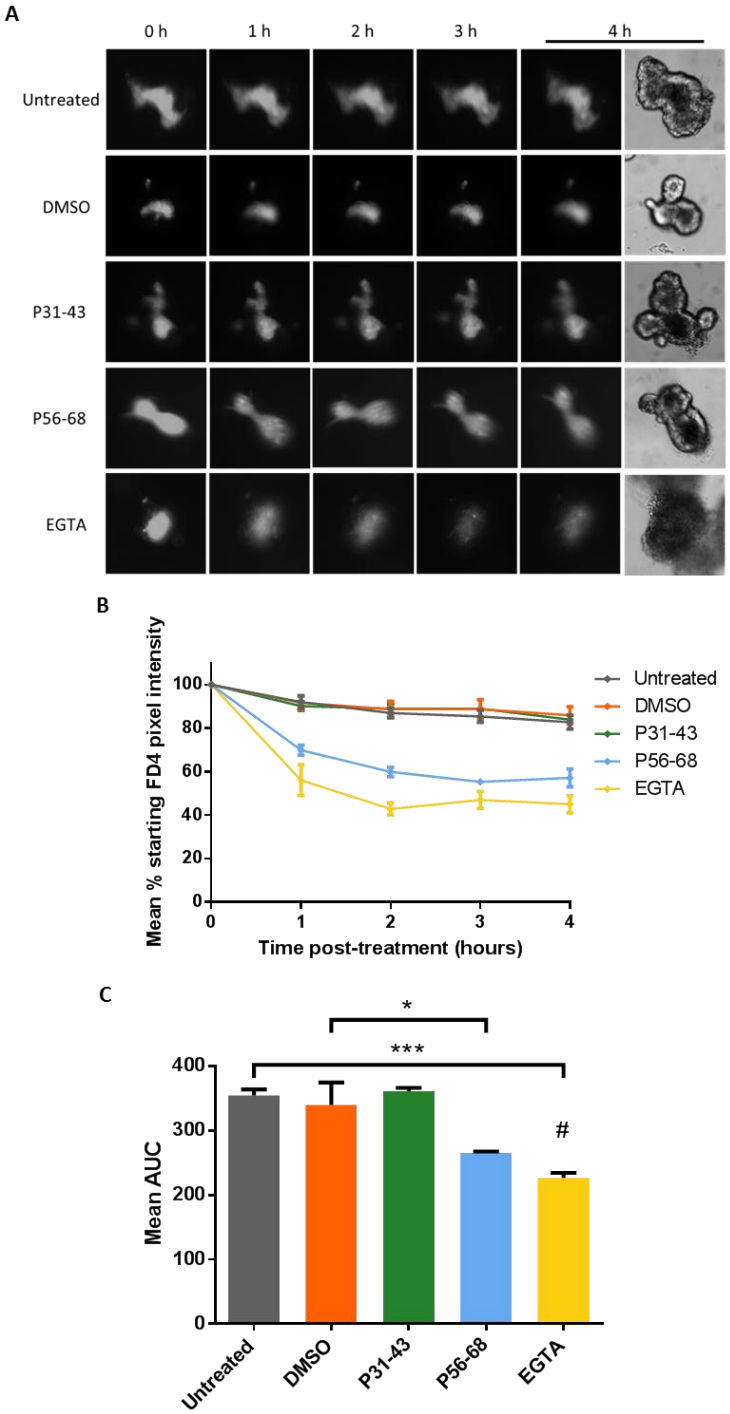

Figure 4.3. Gliadin-derived peptide P56-68 appears to increase epithelial permeability in C57BL/6 enteroids. (A) Representative images showing luminal FD4 fluorescence in enteroids at the indicated time points following treatment with gliadin peptides or 2 mM EGTA. The right-most panel shows the corresponding bright field images of enteroids 4 h post-treatment. **(B)** Quantification of the mean fluorescence intensity within the enteroid lumen at the indicated time points post-treatment. Intensity at each time point for each enteroid was measured relative to its intensity at 0 h (set to 100%). Error bars represent SEM. **(C)** Data shown in panel (B) calculated as mean area under the curve. Significant differences determined by one-way ANOVA; *$p < 0.05$, ***$p < 0.001$, N = 4 (except group marked with #, for which N = 3), n = 2-5 enteroids per group. Error bars represent SEM.

4.5.1.4. Gliadin-derived peptide P56-68 appears to increase epithelial permeability in Nfkb2$^{-/-}$ enteroids

In enteroids derived from *Nfkb2*$^{-/-}$ mice bred on a C57BL/6 background, treatment with 100 µg/mL gliadin P56-68 also resulted in a significant loss of luminal fluorescence intensity compared to vehicle control (**Figure 4.4 A-C**). Whereas mean luminal pixel intensity declined to approximately 60% of its initial value in wild type C57BL/6 enteroids, the decrease in *Nfkb2*$^{-/-}$ enteroids was observed to be approximately 70%. The initial rate of change in *Nfkb2*$^{-/-}$enteroids appeared to be lower, with mean fluorescence intensity only beginning to plateau at 4 hours post-treatment rather than 2 hours as seen in wild type strains (**Figure 4.4 B**). Again, 100 µg/mL gliadin P31-43 had no effect on the rate of fluorescence loss from the enteroid lumen (**Figure 4.4 A-C**). *Nfkb2*$^{-/-}$ enteroids appear to be less sensitive to P56-68-induced loss of FD4 fluorescence (**Figure 4.4 D**).

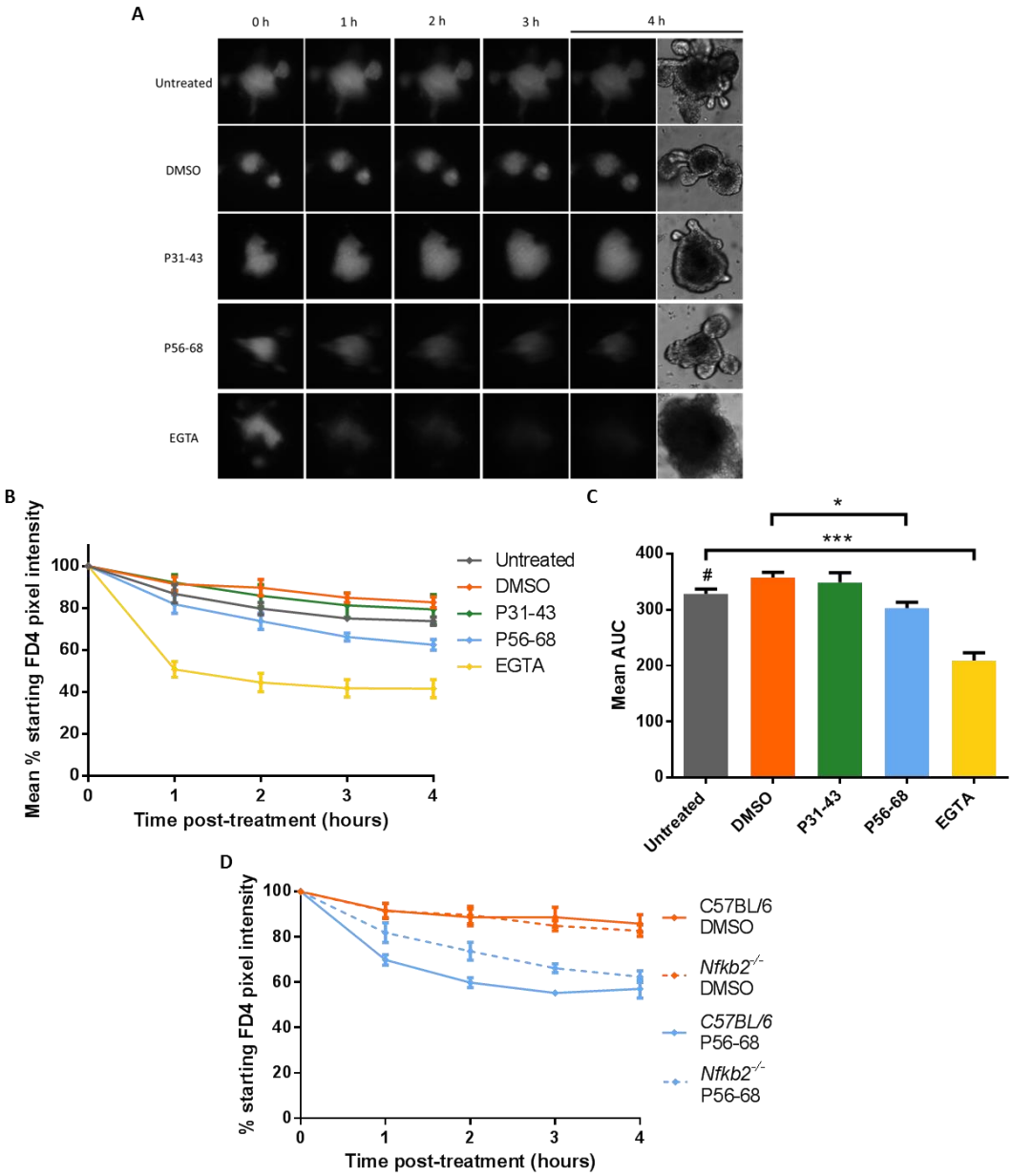

Figure 4.4. Gliadin-derived peptide P56-68 appears to increase epithelial permeability in *Nfkb2*$^{-/-}$ enteroids. (A) Representative images showing luminal FD4 fluorescence in enteroids derived from transgenic *Nfkb2*$^{-/-}$ mice (bred on a C57BL/6 background) at the indicated time points following treatment with vehicle control (0.2% v/v DMSO), 100 µg/mL gliadin P31-43 or P56-68, or 2 mM EGTA. Right-most images show corresponding bright field images of enteroids 4 h post-treatment. **(B)** Quantification of mean fluorescence intensity within enteroid lumen at the indicated time points post-treatment. Intensity at each time point for each enteroid was measured relative to its intensity at 0 h (set to 100%). **(C)** Data shown in panel (B) calculated as area under the curve. Significant differences as determined by one-way ANOVA; *p < 0.05, ***p < 0.001, N = 4 (except group marked #, for which N = 3), n = 2-7 enteroids per group. **(D)** Comparison of luminal FD4 fluorescence in vehicle-treated controls and P56-68-treated enteroids derived from C57BL/6 and *Nfkb2*$^{-/-}$ mouse strains (data from panel (B) and Figure 4.3). All error bars represent SEM.

4.5.2. Effects of gliadin-derived peptides on epithelial cell viability

There is a high rate of cell turnover in the intestine, regulated by proliferation, apoptosis and cell shedding. In enteroids, shed apoptotic cells are observed to accumulate within the enclosed lumen during growth. In enteroids exposed only to 0.2% DMSO vehicle control for 24 hours, some apoptotic cells – marked by positive staining of active caspase 3 – were visualised within the enteroid lumen (**Figure 4.5 A**). As expected, staining was found throughout the cytoplasm of these cells. Some cellular debris was also apparent within the lumen, such as cell fragments with no discernible nucleus. Also apparent in the lumen was the presence of cell debris, such as cell fragments with no discernible nuclei. Cells positive for active caspase 3 were rarely observed within the epithelium of vehicle-treated control enteroids. Following treatment for 24 hours with 100 µg/mL gliadin peptides P31-43 (**Figure 4.5 B**) or P56-68 (**Figure 4.5 C**), the number of apoptotic cells within the lumen did not appear to be increased across more than 20 enteroid sections. There was also no increase in the occurrence of positively stained cells within the epithelium of gliadin peptide-treated enteroids compared to vehicle-treated controls.

Even in untreated enteroids, cells undergoing apoptosis may be observed within the enteroid lumen by TEM, having been shed from the epithelium (**Figure 4.6 A**). Apoptotic cells may be distinguished by several features, including: dense cytoplasm, nuclear fragmentation or complete breakdown of the nuclear membrane, disintegration of organelles and blebbing of the plasma membrane. No evidence of apoptosis was observed within cells of the epithelial monolayer of C57BL/6 enteroids incubated for 2 hours with vehicle control, 100 µg/mL gliadin P31-43 or 100 µg/mL P56-68 (**Figure 4.6 B**). In two gliadin peptide-treated enteroids observed, the overall structure of the epithelium appeared normal. The nuclear membranes remained intact with no signs of increased chromatin condensation. Across the different treatments examined, organelles such as mitochondria, endoplasmic reticulum and Golgi were visible and displayed normal architecture.

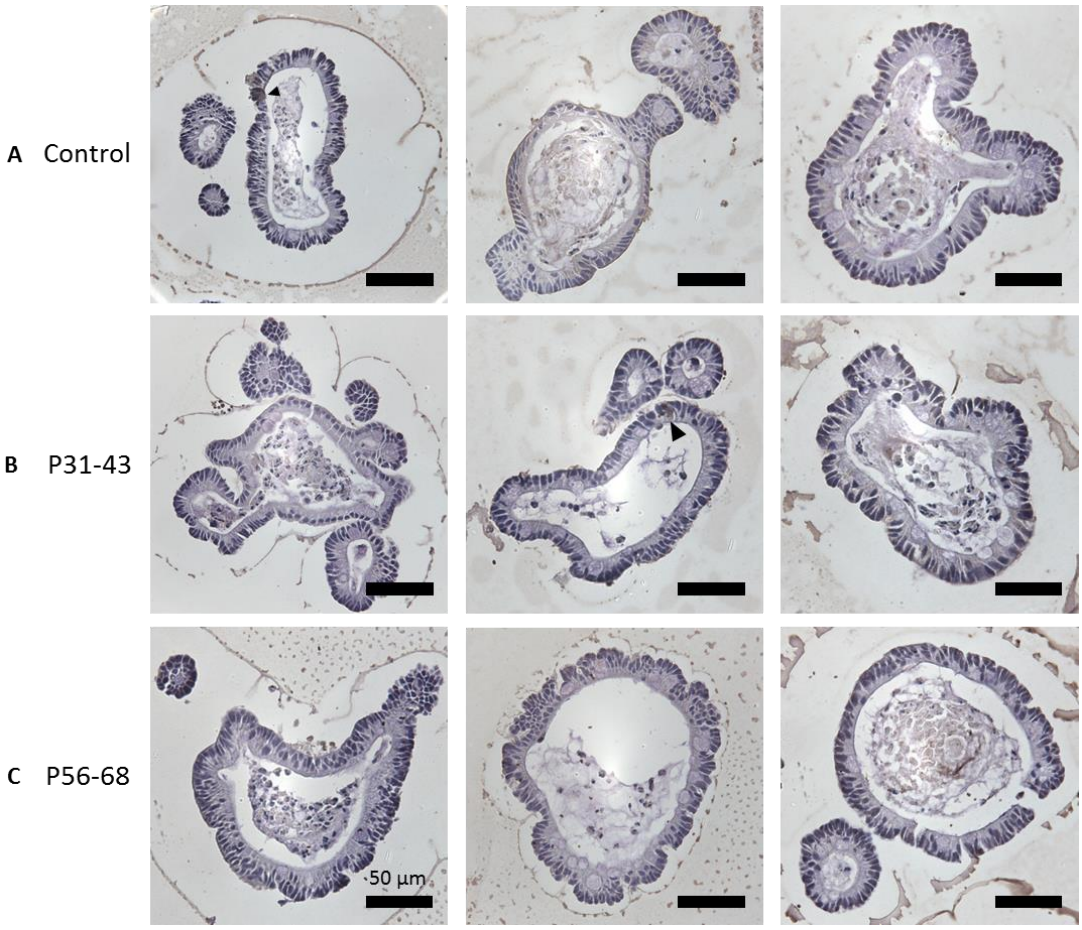

Figure 4.5. Effects of gliadin-derived peptides on epithelial cell death as assessed by active caspase 3 immunohistochemistry. Representative images of sections of C57BL/6 enteroid treated for 24 h with **(A)** vehicle control (0.2% v/v DMSO), **(B)** 100 µg/mL gliadin P31-43, or **(C)** 100 µg/mL gliadin P56-68 with immunohistochemical staining for active caspase 3. Arrow heads indicate examples of individual positively stained cells within the enteroid epithelial monolayer. All scale bars = 50 µm.

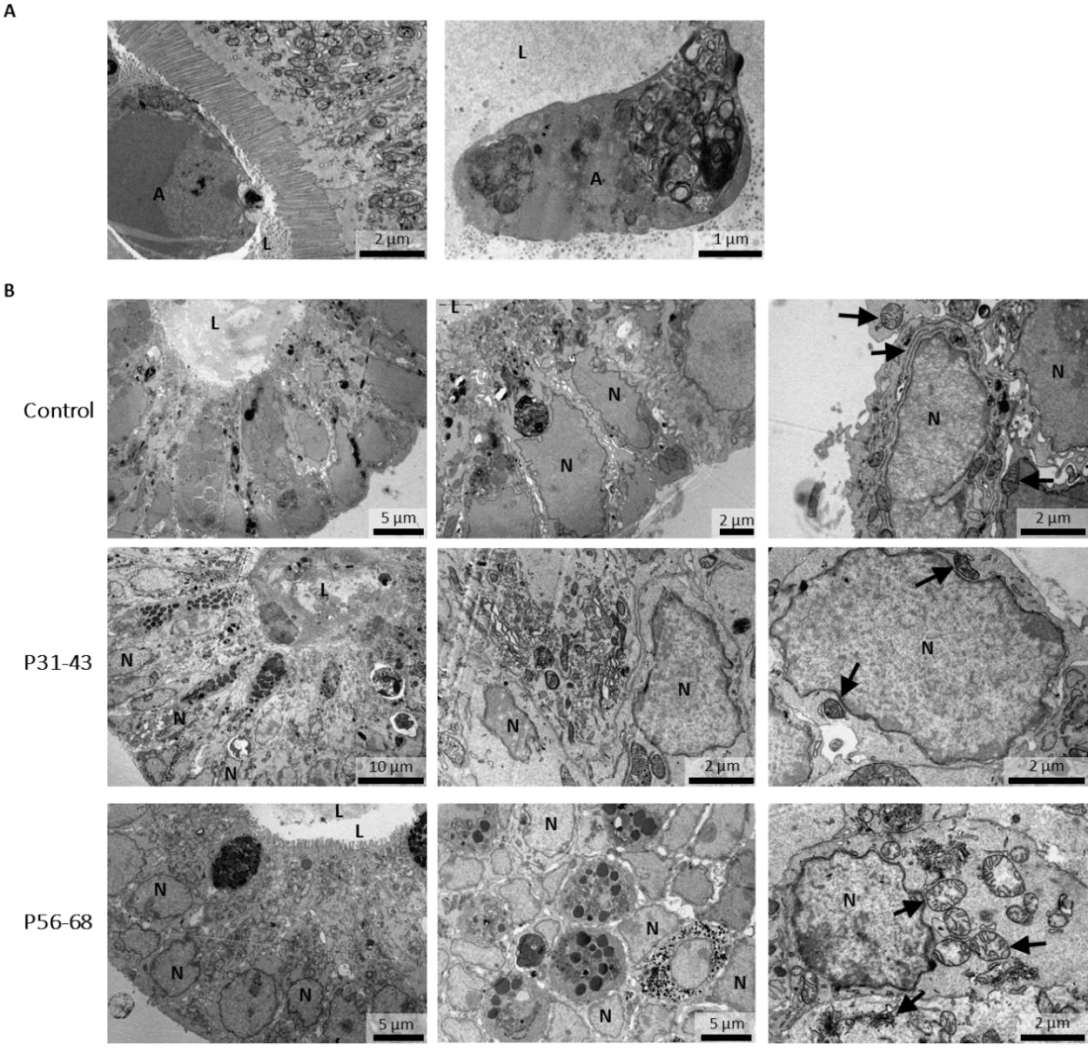

Figure 4.6. Enteroids do not show ultrastructural evidence of reduced viability following treatment with gliadin peptides. (A) TEM images showing apoptotic cells within the lumen of untreated enteroids. In the left image, the apical surface of the epithelium is also visible. **(B)** Representative TEM images of enteroids treated for 2 h with vehicle control or 100 µg/mL gliadin peptides P31-43 or P56-68. Left column shows low magnification overviews of the epithelium. Middle column shows examples of cell nuclei with a healthy appearance. Right column shows high power images of healthy-looking cell nuclei and intact organelles, including mitochondria. Arrows indicate healthy-looking organelles, including mitochondria, endoplasmic reticulum and Golgi apparatus. All scale bars are as indicated. L, lumen; A, apoptotic body; N, nucleus.

4.5.3. Effects of gliadin-derived peptides on cell-cell junctions

4.5.3.1. Gliadin-derived peptides do not alter ultrastructure of cell-cell junctions

Transmission electron microscopy was used to examine changes to cell-cell junctions in the enteroid epithelium in response to gliadin-derived peptides 2 hours post-administration, when changes in permeability in response to gliadin P56-68 were apparent (**Figure 4.2, Figure 4.4**). Enteroids derived from both proximal and distal SI were examined by TEM following 2 hours of treatment with vehicle, P31-43 or P56-68. Since the crypt and villus regions of the intestinal epithelium are structurally and functionally distinct, sections taken from both areas of enteroids were examined.

In all samples, some spaces were observed along the boundary between cells. These were flanked by areas of very close contact. In all samples, cells were tightly held together at the apical surface of the epithelium, where tight junctions are located (**Figure 4.7**). No differences were observed in the appearance of tight junctions in the enteroids treated with gliadin-derived peptides compared to the vehicle control.

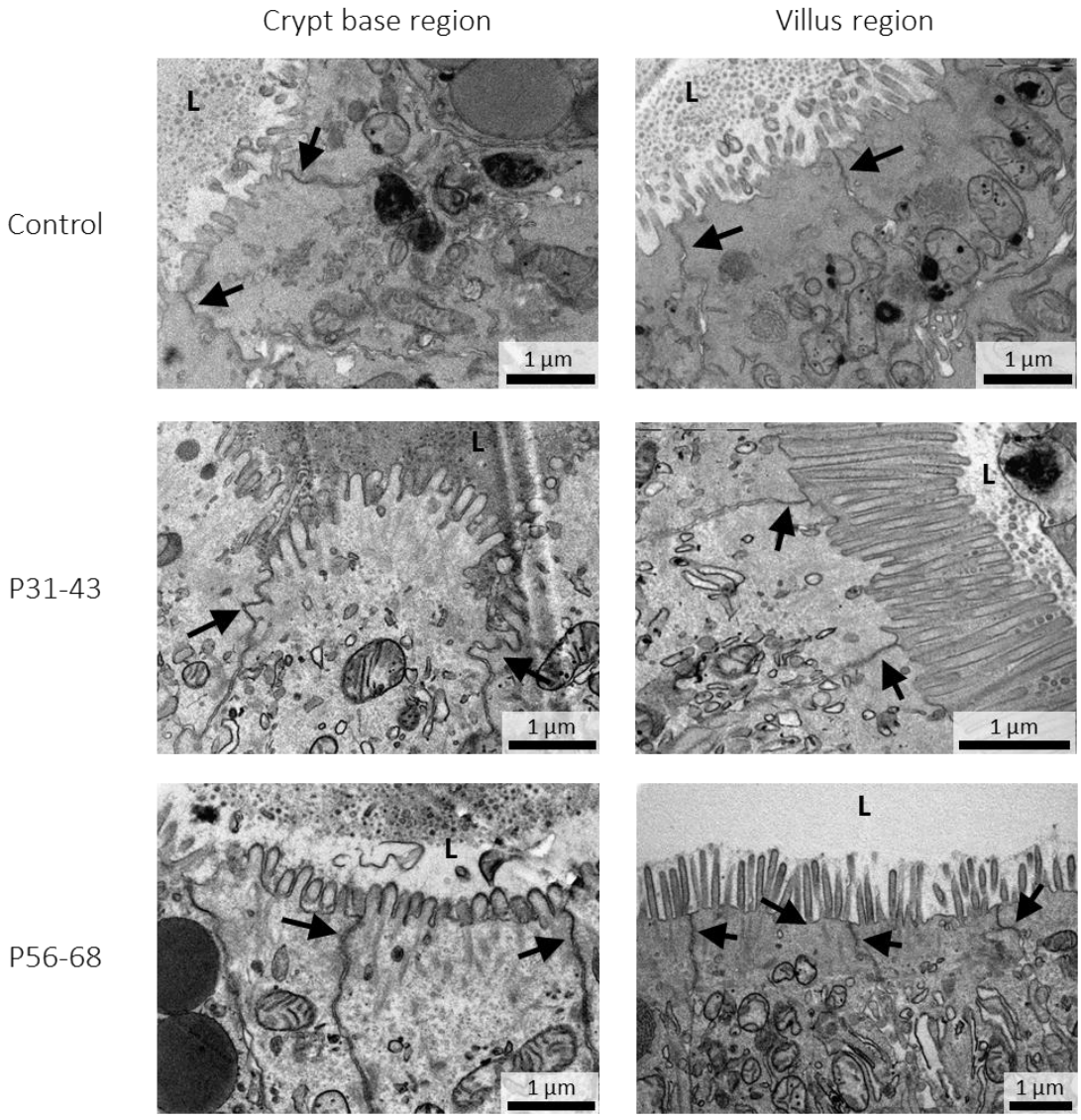

Figure 4.7. Gliadin-derived peptides do not disrupt ultrastructure of cell-cell junctions. Representative TEM images of enteroids following treatment for 2 h with vehicle control (0.2% v/v DMSO) or 100 µg/mL gliadin peptides P31-43 or P56-68. As shown in left and right columns, cell-cell junctions were examined both in crypt base and villus regions of the enteroids. Arrows indicate location of tight junctions. All scale bars correspond to 1 µm.

4.5.3.2. Gliadin-derived peptides do not cause rearrangement of tight junction proteins in differentiated Caco-2 cell monolayers

Tight junctions are known to regulate epithelial permeability (Zihni *et al.*, 2016) and may be regulated by redistribution of junctional proteins away from the cell-cell border (Clayburgh *et al.*, 2005). Furthermore, rearrangement of the actin cytoskeleton, which also regulates

tight junction integrity, has been reported in response to gliadin peptides in rat intestinal epithelial (IEC-6) cells (Clemente *et al.*, 2003). Localisation of key tight junction proteins, occludin and zonula occludens 1 (ZO-1), was therefore investigated as a potential mechanism for increased epithelial permeability following exposure to gliadin peptides. Since it is easier to visualise cell-cell junctions in 2D cell culture, differentiated Caco-2 cell monolayers were used. As the monolayer forms, Caco-2 cells undergo differentiation to adopt a phenotype similar to that of small intestinal enterocytes. Analysis of monolayer transepithelial electrical resistance (TEER) demonstrated that TEER increased over 15-18 days in culture, consistent with full differentiation of the Caco-2 monolayers (Roberts *et al.*, 2010) (**Figure 4.8**).

Following treatment for 2 hours with vehicle control, 100 µg/mL P31-43 or 100 µg/mL P56-68, no difference was observed in the localisation of ZO-1 (**Figure 4.9 A**) or occludin (**Figure 4.10 B**). As expected, both ZO-1 and occludin were observed along the cell-cell junctions. The distribution pattern of both proteins varied within each treatment group. In some regions within in all groups, a double line was visible at the cell-cell junction; in others, the smoothness of the line of the cell junctions varied.

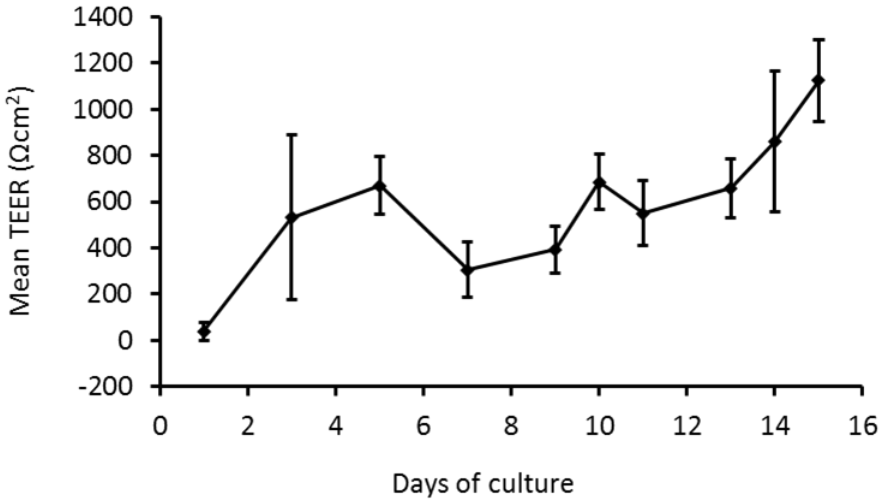

Figure 4.8. Caco-2 cells differentiate to form intact monolayers as assessed by TEER analysis. Transepithelial electrical resistance of Caco-2 cell monolayers cultured on Millicell culture inserts for up to 15 days. Background readings recorded from an unseeded insert incubated in media were subtracted from the raw TEER values. Values shown are multiplied by the area of the Millicell polycarbonate membrane (0.6 cm^2). Data represent mean TEER recordings from n = 21 cultures. Error bars represent SD.

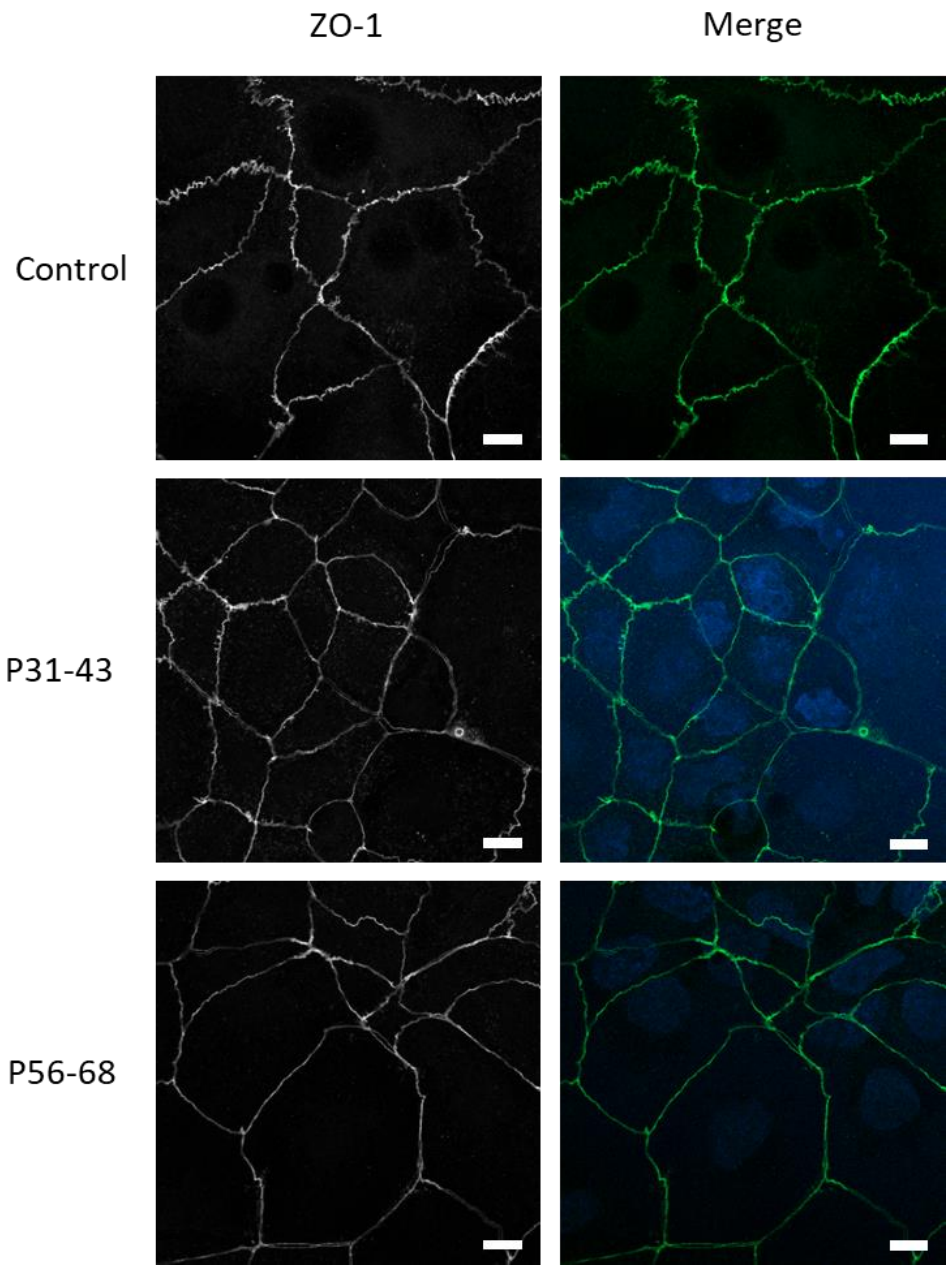

Figure 4.9. Gliadin-derived peptides do not cause rearrangement of ZO-1 in differentiated Caco-2 cell monolayers. Confocal microscopy images of immunofluorescent staining of tight junction protein, ZO-1, in Caco-2 cell monolayers treated for 2 h with vehicle control or 100 µg/mL gliadin P31-43 or P56-68. Monolayers were differentiated for 15-18 days prior to treatment. Cell nuclei are counterstained with Hoechst-33342 (blue). All scale bars = 10 µm.

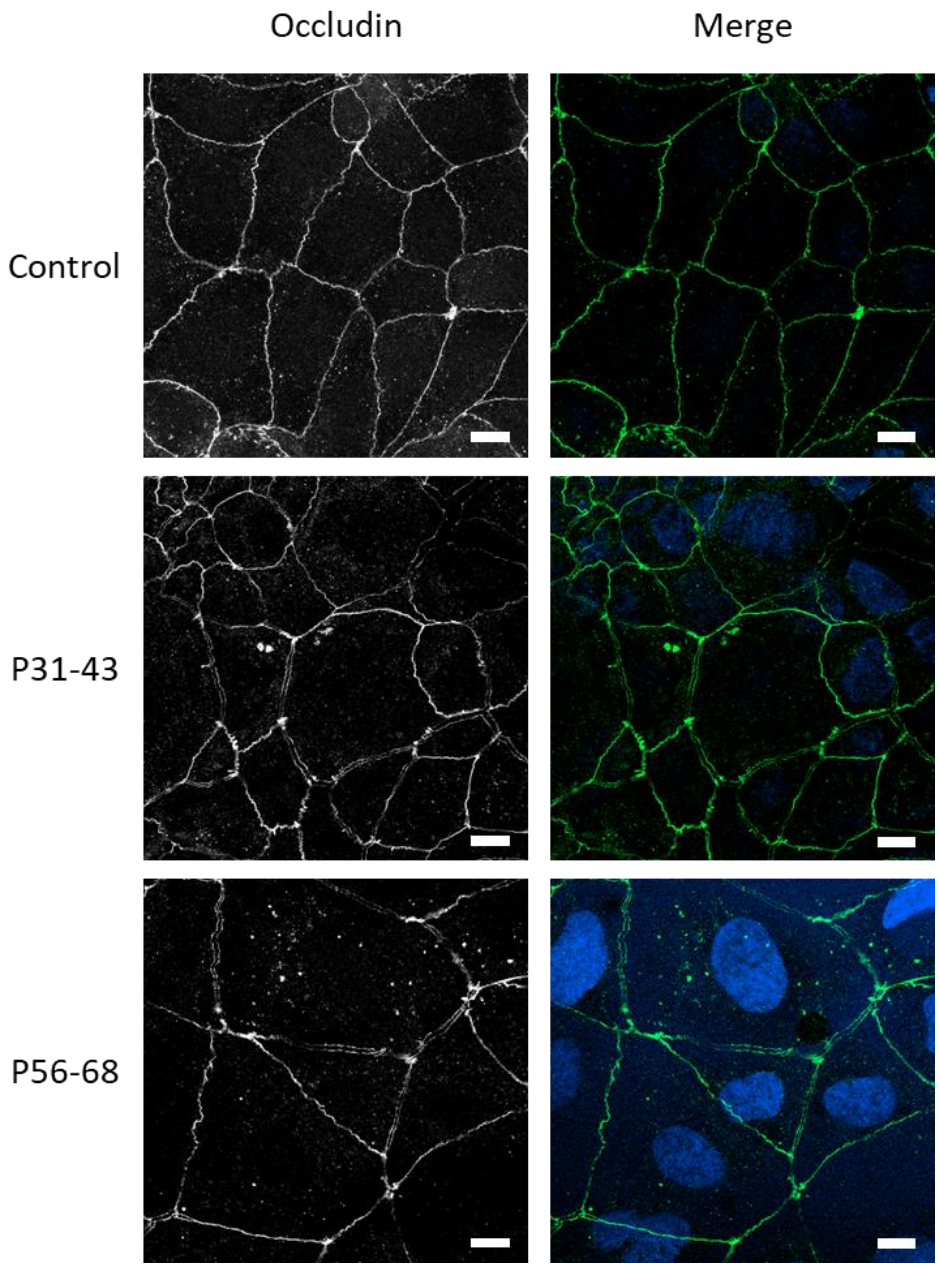

Figure 4.10. Gliadin-derived peptides do not cause rearrangement of occludin in differentiated Caco-2 cell monolayers. Confocal microscopy images of immunofluorescent staining of tight junction protein, occludin, in Caco-2 cell monolayers treated for 2 h with vehicle control or 100 µg/mL gliadin P31-43 or P56-68. Monolayers were differentiated for 15-18 days prior to treatment. Cell nuclei are counterstained with Hoechst-33342 (blue). All scale bars = 10 µm.

4.5.4. Gliadin-derived peptide P56-68 but not P31-43 induced enteroid swelling

During the permeability experiments described above (Section 4.5.1), it was observed that enteroids appeared to swell following treatment with gliadin P56-68. To investigate this possible effect, images collected during the experiments on C57BL/6 enteroids (**Figure 4.3**) were re-analysed to evaluate and compare enteroid area. This revealed that there was indeed an increase in mean percentage area of enteroids treated with 100 μg/mL P56-68 compared to vehicle-treated controls. A peak response was observed at around 2 hours post-treatment (**Figure 4.11 A**). After 2 hours, mean enteroid area decreased slightly but remained elevated above that of controls up to 4 hours post-treatment. This resulted in a significantly greater area under the curve for P56-68-treated enteroids compared to vehicle-treated controls ($p < 0.001$; ANOVA, N = 4, n = 2-5 enteroids per group) (**Figure 4.11 B**). In contrast, the mean area of enteroids treated with 100 μg/mL P31-43 did not change over 4 hours. Addition of 2 mM EGTA also caused a significant increase in mean enteroid area ($p < 0.001$, N = 4 for untreated control, N = 3 for EGTA, n = 2-5); however, this change was likely caused by a different mechanism. Whereas EGTA appeared to cause enterocytes to pull apart, the area increase following P56-68 treatment appeared in bright field images to be due to a rise in luminal volume of the enteroids.

4.5.5. Gliadin P56-68 did not significantly decrease total luminal pixel intensity

Given that altering enteroid area could affect mean pixel intensity, total pixel intensity inside the enteroid perimeter was compared, again for data from C57BL/6 enteroids (**Figure 4.3**). Total pixel intensity is equal to enteroid area multiplied by mean pixel intensity of fluorescence; it is therefore corrected for changes in enteroid area. Using this measure, no significant difference was observed in total pixel intensity within the lumen of C57BL/6 enteroids incubated with 100 μg/mL gliadin P56-68 over 4 hours (**Figure 4.12 A & B**). Gliadin P31-43 also had no effect on total luminal pixel intensity.

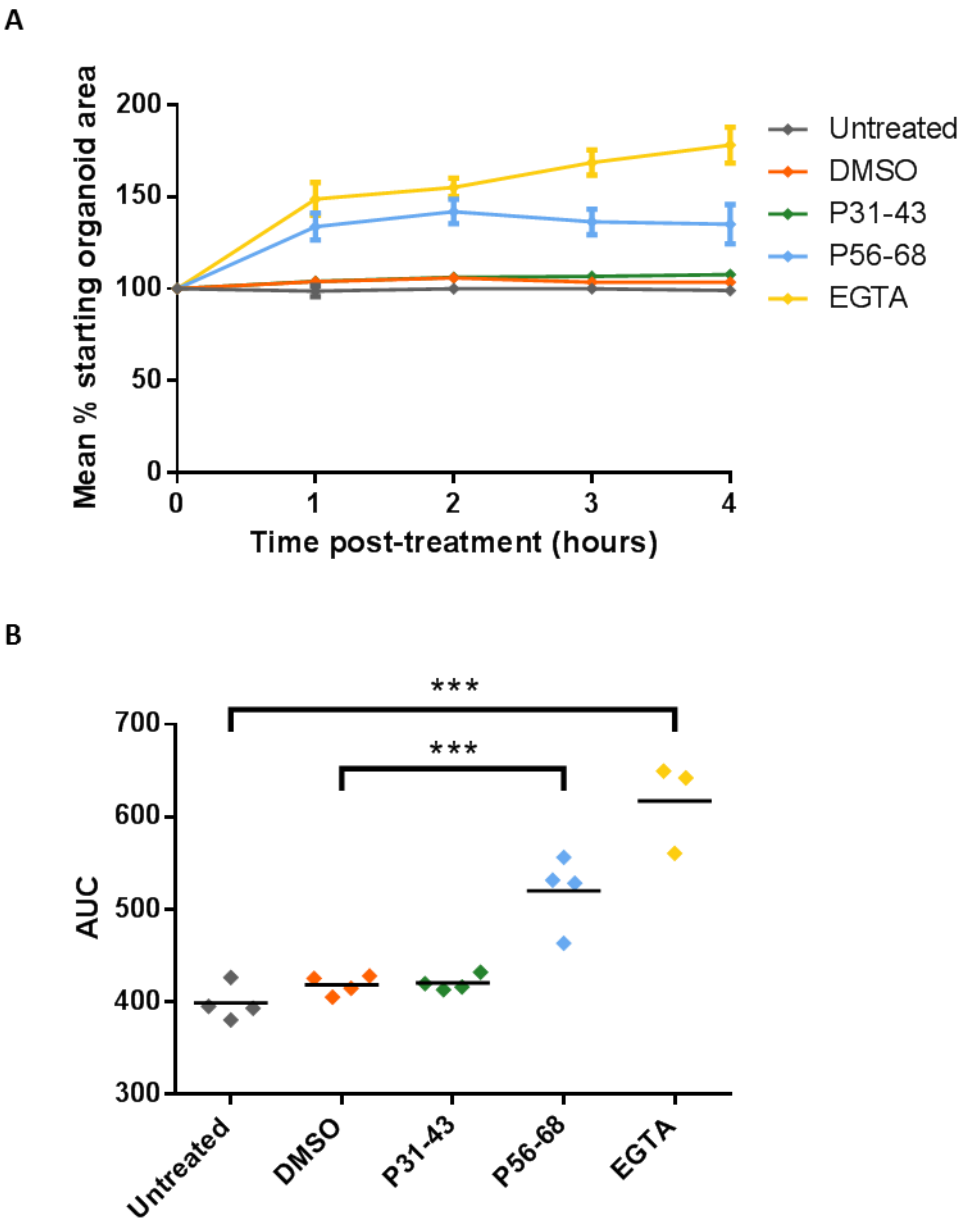

Figure 4.11. Gliadin-derived peptide P56-68 but not P31-43 induces enteroid swelling in permeability experiments. (A) Mean area of enteroids at the indicated time points following treatment with 100 µg/mL gliadin peptides or EGTA. Area refers to surface area determined from the enteroid perimeter in bright field images. Values were calculated relative to the area of each enteroid at 0 h, which was set to 100%. **(B)** Area under the curve was analysed for the data series shown in panel (A). Each symbol represents the mean of an independent experimental repeat. Significant differences were determined using one-way ANOVA; ***$p < 0.001$, N = 3-4, n = 2-5 enteroids per group. Error bars represent SEM.

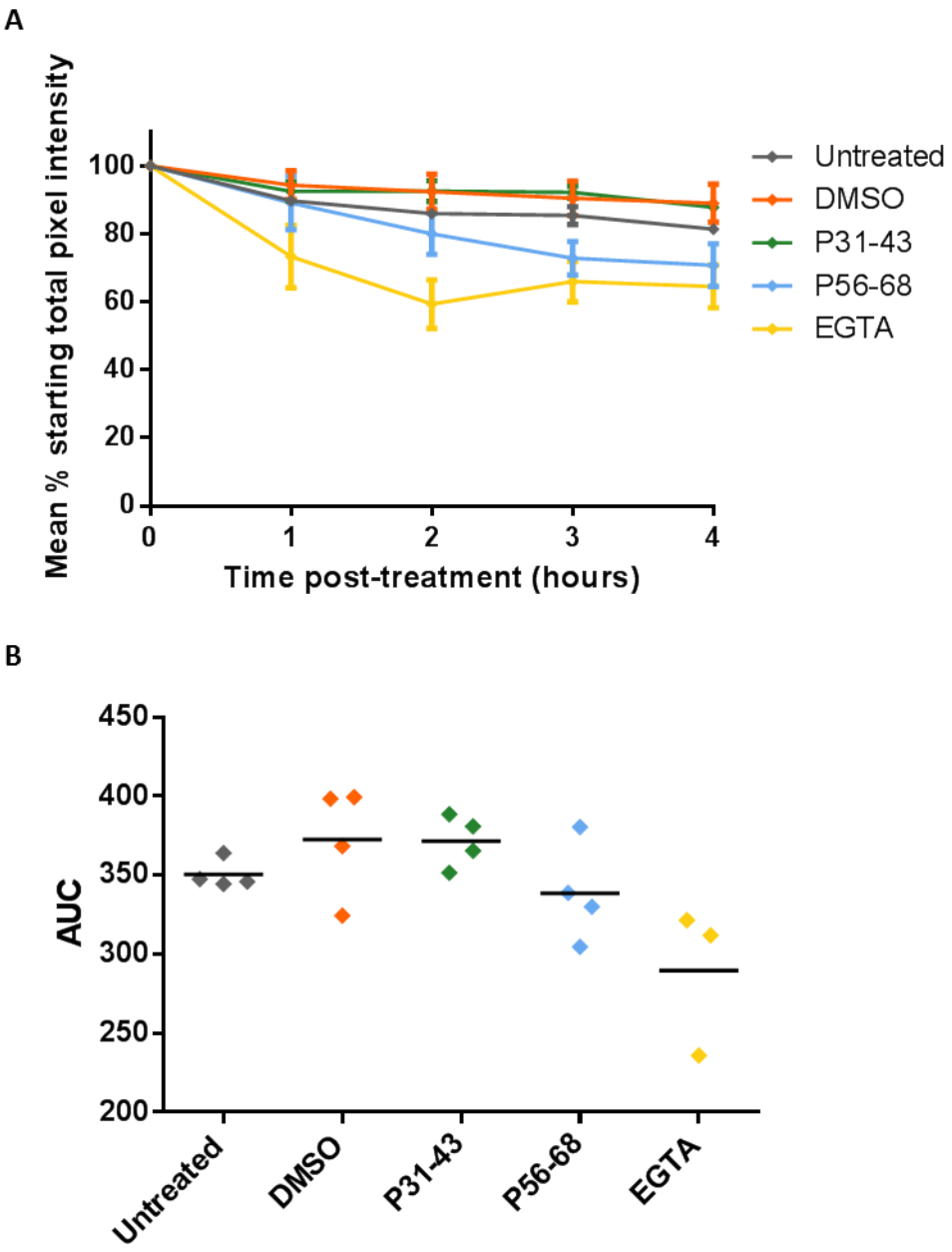

Figure 4.12. Gliadin-derived peptide P56-68 does not significantly decrease total luminal pixel intensity. (A) Change in total pixel intensity within the enteroid lumen following treatment with gliadin peptides or EGTA. Total pixel intensity was calculated as the product of the enteroid area and the mean pixel intensity within this area. Values for each enteroid were calculated relative to the starting total pixel intensity of that enteroid at 0 h. Error bars represent SEM. **(B)** Area under the curve was analysed for the curves shown in (A). Each symbol represents the mean of an independent experimental repeat. No significant differences were observed using one-way ANOVA with selected pairwise comparisons of means using Bonferroni t-tests; N = 3-4, n = 2-5 enteroids per group.

4.5.6. Gliadin P56-68 but not P31-43 induces swelling of BALB/c and *Nfkb2*$^{-/-}$ enteroids

When images from permeability assays of BALB/c enteroids were reanalysed to examine the change in enteroid area, a significant increase in enteroid area was found following treatment with both 2 mM EGTA and 100 µg/mL gliadin P56-68 compared to untreated and vehicle controls respectively. This resulted in a significantly greater calculated area under the curve for both P56-68-treated and EGTA-treated enteroids compared to respective controls (both $p<0.001$; ANOVA, N=6 versus controls N=5, with n=2-6 enteroids per group) (**Figure 4.13 A & B**). In *Nfkb2*$^{-/-}$ enteroids, 2 mM EGTA also caused a significant increase in enteroid area (one-way ANOVA to compare AUC of EGTA-treated enteroids versus untreated controls; $p < 0.001$, N = 4 versus controls N =3, n = 2-7 enteroids per group) (**Figure 4.14 A & B**). A trend towards increased mean area was observed in *Nfkb2*$^{-/-}$ enteroids treated with 100 µg/mL gliadin P56-68 but this difference was not statistically significant.

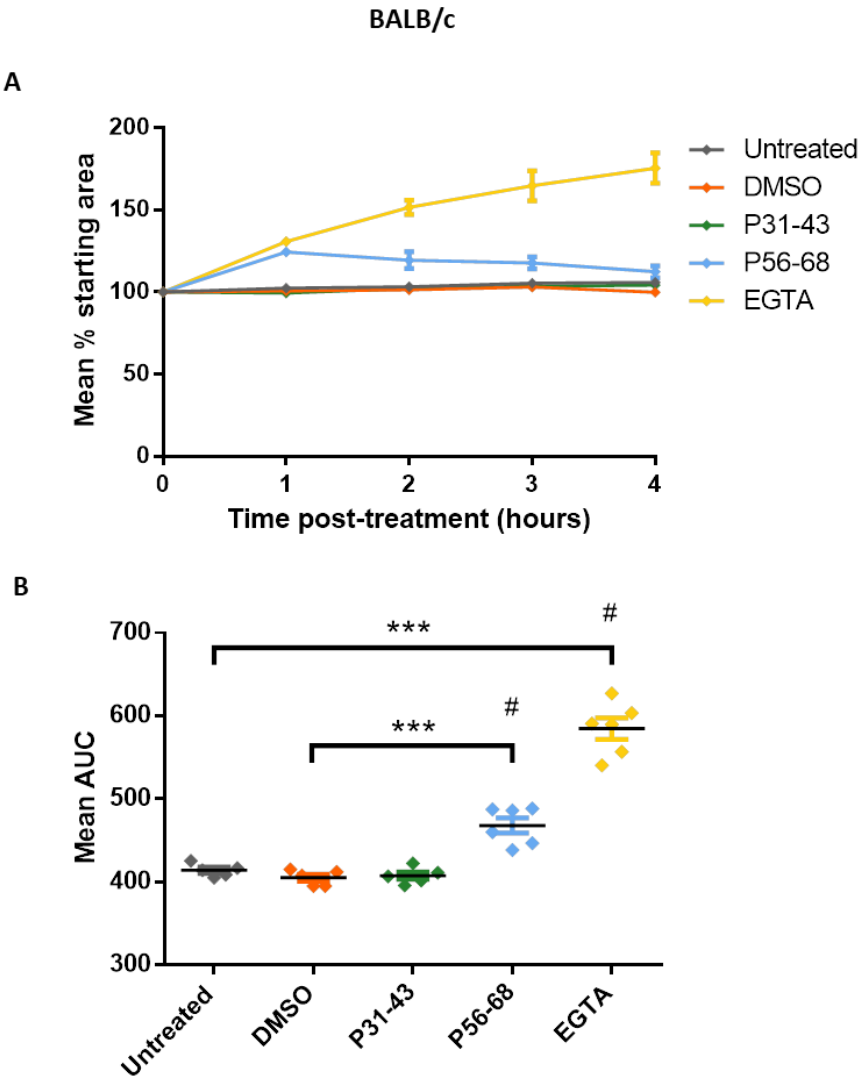

Figure 4.13. Gliadin P56-68 but not P31-43 induces swelling of BALB/c enteroids. (A) Analysis of the change in area of BALB/c enteroids during permeability experiments described in Figure 4.2. **(B)** Area under the curve analysis of the time courses shown in (A). Each symbol represents the mean of one independent biological experiment. Statistical differences were seen using one-way ANOVA; ***p < 0.001, N = 5 separate experimental cultures (except for groups marked #, for which N = 6), n = 2-6 enteroids per group. All error bars represent SEM.

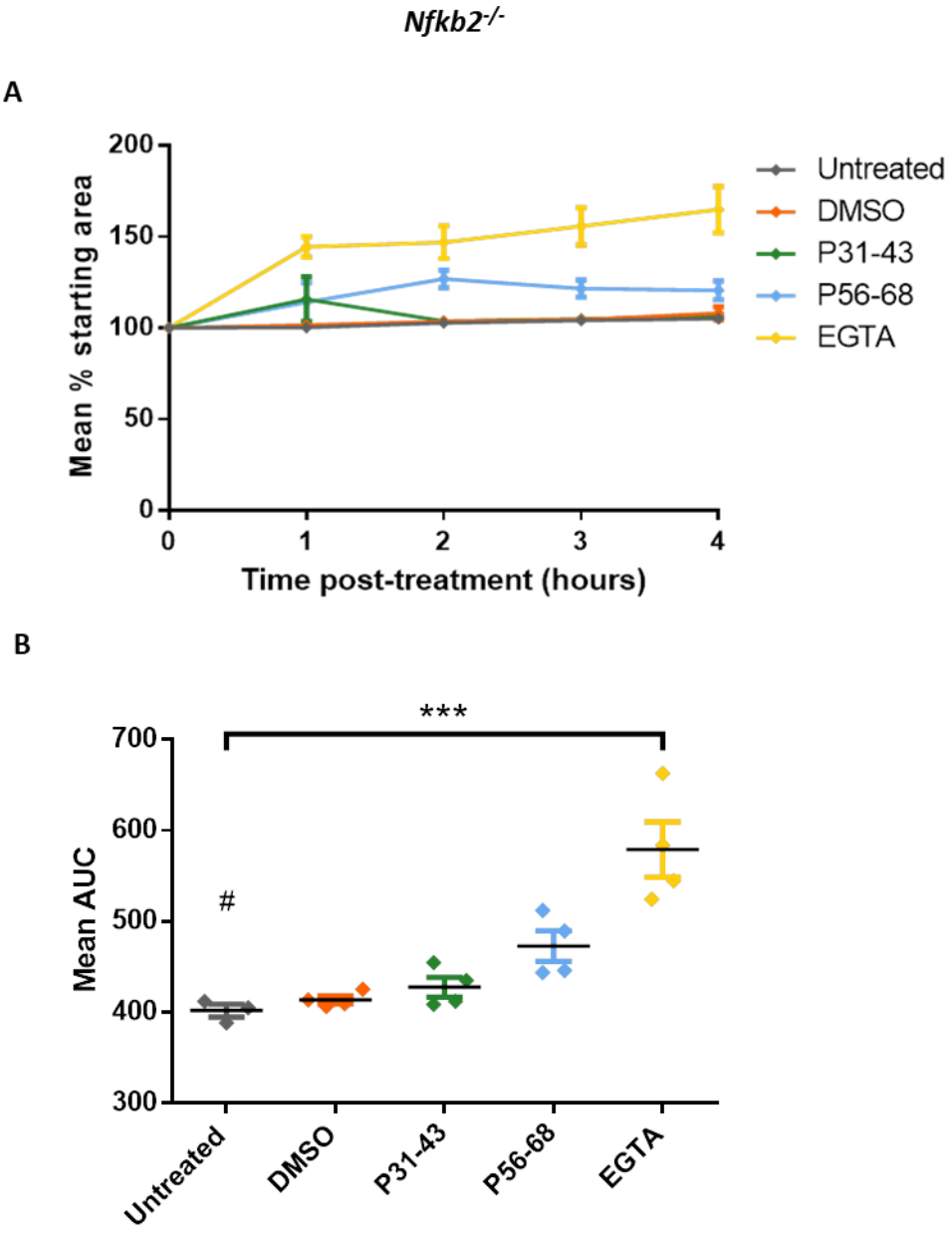

Figure 4.14. Gliadin P56-68 but not P31-43 induces swelling of *Nfkb2*$^{-/-}$ enteroids. (A) Analysis of the change in area of *Nfkb2*$^{-/-}$ enteroids during permeability experiments described in Figure 4.4. **(B)** Area under the curve calculated for the data series shown in panel (A). Each symbol represents the mean of one independent biological experiment. Statistical differences were seen using one-way ANOVA; ***p < 0.001, N = 4 separate experimental cultures (except for groups marked #, for which N = 3), n = 2-7 enteroids per group. All error bars represent SEM.

4.5.7. Gliadin P56-68 induces enteroid swelling due to CFTR-dependent fluid secretion

4.5.7.1. Gliadin P56-68 induces enteroid swelling

To investigate the effect of gliadin P56-68 on enteroid swelling in isolation from the potentially confounding effects of microinjecting fluid into the enteroid lumen, C57BL/6 enteroids were treated on day 2 post-seeding with vehicle (0.2% v/v DMSO) or increasing concentrations of P56-68. Enteroids were tracked by bright field microscopy over 4 hours (**Figure 4.15 A**). Enteroid surface area was used as a surrogate measure of enteroid volume. Control enteroids treated with vehicle showed almost no change in area over 4 hours post-treatment. In contrast, treatment with P56-68 dramatically increased mean percentage enteroid area. Swelling was rapid, being morphologically noticeable at 30 minutes post-treatment (**Figure 4.15 B**). The increase in mean enteroid area after 30 minutes was dose-dependent. Enteroid area peaked after around 1 hour post-treatment, reaching a plateau for up to 4 hours. The mean area of enteroids treated with 50 µg/mL or 100 µg/mL P56-68 increased by around 50-55% compared to pre-treatment, the peak increase in the area of enteroids treated with 25 µg/mL P56-68 was approximately 35%. Analysis of the area under the curve revealed significant differences compared to vehicle with 25, 50 and 100 µg/mL P56-68 (all $p < 0.001$; ANOVA, N = 3, n = 5-8 enteroids per group) (**Figure 4.15 C**).

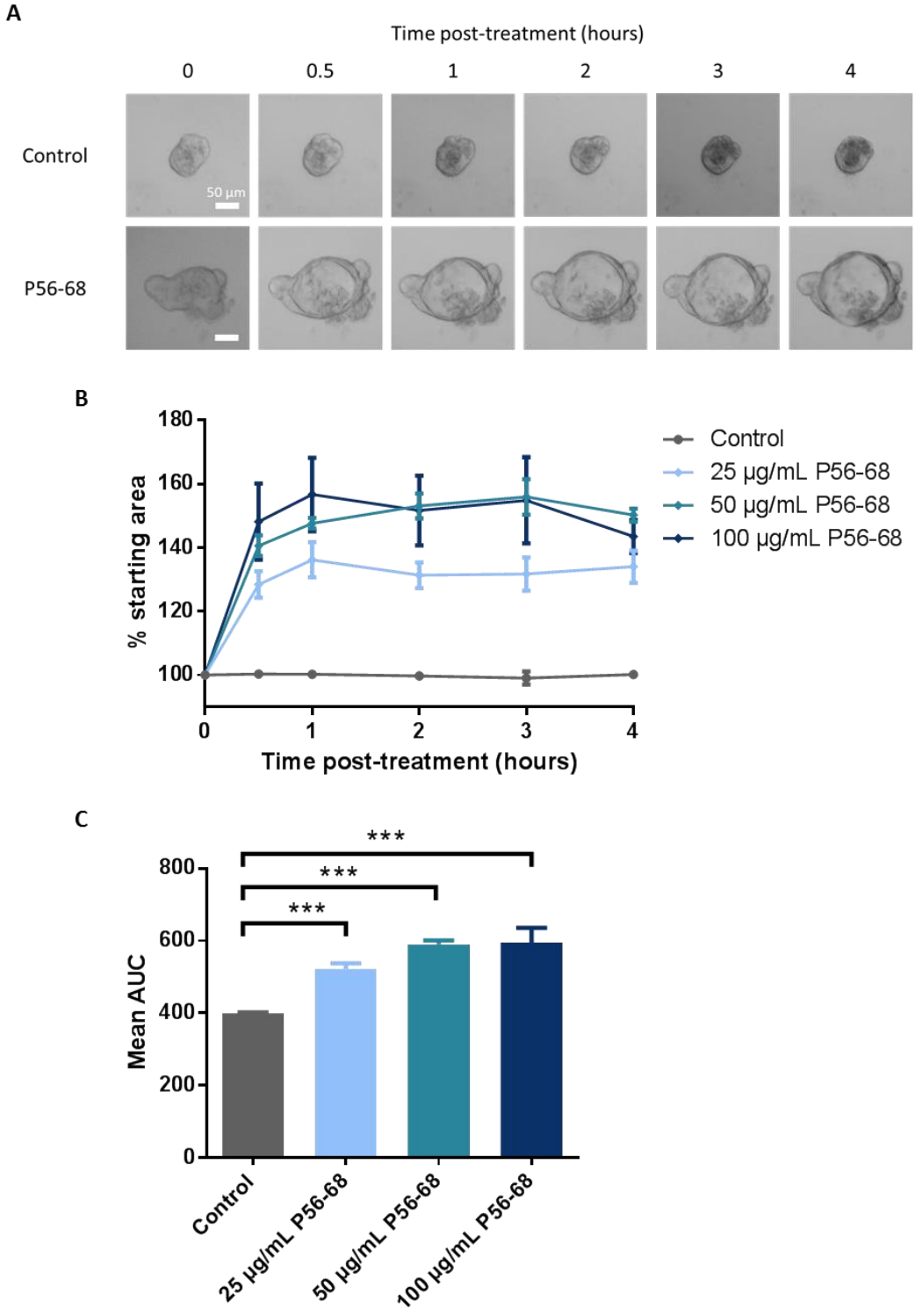

Figure 4.15. Gliadin P56-68 induces enteroid swelling. (A) Representative bright field images of C57BL/6 enteroids at the indicated time points following treatment with vehicle or 25-100 µg/mL gliadin P56-68. **(B)** Mean enteroid area. Error bars represent SEM. **(C)** Area under the curve analysis of the curves shown in (B). One-way ANOVA with Bonferroni correction, ***p <0.001, N = 3, n = 5-8 enteroids per group. Error bars represent SEM.

4.5.7.2. Enteroid swelling induced by P56-68 is similar to that induced by forskolin

Swelling of enteroids has been described previously in response to forskolin (Dekkers *et al.*, 2013). This effect was replicated following treatment of C57BL/6 enteroids on day 2 post-passage with 5 μM forskolin (**Figure 4.16 A**). Forskolin induced a rapid increase in mean percentage enteroid area that was apparent within 0.5 hours and peaked by 1 hour. This increase in enteroid area was sustained for the duration of the experiment (up to 4 hours, **Figure 4.16 B**). This resulted in a significantly greater area under the curve for forskolin-treated enteroids compared to vehicle-treated controls ($p < 0.001$, ANOVA; N = 3, n = 5-8 enteroids per group, **Figure 4.16 C**). The time course of forskolin-induced enteroid swelling was therefore very similar to that induced by gliadin P56-68. The magnitude of the effect was also almost identical, with both resulting in a peak increase in mean enteroid area of approximately 50-55%.

Forskolin-induced swelling is due to activation of the CFTR, a chloride ion channel known to be expressed on the apical membrane of intestinal epithelial cells (Saint-Criq and Gray, 2017). Secretion of chloride ions into the lumen creates an electrochemical and osmotic gradient, drawing sodium ions and water into the lumen (Saint-Criq and Gray, 2017). In enteroids, this results in swelling as the lumen is enclosed. The involvement of CFTR in this effect was confirmed by pre-incubation of the enteroids with 50 μM CFTR-inh-172, a specific inhibitor of CFTR (Thiagarajah *et al.*, 2004; Dekkers *et al.*, 2013). Enteroids pre-treated with CFTR-inh-172 alone showed no change in area, while CFTR-inh-172 significantly reduced the swelling induced by addition of 5 μM forskolin ($p < 0.01$ when comparing AUC of mean percentage area for enteroids treated with forskolin and CFTR-inh-172 versus those treated with forskolin alone; ANOVA, N = 3, n = 5-8 enteroids per group) (**Figure 4.16 C**).

4.5.7.3. Enteroid swelling induced by P56-68 is mediated by CFTR activation

Inhibition of CFTR by pre-incubation with 50 μM CFTR-inh-172 completely abolished the increase in enteroid area induced by 100 μg/mL P56-68 (**Figure 4.17 A-C**). The extent of protection was greater than that afforded by CFTR-inh-172 when used to block forskolin-induced swelling.

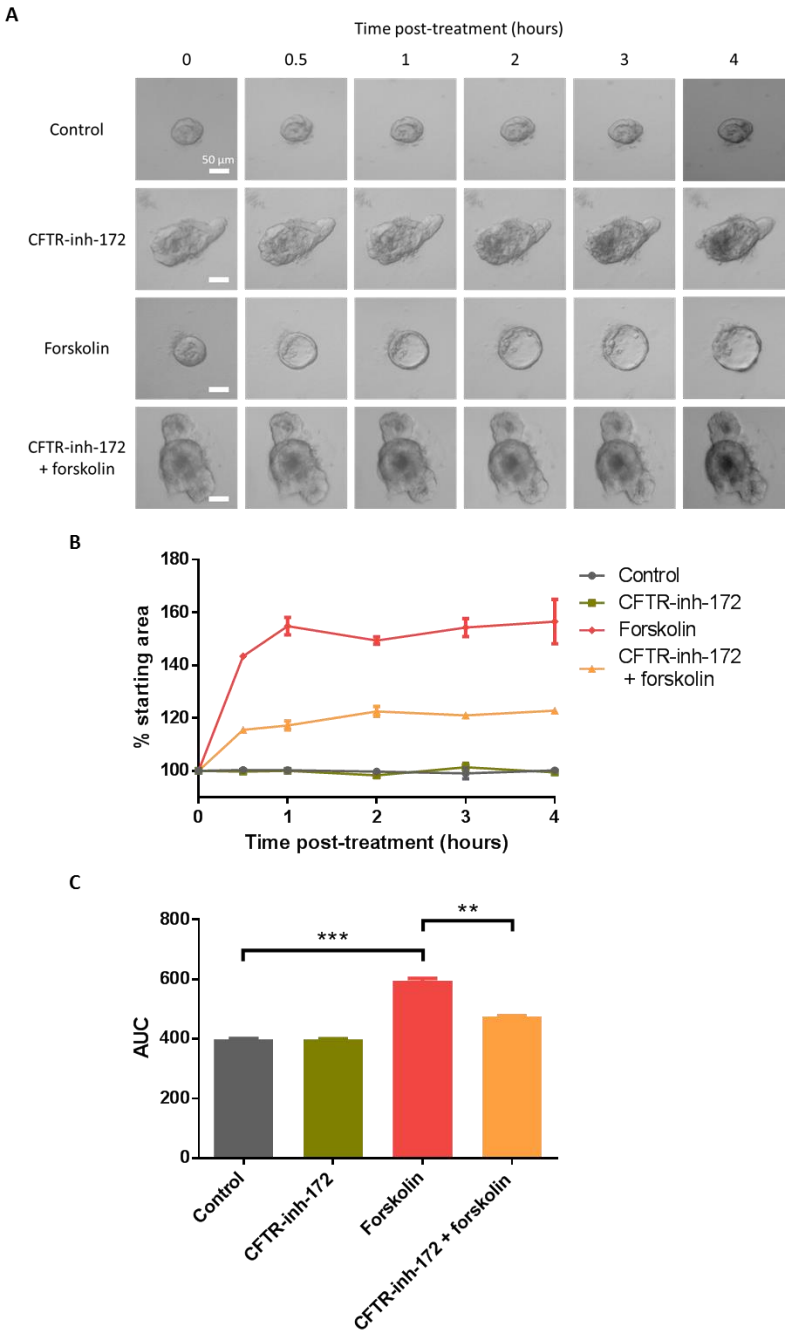

Figure 4.16. Enteroid swelling induced by P56-68 is similar to that induced by forskolin. (A) Representative bright field images of enteroids at the indicated time points following treatment with vehicle control (0.3% DMSO), CFTR-inh-172 (a selective CFTR inhibitor), forskolin alone or forskolin and CFT-172-inh. To block apical chloride channel ion secretion, enteroids were pre-incubated with 50 µM CFTR-inh-172 for 3 h prior to addition of gliadin peptides; CFTR-inh-172 was present for the duration of the experiment. Forskolin was used at dose of 5 µM. **(B)** Mean area of treated enteroids determined from specifying enteroid perimeter in bright field images. Error bars represent SEM. **(C)** Area under the curve analysis of the data series shown in panel (B). Significant differences were observed using one-way ANOVA with selected pairwise comparisons of treatment means using Bonferroni t-tests; ***$p < 0.001$, **$p < 0.01$, N = 3, n = 5-8 enteroids per group. Error bars represent SEM.

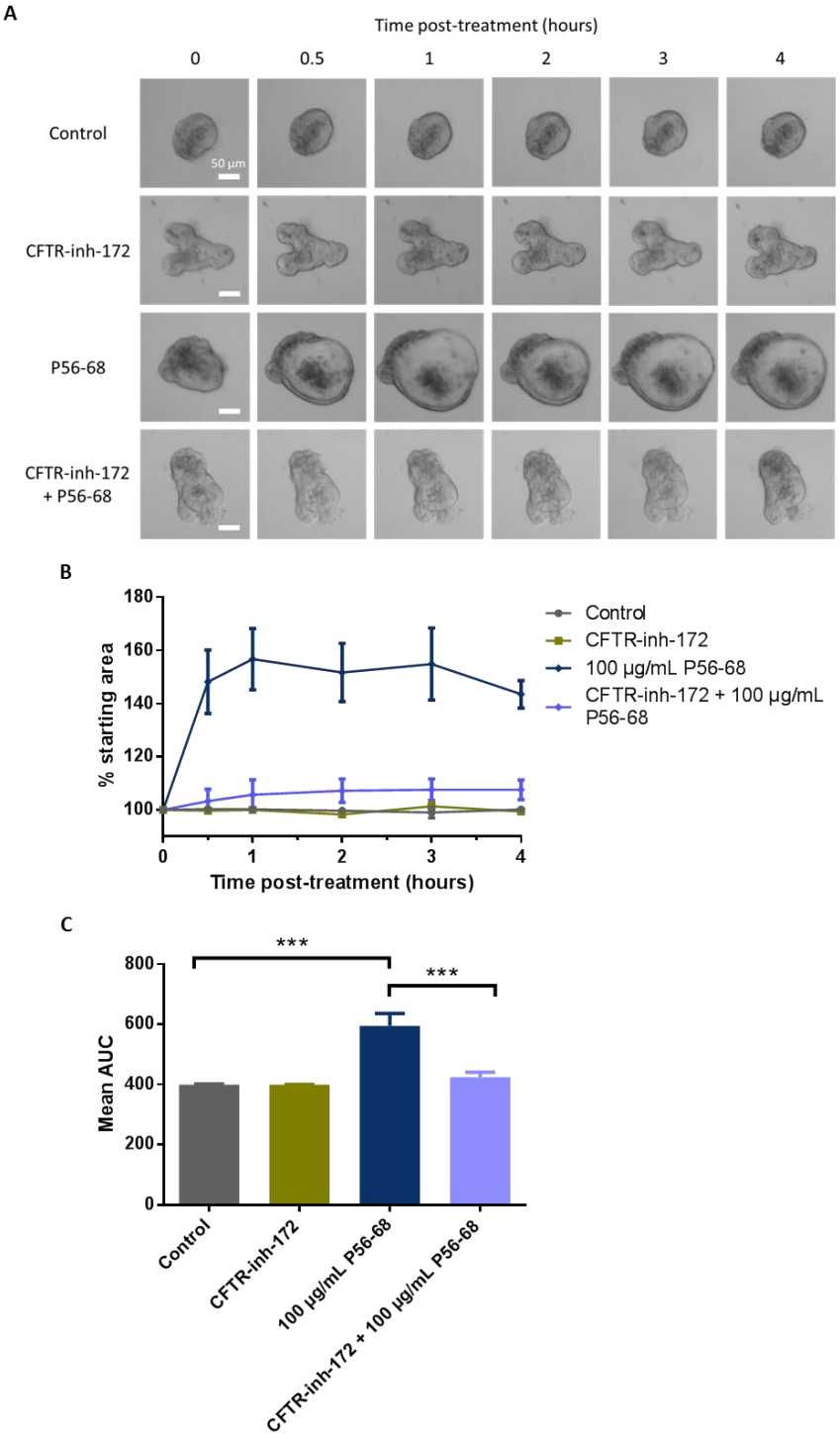

Figure 4.17. Enteroid swelling induced by P56-68 is mediated by CFTR activation. (A) Representative bright field images of C57BL/6 enteroids over 4 h post-treatment with vehicle control (0.3% DMSO) or 100 µg/mL gliadin P56-68, both with and without the apical chloride channel inhibitor CFTR-inh-172 (at 50 µM). Scale bars = 50 µm. **(B)** Quantification of mean enteroid percentage area following the treatments described in panel (A). Error bars = SEM. **(C)** Area under the curve calculated for the data series shown in panel (B). Significant differences determined by one-way ANOVA with selected pairwise comparisons of treatment means using Bonferroni t-tests; ***$p < 0.001$, N = 3, n = 5-8 enteroids per group. Error bars = SEM.

4.5.7.4. Gliadin P31-43 does not induce enteroid swelling

No change in mean enteroid area was recorded in enteroids treated with 100 µg/mL gliadin P31-43 compared to vehicle control (**Figure 4.18 A-C**). There was also no change in enteroid area following treatment with combination of gliadin P31-43 in the presence of 50 µM CFTR-inh-172.

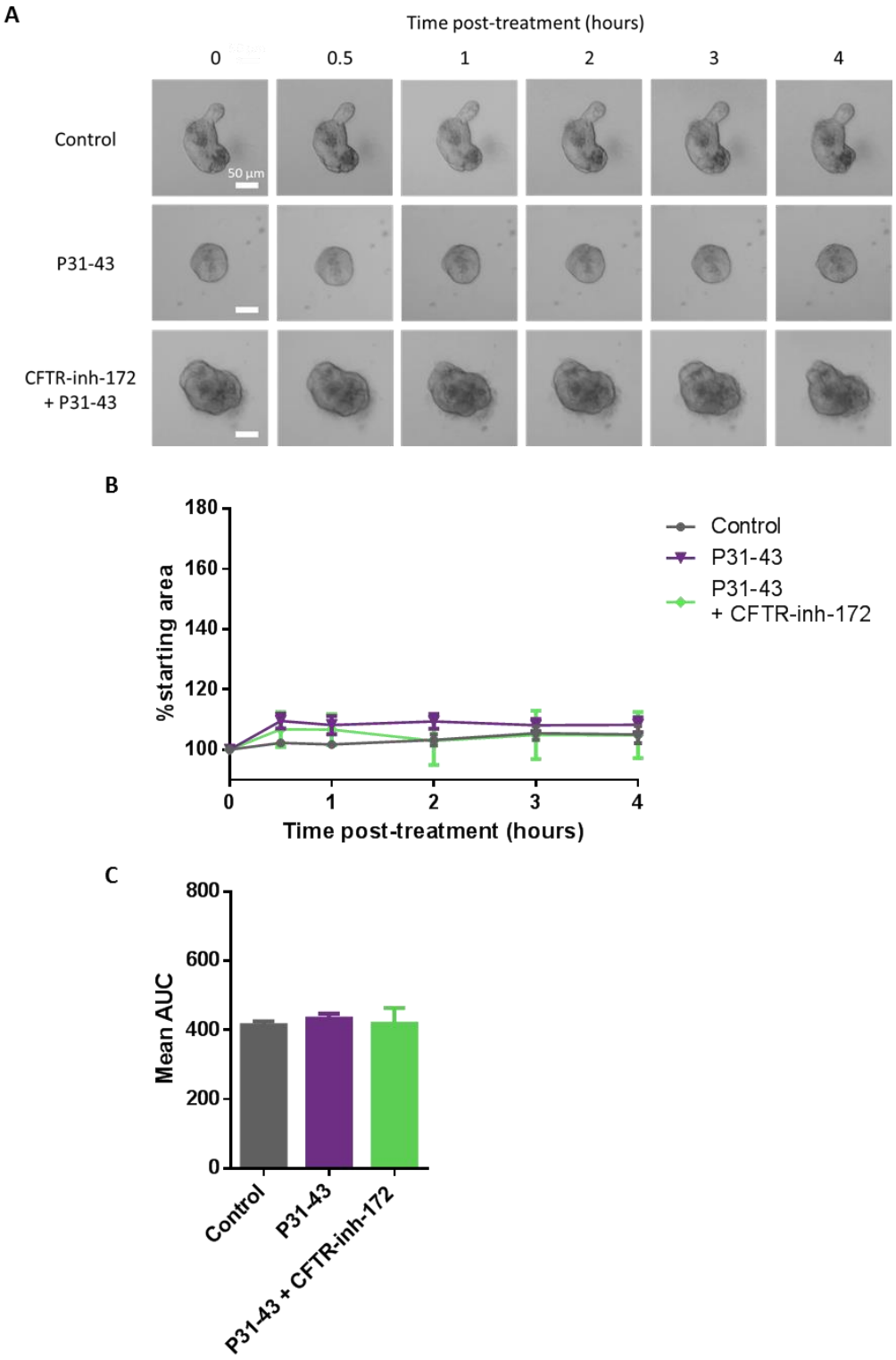

Figure 4.18. Gliadin P31-43 does not induce enteroid swelling. (A) Representative bright field images of C57BL/6 enteroids following treatment with vehicle control (DMSO), 100 µg/mL gliadin P31-43, or 100 µg/mL P31-43 with 50 µM CFTR-inh-172. Scale bars = 50 µm. **(B)** Quantification of enteroid area following the treatments described in (A). Error bars = SEM. **(C)** Area under the curve analysis of (B). Error bars = SEM. No significant differences observed using one-way ANOVA; N = 3, n = 6-8 enteroids per group.

4.5.8. P56-68-induced enteroid swelling is maintained for approximately 4 hours

Time-lapse microscopy using a CytoSMART in-incubator bright field microscope showed that enteroids treated with vehicle (0.2% v/v DMSO) remained a consistent size over the course of 12 hours (**Figure 4.19 A**). In contrast, 100 μg/mL gliadin P56-68 rapidly induced swelling, which was noticeable by 10 minutes post-treatment (**Figure 4.19 B**). Enteroid lumens remained enlarged for approximately 4 hours, then decreased in size again (visible decrease at 6 hours) Following this, enteroids generally remained at this smaller size until at least 12 hours post-treatment. Around 11-12 hours post-treatment, some enteroids appeared to re-swell, albeit to a much lesser degree. Gliadin P31-43 had no dynamic effect on enteroid area (**Figure 4.19 C**).

A Control

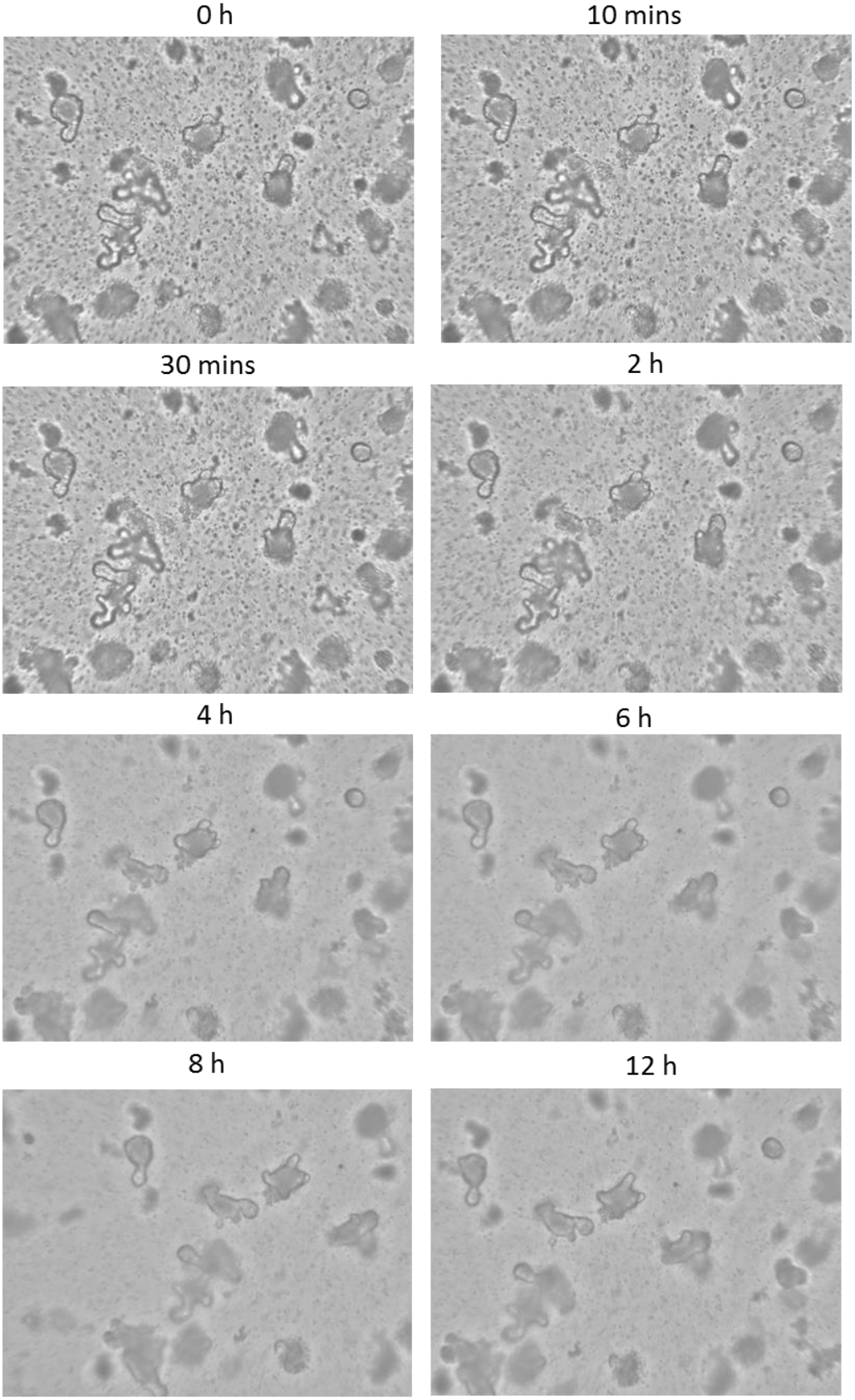

B P56-68

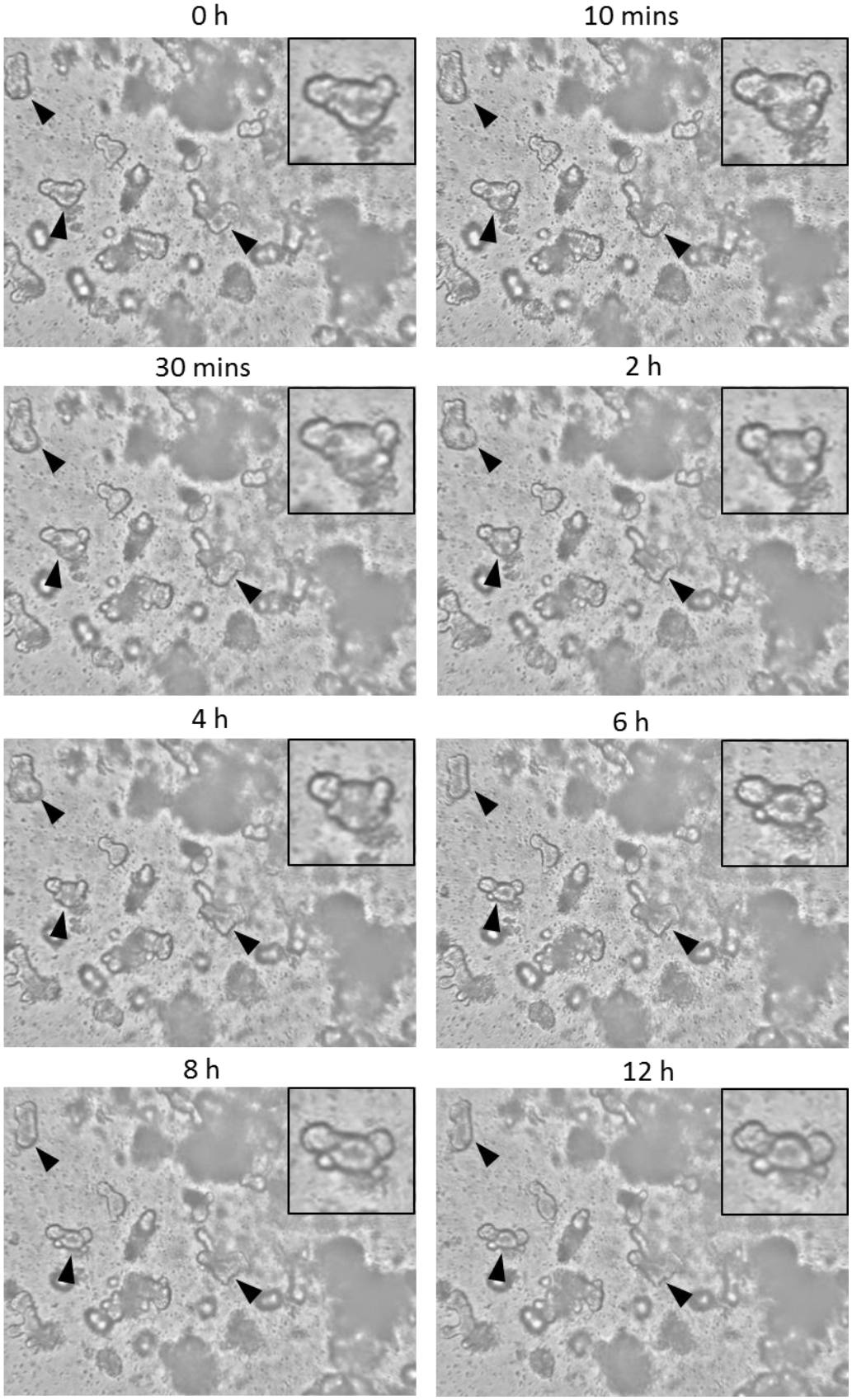

C P31-43

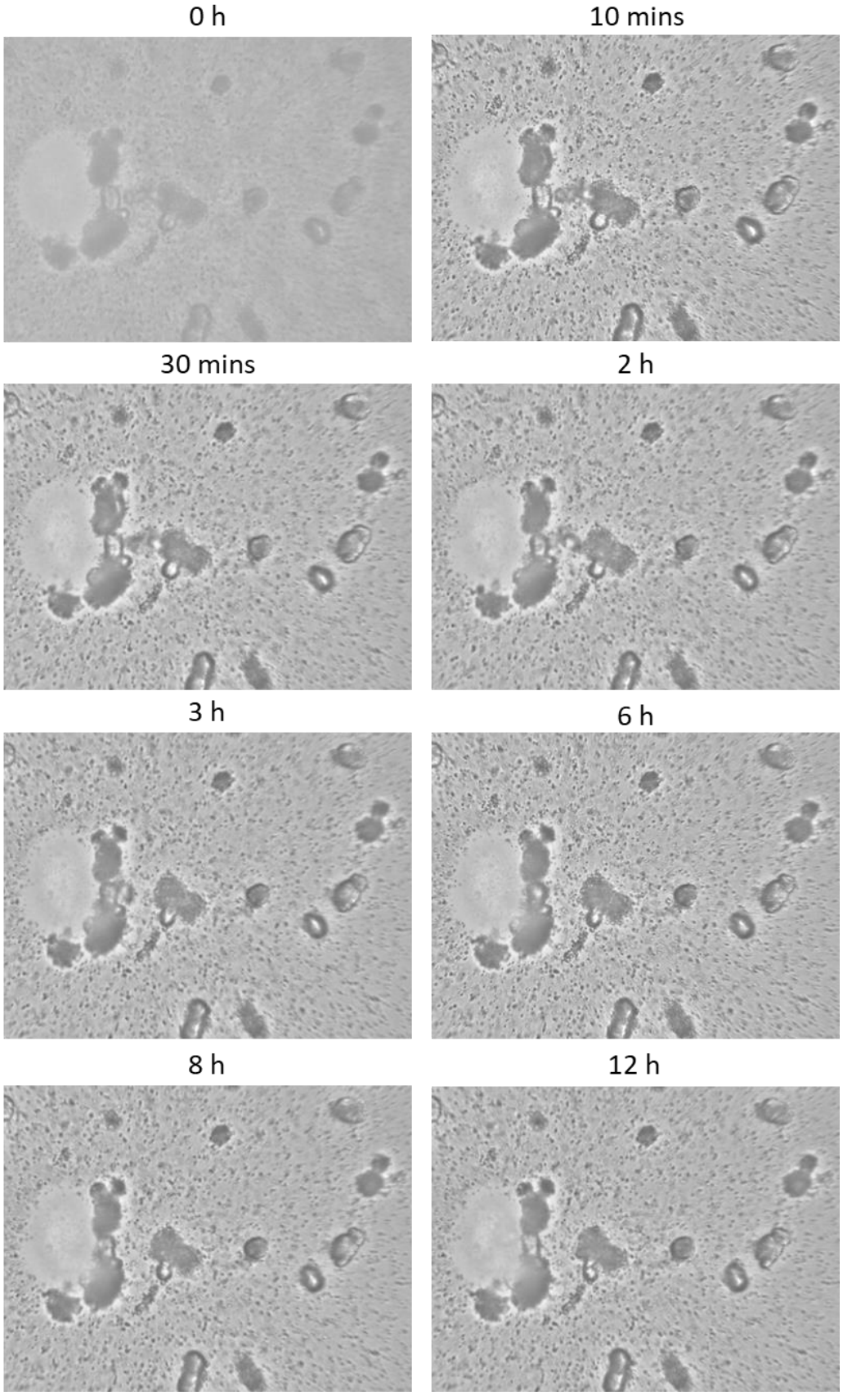

Figure 4.19. P56-68-induced enteroid swelling is maintained for approximately 4 h. Still images taken from 12-h time-lapse videos captured using a CytoSMART in-incubator bright field microscope. Images show C57BL/6 enteroids treated at 0 h with **(A)** vehicle control (0.2% v/v DMSO), **(B)** 100 µg/mL gliadin P56-68, or **(C)** 100 µg/mL gliadin P31-43. Arrow heads indicate examples of individual enteroids that showed an obvious swelling response. Inset images in (B) show 2X magnified images of 100 µg/mL gliadin P56-68-induced enteroid swelling.

4.5.9. Gliadin P56-68 causes luminal swelling, cell stretching and flattening of microvilli

Unlike the normal monolayer epithelium observed in vehicle-treated (0.2% v/v DMSO) control enteroids (**Figure 4.20 A & B**), parts of the lumen were observed by TEM to be greatly engorged in those enteroids fixed following 2 hours of treatment with 100 µg/mL gliadin peptide P56-68 (**Figure 4.20 C-F**). The epithelium of this P56-68-treated enteroid was seen to be both thinner and stretched (**Figure 4.20 C-E**). Cells were markedly elongated laterally. In the area when the lumen was expanded, apical-basolateral diameter measured in P56-68-treated epithelial cells was 4.0 µm ± 0.96 µm (mean ± SEM; diameter measurements taken at 6 sites in 4 different images of the stretch area). In contrast, the mean apical-basolateral diameter of vehicle-treated control epithelial cells was 17.5 µm ± 1.5 µm (SD, 1 cell measured in 4 images of different areas of the enteroid). Of note too, the apical surface of P56-68-treated enteroid epithelial cells appeared almost devoid of microvilli, with only very small, irregular wrinkles visible (**Figure 4.20 E**). In other regions of the same enteroid where no swelling of the lumen was apparent, the apical surface of enterocytes appeared normal, with regular-length microvilli evident (**Figure 4.20 F**).

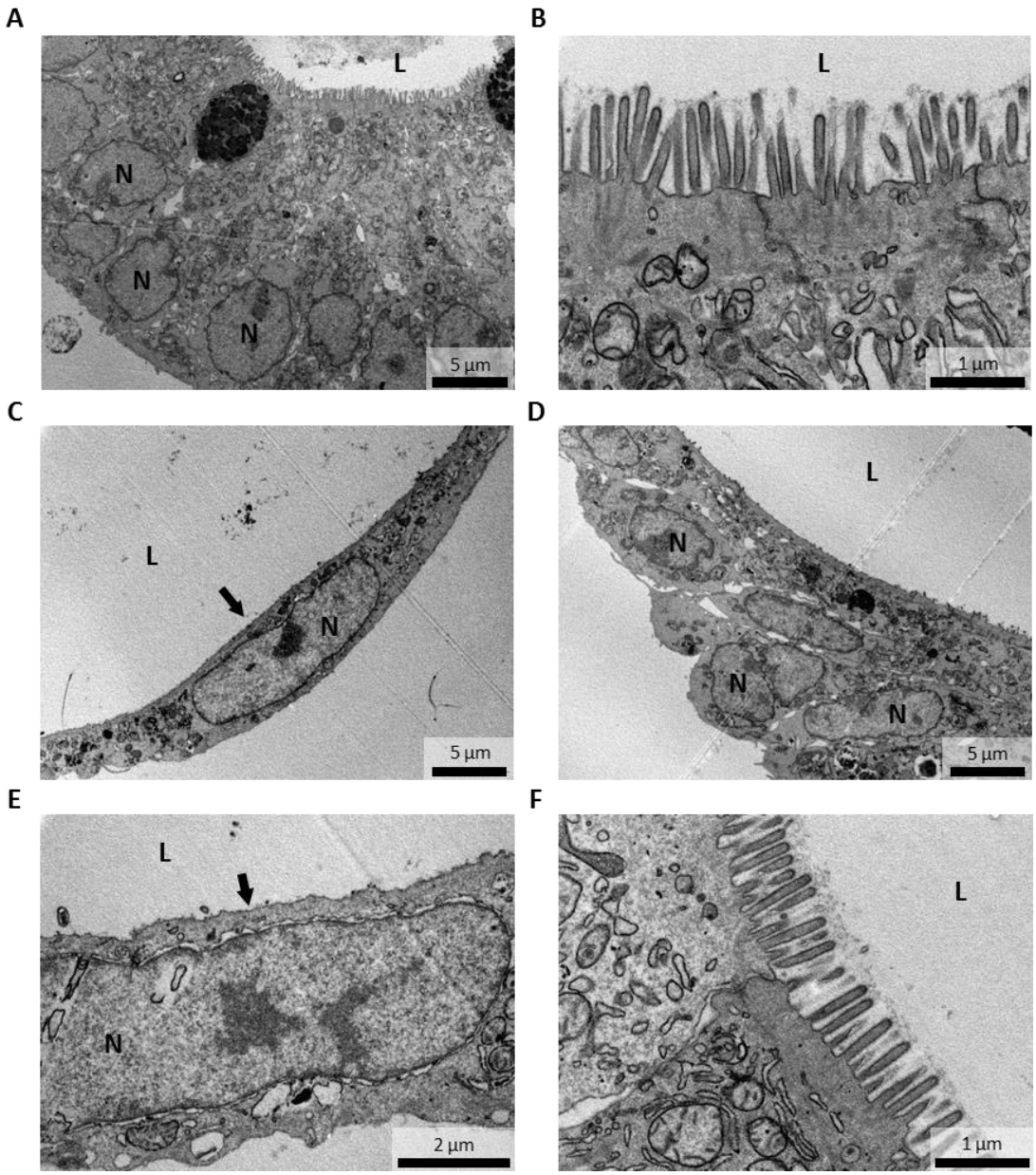

Figure 4.20. Gliadin P56-68 causes luminal swelling, cell stretching and flattening of microvilli. (A & B) TEM images of a control enteroid showing **(A)** an overview of the typical appearance of the epithelium and **(B)** a close-up of microvilli on the apical surface of enterocytes. **(C-F)** Images of an enteroid treated for 2 h with 100 µg/mL P56-68. **(C &D)** Areas of the enteroid where the lumen is enlarged and cells are stretched thin. **(E)** A stretched enterocyte. **(F)** Apical surface of enterocytes in a different part of the same enteroid where normal microvilli are still present. Arrows indicate the apical surface of the cell where microvilli are almost absent. L, lumen; N, nucleus.

4.6. Summary of results

1. A peptide fragment of α-gliadin spanning amino acids 56-68 rapidly induced increased secretion of fluid into the enteroid lumen. The increase in luminal volume peaked around 1 hour after exposure and enteroid area reduced after approximately 4 hours.

2. Enteroid swelling induced by gliadin P56-68 occurred in a dose-dependent manner. The magnitude of the effect was similar with both 50 and 100 μg/mL gliadin P56-68, although a clear effect was still observed with 25 μg/mL gliadin P56-68.

3. Increased intra-enteroid luminal fluid secretion caused by gliadin P56-68 was due to activation of the CFTR, a chloride channel expressed on the apical surface of enterocytes.

4. The swelling response induced by gliadin P56-68 is likely specific to its amino acid sequence, as an otherwise identical size peptide, P31-43 with a different amino acid sequence, had no effect on fluid secretion.

5. Neither gliadin peptide was observed to affect enterocyte cell viability or integrity of tight junctions.

4.7. Discussion

Gluten, and therefore also gliadin, is a common dietary component for the majority of the world's population, being present in foodstuffs made from wheat, barley and rye. Although most dietary proteins are thought to be biologically inert in the gut lumen, gliadin is an example of a protein that interacts with the intestinal wall and has profound pathophysiological consequences in the form of coeliac disease. Although symptoms of coeliac disease can be successfully avoided by removing gluten from the diet, up to two thirds of patients do not adhere, possibly due to the negative impact on quality of life through social isolation and increased food expense (Barratt, Leeds and Sanders, 2011). As a result, many people find it difficult to adhere to a gluten-free diet. In some cases, patients may not respond or become refractory to a gluten-free diet (McAllister, Williams and Clarke, 2018). The condition is also believed to be under-diagnosed, especially in individuals who suffer mainly

extra-intestinal symptoms. It is therefore desirable to understand the pathophysiology of this common disease. While great progress has been made in understanding the immunological events that drive the inflammatory response observed in coeliac disease, many aspects of the pathophysiology of the condition remain poorly understood, in particular the putative direct effects of gliadin-derived peptides on the intestinal epithelium. The studies presented here, using stem cell-derived 3D enteroid cultures, provide evidence that gliadin-derived peptides may indeed directly impact on the physiology of the epithelium, in the absence of an adaptive immune response.

We show that a 13-amino acid peptide (P56-68) constituting a fragment of α-gliadin, rapidly enhances apical fluid secretion (secondary to apical chloride secretion) by intestinal epithelial cells. This effect is dose-dependent, with a highly significant swelling response generated with 25 µg/mL gliadin P56-68. It is difficult to quantify the concentration of this gliadin peptide present in the gut lumen *in vivo* following the ingestion of a gluten-containing meal. This concentration would be dependent on many factors, including the amount of food consumed, the gluten content of the food and the extent to which this particular peptide was generated from digestion of the gliadin present. One study using an antibody-based test to measure the concentration of gluten-derived peptides in urine detected peptides in all subjects on a gluten-containing diet at concentrations up to 604 ng/mL (Moreno *et al.*, 2017). In one patient, approximately 15 ng/mL gluten-derived peptides were detected in the urine following consumption of a single 25 mg oral dose of gluten. Symptoms have been reported in coeliac patients after oral challenge with just milligram daily doses of gluten (Hischenhuber *et al.*, 2006). Given that one slice of bread contains around 8 g gluten and that these peptides are resistant to digestion, it is not unreasonable to suggest that gluten concentration in the gut could reach concentrations in the microgram range, as used in this study.

Our data show that the swelling induced by gliadin P56-68 is mediated by CFTR activity. The CFTR is a major anion channel expressed at the apical membrane of enterocytes throughout the small intestinal epithelium, with capacity for regulated secretion of chloride and bicarbonate ions, whose activity is the main regulator of apical fluid secretion (Field, 2003; Jakab, Collaco and Ameen, 2011; Saint-Criq and Gray, 2017). CFTR activation is triggered by elevated intracellular cyclic adenosine monophosphate (cAMP) and results in secretion of anions, mainly chloride ions, into the intestinal lumen, with sodium ions following via the paracellular pathway down the resulting electrochemical gradient and water following by osmosis.

Whilst in this study we do not address the upstream mechanism of P56-68-mediated CFTR activation, CFTR can be activated in many ways, including phosphodiesterase inhibition, inhibition of CFTR-interacting proteins, or stimulation of adenylate cyclase (Moon *et al.*, 2015). Hyperactivation of the CFTR, for example by cholera toxin-mediated activation of adenylate cyclase, can result in diarrhoea as too much fluid is secreted and overtakes the reabsorbing capacity of the colon (Lencer and Tsai, 2003). Secretory diarrhoea is also an adverse effect of many drugs, including irinotecan and zidovudine, which inhibit cAMP secretion via the CFTR-interacting protein MRP and cause increased local cAMP (Moon *et al.*, 2015). There are therefore myriad pathways by which gliadin P56-68 could activate the CFTR.

A very recent publication reports that gliadin-derived peptide P31-43 inhibits CFTR activity, reportedly mediated by direct binding of P31-43 to one of the CFTR intracellular nucleotide binding domains (Villella *et al.*, 2019). Together, the findings suggest that P31-43-mediated inhibition of CFTR drives epithelial stress and activation of TG2, the enzyme responsible for the deamidation of gliadin peptides that promotes presentation to the adaptive immune system. Evidence was also described of elevated baseline inflammation in the small intestines of CFTR-deficient mice (either CFTR knockout or mutated), which was augmented following oral gliadin administration. In contrast to P31-43, no inhibition of forskolin-induced CFTR activity was reported in Caco-2 cells following 3 hours of treatment with an α-gliadin peptide consisting of amino acids 57-68, which is very similar to P56-68. Although it is difficult to compare this with our own study given the different time points and methodologies, the report of direct binding and regulation of the CFTR by a gliadin-derived peptide is certainly intriguing. This study provides evidence of a peptide similar in size and amino acid composition to P56-68 directly regulating CFTR activity.

From the study presented here, it is not clear whether gliadin P56-68 acts on a cell surface receptor or whether it enters the epithelial cells and interacts with a target inside the cells. Several previous studies have indicated that gliadin-derived peptides are taken up by intestinal epithelial cells via endocytosis (Friis *et al.*, 1992; Ménard *et al.*, 2012; Zimmermann *et al.*, 2014; Barone and Zimmer, 2016). Endocytosis is the suggested mechanism, since uptake was reduced by methyl-β-cyclodextin, a general inhibitor of endocytosis (Schumann *et al.*, 2008; Caputo *et al.*, 2010; Zimmermann *et al.*, 2014); however, some reports suggest there may be differences between the precise mechanisms of endocytosis of P31-43 and P56-68. Uptake of gliadin-derived peptides has also been shown in biopsies from both healthy individuals and those with coeliac disease. One study demonstrated uptake of synthetic gliadin peptides in biopsies from patients with active coeliac disease (Ménard *et al.*, 2012), while a second

reported greater uptake in coeliac patients compared to controls following *in vivo* challenge with digested gliadin (Friis *et al.*, 1992). This indicates that both cell surface receptors and molecules inside the cell are possible targets for P56-68 in activating the CFTR.

One potential limitation of our study is that gliadin peptides were delivered to the basolateral rather than the apical surface of the intestinal epithelium. *In vivo*, the initial exposure of the intestinal epithelium to dietary gliadin would be at the apical surface; however, presentation of gliadin peptides at the basolateral surface is also likely to occur, perhaps especially in coeliac patients in whom defects in epithelial barrier integrity have been reported (van Elburg *et al.*, 1993; Heyman *et al.*, 2012). It is probable that gliadin peptides translocate across the epithelium in order to encounter antigen-presenting cells in the lamina propria and drive the adaptive immune response observed in coeliac disease. Translocation of gliadin peptides has been reported in several studies using epithelial cell lines (Schumann *et al.*, 2008; Bethune *et al.*, 2009). In a macaque model of gluten sensitivity, translocation of gliadin peptides was found only in gluten-sensitive animals (Bethune *et al.*, 2008; Mazumdar *et al.*, 2010), while translocation was only observed in duodenal biopsies derived from patients with active coeliac disease (Matysiak-Budnik *et al.*, 2008). A role for the transferrin receptor in transporting gliadin peptides as a complex with secretory IgA, in a retrograde manner from apical to basal compartments, has also been proposed (Matysiak-Budnik *et al.*, 2008). As mentioned previously, increased permeability of the intestinal epithelium has also been reported during coeliac disease (van Elburg *et al.*, 1993; Heyman *et al.*, 2012), presenting another route by which gliadin peptides may access the basolateral surface.

In our studies, analysis of total FD4 pixel intensity during permeability assays indicated that the effect of gliadin P56-68 on mean FD4 pixel intensity was largely explained by its effect on enteroid swelling, there was still a slight, non-significant trend towards greater loss of FD4 in the P56-68 group. This suggests that this peptide could also have a small effect on epithelial permeability, perhaps contributing to the barrier dysfunction already reported in coeliac patients (van Elburg *et al.*, 1993; Heyman *et al.*, 2012).

A further aspect for consideration is whether the synthetic gliadin peptides undergo modification by TG2 in our system. *In vivo*, glutamine residues within gliadin peptides are deamidated to glutamic acid by TG2; the resulting negative charge makes them ideal ligands for the HLA-DQ2/8 molecules. TG2 is expressed in the lamina propria and expression in the small intestinal epithelium has been reported to increase in active coeliac disease (Esposito *et al.*, 2003). The level of TG2 expression in normal intestinal epithelium has not been well

defined. In this study, we did not assess whether TG2 is present in enteroid cultures. The peptides used in this study both contain multiple glutamine residues that are potential sites for TG2 activity. If TG2 is present, it is possible that the peptides may undergo modification in the cultures, which would increase the physiological relevance of this model.

The aim of our study was to use enteroids to model gliadin-associated pathophysiological epithelial responses, so a key question is the physiological relevance of our findings to conditions of gluten sensitivity in humans. Abnormal activation of the CFTR by gliadin P56-68 *in vivo* could cause excess fluid secretion into the lumen of the small intestine. It is conceivable that this could contribute to bloating and abdominal pain, commonly reported symptoms of coeliac disease, NCWS and many cases of IBS. Although the colon has a significant capacity for reabsorbing water (up to 1.5 L), it can be overwhelmed (Debongnie and Phillips, 1978), for instance in the case of CFTR hyperactivation and fluid secretion caused by enterotoxic pathogens such as *Vibrio cholerae* (Thiagarajah, Donowitz and Verkman, 2015). The action of gliadin P56-68 could therefore contribute to diarrhoea, another key symptom of coeliac disease, NCWS and diarrhoea-associated IBS (IBS-D) (Cooper *et al.*, 1980; Wald, 2012; Murray, Frey and Oliva-Hemker, 2018). If so, our data demonstrating enteroid swelling in response to gliadin-derived peptides suggest a possible diagnostic test for gluten-sensitive IBS or NCWS.

We demonstrated that enhanced fluid secretion triggered by gliadin P56-68 resulted in distension of the intestinal epithelium and disruption of normal microvilli morphology. Since the role of microvilli is to increase the surface area of the epithelium, such an effect *in vivo* could play a role in reduced nutrient absorption. Although largely attributable to villus flattening and damage caused by ongoing inflammation, nutrient malabsorption is a common problem in coeliac patients.

The vast majority of coeliac patients are carriers of the HLA-DQ2/8 alleles whereas the C57BL/6 mice from which our enteroids were derived were not genetically susceptible to gluten sensitivity. Our findings are therefore relevant to both coeliac and non-coeliac individuals but may be a better model of NCWS than coeliac disease. It has been suggested, however, that direct effects of gliadin-derived peptides on the intestinal epithelium may have a role in coeliac disease, particularly in its early stages. Only a small proportion of those who carry HLA-DQ2/8 develop coeliac disease and many other genetic loci have been linked to coeliac disease risk (Abadie *et al.*, 2011), including *NFKB2* and multiple other NF-κB-related genes (Fernandez-Jimenez *et al.*, 2014). Other coeliac-associated loci include genes related to T and B cell function, as well as intestinal barrier function. It is therefore possible that genetic

variants could make certain individuals more susceptible to direct effects of gliadin peptides, such as P56-68, on the epithelium. This could contribute to an individual's risk of developing coeliac disease, or indeed, NCWS.

We did not find evidence of cytotoxic effects induced by gliadin P31-43, including no increase in cell shedding into the lumen, in caspase 3-positive staining, or in localisation of tight junction proteins. This is in agreement with previous findings from our group showing that enteroid circularity does not increase following treatment with synthetic gliadin peptides P31-43 or P56-68 for 24 or 48 hours (personal communication, Andra Vaida and Dr Carrie Duckworth, University of Liverpool). Enteroid circularity is a morphological measure determined from the enteroid perimeter in bright field images; it has been shown by our group to correlate positively with the number of caspase 3-positive cells and is thus a crude measure of enteroid viability. Previous studies have reported alterations of the actin cytoskeleton (Clemente *et al.*, 2003), growth factor-like effects due to interfering with trafficking of the EGFR (Barone *et al.*, 2007, 2010, 2011), IL-15 secretion (Maiuri *et al.*, 2003) and expression of tight junction regulators (Lammers *et al.*, 2008). In contrast, Cerf-Bensussan and colleagues stated that "several unpublished studies including ours have not been able to demonstrate a direct effect of p31-43 or the longer p31-49 peptide on either epithelial lines or leucocytes" (Heyman *et al.*, 2012). One possible explanation is that most of these studies were performed on cell lines, which can show marked variation in phenotype between different laboratories.

The results presented here also highlight the importance of choice of experimental model system. The unique properties of enteroid cultures made it possible to observe the swelling response induced by gliadin P56-68. The self-organisation of enteroids to form distinct basal and luminal compartments makes them ideal models in which to investigate factors affecting secretion into the lumen. This would not have been possible using a 2D cell culture, even a Transwell system, where the apical and basolateral compartments are separated but not restricted in volume. In contrast in enteroids, the closed nature of the lumen means that even small changes in the lumen volume may be detected as a change in enteroid area.

Chapter 5

Characterisation of an enteroid model of M cells and the FAE

5.1. Introduction

M cells are specialised epithelial cells restricted spatially to the follicle-associated epithelium of the intestine, which overlies tertiary lymphoid follicle, such as Peyer's patches in the distal small intestine and mucosal lymphoid follicles of the colon (Ohno, 2016). Although details of the underlying mechanisms remain poorly understood, several studies have indicated that M cells have the ability to take up particles, bacteria and viruses from the gut lumen and translocate them to the basolateral surface of the epithelium (des Rieux *et al.*, 2005; Keita *et al.*, 2008; Hase, Kawano, *et al.*, 2009; Roberts *et al.*, 2010; Nakato *et al.*, 2012; Rios *et al.*, 2016). From here, antigens are thought to be transferred to antigen presenting cells, such as dendritic cells, macrophages and intraepithelial lymphocytes, thereby facilitating generation of immune responses by the gut-associated immune system to antigens present in the gut lumen (Mabbott *et al.*, 2013; Rios *et al.*, 2016).

Given that they represent only a tiny fraction of epithelial cells in the small intestine, M cells are challenging to study *in vivo*. Whilst 2D transformed cell line co-culture models have supported key biological insights into M cell biology, they also have significant limitations in terms of reproducibility, inconsistencies in M cell function, time to develop and cost (Kernéis *et al.*, 1997; Gullberg *et al.*, 2000; Schulte *et al.*, 2000; Martinez-Argudo, Sands and Jepson, 2007). Development of 3D *in vitro* models to facilitate the study of M cells is therefore desirable. Understanding of M cell biology has recently been advanced by the finding that RANKL, a cytokine belonging to the TNF super family, is necessary and sufficient for M cell differentiation (Knoop *et al.*, 2009). Since then, RANKL has been shown to stimulate expansion of the M cell population even in enteroids, which are devoid of immune cells (de Lau *et al.*, 2012). *In vivo*, M cells are restricted to the FAE because their differentiation is driven by a subset of RANKL-expressing mesenchymal cells that reside in the sub-epithelial dome (Nagashima *et al.*, 2017a; Nagashima *et al.*, 2017b). RANKL-stimulated enteroids therefore present a novel model of the FAE in which to investigate M cell biology; however, this model has not so far been fully characterised.

RANKL induces upregulation of an M cell 'master transcription factor', SpiB, which in turn drives expression of several M cell-associated genes, including GP2 (de Lau *et al.*, 2012; Wood, Rios and Williams, 2016). RANKL is known to activate NF-κB signalling via TRAF signalling molecules (Wong *et al.*, 1998); however, the relative requirement for classical versus alternative NF-κB signalling pathways and their distinct NF-κB subunits (Vallabhapurapu and Karin, 2009) in M cell differentiation is unclear. NF-κB subunits RelA and RelB are essential for

development of Peyer's patches in mice (Alcamo *et al.*, 2002; Yilmaz, 2003), although their precise roles in M cell differentiation are unknown. M cell differentiation was recently found to proceed normally in c-Rel-deficient mice (Sehgal *et al.*, 2017).

Previous work has also implicated B cells in M cell differentiation. For instance, work in our research laboratory, and by others, has described a model where Caco-2 human colon carcinoma cells are cultured in the presence of B cells, stimulating the Caco-2 cells to adopt an M cell-like phenotype (Kernéis *et al.*, 1997; Gullberg *et al.*, 2000; des Rieux *et al.*, 2007; Man *et al.*, 2008; Roberts *et al.*, 2010). These cells demonstrate increased expression of M cell markers (Gullberg *et al.*, 2000), M cell-like ultrastructural changes and translocation of beads and bacteria (Roberts *et al.*, 2010, 2013). The identity of the Raji B cell-derived factors responsible for driving this phenotypic change have, however, proved difficult to identify (Gullberg, 2005). Other evidence supporting a role for B cells in M cell differentiation includes the proximity of the FAE to the lymphoid follicle and reports that mice deficient in B cells have fewer M cells (Golovkina *et al.*, 1999; Ebisawa *et al.*, 2011).

5.2. Hypothesis

Stimulation of enteroids with RANKL to induce M cell differentiation will cause perturbations in the differentiation of other epithelial cell types. Differentiation of M cells induced by RANKL requires NF-κB2 alternative pathway signalling and may be promoted by B cell-derived factors.

5.3. Aims

1. To characterise the effects of exogenous RANKL on differentiation of M cells in an enteroid model.

2. To investigate the role of NF-κB alternative pathway in M cell differentiation.

3. To characterise the effect of RANKL on other aspects of enteroid structure and composition.

4. To investigate the effects of B cells and B cell-derived factors on differentiation of M cells.

5.4. Methods

Enteroid culture

Since most Peyer's patches are located in the terminal ileum, all enteroids used in this chapter were derived from the distal region of murine small intestine, unless otherwise stated. To investigate the role of alternative pathway signalling in M cell differentiation, enteroids were established from two mouse strains carrying knockouts of key alternative pathway proteins. $Nfkb2^{-/-}$ mice (on a C57BL/6 background), carrying a germ line mutation of the Nfkb2 gene, have decreased numbers of B cells in their spleen, bone marrow and lymph nodes, in addition to altered structure of secondary lymphoid organs (Caamaño et al., 1998).

$Relb^{-/-}$ mice, carrying a germ line mutation of the Relb gene, display multiple abnormalities, including smaller body mass, inflammatory responses in multiple organs and splenomegaly (Weih et al., 1995). They were bred by crossing heterozygous animals and offspring were genotyped in our laboratory by PCR prior to use in experiments (see Section 2.2 for details). All other enteroids used in this chapter were established from mice of the C57BL/6 strain.

Stimulation of M cell differentiation by RANKL

To induce M cell differentiation, enteroids were treated with 200 ng/mL recombinant murine RANKL at the time of passage. This dose was selected as it has previously been demonstrated to induce robust upregulation of Spib and other M cell-associated genes in enteroid cultures (de Lau et al., 2012; Rouch et al., 2016). Enteroids were exposed to RANKL for either 3 or 6 days, as indicated. For 6-day treatments, RANKL was added again on day 3, ie. when culture medium was replaced. The effect of RANKL on the growth and gross morphology of enteroids was assessed using bright field microscopy.

Quantitative analysis of M cell-associated gene expression

Changes in gene expression in enteroids as a result of RANKL treatment were detected by qPCR. A detailed description of the procedure may be found in Section 2.9. Briefly, Matrigel was dissociated and enteroids were washed and collected by centrifugation. Total RNA was extracted and contaminating DNA was removed by DNase treatment. RNA was then reverse transcribed to cDNA and qPCR was performed with SYBR green, using validated primers specific for mouse *Spib*, *Gp2* and *Rank*. Amplification of a single, specific amplicon was confirmed from melt curves. *Gp2* expression in untreated controls was consistently undetectable across independent repeats, indicating that *Gp2* is truly unexpressed in these

samples. In these cases, an arbitrary value of 40 was imputed (McCall *et al.*, 2014). To reduce bias introduced by normalising experimental samples to these imputed *Gp2* control CT values, data were analysed using the dCT method rather than the ddCT method. CT values for target genes were normalised to the housekeeping gene, *Gapdh*, and are expressed as $2^{-\Delta CT}$ (Schmittgen and Livak, 2008). Statistical tests were not performed given that *Gp2* was not measurable in untreated controls. *Gapdh* mRNA levels were similar in experimental samples and controls.

Immunohistochemical analysis of effect of RANKL epithelial cell lineage markers and SpiB

For immunohistochemical analysis, enteroids were treated for 6 days starting from day 0 post-passage. Enteroids were then fixed and processed to generate paraffin-embedded sections as described in Section 2.7.

Comparing epithelial permeability in control versus RANKL-treated enteroids

The assay used to evaluate epithelial permeability in control and RANKL-treated enteroids was similar to that described in Section 2.10. Enteroids were treated on the day of seeding with 200 ng/mL RANKL. On day 3 post-seeding, a 50:50 mixture of FD4 and AlexaFluor 594-conjugated 10 kDa dextran were microinjected into the enteroid lumen. Instead of allowing 3.5 hours for luminal FD4 to stabilise, images were captured every hour, starting 1 hour post-injection. Image analysis was performed as described in Section 2.10 using ImageJ software.

Production of Raji B cell-conditioned medium

Since B cells have been reported to promote M cell differentiation (Kernéis et al., 1997), Raji B cell-conditioned medium was generated and incubated with enteroids to investigate whether factors secreted by B cells could induce upregulation of M cell-associated genes. Raji B cells are a non-adherent human Burkitt's lymphoma cell line (Karpova et al., 2005). Raji B cell-conditioned media and control media was produced by culturing Raji cells in suspension in DMEM supplemented with 10% v/v FBS and 8 mM L-glutamine for 5 days, then collecting media and removing cells and cell debris by centrifugation. Control media was incubated in tissue culture flasks, at the same time and under the same conditions, but without cells. Conditioned or control medium was incubated with enteroids at a dilution of 50% v/v in normal minigut medium from day 0 post-passage. The resulting medium was supplemented with 50 ng/mL EGF, 100 ng/mL Noggin and 500 ng/mL R-spondin-1, as in complete minigut medium. Medium was replaced on day 3 post-passage and enteroids were harvested for RNA extraction on day 6 post-passage.

Co-culture of Raji B cells and enteroids

For co-culture of enteroids with Raji B cells, 1 x 10^5 cells per well were added to the culture medium overlying enteroid cultures. Various co-culture conditions were assessed: Raji B cells were added on either day 0 or day 3 post-seeding. On day 3 post-seeding, either Raji cells and culture medium were replaced, or the original cells were kept and only the medium was replaced. Enteroids were harvested on day 6 for RNA extraction by removing Raji cells and dissociating Matrigel.

5.5. Results

5.5.1. Effect of RANKL on enteroid growth and morphology

Treatment with 200 ng/mL RANKL had no apparent effects on the growth of enteroids (**Figure 5.1**). Enteroids grow at a similar rate to controls and reached a similar size. Both RANKL-treated and control enteroids display the expected budding morphology.

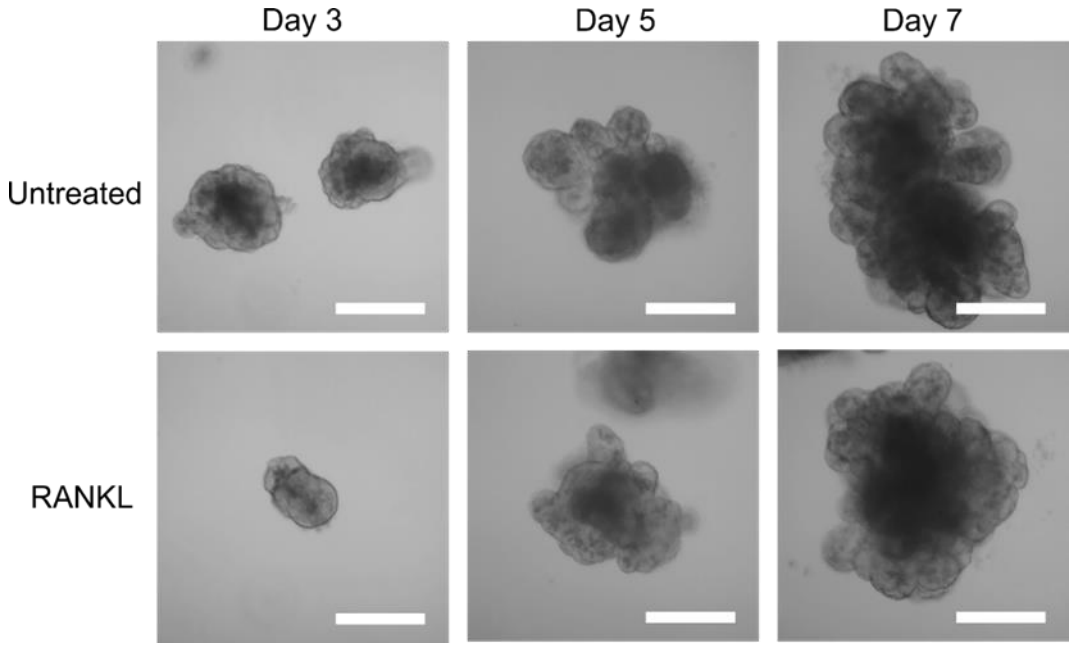

Figure 5.1. Effect of RANKL on enteroid growth. Representative bright field images of enteroids derived from a C57BL/6 mouse treated with 200 ng/mL recombinant murine RANKL. Images were captured on days 3, 5 and 7 post-seeding. RANKL treatment was on day 0. Scale bars represent 100 µm.

5.5.2. Effect of RANKL on M cell-associated gene expression in wild type enteroids

5.5.2.1. Distal enteroids

To confirm whether exogenous RANKL induces M cell differentiation, expression of *Spib* and *Gp2* were analysed following incubation of distal C57BL/6 enteroids with 200 ng/mL RANKL. After 3 days, *Spib* expression relative to *Gapdh* showed a trend to increase in RANKL-treated enteroids compared to controls in each independent experiment, although the size of the increase showed considerable variation and this difference did not reach significance (**Figure 5.2 A**). *Gp2* mRNA was consistently not detected in control enteroids, whereas it was detected in enteroids treated with RANKL. Again, this effect was variable and did not reach significance.

Incubation of distal enteroids with 200 ng/mL RANKL over a longer period – for 6 days from passage – resulted in significant upregulation of both *Spib* and *Gp2* expression, with *Gp2* transcripts again undetectable in control enteroids (**Figure 5.2 B**). In contrast, no significant difference was found in the level of *Rank* expression between controls and RANKL-treated enteroids.

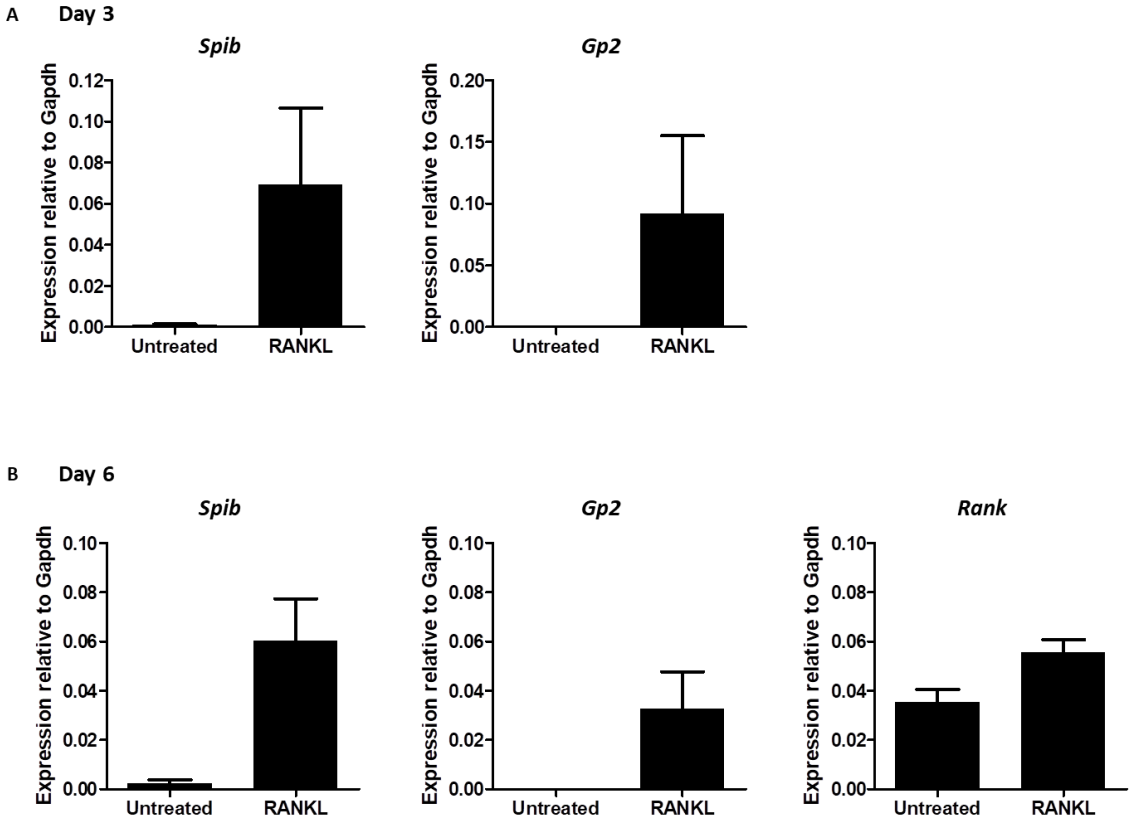

Figure 5.2. Effect of RANKL on M cell-associated gene expression in wild type distal enteroids. (A) Quantification by qPCR of the expression of M cell-associated genes, *Spib* and *Gp2*, in enteroids derived from distal small intestine of C57BL/6 mice treated for 3 d with 200 ng/mL RANKL. Addition of RANKL to enteroid cultures was at the time of seeding. N = 3, n = 3-5 wells enteroids pooled for each condition. **(B)** Quantification by qPCR of the expression of M cell-associated genes, *Spib*, *Gp2* and *Rank*, in C57BL/6 enteroids on day 6 of treatment with 200 ng/mL RANKL. RANKL was added to enteroid cultures at the time of seeding. N = 7, except for *Rank*, for which N = 3, n = 3-5 wells enteroids pooled for each condition. All data measured by qPCR were normalised to the housekeeping gene *Gapdh* and are represented as $2^{-\Delta CT}$. *Gp2* transcript was undetected in all untreated samples at both time points. Error bars represent SEM.

5.5.2.2. M cell differentiation in proximal enteroids

Whilst the majority of Peyer's patches are known to be located in the terminal ileum (Ohno, 2016), proximal intestinal epithelial cells were used to investigate whether they were also capable of supporting M cell differentiation. Expression of M cell-associated genes in response to 200 ng/mL RANKL was therefore analysed in enteroids derived from proximal murine small intestine. After 6 days incubation with RANKL, relative expression of both *Spib* and *Gp2* was increased compared to untreated control enteroids (**Figure 5.3**). The increase relative to *Gapdh* was at least as great, particularly for *Gp2*, as was seen under the same conditions in distal enteroids.

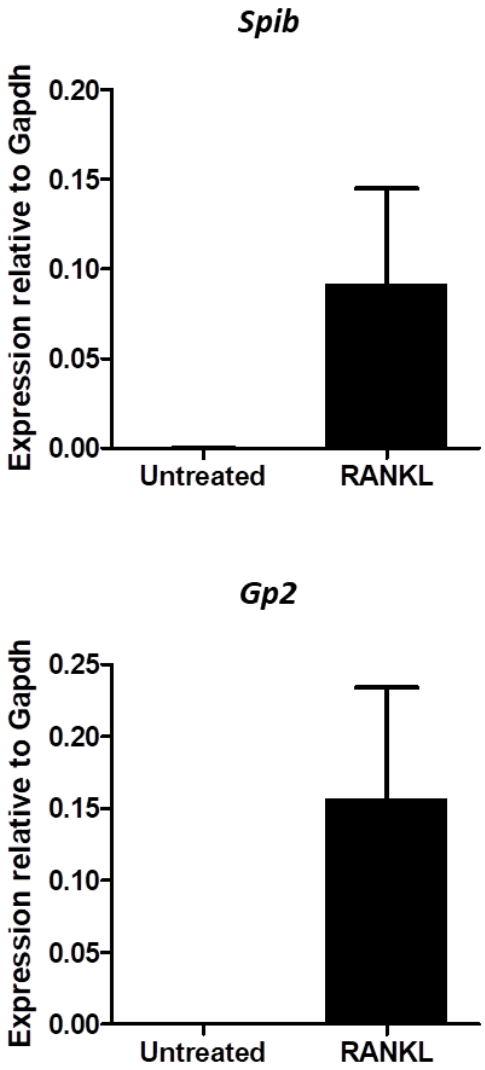

Figure 5.3. RANKL induces upregulation of M cell-associated genes in wild type proximal enteroids. Quantification of mRNA levels of M cell-associated genes in enteroids derived from C57BL/6 murine proximal small intestine on day 6 post-treatment with 200 ng/mL RANKL. Enteroids were first treated with RANKL at the time of seeding. Data measured by qPCR were normalised to the housekeeping gene *Gapdh* and are represented as $2^{-\Delta CT}$. *Gp2* transcript was undetected in all untreated samples. N = 3 independent enteroid cultures derived from different mice. Error bars represent SEM.

5.5.1. Effect of RANKL on expression of M cell marker SpiB

Expression of SpiB was investigated at the protein level by immunohistochemical staining. The specificity of the anti-SpiB antibody was validated in small intestinal tissue from a C57BL/6 mouse containing a Peyer's patch and follicle-associated epithelium (**Figure 5.4 A**). No SpiB-positive cells were visible in control sections (where the staining protocol was performed in the absence of the primary anti-SpiB antibody). Cells with nuclear staining were observed in the dome-like follicle-associated epithelium overlying Peyer's patches, where M cells are known to be located. In contrast, no positively stained nuclei were observed within the epithelium of neighbouring villi.

SpiB-positive cells were extremely rare in untreated enteroids harvested on day 6 post-seeding (**Figure 5.4 B**). In enteroids treated with 200 ng/mL RANKL on the day of seeding, cells with positive nuclear staining were observed. SpiB-positive cells were dispersed throughout the epithelium in both crypt and villus regions of the enteroids, rather than exhibiting any pattern of polarisation or clustering. Quantification of SpiB-positive cells revealed that RANKL treatment resulted in a significant increase in the percentage of SpiB-positive cells per enteroid section from 0.1% ± 0.03% (mean ± SEM) in untreated controls to 14.0% ± 4.6% with RANKL (**Figure 5.4 C**). Efforts to quantify GP2 expression using an anti-GP2 antibody (clone 2F11-C3; MBL International, Massachusetts, USA) did not result in clear, specific staining. Furthermore, efforts to quantify expression and localisation of *Spib* and *Gp2* expression using the RNAscope *in situ* hybridisation assay (Advanced Cell Diagnostics, California, USA) also did not generate a sufficiently strong signal to allow quantification.

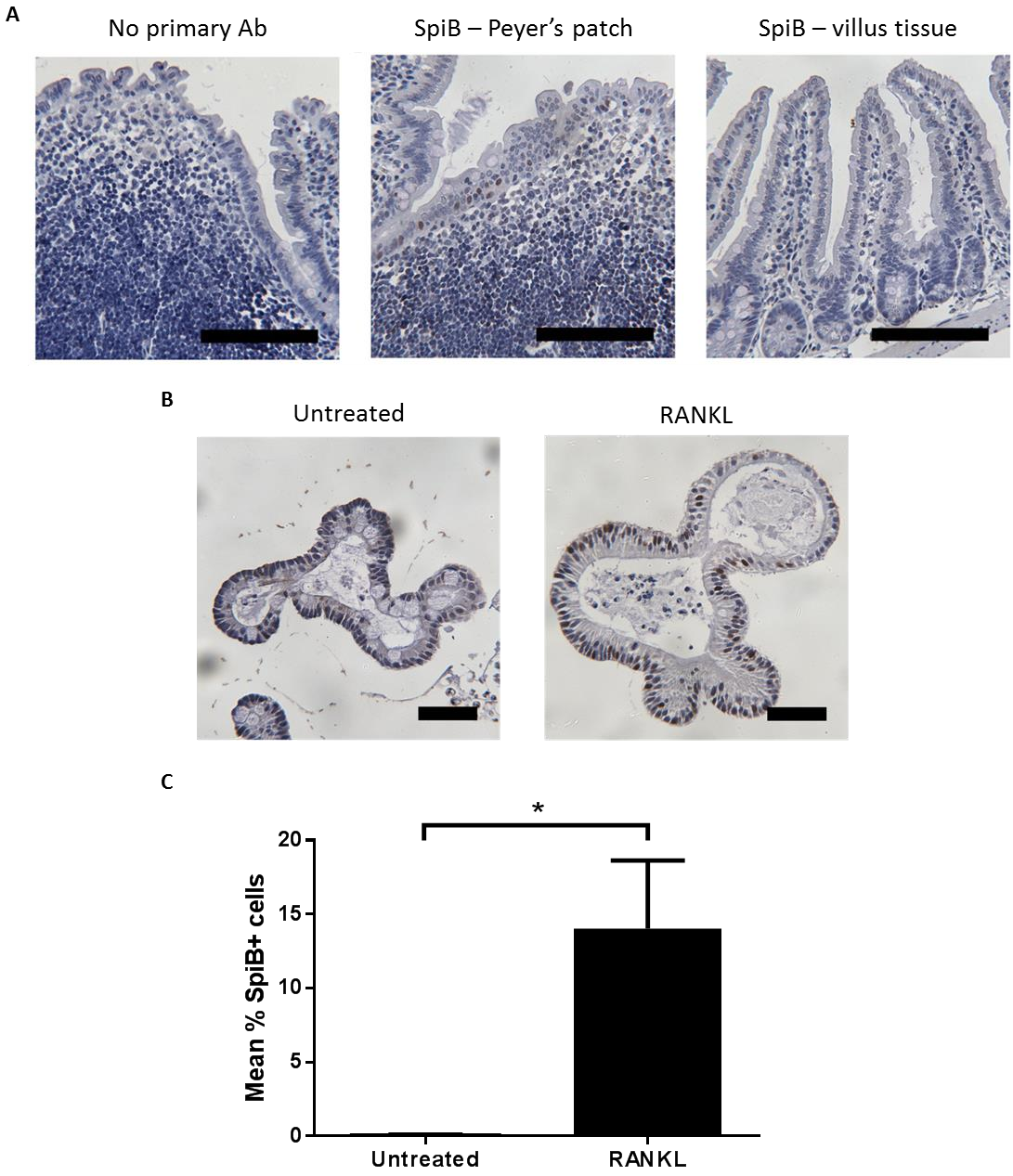

Figure 5.4. Effect of RANKL on expression of M cell marker SpiB in enteroids. (A) Validation of the specificity of the anti-SpiB antibody used. Sections of C57BL/6 mouse small intestine containing Peyer's patches or neighbouring villus tissue were stained with and without anti-SpiB antibody. Scale bars = 100 µm. **(B)** Representative images of immunohistochemical staining for SpiB in sections of enteroids that were untreated or treated for 6 d with 200 ng/mL RANKL. Scale bars = 50 µm. **(C)** Quantification of SpiB-positive cells as a proportion of the total cells per enteroid section. Unpaired t-test, *$p < 0.05$, N = 3 independent enteroid cultures derived from 3 different mice, n = 20-27 enteroid sections per treatment.

5.5.2. Ultrastructural effects of RANKL on enteroids

Peyer's patch M cells *in vivo* have characteristic features visible only by electron microscopy, such as altered apical microvilli and a basolateral pocket in which lymphocytes are frequently observed (Owen and Jones, 1974). While the enteroid model used here did not contain immune cells because it is established from epithelial stem cells, both proximal and distal C57BL/6 enteroids incubated for 3 days with or without 200 ng/mL RANKL were analysed by TEM for evidence of changes towards an M cell phenotype. In crypt and villous domains, the epithelium of proximal (**Figure 5.5 A**) and distal (**Figure 5.5 B**) enteroids treated with RANKL showed a similar overall structure as observed in control enteroids (see Figure 3.3 for further images). Treatment with RANKL clearly did not induce M cell differentiation in all cells within the enteroid epithelium as other differentiated cell types, including Paneth and enteroendocrine cells, were apparent (**Figure 5.6**).

In some areas of RANKL-treated enteroids, epithelial cells exhibited densely packed, regular microvilli typical of those found on mature villous enterocytes *in vivo* (**Figure 5.7 A**). Given that the appearance of microvilli in control enteroids appeared to vary between crypt and villous regions, identification of cells with altered apical microvilli proved somewhat challenging. Several examples, however, were observed of enterocytes with microvilli that were shorter, more irregular, or even absent, than the surrounding cells, which featured well-developed microvilli as described above (**Figure 5.7 B**).

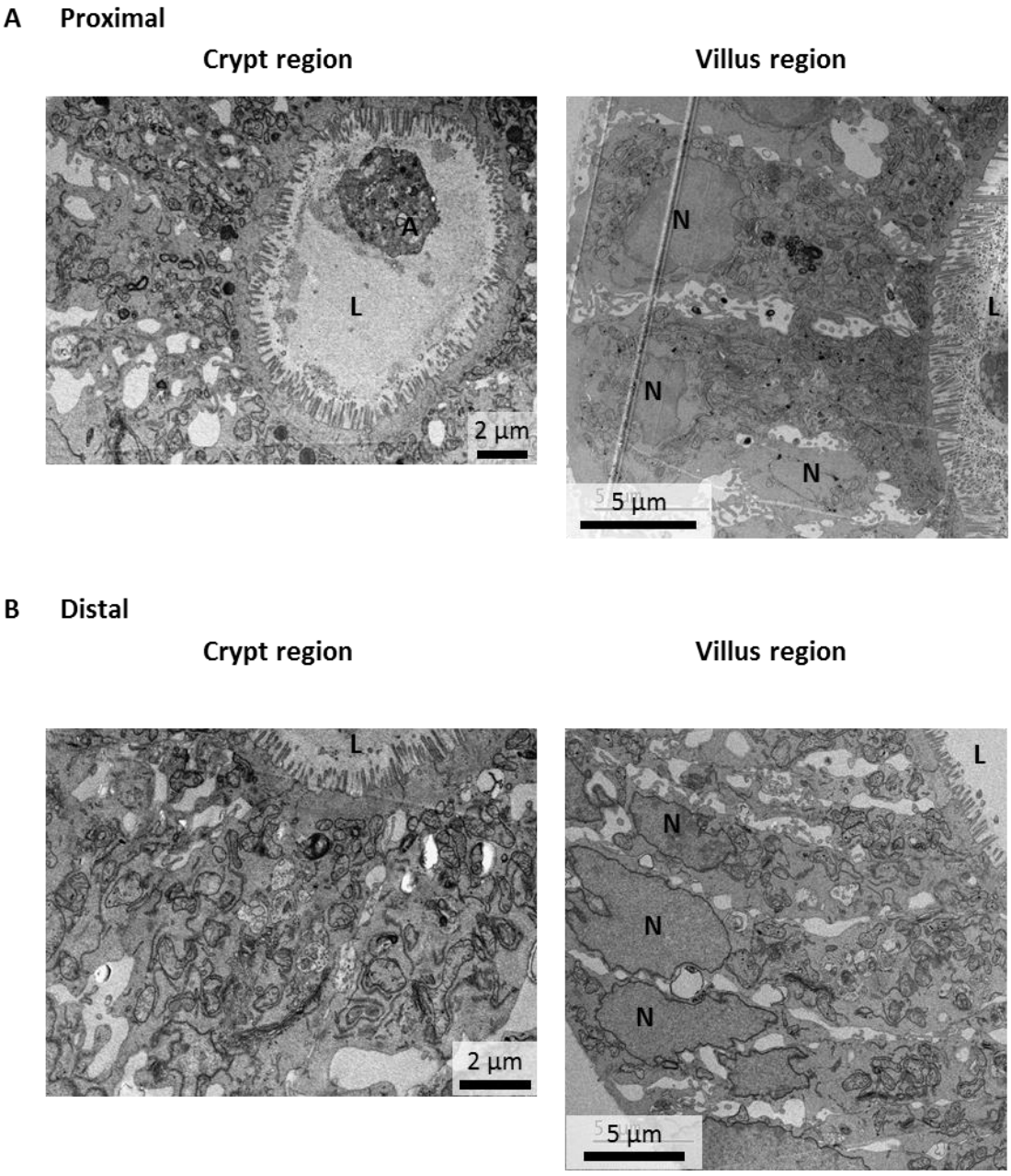

Figure 5.5. Treatment with RANKL does not cause overt structural changes in enteroids. TEM images of **(A)** proximal and **(B)** distal enteroids treated for 3 days with 200 ng/mL RANKL. L, lumen; N, nucleus; A, apoptotic body.

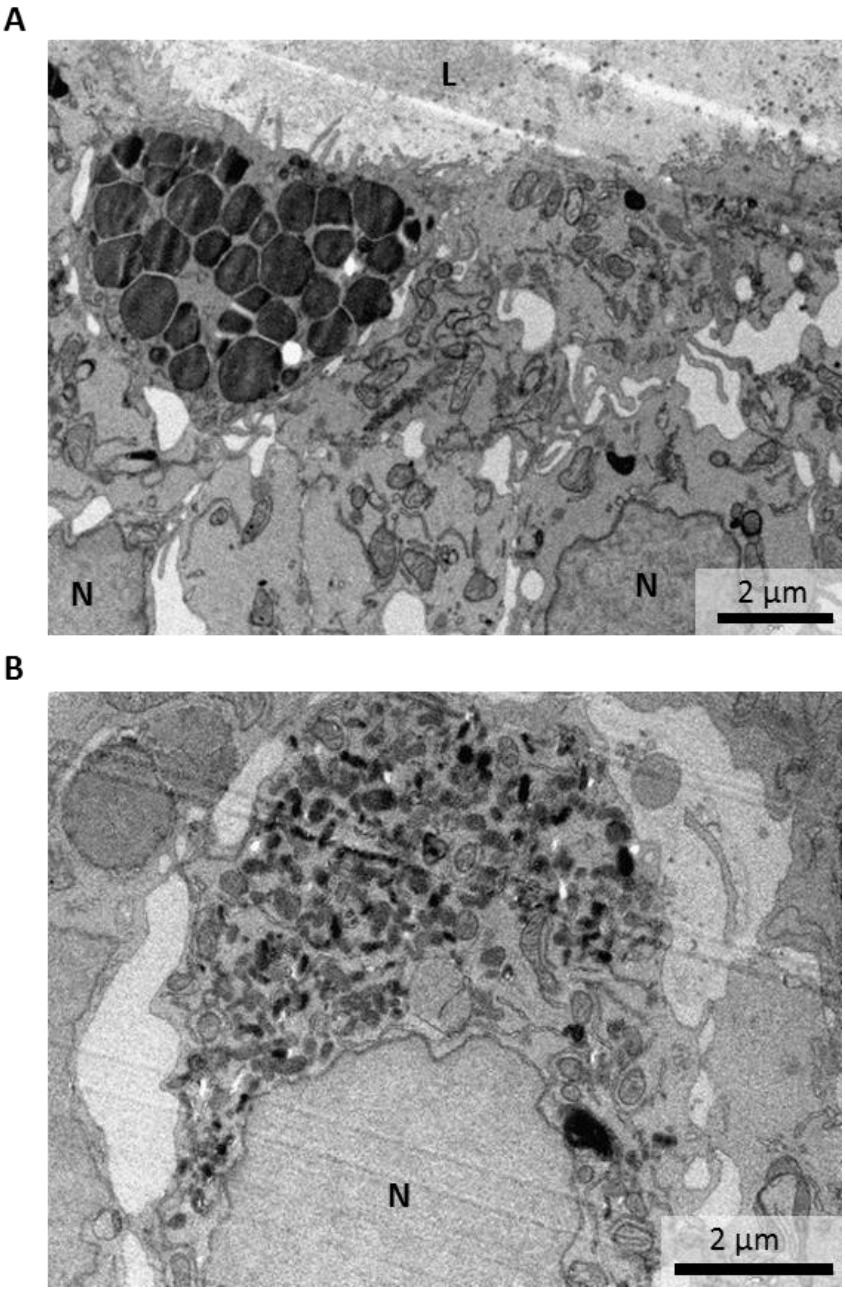

Figure 5.6. Enteroids treated with RANKL still contain other differentiated epithelial cell types. TEM images of **(A)** a Paneth cell and **(B)** a goblet cell in a distal enteroid treated for 3 days with 200 ng/mL RANKL. L, lumen; N, nucleus.

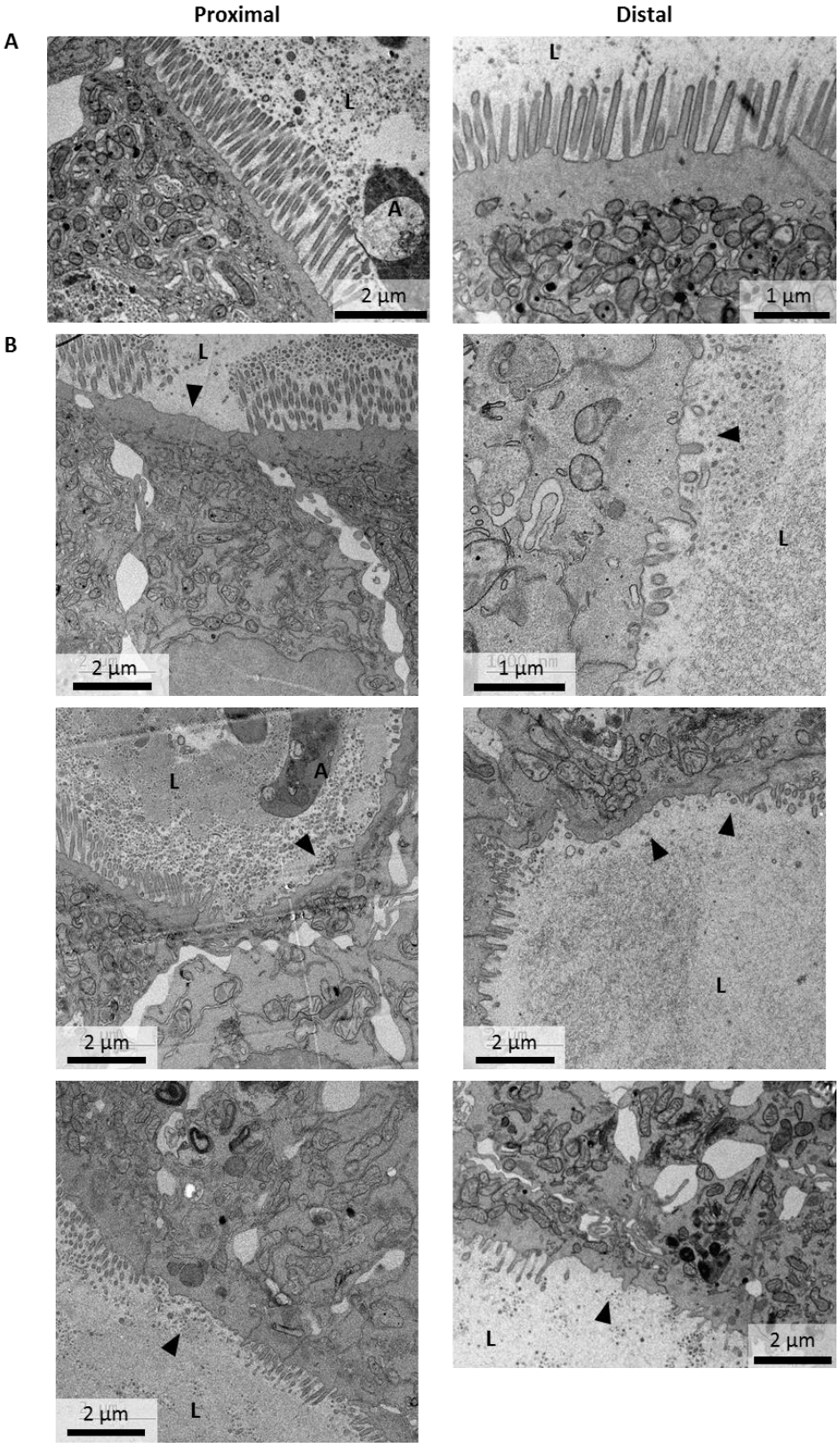

Figure 5.7. Evidence of cells with an M cell phenotype in enteroids treated with RANKL. TEM images of proximal and distal enteroids treated for 3 days with 200 ng/mL RANKL showing **(A)** cells with normal microvilli on the apical surface and **(B)** examples of cells with microvilli that appear short and irregular, typical of murine M cells. Arrowheads indicate the apical surface of cells with M cell-like appearance. L, lumen; A, apoptotic body.

5.5.3. Effect of RANKL on frequency of other epithelial cell types

5.5.3.1. Paneth cells

Given the observation that other epithelial lineages are still present in RANKL-treated enteroids (**Figure 5.6**) and that increased differentiation of M cells must impact on the proportion of the other cell types, the distribution of epithelial cell types was analysed by immunohistochemistry following RANKL treatment. The presence of Paneth cells in both untreated and enteroids exposed to 200 ng/mL RANKL for 6 days was confirmed by immunohistochemical staining (**Figure 5.7 A**). The proportion of cells within each enteroid that were Paneth cells was significantly lower in RANKL-treated enteroids than in controls (**Figure 5.8 B**). In untreated enteroids the mean proportion of cells represented by Paneth cells was 7.8% ± 1.4%, whereas this was reduced to 2.4% ± 0.4% following RANKL treatment.

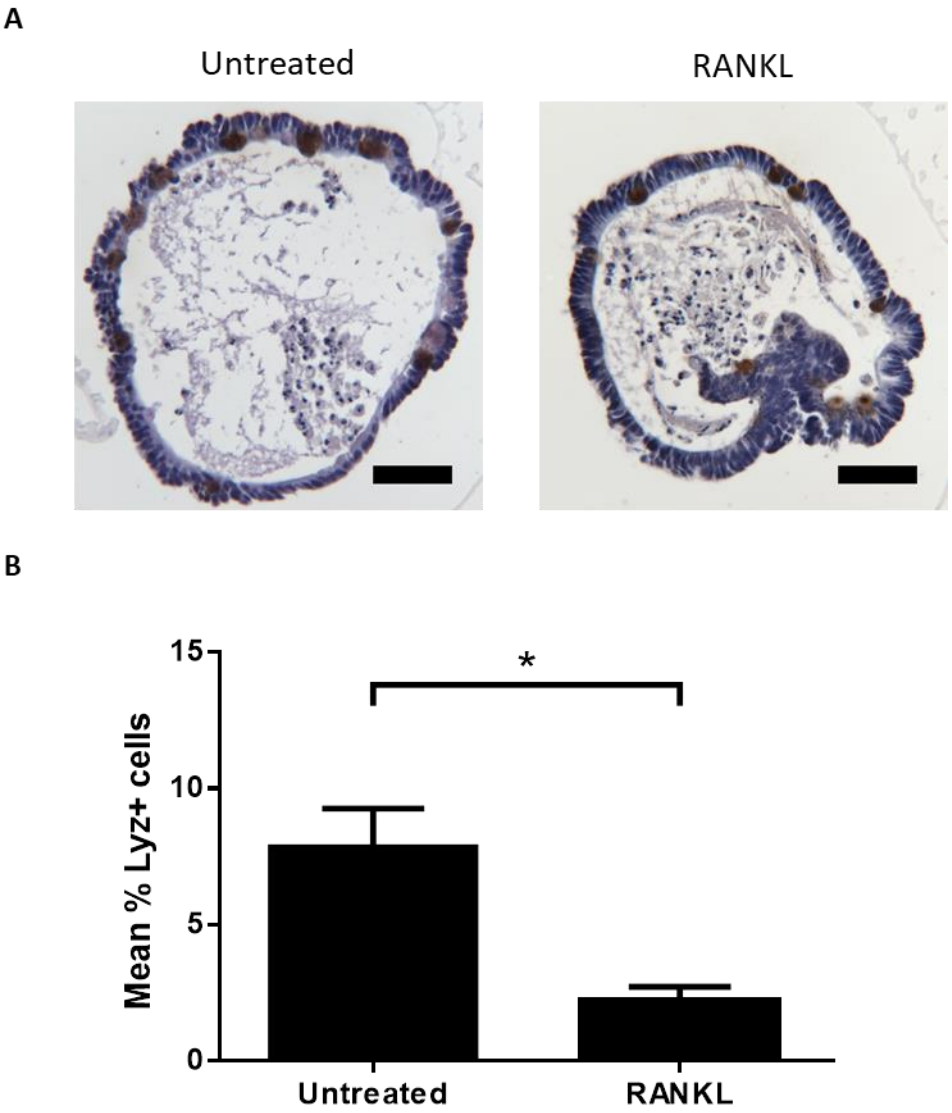

Figure 5.8. Effect of RANKL treatment on frequency of Paneth cells in enteroids. (A) Representative images of immunohistochemical staining for lysozyme (Lyz; a marker for Paneth cells) in sections of enteroids that were untreated or treated for 6 d with 200 ng/mL RANKL. Scale bars represent 50 µm. **(B)** Quantification of Paneth cells as a proportion of the total cells per enteroid section. Unpaired t-test, *p < 0.05. N = 3 independent enteroid cultures derived from 3 different mice, n = 21-29 enteroid sections. Y-axis scaled for comparison of Figures 5.8-11.

5.5.3.2. Goblet cells

Goblet cells were present in control enteroids and in those treated with RANKL (**Figure 5.9 A**). Quantification of the proportion of goblet cells per enteroid section indicated a trend towards fewer goblet cells in enteroids treated with RANKL compared to untreated controls, although this did not reach statistical significance (**Figure 5.9 B**). Untreated enteroids contained 9.3% ± 2.4% goblet cells on average, while those treated with RANKL contained 5.3% ± 0.96% goblet cells.

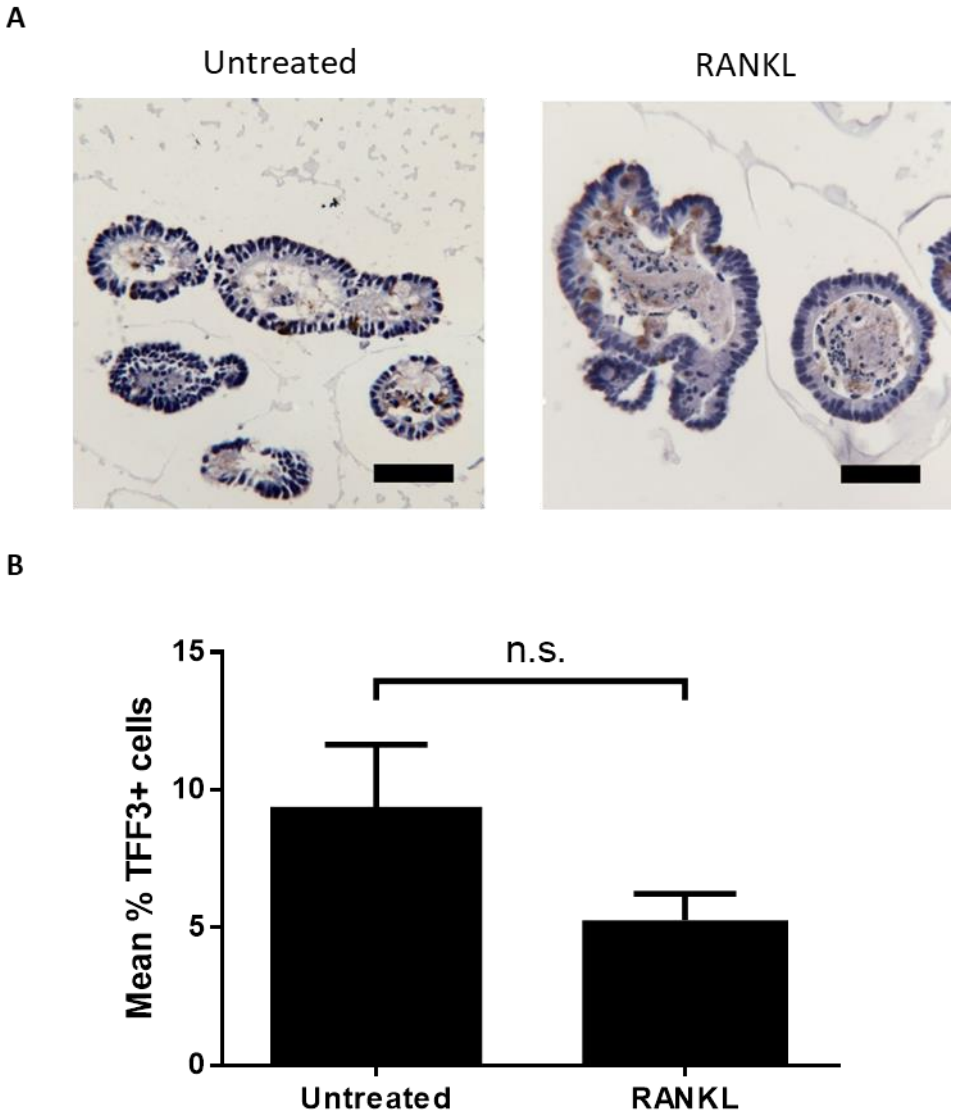

Figure 5.9. Effect of RANKL treatment on frequency of goblet cells in enteroids. (A) Representative images of immunohistochemical staining for trefoil factor 3 (TFF3; a marker for mucus-secreting goblet cells) in sections of enteroids that were untreated or treated for 6 d with 200 ng/mL RANKL. Scale bars represent 50 µm. **(B)** Quantification of goblet cells as a proportion of the total cells per enteroid section. Unpaired t-test, n.s. not significant. N = 3 independent enteroid cultures derived from 3 different mice, n = 26-34 enteroid sections. Y-axis scaled for comparison of Figures 5.8-11.

5.5.3.3. Enteroendocrine cells

Enteroendocrine cells were apparent in both untreated and RANKL-treated enteroids (**Figure 5.10 A**). The mean percentage of the epithelium made up of enteroendocrine cells in untreated enteroids was 1.9% ± 0.4% (**Figure 5.10 B**). This was similar to the percentage of enterocytes identified as enteroendocrine cells in enteroids stimulated with RANKL (2.6% ± 1.7%). No significant difference was found between the proportions of enteroendocrine cells in the two groups.

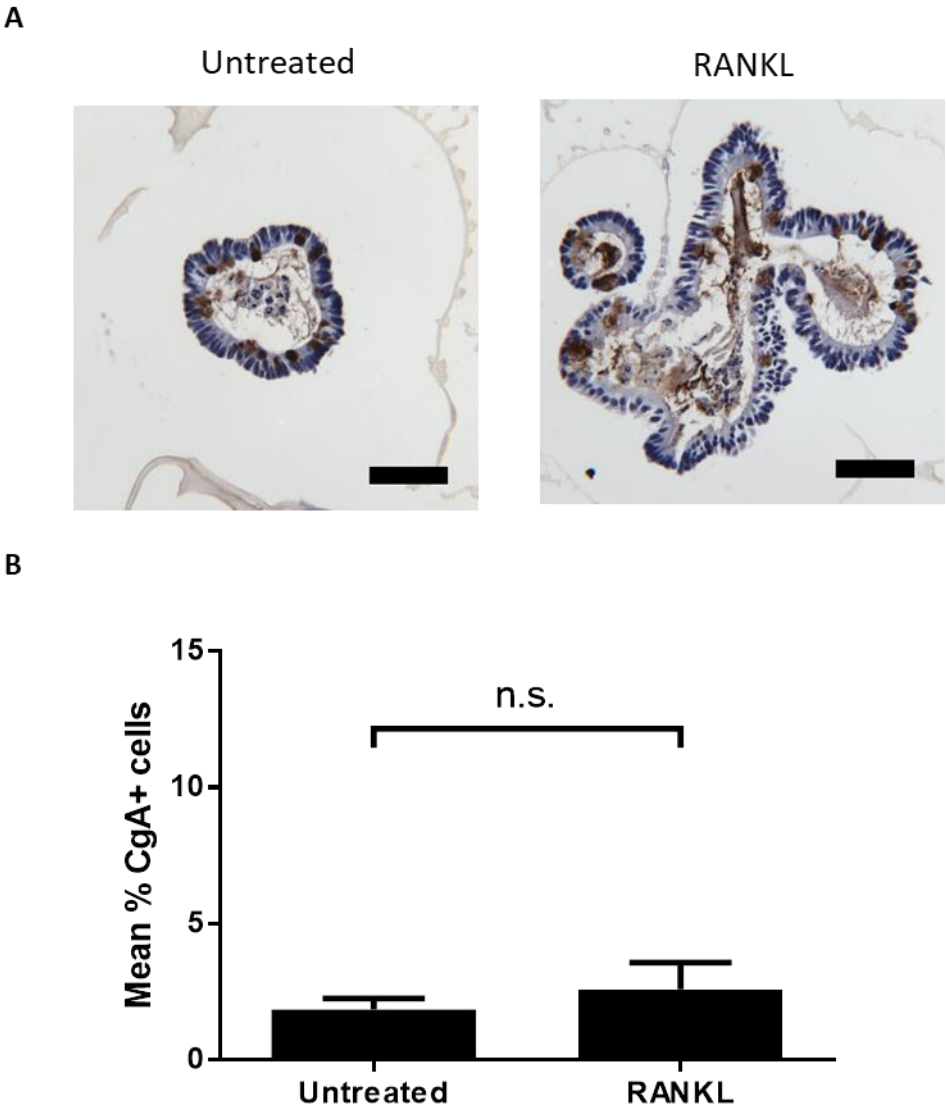

Figure 5.10. Effect of RANKL treatment on frequency of enteroendocrine cells in enteroids. **(A)** Representative images of immunohistochemical staining for chromogranin A (CgA; a marker of enteroendocrine cells) in sections of enteroids that were untreated or treated for 6 d with 200 ng/mL RANKL. Scale bars represent 50 µm. **(B)** Quantification of enteroendocrine cells as a proportion of the total cells per enteroid section. Unpaired t-test, n.s. not significant. N = 3 independent enteroid cultures derived from 3 different mice, n = 20-34 enteroid sections. Y-axis scaled to allow comparison of Figures 5.8-11.

5.5.3.4. Tuft cells

Although they occur infrequently, tuft cells were identified in both untreated controls and in those treated with RANKL (**Figure 5.11 A**). No significant difference was found between the proportions of enterocytes represented by tuft cells in untreated and treated enteroids (**Figure 5.11 B**). In untreated controls, the percentage made up by tuft cells was 1.1% ± 0.02%; in enteroids exposed to RANKL, the percentage was 0.95% ± 0.21%.

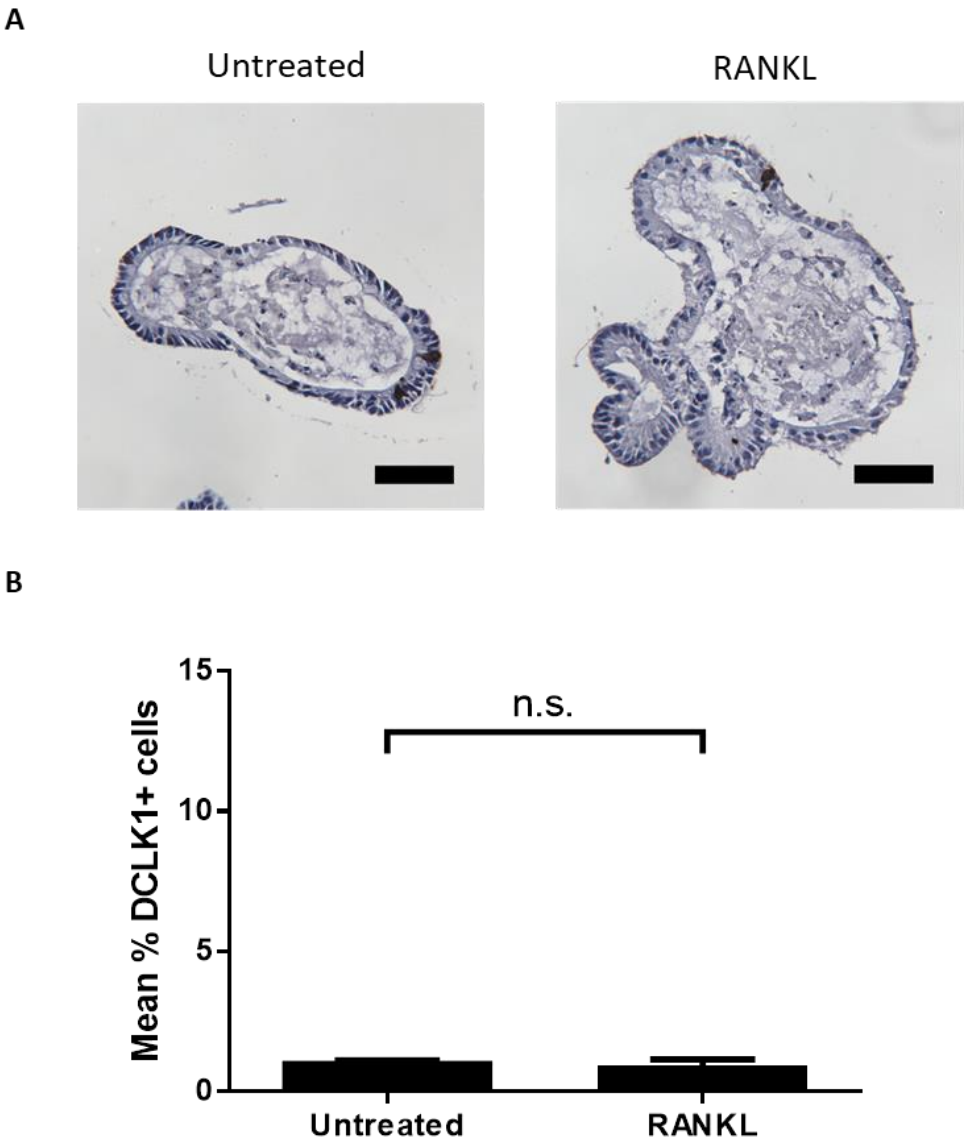

Figure 5.11. Effect of RANKL treatment on frequency of tuft cells in enteroids. (A) Representative images of immunohistochemical staining for doublecortin-like kinase 1 (DCLK1; a marker for mature tuft cells) in sections of enteroids that were untreated or treated for 6 d with 200 ng/mL RANKL. Scale bars represent 50 µm. **(B)** Quantification of tuft cells as a proportion of the total cells per enteroid section. Unpaired t-test, n.s. not significant. N = 3 independent enteroid cultures derived from 3 different mice, n = 21-26 enteroid sections. Y-axis scaled for comparison of Figures 5.8-11.

5.5.4. Effect of RANKL on epithelial permeability in enteroids

A slightly reduced TEER value – an indicator of epithelial permeability – has been reported following stimulation of Caco-2 cells are induced by Raji B cells to adopt an M cell-like phenotype (Roberts *et al.*, 2010). To examine this in RANKL-treated M cell-rich enteroids, permeability of the epithelium to luminally microinjected FD4 was assessed. Both untreated controls and enteroids treated with 200 ng/mL RANKL, added on the day of seeding, showed a similar pattern of gradual loss of luminal FD4 (**Figure 5.12 A**). This was contrasted by the marked increase in the rate of FD4 loss caused by treatment with 2 mM EGTA at 3 hours post-injection. No change was observed in the area of either untreated or RANKL-treated enteroids (**Figure 5.12 B**). This confirms that any change in mean luminal pixel intensity was due to loss of luminal FD4 rather than due to a change in enteroid area.

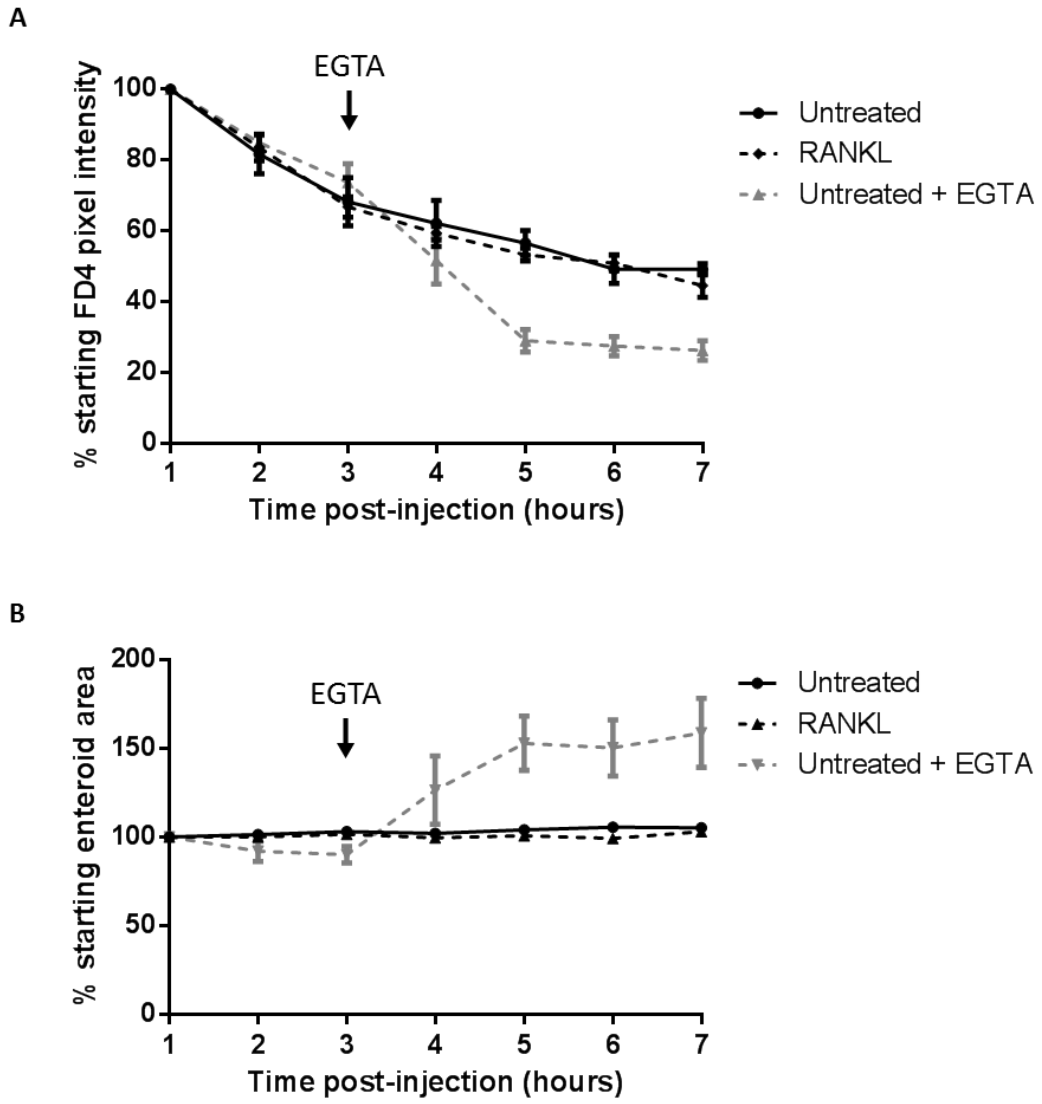

Figure 5.12. Effect of RANKL on epithelial permeability in enteroids. (A) Epithelial permeability of C57BL/6 enteroids treated with 200 ng/mL RANKL for 3 d from the day of seeding was compared to that of untreated enteroids by assessing decline in mean fluorescence intensity within the enteroids. Following microinjection of FD4 into the enteroid lumen, enteroids were monitored over 7 h. Mean luminal pixel intensity at each time point is shown relative to the intensity 1 h post-injection, which was set to 100%. Some untreated enteroids were exposed to 2 mM EGTA 3 h post-injection. N = 4 independent experiments using enteroids derived from 3 different mice, n = 2-7 enteroids per group. Error bars represent SEM. **(B)** Analysis of change in enteroid area throughout the experiment detailed in (A). Data is shown as the percentage change relative to the starting area for each enteroid. Error bars represent SEM.

5.5.1. Role of alternative pathway NF-κB signalling in M cell differentiation

Enteroid cultures were established from *Nfkb2*$^{-/-}$ mice bred on a C57BL/6 background. *Nfkb2*$^{-/-}$ enteroids showed normal appearance and growth (**Figure 5.13 A**). Following 6 days of treatment with 200 ng/mL RANKL, *Nfkb2*$^{-/-}$ enteroids showed a slight, but non-significant, increase in expression of *Spib* mRNA (**Figure 5.13 B**). This was approximately 24 times smaller than the increase found in wild-type C57BL/6 enteroids following the same treatment ((an increase in expression of *Spib* relative to *Gapdh* of 0.006 in *Nfkb2*$^{-/-}$ enteroids compared to 0.091 in wild type enteroids**; Figure 5.2 A**). There was also a very slight increase in expression of *Gp2* in RANKL-treated compared to untreated *Nfkb2*$^{-/-}$ enteroids but, again, this increase was smaller than that seen in wild type C57BL/6 enteroids (**Figure 5.13 C**).

To investigate the role of the alternative NF-κB pathway signalling protein subunit RelB in M cell differentiation, we established enteroids from *Relb*$^{-/-}$ mice bred on a C57BL/6 background. *Relb*$^{-/-}$ enteroids displayed a normal gross morphology and growth (**Figure 5.14 A**). Treatment of *Relb*$^{-/-}$ enteroids with 200 ng/mL RANKL for 6 days from the day of seeding resulted in a slight but non-significant increase in levels of *Spib* mRNA (**Figure 5.14 B**). This increase was notably much less than was observed in C57BL/6 enteroids treated with the same concentration of RANKL (an increase in expression of *Spib* relative to *Gapdh* of 0.007 in *Relb*$^{-/-}$ enteroids compared to 0.091 in wild type enteroids; **Figure 5.2 A**). *Gp2* mRNA was undetectable in both untreated and RANKL-treated enteroids (**Figure 5.14 C**).

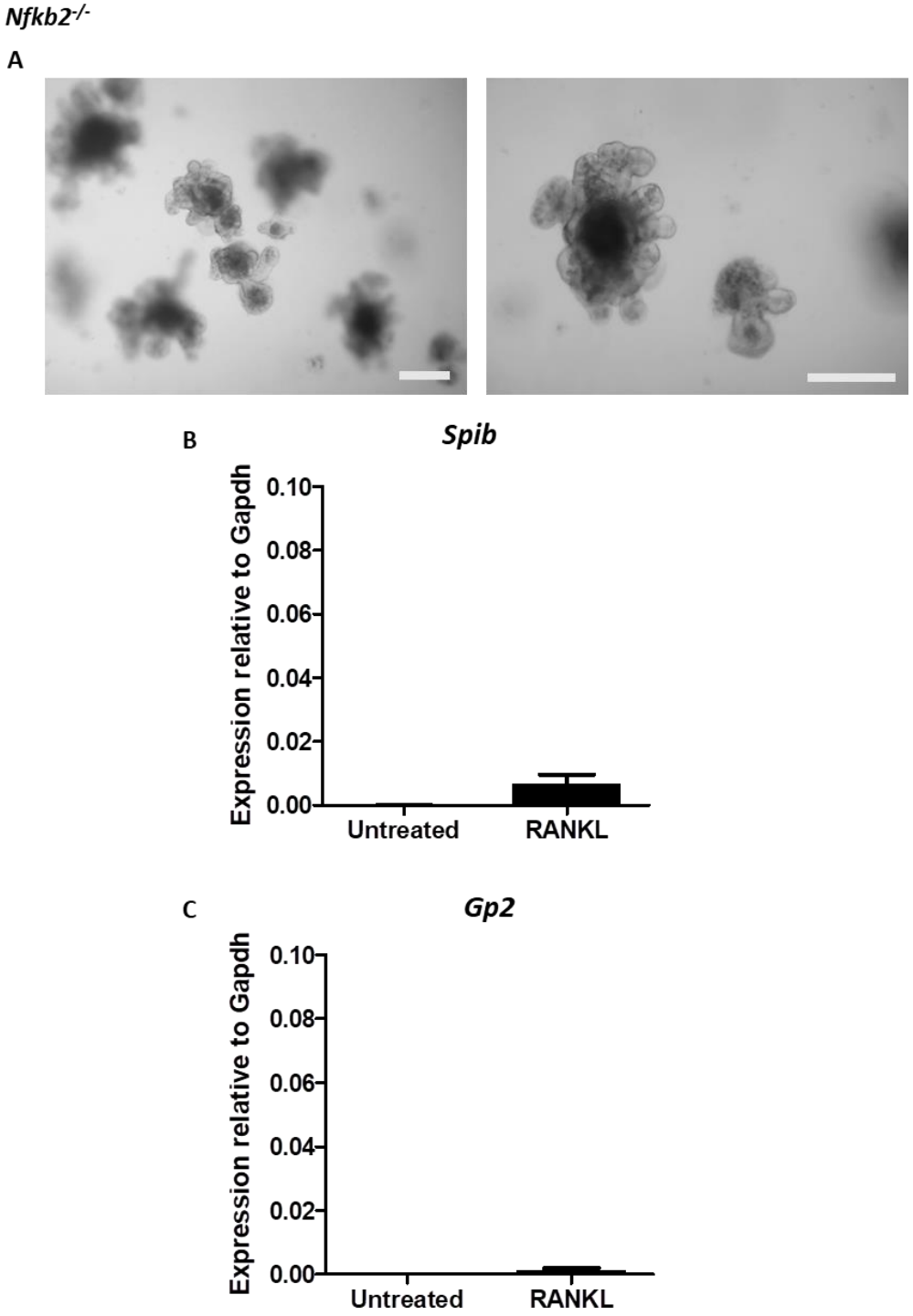

Figure 5.13. Role of NF-κB2 in M cell differentiation in enteroids. (A) Bright field images of untreated *Nfkb2*$^{-/-}$ enteroids on day 6 post-passage. Scale bars = 200 µm. **(B & C)** Quantification of (A) *Spib* and (B) *Gp2* mRNA levels in enteroids derived from distal small intestine of *Nfkb2*$^{-/-}$ mouse bred on a C57BL/6 background on day 6 post-treatment with 200 ng/mL RANKL. Enteroids were first treated with RANKL at the time of seeding. Data measured by qPCR were normalised to the housekeeping gene *Gapdh* and are represented as $2^{-\Delta CT}$. *Gp2* transcript was undetected in all untreated samples. N = 3 independent enteroid cultures derived from different mice; enteroids from 3 wells were pooled for each condition. Error bars represent SEM. Y-axes scaled for comparison with Figure 5.2 B.

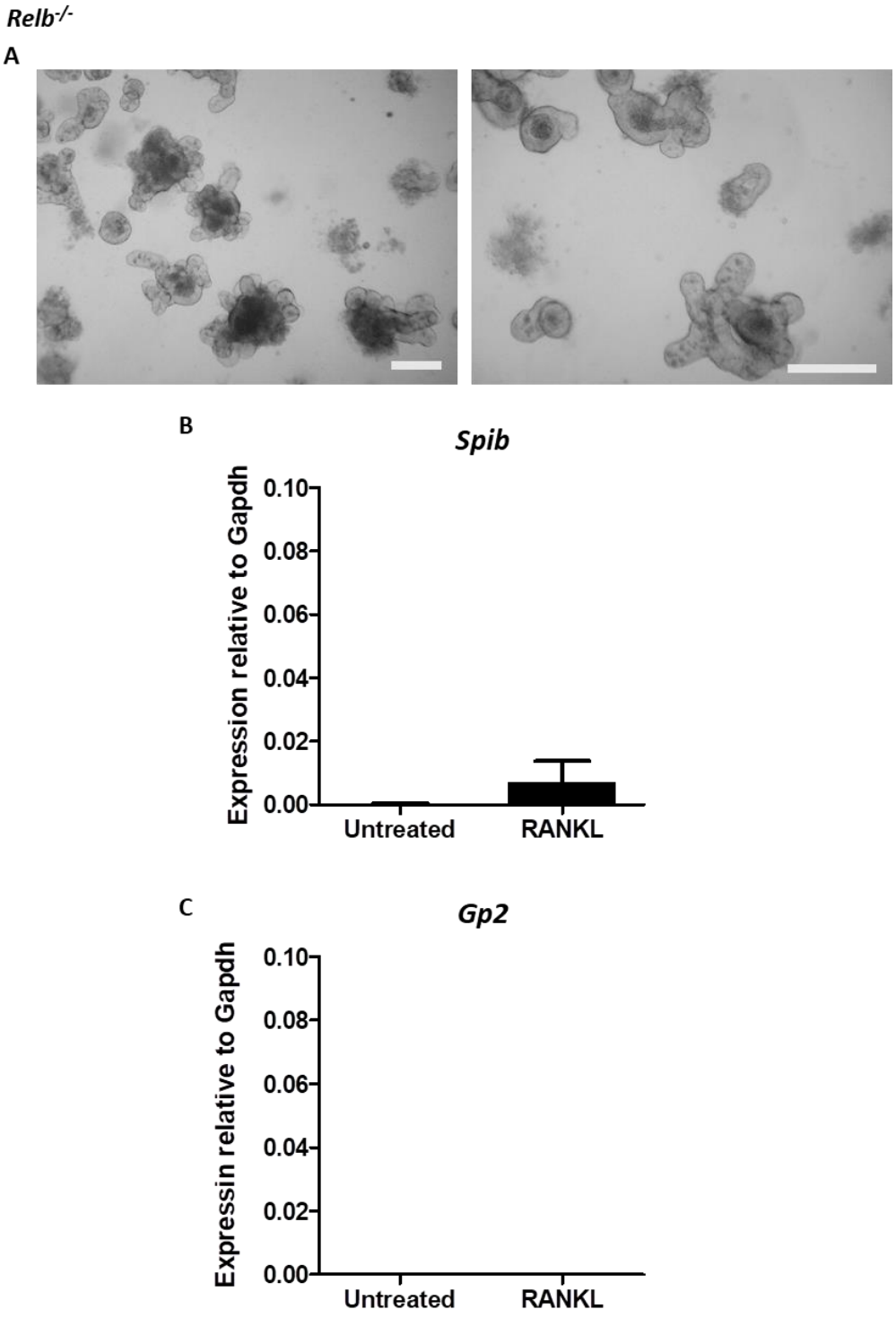

Figure 5.14. Role of RelB in M cell differentiation in enteroids. (A) Bright field images of *Relb*$^{-/-}$ enteroids on day 3 post-passage. Scale bars = 200 µm. **(B & C)** Quantification of (B) *Spib* and (C) *Gp2* mRNA levels in enteroids derived from distal small intestine of *Relb*$^{-/-}$ mice bred on a C57BL/6 background on day 6 post-treatment with 200 ng/mL RANKL. Enteroids were first treated with RANKL at the time of seeding. Data measured by qPCR were normalised to the housekeeping gene *Gapdh* and are represented as $2^{-\Delta CT}$. *Gp2* transcript was undetected in all untreated samples. N = 3 independent enteroid cultures derived from different mice. Error bars represent SEM. Y-axes scaled for comparison with Figure 5.2 B.

5.5.1. Role of B cells in M cell differentiation

Enteroids cultured for 6 days after seeding with a 50:50 ratio of normal enteroid medium and conditioned medium from Raji B cell cultures showed no induction of either *Spib* or *Gp2* expression (**Figure 5.15 A & B**). This was in comparison to enteroids cultured with a 50:50 ratio of enteroid medium and control medium that had been incubated under the same conditions but without Raji B cells.

To investigate the effects of B cells on M cell differentiation, C57BL/6 enteroids were co-cultured with Raji B cells. The Raji cells were added to the medium overlying the Matrigel droplet containing the enteroids. Raji cells were observed to cluster around the periphery of the Matrigel but did not migrate into the Matrigel (**Figure 5.16 A**). Co-culture with the Raji B cells appeared to induce increased expression of *Spib* mRNA, although this response showed large variability and did not reach significance (**Figure 5.16 B**). This was observed after both 3 and 6 days of co-culture. No change was found in the expression of *Gp2* mRNA in enteroids following co-culture with Raji B cells for either 3 or 6 days (**Figure 5.16 C**). *Gp2* mRNA was virtually undetectable in all groups, although was detected in positive control samples treated for 6 days with 200 ng/mL RANKL (**Figure 5.2 B**).

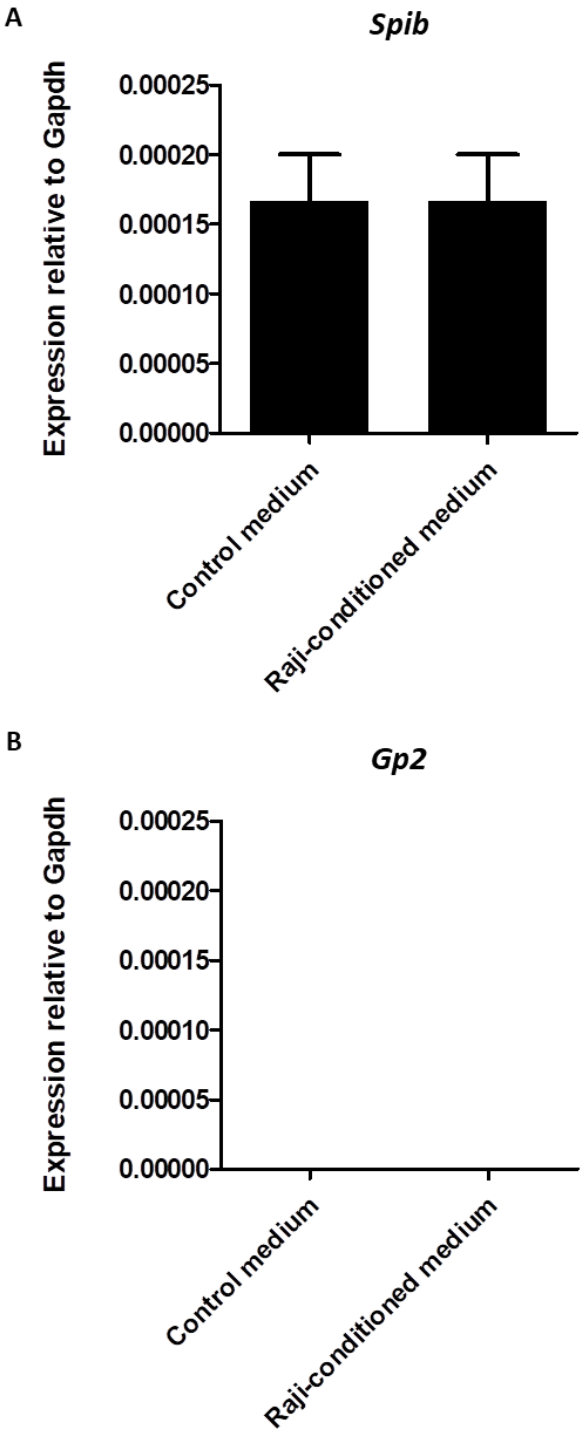

Figure 5.15. Effect of B cell-secreted factors on M cell differentiation in enteroids. Quantification of **(A)** *Spib* and **(B)** *Gp2* mRNA in enteroids derived from distal small intestine of C57BL/6 mice. Enteroids were exposed to 50% control media or 50% Raji B cell-conditioned media for 6 days from the day of seeding. Data measured by qPCR were normalised to the housekeeper gene *Gapdh* and are represented as $2^{-\Delta CT}$. *Gp2* transcript was undetected in all untreated samples. N = 3 independent enteroid cultures derived from different mice. Error bars represent SEM.

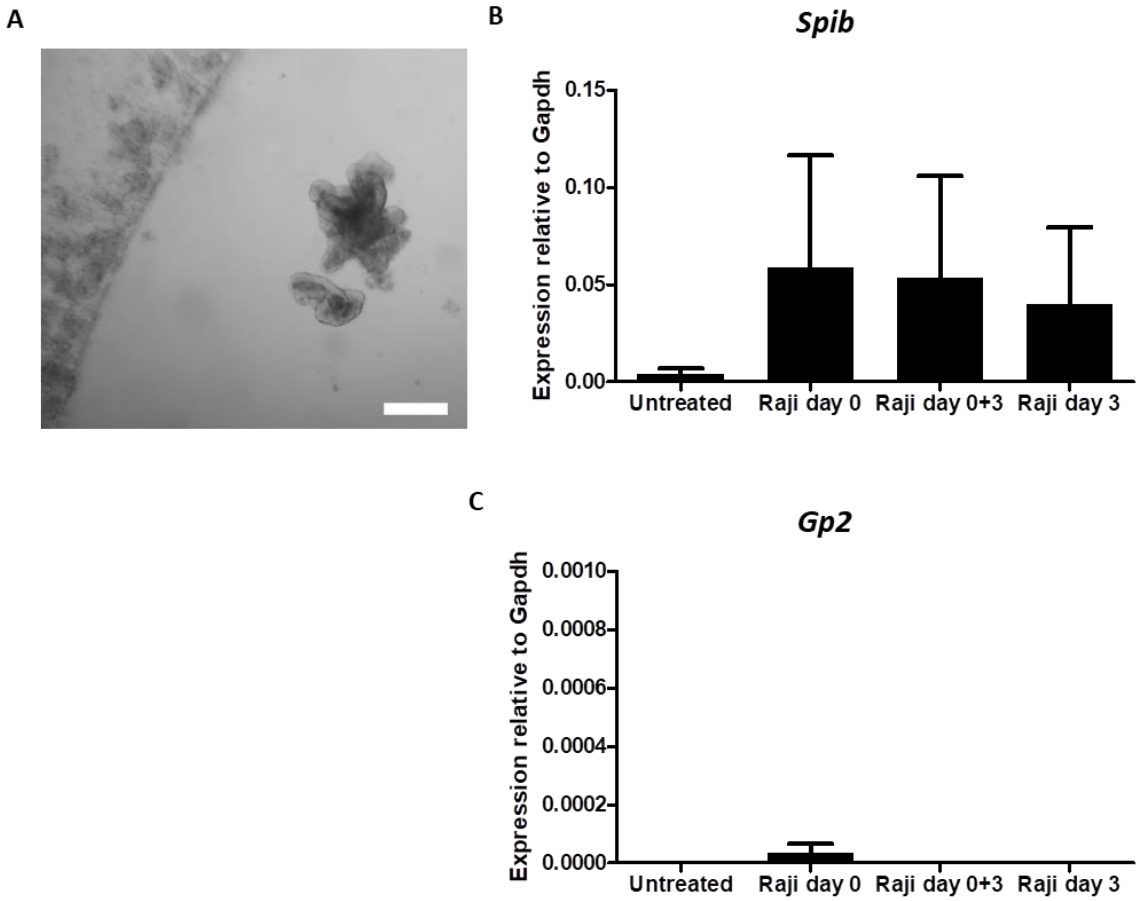

Figure 5.16. Effect of B cells on M cell differentiation in enteroids. (A) Representative bright field image showing the enteroid-Raji B cell co-cultures, with Raji B cells (arrow head) seen in the media overlying enteroids (arrows) within a droplet of Matrigel (M). Image captured on day 6 of co-culture. Scale bar = 200 µm. **(B & C)** Quantification of mRNA levels of M cell-associated genes (B) *Spib* and (C) *Gp2* in enteroids derived from distal small intestine of C57BL/6 mice on day 6 post-seeding. Enteroids were cultured with 1 x 10^5 Raji B cells either from the day of seeding with no replacement of Raji cells, from the day of seeding with replacement of Raji cells on day 3 post-seeding, or with addition of Raji cells on day 3. Data measured by qPCR were normalised to the housekeeping gene *Gapdh* and are represented as $2^{-\Delta CT}$. *Gp2* transcript was undetected in all untreated samples. N = 3 independent enteroid cultures derived from different mice; enteroids from 3 wells were pooled for each condition. Error bars represent SEM.

5.6. Summary of results

1. RANKL induces M cell differentiation in wild type C57BL/6 mouse enteroids, as shown by upregulation of *Spib* and *Gp2* expression and increased expression of SpiB at the protein level.

2. The frequency of Paneth and goblet cells is reduced in enteroids treated with RANKL, while enteroendocrine cell and tuft cell populations remained constant.

3. Alternative pathway NF-κB signalling is required for RANKL-induced M cell differentiation, including a requirement for both NF-κB2 and RelB.

4. B cells are able to induce a limited degree of M cell differentiation, with upregulation of *Spib* but not of *Gp2*, a marker of mature M cells.

5.7. Discussion

Understanding the factors regulating M cell differentiation and function is key to gaining insight into their role in antigen sampling and induction of intestinal immune responses. This will aid development of improved oral vaccines and novel therapies against enteric infections. Progress in this area has been hampered by a lack of robust *in vitro* models of M cells and the FAE; however, recent discoveries have identified that the cytokine RANKL upregulates expression of *Spib*, a master transcription factor that drives M cell differentiation (Knoop *et al.*, 2009; Kanaya *et al.*, 2012). Although the source of RANKL *in vivo* is specialised mesenchymal cells in the sub-epithelial dome of Peyer's patches, the demonstration that exogenous RANKL is sufficient to induce differentiation of M cells in enteroid cultures presents an exciting new model of the FAE (de Lau *et al.*, 2012).

Here, we provide additional evidence in support of these earlier findings, showing in a physiologically relevant, 3D model of the small intestinal epithelium – generated from intestinal crypt stem cells derived from either the proximal or the more relevant distal region – that exogenous RANKL stimulates upregulation of transcription factor *Spib* and M cell marker *Gp2*. Nuclear SpiB is detected in many cells throughout the epithelium following addition of RANKL, demonstrating that upregulated mRNA is translated to increased levels of protein. We further characterised the RANKL-stimulated enteroid model, showing that treatment with RANKL perturbs the usual distribution of different epithelial cell types found in the enteroid

epithelium, resulting in a trend towards fewer TFF3-positive, mucus-secreting goblet cells and significantly fewer lysozyme-positive Paneth cells. Upregulation of *Spib* and *Gp2* by RANKL is shown to require *Nfkb2* and *RelB*, indicating that alternative pathway NF-κB signalling is necessary for M cell differentiation. Finally, a B cell line was also found to be capable of stimulating upregulation of *Spib* but not of *Gp2*, suggesting that B cells do likely promote M cell differentiation but are perhaps not sufficient alone to generate fully mature M cells.

The data presented here are in agreement with the findings of two previous studies showing that RANKL induced upregulation of *Spib* and *Gp2* in murine enteroids (de Lau *et al.*, 2012; Rouch *et al.*, 2016). This is further supported by our demonstration that SpiB expression at the protein level is also increased and evidence from TEM studies showing individual cells within the enteroids that displayed M cell-like characteristics, with irregular apical microvilli. Similar findings have been described in the Caco-2 cell line-based model of M cells, where a variable number of cells with irregular microvilli were identified following co-culture with Raji B cells (Roberts *et al.*, 2010). In their study, Clevers and colleagues also observed increased expression of the receptor *Rank* following RANKL treatment, independently of SpiB (de Lau *et al.*, 2012); however, we found no change in the level of *Rank* mRNA. Elevated levels of RANK expression in M cells or the FAE have not been described in other studies.

In the studies presented here, a large degree of variation was found in the fold changes measured in *Spib* and *Gp2* between independent experiments. Likely explanations for this are a) variation in enteroid seeding density between individual experiments, which could alter the available concentration of RANKL, and b) contamination of RNA samples due to incomplete removal of Matrigel. Since Matrigel is produced by murine cells, it is therefore likely to contain some mouse RNA.

Immunohistochemical analysis of SpiB showed that SpiB was essentially absent in untreated epithelial cells, whereas SpiB expression was observed in approximately 14% ± 4.6% of cells following treatment for 6 days with RANKL. The fact that SpiB was not expressed in all cells, despite all cells presumably receiving the same amount of RANKL stimulation, suggests that a process of lateral inhibition may be occurring; for example, so that M cells inhibit their neighbours from also becoming M cells. Such a mechanism could be a way of limiting the number of M cells within the FAE. This is in agreement with previous reports that the distribution of M cells in the FAE is spatially regulated so that they are dispersed across the FAE rather than forming clusters (Wang *et al.*, 2011; Hsieh and Lo, 2012). Hsieh and Lo observed that conditional deletion of either Notch, or its ligand Jagged1, resulted in increased clustering

of M cells within the FAE, suggesting that Notch signalling may be involved in patterning of M cell distribution via lateral inhibition (Hsieh and Lo, 2012). Notch signalling is known to coordinate complex spatial arrangement of cell types during development of other tissues, such as in the Drosophila eye disc and mammalian inner ear (Hsieh and Lo, 2012).

In this respect, RANKL-stimulated enteroids appear to be a good model of the FAE. Here, 14.0% ± 4.6% of cells within the enteroid epithelium were SpiB-positive following RANKL treatment, which is comparable to the approximately 10% of cells within the FAE that have previously been reported to be M cells (Mabbott *et al.*, 2013). In variations on the Caco-2 cell line model, one study reported that 20-70% of cells within a monolayer co-cultured with Raji B cells were observed to adopt an M cell-like morphology, without clearly defined apical microvilli (Roberts *et al.*, 2010); another study reported a conversion rate of between 15-30% based on morphological analysis (des Rieux *et al.*, 2007).

In addition to promoting M cell differentiation, the data presented here show that exogenous RANKL also reduced the proportion of Paneth cells, and likely also the number of goblet cells, present in the enteroid epithelium. In support of this, elevated goblet cell numbers have been observed in the FAE of mice with an epithelium-specific deletion of *Traf6* (Kanaya *et al.*, 2018). This effect could be a consequence of increased M cell differentiation, leaving fewer progenitor cells available to be directed into the other epithelial lineages, or due to redirection (specifically of Paneth and goblet cell progenitors) towards the M cell fate. Alternatively, RANKL may inhibit Paneth and goblet cell differentiation via an (as yet unknown) independent mechanism. Furthermore, goblet and M cell populations are expanded in mice following conditional deletion of *Notch1* and reduced following deletion of *Jag1* (encoding Jagged1) (Hsieh and Lo, 2012). These findings are in line with the data presented here and support the hypothesis that M cells and goblet cells share a common precursor, or at least similar lineage commitment requirements (Kanaya *et al.*, 2018). Furthermore, they also support the relevance of RANKL-stimulated enteroids as a model of the FAE, where goblet and Paneth cells are reported to be less abundant *in vivo* (Neutra, Mantis and Kraehenbuhl, 2001).

We provide evidence that both NF-κB2 and RelB are required for RANKL-induced upregulation of *Spib* and *Gp2*, suggesting that alternative pathway NF-κB signalling is essential for M cell differentiation (**Figure 5.17**). These data are in agreement with a very recent study demonstrating that the increased expression of M cell markers in response to RANKL is largely abolished in enteroids generated from an independent strain of $Relb^{-/-}$ mice (Kanaya *et al.*, 2018). Overexpression of *Relb* and *Nfkb2* in the enteroids was also sufficient to upregulate *Spib*

but not *Gp2*. The same study showed that canonical NF-κB signalling is also important for M cell differentiation as inhibition of IκB kinase-β – a crucial component of the canonical pathway – impaired upregulation of M cell markers in response to RANKL (Kanaya *et al.*, 2018). Overexpressing canonical pathway subunits, NF-κB1 and RelA, also induced M cell markers but to a lesser degree than RANKL or NF-κB2/RelB (Kanaya *et al.*, 2018). Conversely, expression of *Spib* and functional maturation of M cells was shown to be unaffected in c-Rel-deficient mice (Sehgal *et al.*, 2017).

Findings from another very recent study indicate that a second transcription factor, Sox8, acts independently of SpiB to drive M cell differentiation in response to RANKL (Kimura *et al.* 2019). The authors reported that Sox8 is upregulated in a RelB-dependent manner following RANKL stimulation and is necessary for induction of *Gp2* expression by RANKL. Direct binding of Sox8 to the *Gp2* promoter region was demonstrated; however, similarly to SpiB, Sox8 alone was insufficient to generate mature $GP2^+$ M cells and the authors suggest that SpiB may contribute to *Gp2* induction by upregulating factors that stabilise Sox8 binding to DNA.

Aside from RANKL signalling, there is also evidence that B cells have a role in promoting M cell differentiation (Kernéis *et al.*, 1997; des Rieux *et al.*, 2005; Ebisawa *et al.*, 2011). The data presented here support this conclusion as we show that enteroids co-cultured with B cells express elevated levels of *Spib* mRNA. Co-cultured enteroids did not, however, show any change in expression of *Gp2*. This indicates that B cell-derived signals are insufficient to generate mature M cells. A limitation of our study is that we did not investigate whether co-cultured enteroids contained functional M cells capable of transcytosis. No change in *Spib* expression is observed when enteroids are treated with a mixture of normal culture medium and medium conditioned by the same B cells. This might suggest that B cell-induced upregulation of *Spib* requires cell-cell contact; however, B cells in co-cultures did not appear to migrate into the Matrigel to a great extent so contact was likely to have been limited. It is possible that crosstalk between epithelial cells and B cells is required to induce expression or secretion of the M cell-promoting factors. Alternatively, it is also possible that the relevant factors are quite unstable or were not present at sufficient concentrations in the conditioned medium to stimulate *Spib* upregulation.

It should also be noted that the species difference between murine epithelium and human Raji B cells may have reduced the effect of B cells on the epithelial cells. Evidence to support this comes from the study of Pringault and colleagues, where they observed that B cells isolated from Peyer's patches of mice were ~5 times more effective at transforming Caco-2 cells to

functional M-like cells than human Raji B cells, as determined by enhanced translocation of latex particles (Kernéis *et al.*, 1997). As well as secreted soluble factors – likely candidates including TGF-β and RANTES (Gullberg, 2005) – their study also indicated that cell-cell contact between B cells and epithelial cells is required in this system to support transformation to M-like cells (Kernéis *et al.*, 1997). Cell surface expression of β1-integrins may play a key role here in enhancing M cell functionality (Gullberg *et al.*, 2006). In the study presented here, significant Raji B cell contact with epithelial cells was restricted by the Matrigel barrier.

Overall, the evidence presented here provide important characterisation of RANKL-stimulated enteroids as a novel *in vitro* model of the FAE and are in agreement with others' recent findings on the role of NF-κB alternative pathway signalling in M cell differentiation. Enteroids are a uniquely useful for unpicking the role of epithelium-intrinsic factors in M cell differentiation, given the opportunity they allow to isolate the epithelium from immune and stromal components. Given the close resemblance of these enteroids to the FAE *in vivo* – further characterised in the present study – this model will be a powerful tool for investigating the mechanisms of antigen sampling in this specialised region. One report published during the course of our own studies has begun to address this field, using 2D adult intestinal stem cell-derived cultures stimulated with RANKL to investigate uptake of S. *Typhimurium* (Rouch *et al.*, 2016).

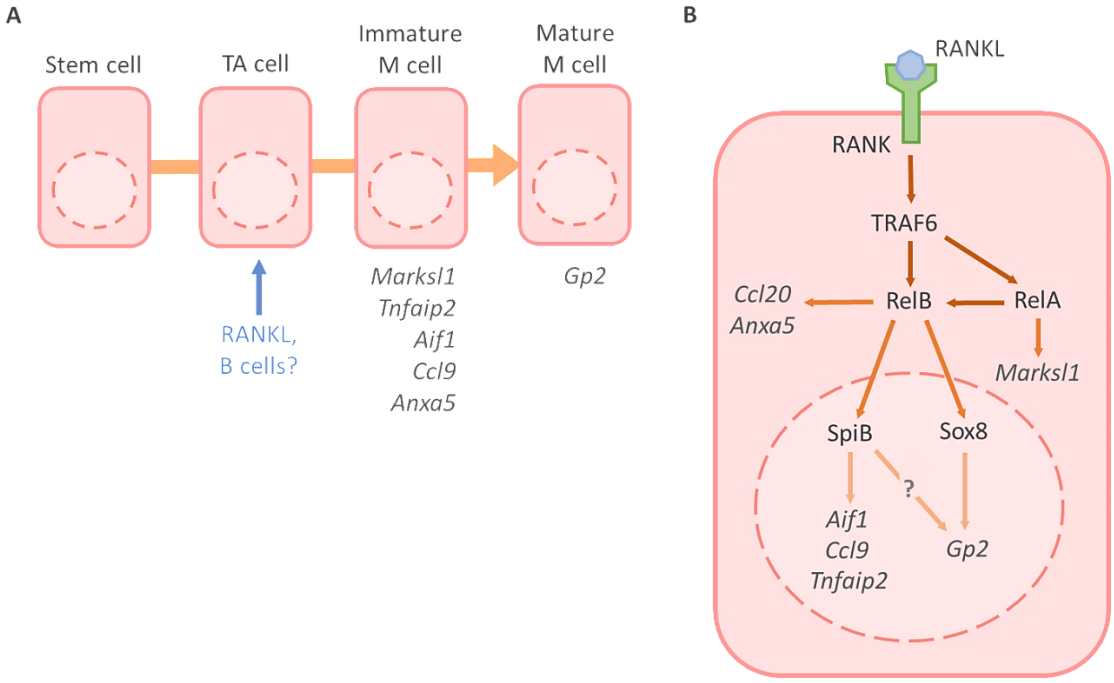

Figure 5.17. Current understanding of the molecular pathways regulating M cell differentiation. (A) M cell differentiation is driven by RANKL acting via its receptor, RANK, which is expressed throughout the epithelium. The endogenous source of RANKL is mesenchymal M cell inducer (MCi) cells in the sub-epithelial dome of Peyer's patches. Some evidence also suggests that B cells may promote M cell differentiation by a currently unknown mechanism. **(B)** Downstream of RANK, TRAF6 drives both classical (RelA) and alternative (NF-κB2/RelB) NF-κB signalling. The classical pathway upregulates expression of the M cell-associated gene *Marcksl1*, while RelB is required for induction of key transcription factors, SpiB and Sox8. SpiB drives M cell differentiation by upregulating M cell-associated genes, including *Ccl9*, *Aif1* and *Tnfaip2* but seems to be insufficient to drive M cell maturation via expression of *Gp2* alone. Sox8 is necessary for *Gp2* expression, likely though direct binding of the *Gp2* promoter, while SpiB may contribute by upregulating additional regulatory co-factors. Other M cell-related genes, eg. *Anxa5*, are also thought to be induced by RelB signalling, independently of SpiB. Figure adapted from (Kimura *et al.*, 2019) and (Kanaya *et al.*, 2018).

Chapter 6

Development of a fluorescent long polar fimbriae adhesin fusion protein to investigate targeting and uptake in M cell-rich enteroids

6.1. Introduction

The FAE is an important interface as its antigen sampling activity allows immune cells to survey the contents of the gut lumen and respond accordingly. Several studies have demonstrated the ability of FAE cells to bind and take up a range of external particles, including beads and even whole bacteria (Kernéis *et al.*, 1997; Gullberg *et al.*, 2000; de Lau *et al.*, 2012; Rouch *et al.*, 2016). This immune surveillance is required for normal intestinal IgA responses (Rios *et al.*, 2016). This function of the FAE is also exploited by enteropathogens as route of invasion, making the FAE important as a site of infection initiation (Miller, 2007).

Uptake of bacteria by M cells within the FAE is thought to occur via specific ligand-receptor interactions, although few examples have so far been described. Uptake of several bacteria, including *S.* Typhimurium and *E. coli*, is mediated by the interaction of M cell-expressed GP2 with bacterial adhesion FimH, a component of bacterial type I pili (Hase, Kawano, *et al.*, 2009). Closely related to the *fim* operon encoding type I pili is the *lpf* operon, which encodes long polar fimbriae, another type of bacterial adhesion molecule (Bäumler and Heffron, 1995). The *lpf* operon contains 5 genes, of which *lpfA* encodes the major fimbrial subunit. Like the type I fimbrial adhesin FimH, long polar fimbriae adhesin (LpfA) has also been shown to mediate preferential binding of *S.* Typhimurium and Crohn's disease-associated adherent, invasive *E. coli* (AIEC) to M cells of the FAE (Baumler *et al.*, 1996; Chassaing *et al.*, 2011).

In Chapter 5 of this thesis, it was confirmed that M cell differentiation can be induced in enteroid cultures by addition of exogenous RANKL, thus generating a highly physiologically relevant *in vitro* model of the FAE. This system could be used to investigate interactions of bacteria and their components with epithelial cells of the FAE. Due to the 3D nature of enteroids, luminal and basolateral compartments are separated, making it possible to study translocation or transcytosis of bacteria and antigens across the epithelium; however, delivery of substances to the luminal compartment in the enteroid model is only possible via microinjection.

In Chapter 3 of this thesis, an assay to evaluate epithelial permeability was described, where a fluorescent dye was successfully microinjected into the enteroid lumen. These results confirm that this technique is possible. Although injection of a suspension of whole bacterial into the enteroid lumen has been described (Forbester *et al.*, 2015; Leslie *et al.*, 2015), it is significantly more technically challenging. Injection of a suspension of fluorescently labelled microspheres with a diameter of 1 µm was also impractical due to clogging of the needle opening.

Efforts were made to increase the dimensions of micropipettes to allow for the larger particles to pass through the tip; however, this resulted in greater difficulty in piercing the enteroid epithelium and significant damage to the enteroid epithelium. With this also comes an increased probability the injected substance leaking out of the enteroid lumen at disrupted sites. These issues were also encountered when using pre-pulled microcapillaries with a larger opening. An additional disadvantage of using inert latex microspheres is that they do not feature any of the bacterial surface molecules that are potential specific M cell receptors.

An alternative approach was therefore pursued. Given the availability of a plasmid harbouring the gene encoding the *S.* Typhimurium long polar fimbriae major subunit, LpfA (Humphries *et al.*, 2003), it was decided to construct a fusion protein that might be used to track the bacterial adhesion molecule by time-lapse confocal microscopy following injection into M cell-rich (RANKL-treated) enteroids. With no issues of particle size, microinjection of this recombinant protein could be performed in the same manner as previously described for FITC-dextran. This chapter describes the generation of a construct to produce such a fusion protein of LpfA and a fluorescent protein. A second construct is also generated to produce mCherry alone, for use as a negative control in the intended experiments described above.

6.2. Hypothesis

Recombinant LpfA, the major adhesion subunit of bacterial Lpf, can be used as a surrogate to track targeting, adhesion and transcellular uptake of *S.* Typhimurium by M cells in an enteroid model of the FAE.

6.3. Aim

To generate a fusion protein consisting of the *S.* Typhimurium adhesion protein, LpfA, and fluorescent protein, mCherry, that may be injected into the enteroid lumen and tracked by fluorescence microscopy to model bacterial adhesion and uptake in the enteroid model of the FAE.

6.4. Methods

Plasmids

The plasmid pAH97 and empty vector pGEX-4T-2 were generously provided by Professor Andreas Bäumler (Department of Medical Microbiology and Immunology, University of California, Davis, USA). pGEX-4T-2 is a bacterial plasmid for expressing glutathione (N-terminally tagged) S-transferase (GST) fusion proteins, containing the sequence encoding GST inserted immediately before the multiple cloning site (**Figure 6.1**). The GST tag facilitates purification of the expressed protein and a thrombin cleavage site at the end of the GST sequence allows removal of the GST tag if desired. pAH97 is a pGEX-4T-2 construct expressing *S.* Typhimurium LpfA for generation of a GST-LpfA fusion protein (**Figure 6.2**). Generation of the pAH97 plasmid had been performed by PCR amplification of the sequence encoding the major fimbrial subunit, LpfA, using overhanging primers to add a BamHI restriction site at the 5' end and an XbaI site at the 3' end of the resulting amplicon (Humphries *et al.*, 2003). This had then been blunt-end cloned into the pCR2.1 vector, before being cut out and cloned in-frame with GST into the pGEX-4T-2 vector using BamHI and EcoRI (**Figure 6.3**) (Humphries *et al.*, 2003).

The TOPO-mCherry cloning vector that carries the mCherry cDNA encoding a 26.7 kDa red fluorescent protein (587 nm/610 nm excitation/emission maxima) was a kind gift from Dr Massimiliano Stagi (Department of Cellular & Molecular Physiology, University of Liverpool, UK), originally from originally from Tyler Jacks (Addgene plasmid # 68490; Akama-Garren *et al.*, 2016) (**Figure 6.4**).

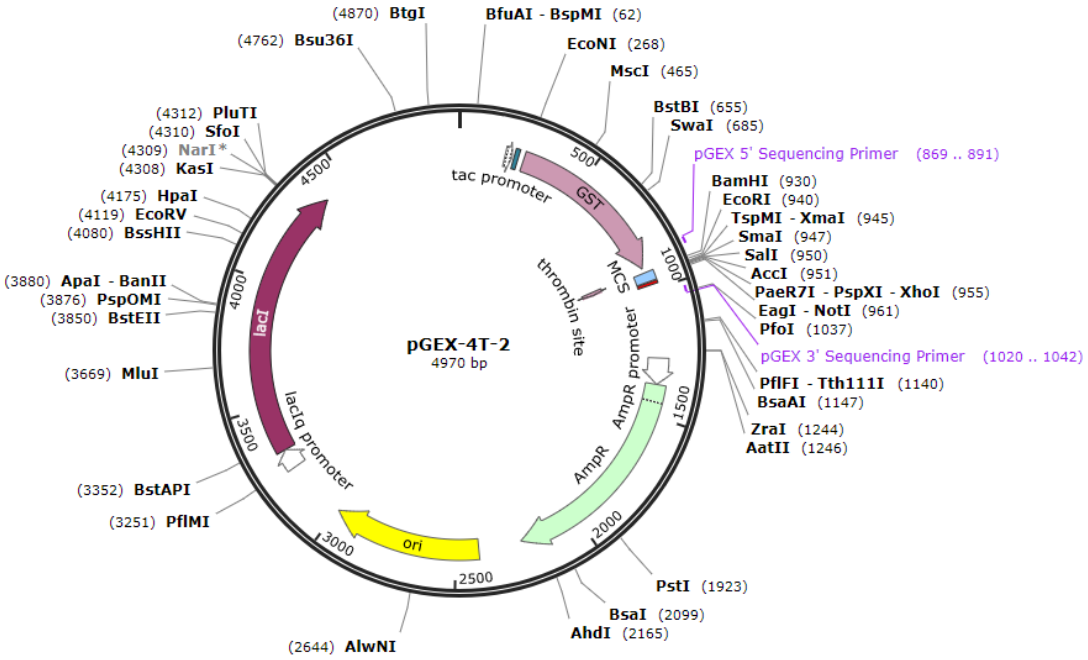

Figure 6.1. Map of pGEX-4T-2 plasmid. pGEX-4T-2 is a vector for expression of GST-tagged recombinant proteins. Figure made using SnapGene Viewer (GSL Biotech, Chicago, IL, USA) with sequence from Addgene (https://www.addgene.org/vector-database/2877/).

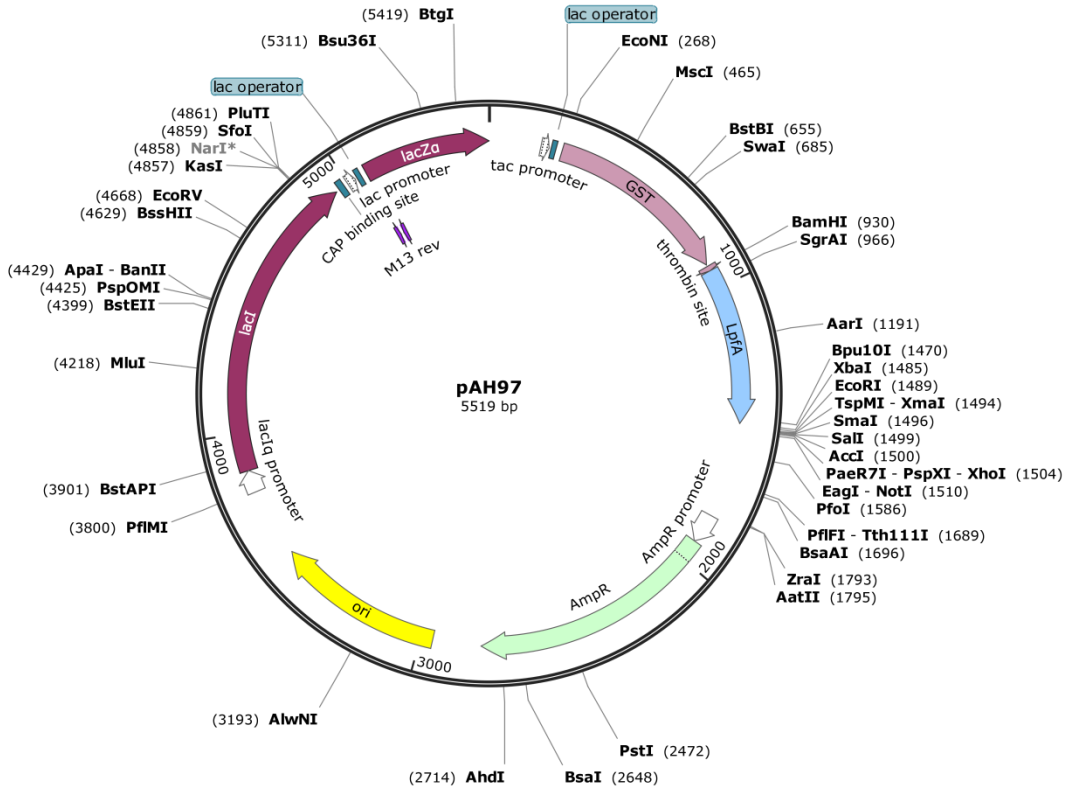

Figure 6.2. Map of pAH97 plasmid. pAH97 is a pGEX-4T-2 construct expressing *S.* Typhimurium LpfA, for generation of a GST-LpfA fusion protein. LpfA is the major subunit of the long polar fimbrial operon. The expression product of pAH97 is therefore LpfA with a GST tag at the N-terminus. The sequence encoding LpfA was originally amplified by PCR from *S.* Typhimurium strain SR11 (Humphries *et al.*, 2003).

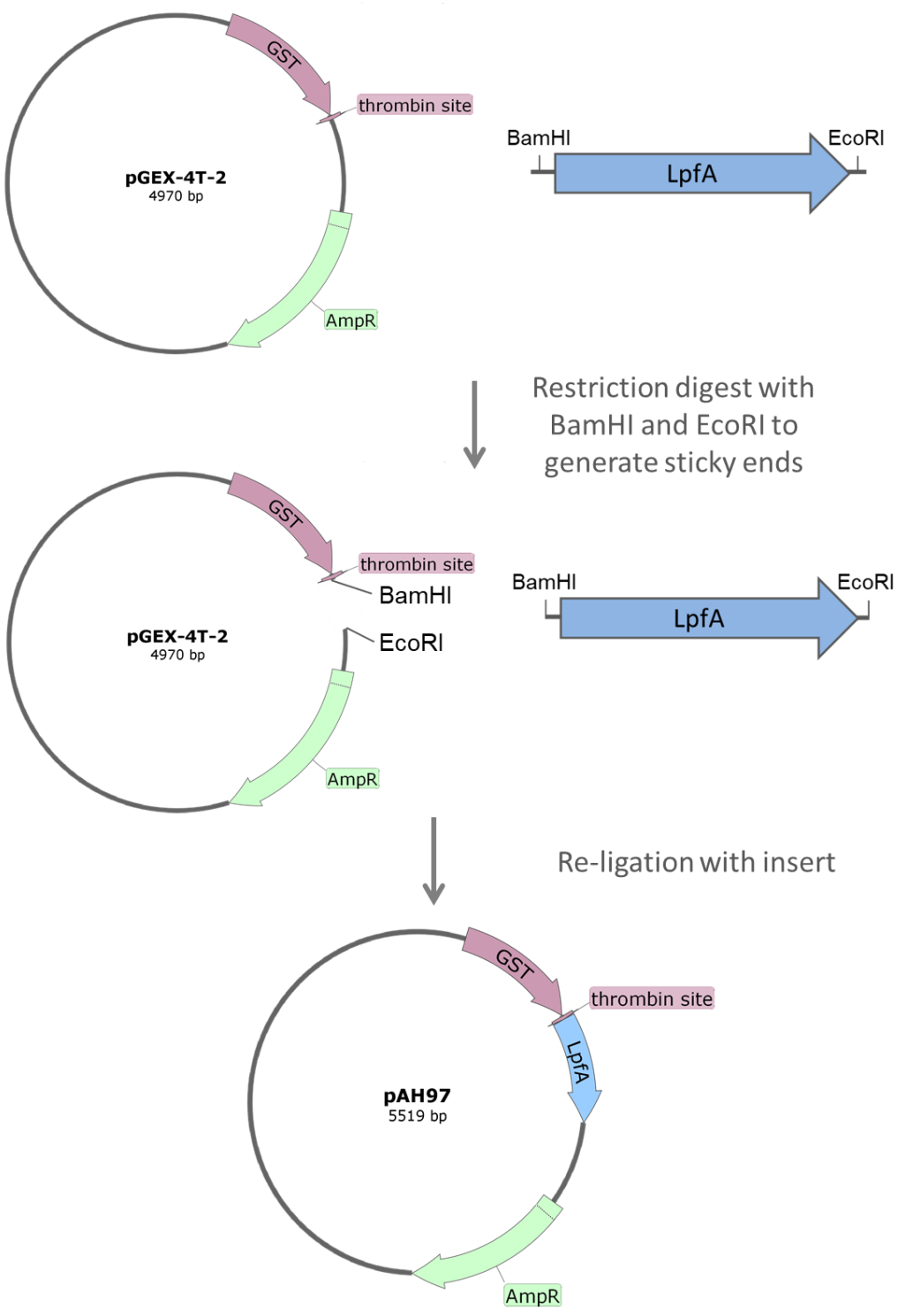

Figure 6.3. Schematic showing steps performed by Baumler and colleagues to construct pAH97 plasmid encoding GST-LpfA fusion protein. Both pGEX-4T-2 vector and PCR-amplified LpfA gene fragment were digested with BamHI and EcoRI to generate sticky ends, then insert was ligated into the vector.

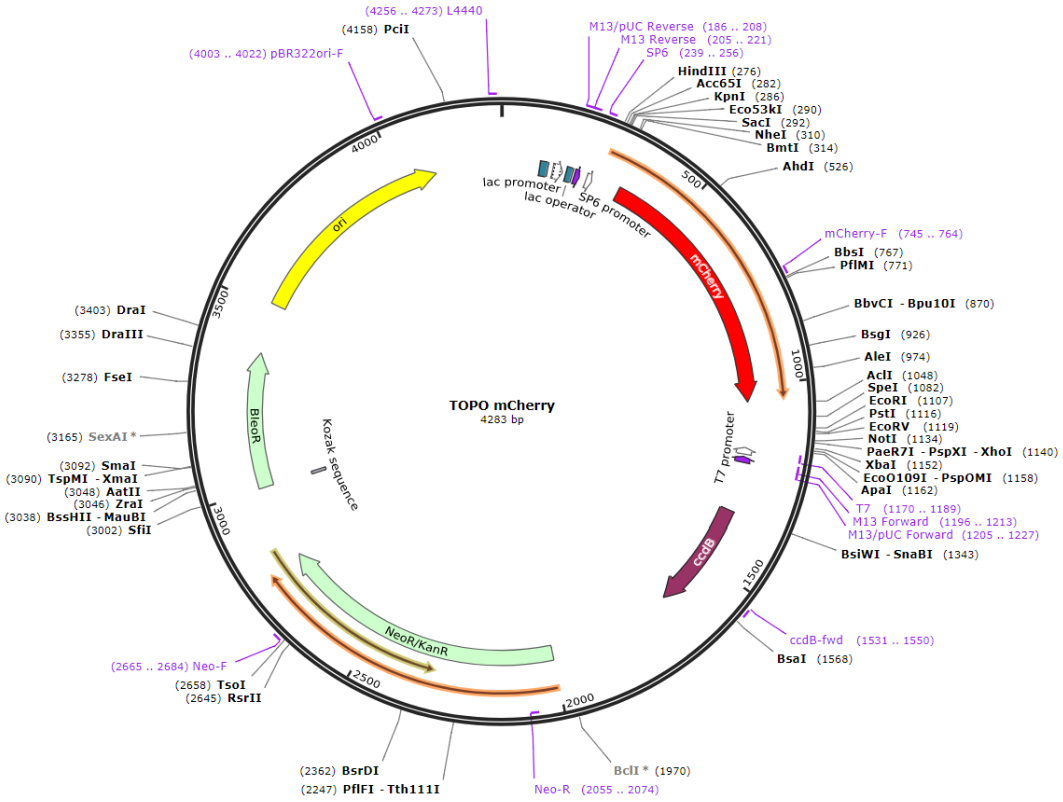

Figure 6.4. Map of TOPO mCherry plasmid. Figure from Addgene, plasmid #68490; http://n2t.net/addgene:68490. TOPO mCherry construct contains a 714 bp insert encoding mCherry, a red fluorescent protein.

Bacterial strains and growth conditions

E. coli strain DH5α transformed with either pGEX-4T-2 or pAH97 were grown from frozen stocks stored on Protect bacterial storage beads (Thermo Fisher Scientific) at -80°C. Competent BL21 (DE3) *E. coli* (Stratagene, now Agilent, Santa Clara, CA, USA) were transformed with new constructs since this strain allows high-level protein expression. For routine culture, both strains were grown on Luria Bertani (LB) agar under aerobic conditions at 37°C or in LB broth at 37°C with shaking overnight at 200 rpm.

Isolation of plasmid DNA

To isolate plasmid DNA, frozen stocks of transformed DH5α cells carrying either pGEX-4T-2 or pAH97 were streaked on Luria-Bertani (LB) agar plates containing 100 µg/mL ampicillin (Sigma-Aldrich) and cultured overnight at 37°C. Three single colonies from each plate were inoculated

into 25 mL LB broth supplemented with 100 µg/mL ampicillin and grown overnight at 37°C with shaking. Cells were harvested from 3 mL of the overnight culture by centrifugation at 4500 x *g* for 16 minutes at 4°C. Plasmid DNA was isolated using a QIAprep spin miniprep kit (Qiagen) and eluted in nuclease-free water. The concentration of plasmid DNA was determined by spectrophotometry using a Nanodrop Lite.

Amplification of mCherry sequence by PCR

The approach used to generate mCherry fusion constructs is summarised in **Figure 6.5**. Primers were designed to amplify the mCherry sequence with overhangs containing restriction sites for either BamHI (G^GATCC) and EcoRI (G^AATTC) or XbaI (C^TCAGA) and EcoRI restriction enzymes (RE), for cloning into pGEX-4T-2 and pAH97, respectively. Primers were synthesised by Eurogentec (Southampton, UK). Primer sequences are shown in **Table 6.1**. Standard PCR was performed with Q5 high-fidelity DNA polymerase and Q5 High GC Enhancer (New England Biolabs, Hitchin, UK) using 50 or 100 ng TOPO mCherry as template. A negative control reaction was performed without template DNA. Details of the PCR components are shown in **Table 6.2**. PCR was performed in a Multigene Optimax thermal cycler (Labnet) with the conditions described in **Table 6.3**. PCR products were purified to remove impurities such as primers, nucleotides and salts using the QIAquick PCR purification kit (Qiagen) and eluted in nuclease-free water. PCR products were separated by gel electrophoresis at 100 V in agarose gels of the percentages indicated with tris-acetate-EDTA (TAE) buffer, containing 1X SYBR Safe DNA gel stain (Invitrogen) and were visualised using a Biorad Universal Hood II transilluminator.

Table 6.1. Sequences of primers used to amplify and add restriction sites to mCherry sequence. Underlined sequences show the location of restriction sites for the noted enzymes; ^ indicates the cutting site.

Primer	***Sequence (5'-3')***
Forward (XbaI)	TGCT^CTAGAATCGCAAGCAAGGGCGAGGAGGA
Forward (BamHI)	TGCG^GATCCATCGCAAGCAAGGGCGAGGAGGA
Reverse (EcoRI)	CCGG^AATTCAAGACTTGTACAGCTCGTCC

Table 6.2. Components of standard PCR to amplify mCherry sequence.

Component	***50 µL reaction***	***Final concentration***
5X Q5 reaction buffer	10	1X
10 mM dNTPs	1	200 µM
10 µM forward primer	2.5	0.5 µM
10 µM reverse primer	2.5	0.5 µM
Template DNA	50 ng/100 ng	

Table 6.3. Thermal cycling conditions used for standard PCR to amplify mCherry sequence.

Step	***Number of cycles***	***Temperature (°C)***	***Time (s)***
Initial denaturation	1	98	45
Denaturation	30	98	15
Annealing		60	30
Extension		72	60
Final extension	1	72	120

Restriction digests

A restriction digest was performed using NcoI (Promega, Madison, WI, USA) to verify the amplified mCherry sequence. The resulting fragments were separated by gel electrophoresis as above and their sizes were compared to expected fragments. Restriction digestion was also used to generate complementary sticky ends in recipient plasmids and inserts to facilitate cloning. For cloning into pGEX-4T-2, vector and insert were digested with BamHI and EcoRI; for cloning into pAH97, digests of vector and respective insert were performed with XBaI and EcoRI. All digests were carried out at 37°C for 15 minutes, followed by 5 minutes at 80°C to inactivate the enzymes.

DNA ligation

Ligation of mCherry into pAH97 and pGEX-4T-2 was performed with T4 DNA ligase (Promega) and 10 ng linearised vector DNA. The ratio of vector to insert DNA was 1:3. The template for ligation reactions is shown in **Table 6.4**. The reaction was allowed to proceed at 15°C overnight.

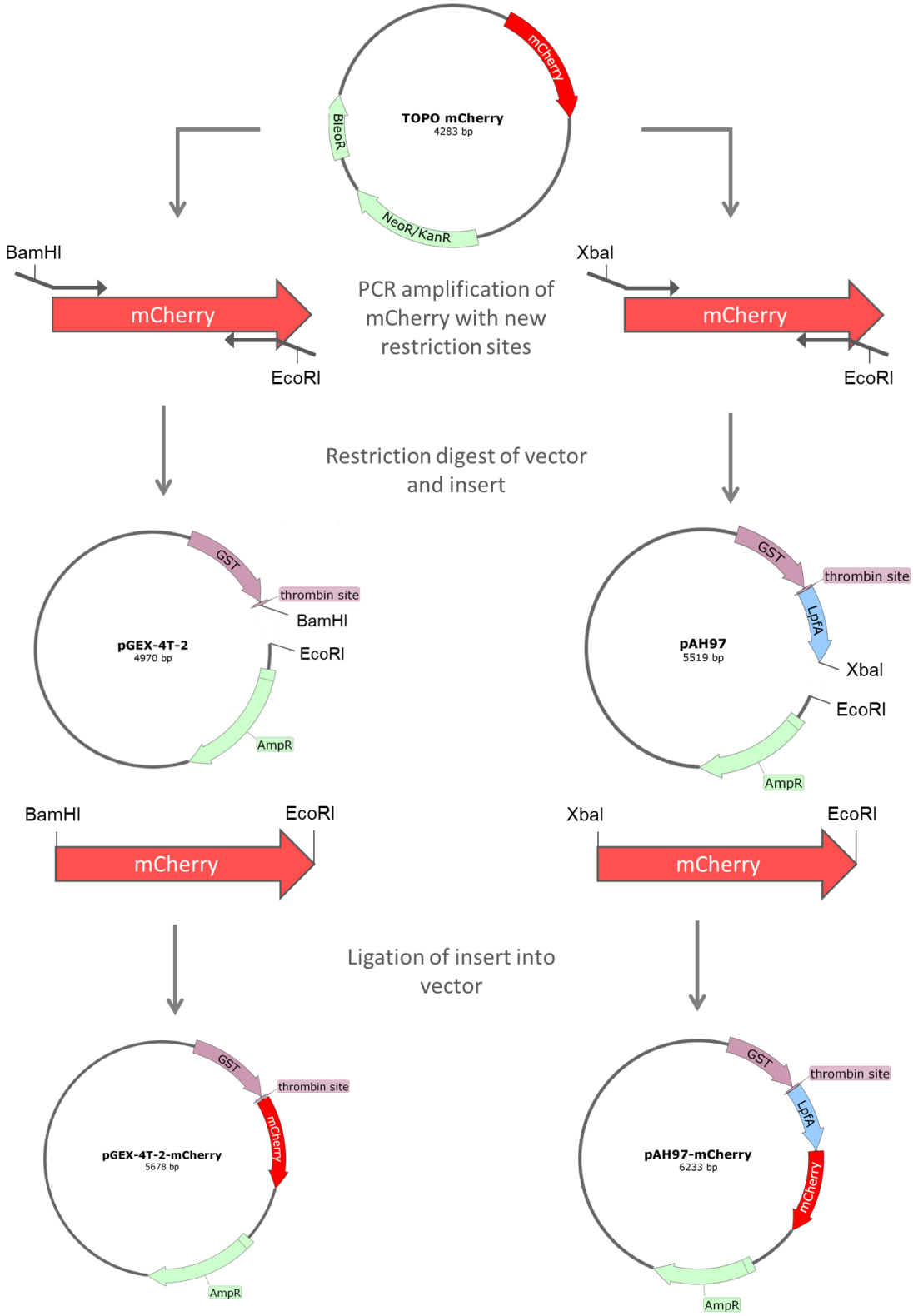

Figure 6.5. Schematic showing steps performed to generate constructs to express GST-mCherry and GST-LpfA-mCherry fusion proteins. The sequence encoding mCherry protein was amplified by PCR from the TOPO mCherry plasmid using primer sets with overhangs to introduce the indicated restriction sites. Both mCherry amplicon and vectors (either pGEX-4T-2 or pAH97) were digested with restriction enzymes to produce sticky ends as shown. Finally, inserts were ligated into vectors to produce the desired constructs.

Table 6.4. Composition of DNA ligation reactions.

Component	***Volume (µL)***	***Final concentration***
Vector DNA		10 ng
Insert DNA for: pAH97 pGEX-4T-2		 4 ng 4.4 ng
Ligase 10X buffer	1	1X
T4 DNA ligase	0.25	
Nuclease-free H_2O	to 10	

Transformation of ligated constructs into competent bacteria

BL21 (DE3) competent *E. coli* (Stratagene) were used for transformation with the ligation product. BL21 (DE3) cells were thawed on ice in 14 mL round-bottom Falcon tubes and 25 mM β-mercaptoethanol was added. They were then incubated for 10 minutes on ice with occasional swirling to mix. One µL ligation reaction (or control pUC18 DNA) was added and the cells were incubated for 30 minutes on ice. Cells were heat shocked at 42°C for 45 seconds, followed by 2 minutes on ice. Cells were allowed to grow in antibiotic-free Super Optimal broth with Catabolite repression (SOC) medium at 37°C for 1 hour with shaking, then 150 µL of transformation mixture was plated on LB agar plates containing 100 µg/mL ampicillin and cultured overnight at 37°C.

DNA sequencing

Plasmid DNA was extracted from 5 mL overnight cultures of transformed BL21 (DE3) cells using the QIAprep Spin Miniprep Kit (Qiagen) and eluted in nuclease-free water. DNA sequencing was performed by DNA Sequencing & Services (MRC I PPU, School of Life Sciences, University of Dundee, Scotland, www.dnaseq.co.uk) using Applied Biosystems Big-Dye Ver 3.1 chemistry on an Applied Biosystems model 3730 automated capillary DNA sequencer. Standard pGEX forward (CCAGCAAGTATATAGCATGG) and reverse primers (CCGGGAGCTGCATGTGTCAGAGG) were used. Sequence analysis and creation of plasmid maps was performed using SnapGene software (GSL Biotech, Chicago, USA).

Expression of proteins from transformed bacteria

Single colonies were cultured overnight in 20 mL LB broth containing 100 µg/mL ampicillin. The following day, 200 µL of these starter cultures were inoculated into 5 mL of LB broth with 100

μg/mL ampicillin and cultured at 37°C with shaking until they reached an optical density at 600 nm (OD_{600}) of 0.6-0.8. OD_{600} was measured using a GeneQuant Pro Spectrophotometer. 1 mL sample of the culture was removed for use as uninduced controls. To induce protein expression, the remaining culture was incubated at 27°C for a further 4 hours with 0.5 mM isopropyl β-D-1-thiogalactopyranoside (IPTG, Sigma-Aldrich). Induced cells in 1 mL were collected by centrifugation at 13,000 x *g*.

To verify protein expression, both induced and non-induced cells were lysed by boiling for 5 minutes in Laemmli sample buffer (with 1% v/v β-mercaptoethanol) for SDS-polyacrylamide gel electrophoresis (PAGE). Samples were separated by SDS-PAGE using 4% w/v acrylamide stacking and 12% w/v resolving gels at 50 V for 30 minutes, followed by 1 hour at 140 V. To fix proteins, gels were incubated for 30 minutes in 7% v/v acetic acid in 40% v/v methanol. Gels were then incubated for 1.5 hours in staining solution (0.5 mg/mL Coomassie Brilliant Blue G dye in 25% methanol). To destain, gels were rinsed for 1 minute in 10% v/v acetic acid in 25% v/v methanol, then rinsed with 25% v/v methanol, and finally agitated in 25% v/v methanol overnight. Coomassie staining of proteins was visualised using a BioRad Chemi Doc XRS+ system.

6.5. Results

6.5.1. Amplification of mCherry sequence from TOPO mCherry

PCR amplification of the mCherry sequence from the TOPO mCherry generated a product of between 700-800 bp, corresponding with the expected product of around 732 bp (**Figure 6.6 A & B**). The expected band consists of the mCherry sequence with the additional sequences introduced at either end containing restriction sites for enzymes EcoRI and XbaI. Amplification of mCherry in a separate PCR with an alternative reverse primer to introduce a BamHI site at the 3' end also resulted in a single product of 700-800 bp (not shown). The identity of the insert was confirmed by restriction digest with NcoI, which generated fragments of the expected sizes of 444 and 287 bp (**Figure 6.7 A & B**).

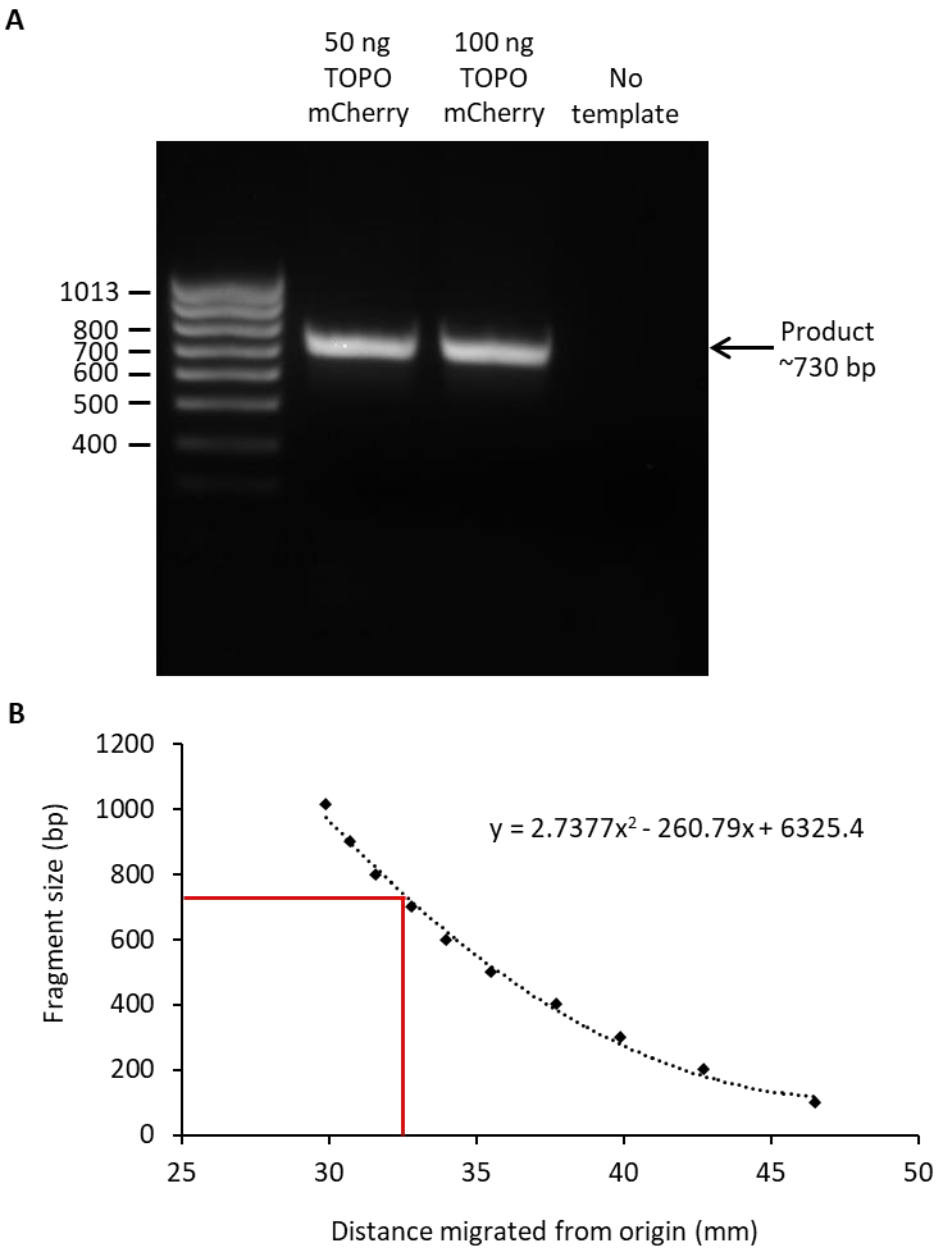

Figure 6.6. Amplification of mCherry sequence by PCR. (A) Gel electrophoresis in a 1.2% w/v agarose gel of products following PCR amplification of mCherry from TOPO mCherry plasmid with primers to introduce EcoRI and XBaI sites at either end. Expected product size was 732 bp. **(B)** Plot of distance migrated against DNA fragment size for DNA ladder in (A). PCR product was determined to have migrated 32.6 mm. Using the equation of the fitted curve, the size of the PCR product was therefore determined to be approximately 731 bp.

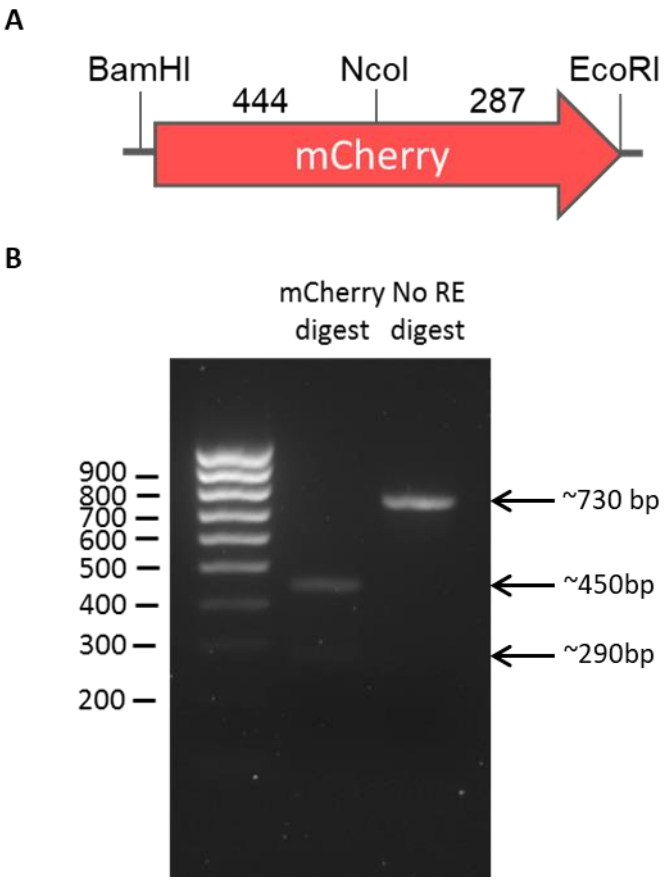

Figure 6.7. Restriction digestion of mCherry PCR amplicon. (A) Schematic showing expected results of digestion of mCherry amplicon with NcoI. The undigested mCherry amplicon is expected to be 731 bp in size. Digestion with NcoI is expected to result in two fragments of 444 and 287 bp. Gel electrophoresis in a 2% w/v agarose gel of products from digestion of mCherry PCR product with NcoI. Lane 1 contains the digestion products; lane 2 contains the products of a control reaction performed without restriction enzyme. Ladder is 1 kb DNA ladder (New England Biolabs).

6.5.3. Cloning of mCherry sequence into pGEX-4T-2 and pAH97

To generate complementary sticky ends, plasmids and inserts were digested simultaneously with either BamHI and EcoRI (for pGEX-4T-2) or XBaI and EcoRI (for pAH97) and inserts were ligated into plasmids to generate the new constructs, pGEX-4T-2-mCherry and pAH97-mCherry (**Figure 6.8**). Competent BL21 (DE3) *E. coli* were transformed with the ligation product and grown on selective agar plates. No colonies were observed on control plates where only vector was included in the ligation reaction, indicating a low level of vector self-ligation. Many colonies were observed on the positive control plate where cells were transformed with pUC18. Colonies were also observed on the plates spread with cells transformed with ligation mixture that contained both vector and insert, suggesting successful transformation.

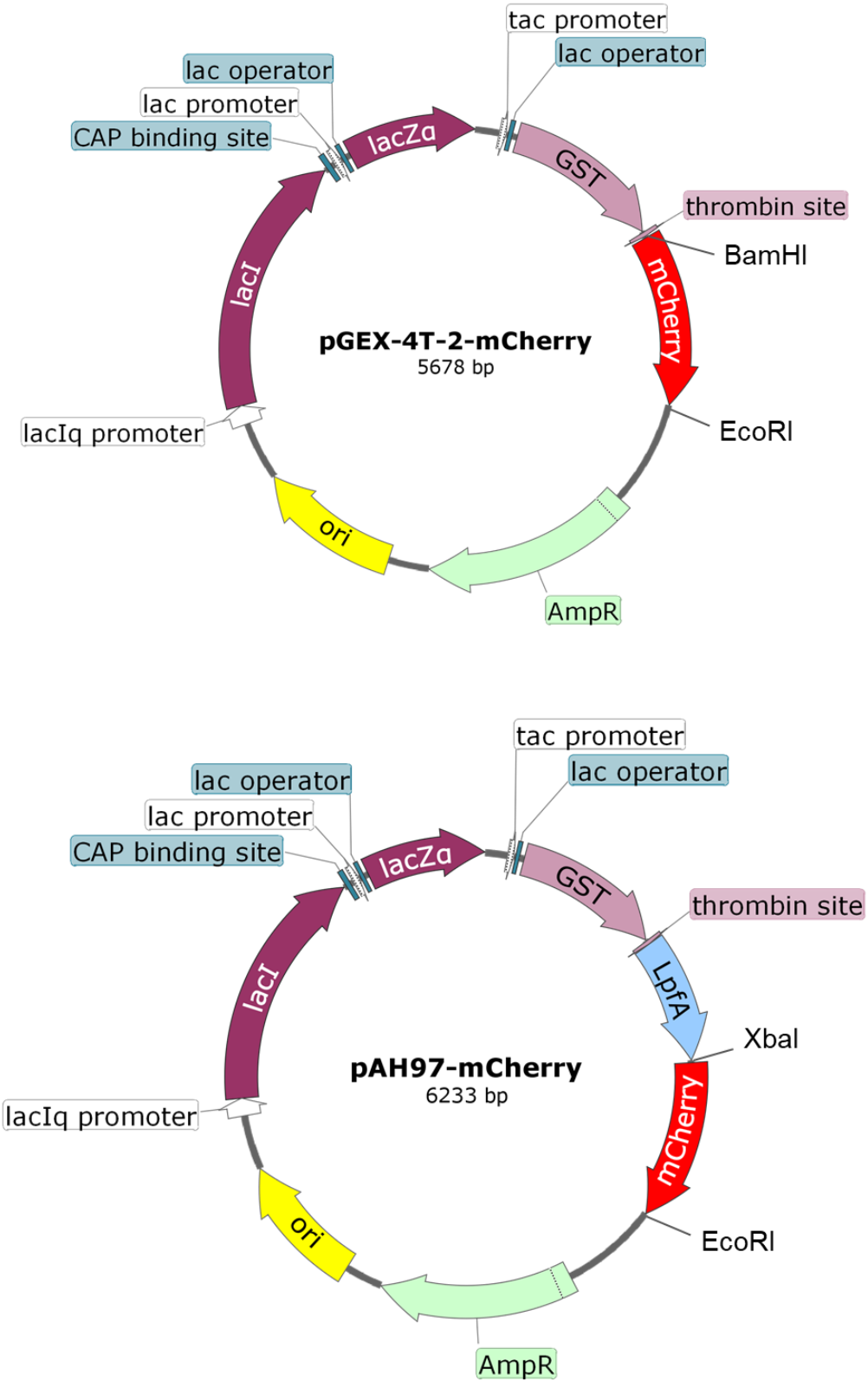

Figure 6.8. Plasmid maps showing the structure of new plasmids pGEX-4T-2-mCherry and pAH97-mCherry.

To confirm successful transformation, five colonies from each transformation were selected and DNA was extracted. PCR was performed using the same primers described in **Table 6.1** to amplify the mCherry sequence where present. A PCR product corresponding with the expected size of the mCherry sequence was amplified from four colonies transformed with pGEX-4T-2-mCherry ligations and two colonies transformed with pAH97-mCherry ligations (**Figure 6.9**). Construction of the correct fusion proteins was also confirmed by DNA sequencing (see **Appendix** for full sequences).

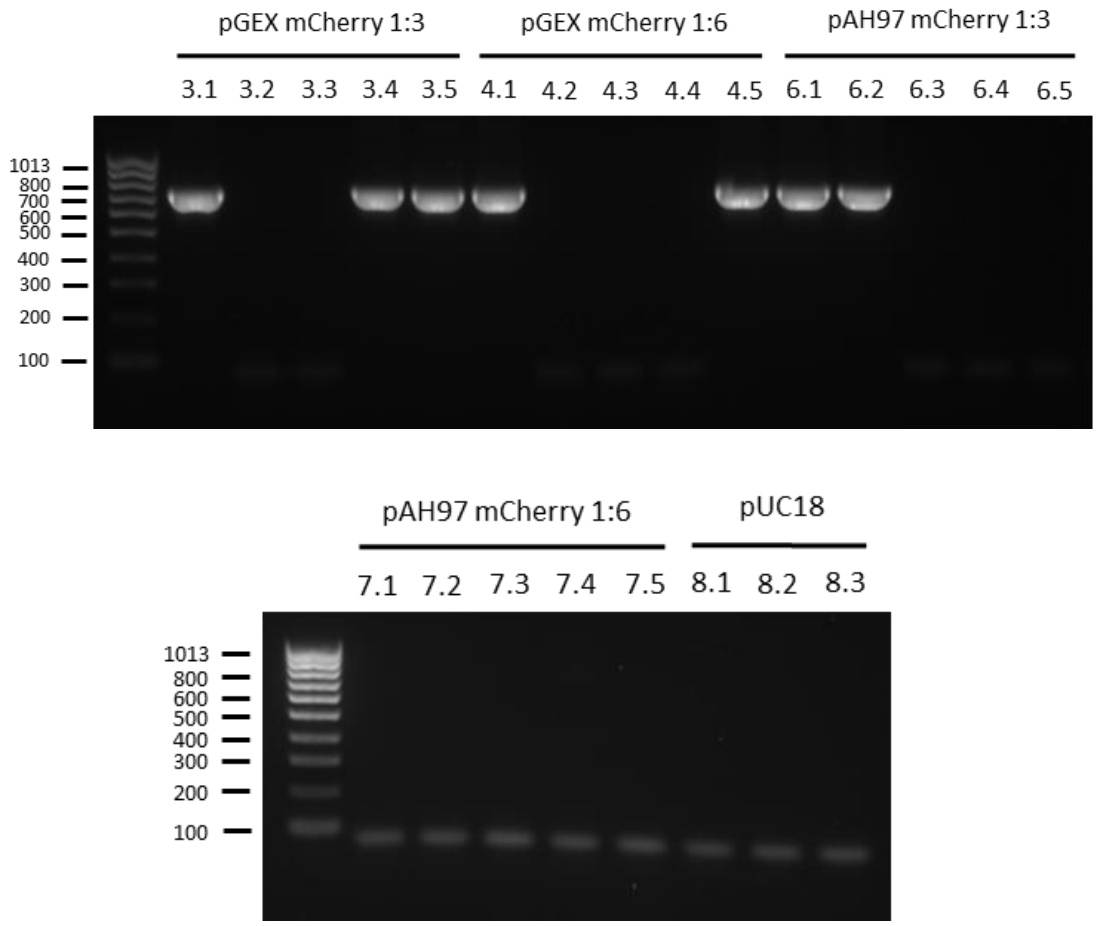

Figure 6.9. Validation of bacterial transformation by PCR amplification of mCherry sequence. Gel electrophoresis of PCR for mCherry to confirm transformation of colonies. Each lane corresponds to a single colony of cells transformed with the ratio of vector: insert indicated above. Gel was 1.5% w/v agarose. Ladder is 100 bp Hyperladder IV (Bioline).

6.5.4. Expression and purification of GST-mCherry and GST-LpfA-mCherry

Expression was induced by IPTG in colonies indicated to be transformed by PCR (**Figure 6.8**). Analysis by SDS-PAGE showed that a new protein of approximately 50 kDa was present following IPTG induction in all cells transformed with pGEX-4T-2-mCherry (**Figure 6.9**). This corresponds with the expected size for GST-mCherry of approximately 53 kDa. In cells transformed with pAH97-mCherry, a new band was detected between 50-70 kDa following induction of protein expression, which matches the expected size of 67 kDa for the GST-LpfA-mCherry fusion protein.

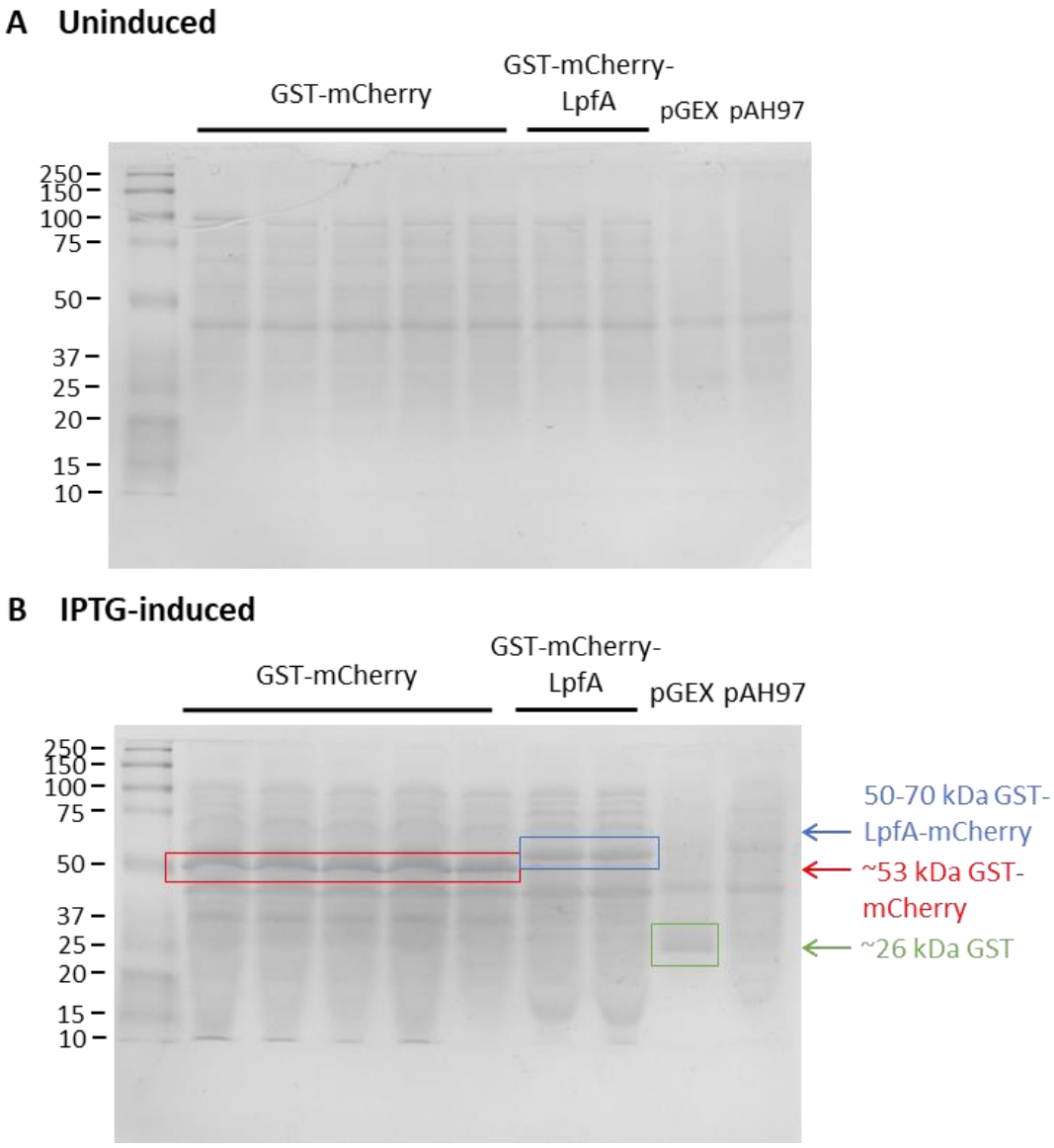

Figure 6.10. Confirmation of protein expression by Coomassie blue staining of bacterial lysates separated by SDS-PAGE. (A) Lysates of bacteria transformed with pGEX-4T-2-mCherry construct, collected prior to IPTG induction. **(B)** Lysates of bacteria transformed with pAH97-mCherry construct following 4 hours of IPTG induction. pGEX and pAH97 refer to untransformed bacteria carrying the original plasmids for GST and GST-LpfA, into which mCherry was inserted. Protein markers are Precision Plus Protein Kaleidoscope Prestained Protein standards (BioRad).

6.6. Summary of results

1. The sequence encoding mCherry was cloned by PCR into pGEX-4T-2 and pAH97 plasmids to create constructs encoding a GST-tagged mCherry-LpfA fusion protein and a control GST-mCherry fusion protein.

2. Successful cloning was demonstrated by PCR and by sequencing.

3. Constructs were transformed into competent *E. coli* and protein expression was demonstrated.

6.7. Discussion

As demonstrated previously for GP2 and FimH, specific ligand-receptor interactions contribute to adhesion, uptake and translocation of bacteria by M cells, which in turn leads to antigen-specific immune responses in the mucosa (Hase, Kawano, *et al.*, 2009). Overall, however, the mechanisms of antigen binding, uptake and translocation that contribute to antigen sampling by FAE M cells remain poorly characterised, which is currently hindering progress in development of oral vaccine strategies and therapies against enteric pathogens. The results presented here demonstrate construction of a GST-tagged fusion protein consisting of the *S.* Typhimurium adhesin, LpfA, fused to mCherry. Since LpfA has been shown to mediate adhesion of adherent-adhesive *E. coli* to the FAE, this construct will act as a tool to enable further investigation of interactions between enteric bacteria and intestinal epithelial cells, including M cells. We also generate a second fusion protein of GST and mCherry alone, which will act as a negative control in parallel experiments.

Further work is needed before the fusion proteins can be used in such experiments. Here, we demonstrate that proteins corresponding with the expected size of the designed constructs are expressed by transformed *E. coli*; however, expression conditions may require optimisation to improve the level of expression or to avoid protein insolubility. Protein expression may then be performed on a larger scale. Following cell lysis, soluble protein may be purified using glutathione columns, to which the GST-tagged proteins will selectively bind. The thrombin site located at the C-terminal end of the GST tag will allow for on-column cleavage of the GST tag and the remaining portions of the fusion proteins may be eluted. Finally, contaminating thrombin must be removed by incubating with *p*-aminobenzamidine.

Following purification, it will be possible to inject the fusion proteins into the lumens of enteroids that have been stimulated with RANKL to induce differentiation of M cells. Unlike injecting whole bacterial particles, this will not require a larger microcapillary and should not therefore cause excessive damage to the epithelium of the enteroids. Injected enteroids may be incubated for different durations, before being fixed and stained with a fluorescently labelled phalloidin to delineate the cell boundaries. M cells may also be identified by fluorescent immunostaining of specific markers, such as SpiB or GP2. Examination by confocal fluorescence microscopy will allow the injected fluorescent bacterial adhesion protein to be tracked, with the hypothesis that it will accumulate at the apical surface of M cells and may even be taken up by M cells, as has been observed for FimH-expressing bacteria (Hase, Kawano, *et al.*, 2009). If protein is taken up, clusters might be apparent in intracellular vesicles. In addition to the microinjection approach, the proteins generated here could also be useful in assays where enteroids are cultured as 2D monolayers (Rouch *et al.*, 2016).

A potential limitation of this approach is that a single isolated bacterial adhesin may be insufficient to stimulate uptake by M cells. Uptake may require M cell receptors to bind to multiple ligands on the same particle. For example, it has been proposed that the role of GP2, a protein secreted by the pancreas, may be to effectively opsonise bacterial particles in the small intestine by binding to FimH on bacterial type 1 pili and polymerising with surface-expressed GP2 on M cells of the FAE (Ohno and Hase, 2010). It is also possible that additional signals, for example via pattern recognition or cytokine receptors, may be required to activate endocytosis of particles by M cells, or to promote their functional maturity. For instance, TNF has been seen to enhance expression of M cell markers in the RANKL-stimulated enteroid model (Wood, Rios and Williams, 2016). In any case, it should still be possible to observe any clustering of the LpfA fusion protein at the apical surface of M cells.

Chapter 7

Summary of key findings

1. The distribution of different epithelial lineages varies between proximal and distal small intestine, with both Paneth and goblet cells being more abundant in distal compared to proximal small intestine.

2. Murine enteroids established from proximal and distal regions of the small intestine retain region-specific characteristics during *in vitro* culture, in particular, mimicking the cell type composition of their parent tissue.

3. An assay is developed to evaluate epithelial permeability in a 3D enteroid model.

4. Permeability of the epithelium to FD4 is very similar in enteroids derived from proximal and distal small intestine.

5. A peptide fragment of α-gliadin spanning amino acids 56-68 (P56-68) rapidly induces activation of the CFTR chloride channel in a dose-dependent manner, causing enhanced apical fluid secretion by small intestinal enterocytes.

6. The effect of P56-68 on fluid secretion by enterocytes is specific to the peptide sequence, since another peptide of identical length and similar amino acid composition (P31-43) has no effect.

7. The cytokine, RANKL, is confirmed to induce M cell differentiation in mouse enteroid cultures derived from both proximal and distal small intestine.

8. Alternative pathway NF-κB signalling is essential for RANKL-induced M cell differentiation, as enteroids deficient in NF-κB2 or RelB – key components of the alternative pathway – did not exhibit upregulation of M cell-associated genes in response to RANKL.

9. B cells appear to promote M cell differentiation but are insufficient to induce fully mature M cells.

10. Plasmid constructs were generated to allow production of a fluorescently labelled bacterial surface adhesion protein, which can be microinjected into the enteroid lumen to enable investigation of adhesion, uptake and translocation by M cells.

Chapter 8

Final discussion

8.1. Concluding discussion

The intestinal epithelium forms a dynamic barrier, allowing the essential passage of water, ions and nutrients while excluding microbes from the intestinal tissue. Specialised follicle-associated epithelium samples luminal antigens, facilitating generation of protective mucosal immune responses, including secretion of IgA back across the epithelium into the lumen. Growing evidence supports an integral role for epithelial barrier function in maintaining normal intestinal homeostasis. Impaired epithelial barrier integrity has been implicated in a number of pathological states, both intestinal and systemic (Odenwald and Turner, 2016).

Intestinal permeability is increased in patients with IBD and the beneficial effect of anti-TNF therapies is thought to be by inhibition of the pro-inflammatory immune response, which allows mucosal healing, but also by inhibiting direct detrimental effects of TNF on tight junction integrity (Odenwald and Turner, 2016). Patients with coeliac disease also display enhanced epithelial permeability and abnormal transport of gliadin-derived peptides has been reported (van Elburg *et al.*, 1993; Heyman *et al.*, 2012). Disruption of epithelial barrier function also occurs during various infections; for example, effectors produced by *S.* Typhimurium, *Vibrio cholera* and enteropathic *E. coli* alter expression and localisation of tight junction proteins (König *et al.*, 2016).

Defects in barrier function may also have effects far beyond the intestine. Altered intestinal permeability has been reported in patients with systemic autoimmune diseases, such as type 1 diabetes and graft versus host disease (Odenwald and Turner, 2013). Abnormal exposure to foreign antigens has been proposed to play a role in development of these conditions (Fasano and Shea-Donohue, 2005). In all cases, however, it is difficult to prove whether alterations in intestinal barrier function are drivers of pathogenesis or whether they occur as a consequence of the pre-existing disorder.

Given the complexity of assessing intestinal permeability *in vivo* (Camilleri *et al.*, 2012), relevant *in vitro* models could be very valuable. Since they were first described, the use of enteroid models to study the intestinal epithelium has become widespread (Sato *et al.*, 2009; Huch *et al.*, 2017). The technique has since been expanded to different regions of the gastrointestinal tract and other organs, including stomach (Barker *et al.*, 2010), colon (Sato, Stange, *et al.*, 2011), liver (Huch *et al.*, 2015) and brain (Lancaster *et al.*, 2013). Adult stem cell-derived enteroids offer several advantages over traditional 2D cell line models: enteroids contain primary, untransformed cells and multiple differentiated cell types; it is possible to derive cultures from humans, mice or other animals; cultures may be maintained long-term and expanded *in vitro*; and finally, enteroids are amenable to genetic manipulation and standard laboratory techniques.

Data presented in this thesis support the unique physiological relevance of enteroids, showing that they maintain a cell type composition specific to the region of the small intestine from which they were established. This evidence supports the finding that regional identity is intrinsically programmed in intestinal stem cells (Middendorp *et al.*, 2014; Kraiczy *et al.*, 2017), suggesting in addition that a region-specific differentiation programme is also intrinsically coded.

Enteroids have been used in the present studies as a model to probe different aspects of epithelial barrier function. As a key indicator of epithelial barrier function, an assay based on luminal microinjection of a florescent dye was developed to evaluate permeability of the enteroid epithelium to macromolecules. This assay was used to demonstrate that enteroids derived from proximal or distal segments of the small intestine exhibit similar permeability and to assess changes in permeability in response to common dietary peptides generated during digestion of gluten. Although neither peptide had a significant effect on epithelial permeability, we observed unexpectedly that one peptide caused significant enteroid swelling. This effect was shown to be mediated by the CFTR, indicating that increased apical chloride ion secretion is activated, leading to osmotic movement of fluid into the enteroid lumen.

The physiological relevance, if any, of this phenomenon remains to be investigated. Further work will be required to determine whether gliadin P56-68 exerts the same effects in humans and whether this contributes to symptoms. These preliminary findings do, however, suggest a new hypothesis that indigestible gliadin fragments activate CFTR expressed by small intestinal enterocytes, resulting in increased movement of fluid into the gut lumen, which contributes to bloating, abdominal pain and diarrhoea reported by patients with coeliac disease, NCWS and gluten-sensitive IBS. While this effect of P56-68 should occur in all individuals, genetic factors may alter susceptibility and a recent magnetic resonance imaging study suggested that patients with IBS are hypersensitive to intestinal distension produced by ingestion of fermentable carbohydrates (Major *et al.*, 2017).

Finally, we used enteroids to examine development of M cells, a rare cell type that play an important role in epithelial barrier function by sampling luminal antigens and therefore facilitating mucosal sIgA responses. The evidence we present provides further support for recent findings showing the importance of alternative pathway NF-κB signalling for M cell differentiation (Kanaya *et al.*, 2018). Analysis of co-cultures of enteroids with Raji B cells also supported a role for B cells in promoting M cell development, as suggested previously (Kernéis *et al.*, 1997; Gullberg *et al.*, 2000; Ebisawa *et al.*, 2011). Raji B cells did not, however, induce upregulation of mature M cell marker, *Gp2*, suggesting that RANKL is also required.

Overall, enteroids present an exciting new intestinal model, particularly for investigation of epithelial barrier function (Nakamura, 2018). This has already begun to be exploited in recent studies reporting the use of enteroids to characterise epithelial factors that regulate barrier function. For example, demonstrating that altered mucus secretion in enteroids established from patients with cystic fibrosis (Liu *et al.*, 2015) and that autophagy regulates intestinal barrier function and protects from experimental colitis(Pott, Kabat and Maloy, 2018).

Furthermore, enteroids have proved useful for examining immune cell regulation of epithelial barrier function. For instance, it has been shown that interferon-γ regulates secretion of antimicrobial peptides by Paneth cells and mucus secretion (Farin *et al.*, 2014). Enteroid-macrophage and enteroid-intraepithelial lymphocyte co-culture models have also been described (Nozaki *et al.*, 2016; Noel *et al.*, 2017). Given that they contain only epithelial cells and contain distinct luminal and basolateral compartments, enteroids allow a reductionist approach to unpicking epithelium-intrinsic factors that regulate barrier function. As

demonstrated here, additional complexity may be added if desired through co-culture with immune or stromal cells.

Finally, the utility of enteroids to study host-microbe interactions has also been demonstrated and much discussed (Bartfeld, 2016; Hill and Spence, 2016; Leslie and Young, 2016). Intestinal organoids derived from human pluripotent stem cells were colonised by *C. difficile* following microinjection into the lumen, resulting in impaired epithelial barrier function (Leslie *et al.*, 2015). In a similar model, luminal microinjection of *S.* Typhimurium altered cytokine expression by the epithelium (Forbester *et al.*, 2015). In murine enteroids derived from adult stem cells, *S.* Typhimurium disrupted tight junctions following colonisation from the basolateral surface of the epithelium (Zhang *et al.*, 2014), while growth of luminally injected *S.* Typhimurium was found to be inhibited by α-defensins, a form of antimicrobial peptides secreted by Paneth cells (Wilson *et al.*, 2015).

A limitation of the enteroid model in relation to studying epithelial barrier function is that the luminal surface of the epithelium, most relevant for most infections, is not easily accessible. Microinjection, particularly of large bacterial particles, is technically difficult and not amenable to large-scale experiments. Additionally, standard protocols for enteroid culture involve suspension of the enteroids in Matrigel, a solid gel matrix. Since it contains mouse proteins, DNA and RNA, it is important that Matrigel is completely removed prior to further analysis. The presence of Matrigel also hinders rapid isolation and fixation necessary during certain time course experiments. Alternative configurations of enteroid culture are a possible solution; for example, protocols have been developed to grow enteroids as polarised 2D monolayers, which still feature multiple differentiated cell types (Moon *et al.*, 2015; VanDussen *et al.*, 2015; Scott *et al.*, 2016). With the luminal surface easily accessible, monolayer cultures have been used to investigate uptake of *S.* Typhimurium by RANKL-induced M cells (Rouch *et al.*, 2016) and transcytosis of IgA (Moon *et al.*, 2014), although in our own experience we struggled to generate confluent monolayers and retain the capacity for expansion. There is also great interest in developing alternative matrices, which could have a precisely defined composition and allow customisation to include different aspects of the extracellular matrix (Gjorevski *et al.*, 2016; Cruz-Acuña *et al.*, 2017).

With our increasing understanding of the role and regulation of intestinal epithelial barrier function, it seems likely that the epithelial barrier will become a target for therapeutic interventions (Odenwald and Turner, 2016). Many currently used drugs have adverse off-target effects on the intestinal epithelium, including commonly prescribed proton pump inhibitors, which increase epithelial permeability through an unknown mechanism that may involve effects on tight junction regulation by the actin-myosin cytoskeleton (König *et al.*, 2016). Currently, the only drug designed to enhance epithelial barrier integrity is larazotide, a synthetic peptide that blocks zonulin receptors, whose activation otherwise increases epithelial permeability by regulating tight junctions (Fasano, 2011). Larazotide is currently entering phase III clinical trials for treatment of coeliac disease. Engraftment of stem cells is also under investigation as a potential therapy to repair epithelial barrier function (Yui *et al.*, 2012, 2018; Fukuda *et al.*, 2014). This approach has revealed interesting insights about regional identity and epithelial repair, but its clinical application is still a long way off.

8.2. Implications for future studies

While the data presented here provide further evidence that intestinal stem cells retain region-specific characteristics in *in vitro* enteroid cultures, further investigation is required to determine the extent to which region-specific cell type composition is retained over multiple passages. Quantification of each cell lineage in enteroids following different numbers of passages would be interesting, as would a more in-depth examination of enteroendocrine cell sub-populations. Since chromogranin A expression level shows greater variation in peptide hormone-storing enteroendocrine cells, specific immunostaining of their peptide hormone products, such as gastric inhibitory peptide and cholecystokinin may allow a higher resolution survey of epithelial cell populations.

These results also demonstrate that the origin of crypts used to establish enteroid cultures is relevant to their function and should therefore be a consideration during design of future studies. As the use of enteroid models is becoming more widespread, variations on the original culture protocols described by the Clevers group are also arising (Sato *et al.*, 2009). Development of alternative protein matrices is likely to compound the issue of inter-study variability in terms of culture conditions. Thorough characterisation of cultures, including of their cell type composition, will therefore aid comparison between different studies.

We also present evidence that a fragment of α-gliadin, generated during digestion of dietary gluten (Shan, 2002), causes apical fluid secretion by the epithelium as a result of CFTR activation but the upstream mechanism and physiological relevance of this finding remain unclear. Fluorescently labelled peptides would be useful tools to answer the question of how gliadin P56-68 induces CFTR activation, allowing peptides to be tracked to determine whether they are taken up into epithelial cells. Previous studies demonstrate that this approach is feasible, reporting entry of labelled peptides into Caco-2 cells via endocytosis (Schumann *et al.*, 2008; Barone *et al.*, 2010), a conclusion supported by studies using gliadin-specific antibodies to track peptide uptake (Friis *et al.*, 1992; Zimmer *et al.*, 2010). The studies also suggest that gliadin peptides P31-43 and P56-68 may be differently trafficked in the endocytic system, which could contribute to the difference in their effects on the CFTR.

The major pathway of CFTR activation is cAMP-dependent phosphorylation of its regulatory domain by protein kinase A (Moran, 2017). This is usually the result of stimulation by mediators such as glucagon, vasoactive intestine peptide, or adenosine, which activate adenylate cyclase, although some molecules act indirectly on CFTR by modulating other kinases and phosphodiesterases. A number of small molecules have also been reported to activate CFTR through direct binding (Becq *et al.*, 2011). To determine the mechanism of gliadin P56-68-induced CFTR activation, it would be interesting to perform a screen to identity activation of upstream kinases and to determine whether P56-68 induces concurrent intracellular cAMP elevation, for which immunoassays are available (Ma, Vetrivel, *et al.*, 2002).

Gliadin peptide fragments clearly reach the lamina propria in coeliac patients in order to interact with HLA DQ2/8-positive T cells antigen-presenting cells. To model the earliest stages of gliadin interaction with the intestinal epithelium, however, it would be desirable to deliver gliadin peptides to the luminal surface of the epithelium rather than the basolateral surface, as

in these studies. We conducted preliminary experiments where gliadin peptides or forskolin were microinjected into the enteroid lumen; however, it seems that this approach did not produce sufficiently high concentrations of the injected material within the enteroid lumen, as neither P56-68 nor forskolin induced any swelling. Given that luminal volume varies between enteroids, it would be difficult to achieve a reproducible concentration in the lumen using this technique.

It will also be necessary to address the question of whether the observed action of gliadin P56-68 is physiologically and clinically relevant in humans. To this end, fluid secretion could be investigated in human-derived enteroids using the swelling assay; this has previously been demonstrated with enteroids derived from cystic fibrosis patients (Dekkers *et al.*, 2013). If tissue, or blood samples to generate iPSC-derived organoids, could be obtained from patients, this assay might help to determine whether the epithelium of patients with coeliac disease, NCWS or gluten-sensitive IBS shows greater sensitivity to the P56-68-induced fluid secretion. Another informative experiment would be to deliver the synthetic gliadin peptides to mice via oral gavage and monitor for evidence of diarrhoea. It might also be possible to measure fluid secretion in response to injection of gliadin peptides in a ligated ileal loop model (Caserta *et al.*, 2011).

The data presented here indicate that enteroids are a suitable model in which to assess effects of food components on epithelial permeability and secretion. It would be interesting to use this model to examine the effects of dietary fibre, fat and emulsifiers, which have already been shown by our group and others to alter epithelial barrier function (Cani *et al.*, 2008; Roberts *et al.*, 2010, 2013; Chassaing *et al.*, 2015).

Our characterisation of factors regulating M cell differentiation indicates a key role for NF-κB alternative pathway signalling. Although recent studies have also demonstrated the essential role of NF-κB signalling (Kanaya *et al.*, 2018), the precise factors required for full differentiation into mature, functional M cells remain unknown. A previous study identified SpiB-independent regulation of certain M cell-specific genes, including *Marcksl1* and *Anxa5* (Kanaya *et al.*, 2012), while a recent study suggested that *Spib* expression alone is not sufficient to produce fully differentiated, *Gp2*-expressing M cells (Kanaya *et al.*, 2018). The authors propose that additional pathways, such as the MAPK pathway, may also be involved, making these interesting targets for future studies.

We also present data suggesting that B cell-derived factors drive *Spib* upregulation, which could in turn promote M cell development. B cells have previously been implicated in M cell differentiation (Kernéis *et al.*, 1997; Gullberg *et al.*, 2000; Ebisawa *et al.*, 2011), but the identities of the factors involved are so far unknown. In the context of the enteroid model, it would be interesting to examine whether co-culture with B cells enhances M cell differentiation stimulated by RANKL. The model could also be improved by using primary isolated murine B cells, although the culture conditions would likely require optimisation. Intraepithelial lymphocytes co-cultured with enteroids within the Matrigel were observed to interact with and migrate between enterocytes (Nozaki *et al.*, 2016). Since B cells are found in close proximity to M cells in Peyer's patches, it is possible that such cell-cell contact would enhance the effect of B cells on M cell differentiation.

The regulation of M cell fate determination is also currently poorly understood. Examination of the distribution of M cells in RANKL-stimulated enteroids might help to elucidate the underlying mechanisms. Given the scattered distribution of M cells observed in previous studies, it is likely that M cell differentiation is regulated by lateral inhibition, possibly involving the influence of Jagged1 and Notch (Hsieh and Lo, 2012).

The development of clustered regularly interspaced short palindromic repeats (CRISPR)-Cas9 technologies has opened up numerous possibilities for gene editing and application of the technique to enteroids has already been demonstrated (Schwank *et al.*, 2013; Driehuis and Clevers, 2017).

Although we demonstrate upregulation of *Spib* expression following RANKL treatment at both mRNA and protein levels, it will be necessary to demonstrate that these M cells are capable of antigen uptake and translocation. During preliminary experiments, we struggled to inject larger particles, such as beads, into the enteroid lumen without causing extensive damage to the enteroid epithelium. To address this challenge, we generated a plasmid construct to allow production of a fluorescently labelled version of LpfA, a bacterial adhesin subunit. This protein will be easily injectable and allow investigation of whether LpfA binds specifically to M cells, as it has previously been shown to mediate selective binding of *S.* Typhimurium to the FAE (Baumler, Tsolis and Heffron, 1996). The LpfA fusion protein with allow modelling of bacterial adhesion, uptake and translocation in M cells.

References

Abadie, V. *et al.* (2011) 'Integration of genetic and immunological insights into a model of celiac disease pathogenesis', *Annual Review of Immunology*, 29(1), pp. 493–525. doi: 10.1146/annurev-immunol-040210-092915.

Aguzzi, A., Kranich, J. and Krautler, N. J. (2014) 'Follicular dendritic cells: origin, phenotype, and function in health and disease', *Trends in Immunology*, 35(3), pp. 105–113. doi: 10.1016/j.it.2013.11.001.

Ahmad, T. *et al.* (2017) 'A comparison of three Peyer's patch "M-like" cell culture models: particle uptake, bacterial interaction, and epithelial histology', *European Journal of Pharmaceutics and Biopharmaceutics*, 119, pp. 426–436. doi: 10.1016/j.ejpb.2017.07.013.

Akama-Garren, E. H. *et al.* (2016) 'A modular assembly platform for rapid generation of DNA constructs', *Scientific Reports*, 6(1), p. 16836. doi: 10.1038/srep16836.

Akiyama, N. *et al.* (2014) 'Limitation of immune tolerance–inducing thymic epithelial cell development by Spi-B–mediated negative feedback regulation', *The Journal of Experimental Medicine*, 211(12), pp. 2425–2438. doi: 10.1084/jem.20141207.

Albac, S. *et al.* (2016) 'Candida albicans is able to use M cells as a portal of entry across the intestinal barrier in vitro', *Cellular Microbiology*, 18(2), pp. 195–210. doi: 10.1111/cmi.12495.

Alcamo, E. *et al.* (2002) 'Requirement for the NF-κB family member RelA in the development of secondary lymphoid organs', *The Journal of Experimental Medicine*, 195(2), pp. 233–244. doi: 10.1084/jem.20011885.

Alexander, C. and Rietschel, E. T. (2001) 'Bacterial lipopolysaccharides and innate immunity', *Journal of Endotoxin Research*, 7(3), pp. 167–202. doi: 10.1179/096805101101532675.

Anderle, P. *et al.* (2005) 'Changes in the transcriptional profile of transporters in the intestine along the anterior-posterior and crypt-villus axes.', *BMC Genomics*, 6(69). doi: 10.1186/1471-2164-6-69.

Anderson, D. M. *et al.* (1997) 'A homologue of the TNF receptor and its ligand enhance T-cell growth and dendritic-cell function.', *Nature*, 390(6656), pp. 175–179. doi: 10.1038/36593.

Anderson, R. P. *et al.* (2000) 'In vivo antigen challenge in celiac disease identifies a single transglutaminase-modified peptide as the dominant A-gliadin T-cell epitope', *Nature Medicine*, 6(3), pp. 337–342. doi: 10.1038/73200.

Araújo, F. *et al.* (2016) 'In vitro M-like cells genesis through a tissue-engineered triple-culture intestinal model', *Journal of Biomedical Materials Research Part B: Applied Biomaterials*, 104(4), pp. 782–788. doi: 10.1002/jbm.b.33508.

Arentz-Hansen, H. *et al.* (2000) 'The intestinal T cell response to alpha-gliadin in adult celiac disease is focused on a single deamidated glutamine targeted by tissue transglutaminase.', *The Journal of Experimental Medicine*, 191(4), pp. 603–12. doi: 10.1084/jem.191.4.603.

Asai, T. and Morrison, S. L. (2013) 'The SRC family tyrosine kinase HCK and the ETS family transcription factors SPIB and EHF regulate transcytosis across a human follicle-associated epithelium model', *Journal of Biological Chemistry*, 288(15), pp. 10395–10405. doi: 10.1074/jbc.M112.437475.

Aziz, I., Hadjivassiliou, M. and Sanders, D. S. (2015) 'The spectrum of noncoeliac gluten sensitivity', *Nature Reviews Gastroenterology & Hepatology*, 12(9), pp. 516–526. doi:

10.1038/nrgastro.2015.107.

Barker, N. *et al.* (2007) 'Identification of stem cells in small intestine and colon by marker gene Lgr5', *Nature*, 449(7165), pp. 1003–1007. doi: 10.1038/nature06196.

Barker, N. *et al.* (2010) 'Lgr5(+ve) stem cells drive self-renewal in the stomach and build long-lived gastric units in vitro.', *Cell Stem Cell*, 6(1), pp. 25–36. doi: 10.1016/j.stem.2009.11.013.

Barone, M. V. *et al.* (2007) 'Growth factor-like activity of gliadin, an alimentary protein: implications for coeliac disease.', *Gut*, 56(4), pp. 480–8. doi: 10.1136/gut.2005.086637.

Barone, M. V. *et al.* (2010) 'Gliadin peptide P31-43 localises to endocytic vesicles and interferes with their maturation.', *PLoS ONE*, 5(8), p. e12246. doi: 10.1371/journal.pone.0012246.

Barone, M. V. *et al.* (2011) 'Gliadin-mediated proliferation and innate immune activation in celiac disease are due to alterations in vesicular trafficking', *PLoS ONE*, 6(2). doi: 10.1371/journal.pone.0017039.

Barone, M. V. and Zimmer, K. P. (2016) 'Endocytosis and transcytosis of gliadin peptides', *Molecular and Cellular Pediatrics*, 3(1), p. 8. doi: 10.1186/s40348-015-0029-z.

Barratt, S. M., Leeds, J. S. and Sanders, D. S. (2011) 'Quality of life in coeliac disease is determined by perceived degree of difficulty adhering to a gluten-free diet, not the level of dietary adherence ultimately achieved', *Journal of Gastrointestinal and Liver Diseases*, 20(3), pp. 241–245.

Bartfeld, S. (2016) 'Modeling infectious diseases and host-microbe interactions in gastrointestinal organoids', *Developmental Biology*, 420(2), pp. 262–270. doi: 10.1016/j.ydbio.2016.09.014.

Bastide, P. *et al.* (2007) 'Sox9 regulates cell proliferation and is required for Paneth cell differentiation in the intestinal epithelium', *Journal of Cell Biology*, 178(4), pp. 635–648. doi: 10.1083/jcb.200704152.

Battle, M. A. *et al.* (2008) 'GATA4 is essential for jejunal function in mice.', *Gastroenterology*, 135(5), pp. 1676-1686.e1. doi: 10.1053/j.gastro.2008.07.074.

Bäumler, A. J. and Heffron, F. (1995) 'Identification and sequence analysis of lpfABCDE, a putative fimbrial operon of Salmonella typhimurium.', *Journal of Bacteriology*, 177(8), pp. 2087–2097. doi: 10.1128/jb.177.8.2087-2097.1995.

Baumler, A. J., Tsolis, R. M. and Heffron, F. (1996) 'The lpf fimbrial operon mediates adhesion of Salmonella typhimurium to murine Peyer's patches.', *Proceedings of the National Academy of Sciences*, 93(1), pp. 279–283. doi: 10.1073/pnas.93.1.279.

Becq, F. *et al.* (2011) 'Pharmacological therapy for cystic fibrosis: From bench to bedside', *Journal of Cystic Fibrosis*, 10, pp. S129–S145. doi: 10.1016/S1569-1993(11)60018-0.

Bennett, K. M. *et al.* (2016) 'Induction of colonic M cells during intestinal inflammation', *The American Journal of Pathology*, 186(5), pp. 1166–1179. doi: 10.1016/j.ajpath.2015.12.015.

Bethune, M. T. *et al.* (2008) 'Transepithelial transport and enzymatic detoxification of gluten in gluten-sensitive rhesus macaques', *PLoS ONE*, 3(3). doi: 10.1371/journal.pone.0001857.

Bethune, M. T. *et al.* (2009) 'Interferon-gamma released by gluten-stimulated celiac disease-specific intestinal T cells enhances the transepithelial flux of gluten peptides.', *The Journal of*

Pharmacology and Experimental Therapeutics, 329(2), pp. 657–68. doi: 10.1124/jpet.108.148007.

Beuling, E. *et al.* (2011) 'GATA factors regulate proliferation, differentiation, and gene expression in small intestine of mature mice', *Gastroenterology*, 140(4), pp. 1219–1229. doi: 10.1053/j.gastro.2011.01.033.

Bevins, C. L. and Salzman, N. H. (2011) 'Paneth cells, antimicrobial peptides and maintenance of intestinal homeostasis', *Nature Reviews Microbiology*, 9(5), pp. 356–368. doi: 10.1038/nrmicro2546.

Biesiekierski, J. R. *et al.* (2011) 'Gluten causes gastrointestinal symptoms in subjects without celiac disease: a double-blind randomized placebo-controlled trial', *American Journal of Gastroenterology*, 106(3), pp. 508–514. doi: 10.1038/ajg.2010.487.

Biesiekierski, J. R. *et al.* (2013) 'No effects of gluten in patients with self-reported non-celiac gluten sensitivity after dietary reduction of fermentable, poorly absorbed, short-chain carbohydrates', *Gastroenterology*, 145(2), pp. 320-328.e3. doi: 10.1053/j.gastro.2013.04.051.

Birchenough, G. M. H. *et al.* (2015) 'New developments in goblet cell mucus secretion and function', *Mucosal Immunology*, 8(4), pp. 1–8. doi: 10.1038/mi.2015.32.

Bischoff, S. C. *et al.* (2014) 'Intestinal permeability – a new target for disease prevention and therapy', *BMC Gastroenterology*, 14(1), p. 189. doi: 10.1186/s12876-014-0189-7.

Bjerknes, M. and Cheng, H. (2010) 'Cell lineage metastability in Gfi1-deficient mouse intestinal epithelium', *Developmental Biology*, 345(1), pp. 49–63. doi: 10.1016/j.ydbio.2010.06.021.

Bosse, T. *et al.* (2006) 'Gata4 is essential for the maintenance of jejunal-ileal identities in the adult mouse small intestine', *Molecular and Cellular Biology*, 26(23), pp. 9060–9070. doi: 10.1128/MCB.00124-06.

Bowcutt, R. (2014) 'Heterogeneity across the murine small and large intestine', *World Journal of Gastroenterology*, 20(41), p. 15216. doi: 10.3748/wjg.v20.i41.15216.

Boyce, B. F. and Xing, L. (2007) 'Biology of RANK, RANKL, and osteoprotegerin', *Arthritis Research & Therapy*, 9(Suppl 1), p. S1. doi: 10.1186/ar2165.

Bröer, S. (2008) 'Amino Acid Transport Across Mammalian Intestinal and Renal Epithelia', *Physiological Reviews*, 88(1), pp. 249–286. doi: 10.1152/physrev.00018.2006.

Buczacki, S. J. a *et al.* (2013) 'Intestinal label-retaining cells are secretory precursors expressing Lgr5', *Nature*, 495(7439), pp. 65–69. doi: 10.1038/nature11965.

Bullen, T. F. *et al.* (2006) 'Characterization of epithelial cell shedding from human small intestine', *Laboratory Investigation*, 86(10), pp. 1052–1063. doi: 10.1038/labinvest.3700464.

Caamaño, J. H. *et al.* (1998) 'Nuclear factor (NF)-kappa B2 (p100/p52) is required for normal splenic microarchitecture and B cell-mediated immune responses.', *The Journal of Experimental Medicine*, 187(2), pp. 185–96. doi: 10.1002/cne.902980205.

Camarca, A. *et al.* (2009) 'Intestinal T cell responses to gluten peptides are largely heterogeneous: implications for a peptide-based therapy in celiac disease', *The Journal of Immunology*, 182(7), pp. 4158–4166. doi: 10.4049/jimmunol.0803181.

Camilleri, M. *et al.* (2012) 'Intestinal barrier function in health and gastrointestinal disease',

Neurogastroenterology and Motility, 24(6), pp. 503–512. doi: 10.1111/j.1365-2982.2012.01921.x.

Cani, P. D. *et al.* (2008) 'Changes in gut microbiota control metabolic endotoxemia-induced inflammation in high-fat diet-induced obesity and diabetes in mice.', *Diabetes*, 57(6), pp. 1470–81. doi: 10.2337/db07-1403.

Capaldo, C. T. and Nusrat, A. (2009) 'Cytokine regulation of tight junctions.', *Biochimica et Biophysica Acta*, 1788(4), pp. 864–71. doi: 10.1016/j.bbamem.2008.08.027.

Caputo, I. *et al.* (2010) 'Celiac anti-tissue transglutaminase antibodies interfere with the uptake of alpha gliadin peptide 31-43 but not of peptide 57-68 by epithelial cells.', *Biochimica et Biophysica Acta*, 1802(9), pp. 717–27. doi: 10.1016/j.bbadis.2010.05.010.

Casella, G. *et al.* (2018) 'Non celiac gluten sensitivity and diagnostic challenges.', *Gastroenterology and hepatology from bed to bench*, 11(3), pp. 197–202. Available at: http://www.ncbi.nlm.nih.gov/pubmed/30013742.

Caserta, J. A. *et al.* (2011) 'Development and Application of a Mouse Intestinal Loop Model To Study the In Vivo Action of Clostridium perfringens Enterotoxin', *Infection and Immunity*, 79(8), pp. 3020–3027. doi: 10.1128/IAI.01342-10.

Casteleyn, C. *et al.* (2013) 'M cell specific markers in man and domestic animals: Valuable tools in vaccine development', *Comparative Immunology, Microbiology and Infectious Diseases*, 36(4), pp. 353–364. doi: 10.1016/j.cimid.2013.03.002.

Catassi, C. *et al.* (2017) 'The overlapping area of non-celiac gluten sensitivity (NCGS) and wheat-sensitive irritable bowel syndrome (IBS): an update.', *Nutrients*, 9(11). doi: 10.3390/nu9111268.

Chassaing, B. *et al.* (2011) 'Crohn disease-associated adherent-invasive E. coli bacteria target mouse and human Peyer's patches via long polar fimbriae', *Journal of Clinical Investigation*, 121(3), pp. 966–975. doi: 10.1172/JCI44632.

Chassaing, B. *et al.* (2015) 'Dietary emulsifiers impact the mouse gut microbiota promoting colitis and metabolic syndrome', *Nature*, 519(7541), pp. 92–96. doi: 10.1038/nature14232.

Chen, C. *et al.* (2009) 'Pdx1 inactivation restricted to the intestinal epithelium in mice alters duodenal gene expression in enterocytes and enteroendocrine cells', *American Journal of Physiology-Gastrointestinal and Liver Physiology*, 297(6), pp. G1126–G1137. doi: 10.1152/ajpgi.90586.2008.

Chen, L., Tuo, B. and Dong, H. (2016) 'Regulation of intestinal glucose absorption by ion channels and transporters', *Nutrients*, 8(1), pp. 1–11. doi: 10.3390/nu8010043.

Chiba, S. *et al.* (2011) 'Listerial invasion protein internalin B promotes entry into ileal Peyer's patches in vivo', *Microbiology and Immunology*, 55(2), pp. 123–129. doi: 10.1111/j.1348-0421.2010.00292.x.

Chieppa, M. *et al.* (2006) 'Dynamic imaging of dendritic cell extension into the small bowel lumen in response to epithelial cell TLR engagement', *The Journal of Experimental Medicine*, 203(13), pp. 2841–2852. doi: 10.1084/jem.20061884.

Ciccocioppo, R., Di Sabatino, A. and Corazza, G. R. (2005) 'The immune recognition of gluten in coeliac disease', *Clinical and Experimental Immunology*, 140(3), pp. 408–416. doi:

10.1111/j.1365-2249.2005.02783.x.

Clark, M. A. *et al.* (1993) 'Differential expression of lectin-binding sites defines mouse intestinal M-cells.', *Journal of Histochemistry & Cytochemistry*, 41(11), pp. 1679–1687. doi: 10.1177/41.11.7691933.

Clark, M. A. *et al.* (1994) 'Preferential interaction of Salmonella typhimurium with mouse Peyer's patch M cells', *Research in Microbiology*, 145(7), pp. 543–552. doi: 10.1016/0923-2508(94)90031-0.

Clayburgh, D. R. *et al.* (2005) 'Epithelial myosin light chain kinase-dependent barrier dysfunction mediates T cell activation-induced diarrhea in vivo.', *The Journal of Clinical Investigation*, 115(10), pp. 2702–15. doi: 10.1172/JCI24970.

Clemente, M. G. *et al.* (2003) 'Early effects of gliadin on enterocyte intracellular signalling involved in intestinal barrier function.', *Gut*, 52(2), pp. 218–23. doi: 10.1136/gut.52.2.218.

Clevers, H. (2013) 'The intestinal crypt, a prototype stem cell compartment', *Cell*, 154(2), pp. 274–284. doi: 10.1016/j.cell.2013.07.004.

Clevers, H. C. and Bevins, C. L. (2013) 'Paneth cells: maestros of the small intestinal crypts', *Annual Review of Physiology*, 75(1), pp. 289–311. doi: 10.1146/annurev-physiol-030212-183744.

Collins, F. L. *et al.* (2017) 'Temporal and regional intestinal changes in permeability, tight junction, and cytokine gene expression following ovariectomy-induced estrogen deficiency', *Physiological Reports*, 5(9), pp. 1–22. doi: 10.14814/phy2.13263.

Comelli, E. M. *et al.* (2009) 'Biomarkers of human gastrointestinal tract regions', *Mammalian Genome*, 20(8), pp. 516–527. doi: 10.1007/s00335-009-9212-7.

Cooper, B. T. *et al.* (1980) 'Gluten-sensitive diarrhea without evidence of celiac disease.', *Gastroenterology*, 79(5 Pt 1), pp. 801–6. Available at: http://www.gastrojournal.org/article/0016-5085(81)90689-2/pdf.

Crosnier, C., Stamataki, D. and Lewis, J. (2006) 'Organizing cell renewal in the intestine: stem cells, signals and combinatorial control', *Nature Reviews Genetics*, 7(5), pp. 349–359. doi: 10.1038/nrg1840.

Cruz-Acuña, R. *et al.* (2017) 'Synthetic hydrogels for human intestinal organoid generation and colonic wound repair', *Nature Cell Biology*, 19(11), pp. 1326–1335. doi: 10.1038/ncb3632.

Dawson, P. A. and Karpen, S. J. (2015) 'Intestinal transport and metabolism of bile acids', *Journal of Lipid Research*, 56(6), pp. 1085–1099. doi: 10.1194/jlr.R054114.

Debard, N. *et al.* (2001) 'Effect of mature lymphocytes and lymphotoxin on the development of the follicle-associated epithelium and M cells in mouse Peyer's patches.', *Gastroenterology*, 120(5), pp. 1173–82. doi: 10.1053/gast.2001.22476.

Debongnie, J. C. and Phillips, S. F. (1978) 'Capacity of the human colon to absorb fluid.', *Gastroenterology*, 74(4), pp. 698–703. Available at: http://www.ncbi.nlm.nih.gov/pubmed/631507.

Dedhia, P. H. *et al.* (2016) 'Organoid models of human gastrointestinal development and disease', *Gastroenterology*, 150(5), pp. 1098–1112. doi: 10.1053/j.gastro.2015.12.042.

Dekkers, J. F. *et al.* (2013) 'A functional CFTR assay using primary cystic fibrosis intestinal organoids', *Nature Medicine*, 19(7), pp. 939–945. doi: 10.1038/nm.3201.

Donaldson, D. S. *et al.* (2012) 'M cell-depletion blocks oral prion disease pathogenesis', *Mucosal Immunology*, 5(2), pp. 216–225. doi: 10.1038/mi.2011.68.

Donaldson, D. S. *et al.* (2016) 'Increased abundance of M cells in the gut epithelium dramatically enhances oral prion disease susceptibility', *PLOS Pathogens*, 12(12), p. e1006075. doi: 10.1371/journal.ppat.1006075.

Driehuis, E. and Clevers, H. (2017) 'CRISPR/Cas 9 genome editing and its applications in organoids', *American Journal of Physiology - Gastrointestinal and Liver Physiology*, 312(3), pp. G257–G265. doi: 10.1152/ajpgi.00410.2016.

Du, L. *et al.* (2018) 'Targeted delivery of GP5 antigen of PRRSV to M cells enhances the antigen-specific systemic and mucosal immune responses', *Frontiers in Cellular and Infection Microbiology*, 8(January), p. 7. doi: 10.3389/fcimb.2018.00007.

Dutta, D., Heo, I. and Clevers, H. (2017) 'Disease modeling in stem cell-derived 3D organoid systems', *Trends in Molecular Medicine*, 23(5), pp. 393–410. doi: 10.1016/j.molmed.2017.02.007.

Ebisawa, M. *et al.* (2011) 'CCR6hiCD11cint B cells promote M-cell differentiation in Peyer's patch', *International Immunology*, 23(4), pp. 261–269. doi: 10.1093/intimm/dxq478.

van Elburg, R. M. *et al.* (1993) 'Intestinal permeability in patients with coeliac disease and relatives of patients with coeliac disease.', *Gut*, 34(3), pp. 354–7. doi: 10.1136/gut.34.3.354.

Engelstoft, M. S. *et al.* (2015) 'Research resource: A chromogranin A reporter for serotonin and histamine secreting enteroendocrine cells.', *Molecular Endocrinology*, 29(11), pp. 1658–71. doi: 10.1210/me.2015-1106.

Ermund, A. *et al.* (2013) 'Studies of mucus in mouse stomach, small intestine, and colon. I. Gastrointestinal mucus layers have different properties depending on location as well as over the Peyer's patches', *American Journal of Physiology-Gastrointestinal and Liver Physiology*, 305(5), pp. G341–G347. doi: 10.1152/ajpgi.00046.2013.

van Es, J. H., van Gijn, M. E., *et al.* (2005) 'Notch/gamma-secretase inhibition turns proliferative cells in intestinal crypts and adenomas into goblet cells.', *Nature*, 435(7044), pp. 959–63. doi: 10.1038/nature03659.

van Es, J. H., Jay, P., *et al.* (2005) 'Wnt signalling induces maturation of Paneth cells in intestinal crypts', *Nature Cell Biology*, 7(4), pp. 381–386. doi: 10.1038/ncb1240.

Esposito, C. *et al.* (2003) 'Expression and enzymatic activity of small intestinal tissue transglutaminase in celiac disease.', *The American Journal of Gastroenterology*, 98(8), pp. 1813–1820. doi: 10.1111/j.1572-0241.2003.07582.x.

Fagarasan, S. (2002) 'Critical roles of activation-induced cytidine deaminase in the homeostasis of gut flora', *Science*, 298(5597), pp. 1424–1427. doi: 10.1126/science.1077336.

Farin, H. F. *et al.* (2014) 'Paneth cell extrusion and release of antimicrobial products is directly controlled by immune cell-derived IFN-γ.', *The Journal of Experimental Medicine*, 211(7), pp. 1393–405. doi: 10.1084/jem.20130753.

Fasano, A. (2011) ‘Zonulin and its regulation of intestinal barrier function: the biological door to inflammation, autoimmunity, and cancer’, *Physiological Reviews*, 91(1), pp. 151–175. doi: 10.1152/physrev.00003.2008.

Fasano, A. and Shea-Donohue, T. (2005) ‘Mechanisms of Disease: the role of intestinal barrier function in the pathogenesis of gastrointestinal autoimmune diseases’, *Nature Clinical Practice Gastroenterology & Hepatology*, 2(9), pp. 416–422. doi: 10.1038/ncpgasthep0259.

Fatehullah, A., Tan, S. H. and Barker, N. (2016) ‘Organoids as an in vitro model of human development and disease’, *Nature Cell Biology*, 18(3), pp. 246–254. doi: 10.1038/ncb3312.

Fernandez-Jimenez, N. *et al.* (2014) ‘Coregulation and modulation of NF B-related genes in celiac disease: uncovered aspects of gut mucosal inflammation’, *Human Molecular Genetics*, 23(5), pp. 1298–1310. doi: 10.1093/hmg/ddt520.

Field, M. (2003) ‘Intestinal ion transport and the pathophysiology of diarrhea’, *Journal of Clinical Investigation*, 111(7), pp. 931–943. doi: 10.1172/JCI200318326.

van der Flier, L. G. and Clevers, H. (2009) ‘Stem cells, self-renewal, and differentiation in the intestinal epithelium’, *Annual Review of Physiology*, 71(1), pp. 241–260. doi: 10.1146/annurev.physiol.010908.163145.

Forbes, S. J. *et al.* (2011) ‘Transient suppression of Shigella flexneri type 3 secretion by a protective O-antigen-specific monoclonal IgA’, *mBio*, 2(3), pp. 9–12. doi: 10.1128/mBio.00042-11.

Forbester, J. L. *et al.* (2015) ‘Interaction of Salmonella enterica serovar Typhimurium with intestinal organoids derived from human induced pluripotent stem cells’, *Infection and Immunity*, 83(7), pp. 2926–2934. doi: 10.1128/IAI.00161-15.

Fre, S. *et al.* (2005) ‘Notch signals control the fate of immature progenitor cells in the intestine’, *Nature*, 435(7044), pp. 964–968. doi: 10.1038/nature03589.

Friis, S. *et al.* (1992) ‘Gliadin uptake in human enterocytes. Differences between coeliac patients in remission and control individuals.’, *Gut*, 33(11), pp. 1487–92. Available at: http://www.ncbi.nlm.nih.gov/pubmed/1452073.

Fukuda, M. *et al.* (2014) ‘Small intestinal stem cell identity is maintained with functional Paneth cells in heterotopically grafted epithelium onto the colon’, *Genes & Development*, 28(16), pp. 1752–1757. doi: 10.1101/gad.245233.114.

Furness, J. B. *et al.* (2013) ‘The gut as a sensory organ’, *Nature Reviews Gastroenterology & Hepatology*, 10(12), pp. 729–740. doi: 10.1038/nrgastro.2013.180.

Gebert, A. and Posselt, W. (1997) ‘Glycoconjugate expression defines the origin and differentiation pathway of intestinal M-cells’, *Journal of Histochemistry & Cytochemistry*, 45(10), pp. 1341–1350. doi: 10.1177/002215549704501003.

Gerbe, F. and Jay, P. (2016) ‘Intestinal tuft cells: epithelial sentinels linking luminal cues to the immune system’, *Mucosal Immunology*, 9(6), pp. 1353–1359. doi: 10.1038/mi.2016.68.

Giannasca, P. J. *et al.* (1999) ‘Human intestinal M cells display the sialyl Lewis A antigen.’, *Infection and Immunity*, 67(2), pp. 946–53. Available at: http://www.ncbi.nlm.nih.gov/pubmed/9916113.

Gibson, P. R., Skodje, G. I. and Lundin, K. E. A. (2017) 'Non-coeliac gluten sensitivity', *Journal of Gastroenterology and Hepatology*, 32, pp. 86–89. doi: 10.1111/jgh.13705.

Gicheva, N. *et al.* (2016) 'Siglec-F is a novel intestinal M cell marker', *Biochemical and Biophysical Research Communications*, 479(1), pp. 1–4. doi: 10.1016/j.bbrc.2016.08.055.

Gjorevski, N. *et al.* (2016) 'Designer matrices for intestinal stem cell and organoid culture', *Nature*, 539(7630), pp. 560–564. doi: 10.1038/nature20168.

Golovkina, T. V *et al.* (1999) 'Organogenic role of B lymphocytes in mucosal immunity.', *Science*, 286(5446), pp. 1965–8. doi: 10.1126/science.286.5446.1965.

Gonzalez-Hernandez, M. B. *et al.* (2013) 'Murine norovirus transcytosis across an in vitro polarized murine intestinal epithelial monolayer is mediated by M-like cells', *Journal of Virology*, 87(23), pp. 12685–12693. doi: 10.1128/JVI.02378-13.

Gregorieff, A. *et al.* (2009) 'The Ets-domain transcription factor Spdef promotes maturation of goblet and Paneth cells in the intestinal epithelium', *Gastroenterology*, 137(4), pp. 1333-1345.e3. doi: 10.1053/j.gastro.2009.06.044.

Gullberg, E. *et al.* (2000) 'Expression of specific markers and particle transport in a new human intestinal M-cell model', *Biochemical and Biophysical Research Communications*, 279(3), pp. 808–813. doi: 10.1006/bbrc.2000.4038.

Gullberg, E. (2005) *Particle transcytosis across the human intestinal epithelium. Model development and target identification for improved drug delivery.* Uppsala University.

Gullberg, E. *et al.* (2006) 'Identification of cell adhesion molecules in the human follicle-associated epithelium that improve nanoparticle uptake into the Peyer's patches', *Journal of Pharmacology and Experimental Therapeutics*, 319(2), pp. 632–639. doi: 10.1124/jpet.106.107847.

Gullberg, E. and Söderholm, J. D. (2006) 'Peyer's patches and M cells as potential sites of the inflammatory onset in Crohn's disease', *Annals of the New York Academy of Sciences*, 1072, pp. 218–232. doi: 10.1196/annals.1326.028.

Gunawardene, A. R., Corfe, B. M. and Staton, C. a. (2011) 'Classification and functions of enteroendocrine cells of the lower gastrointestinal tract', *International Journal of Experimental Pathology*, 92(4), pp. 219–231. doi: 10.1111/j.1365-2613.2011.00767.x.

Haegebarth, A. *et al.* (2006) 'Protein tyrosine kinase 6 negatively regulates growth and promotes enterocyte differentiation in the small intestine', *Molecular and Cellular Biology*, 26(13), pp. 4949–4957. doi: 10.1128/MCB.01901-05.

Han, Z. *et al.* (1997) 'A sequential two-step mechanism for the production of the mature p17:p12 form of caspase-3 in vitro', *Journal of Biological Chemistry*, 272(20), pp. 13432–13436. doi: 10.1074/jbc.272.20.13432.

Hase, K. *et al.* (2005) 'Distinct gene expression profiles characterize cellular phenotypes of follicle-associated epithelium and M cells', *DNA Research*, 12(2), pp. 127–137. doi: 10.1093/dnares/12.2.127.

Hase, K. *et al.* (2006) 'The membrane-bound chemokine CXCL16 expressed on follicle-associated epithelium and M cells mediates lympho-epithelial interaction in GALT', *The Journal of Immunology*, 176(1), pp. 43–51. doi: 10.4049/jimmunol.176.1.43.

Hase, K., Kimura, S., *et al.* (2009) 'M-Sec promotes membrane nanotube formation by interacting with Ral and the exocyst complex', *Nature Cell Biology*, 11(12), pp. 1427–1432. doi: 10.1038/ncb1990.

Hase, K., Kawano, K., *et al.* (2009) 'Uptake through glycoprotein 2 of FimH+ bacteria by M cells initiates mucosal immune response', *Nature*, 462(7270), pp. 226–230. doi: 10.1038/nature08529.

Heyman, M. *et al.* (2012) 'Intestinal permeability in coeliac disease: insight into mechanisms and relevance to pathogenesis.', *Gut*, 61(9), pp. 1355–64. doi: 10.1136/gutjnl-2011-300327.

Hill, D. R. and Spence, J. R. (2016) 'Gastrointestinal organoids: understanding the molecular basis of the host–microbe interface', *CMGH Cellular and Molecular Gastroenterology and Hepatology*, 3(2), pp. 138–149. doi: 10.1016/j.jcmgh.2016.11.007.

Hischenhuber, C. *et al.* (2006) 'Review article: Safe amounts of gluten for patients with wheat allergy or coeliac disease', *Alimentary Pharmacology and Therapeutics*, 23(5), pp. 559–575. doi: 10.1111/j.1365-2036.2006.02768.x.

Hollon, J. *et al.* (2015) 'Effect of gliadin on permeability of intestinal biopsy explants from celiac disease patients and patients with non-celiac gluten sensitivity', *Nutrients*, 7(3), pp. 1565–1576. doi: 10.3390/nu7031565.

Hondo, T. *et al.* (2016) 'Cyclophilin A is a new M cell marker of bovine intestinal epithelium', *Cell and Tissue Research*, 364(3), pp. 585–597. doi: 10.1007/s00441-015-2342-1.

Hsieh, E. H. and Lo, D. D. (2012) 'Jagged1 and Notch1 help edit M cell patterning in Peyer's patch follicle epithelium', *Developmental and Comparative Immunology*, 37(2), pp. 306–312. doi: 10.1016/j.dci.2012.04.003.

Hu, J. L. *et al.* (2018) 'Opportunities for organoids as new models of aging', 217(1), pp. 1–12. doi: 10.1083/jcb.201709054.

Huch, M. *et al.* (2015) 'Long-term culture of genome-stable bipotent stem cells from adult human liver', *Cell*, 160(1–2), pp. 299–312. doi: 10.1016/j.cell.2014.11.050.

Huch, M. *et al.* (2017) 'The hope and the hype of organoid research', *Development*, 144(6), pp. 938–941. doi: 10.1242/dev.150201.

Hugenholtz, F. and de Vos, W. M. (2018) 'Mouse models for human intestinal microbiota research: a critical evaluation', *Cellular and Molecular Life Sciences*, 75(1), pp. 149–160. doi: 10.1007/s00018-017-2693-8.

Humphries, A. D. *et al.* (2003) 'The use of flow cytometry to detect expression of subunits encoded by 11 Salmonella enterica serotype Typhimurium fimbrial operons', *Molecular Microbiology*, 48(5), pp. 1357–1376. doi: 10.1046/j.1365-2958.2003.03507.x.

In, J. G. *et al.* (2016) 'Human mini-guts: new insights into intestinal physiology and host-pathogen interactions.', *Nature reviews. Gastroenterology & hepatology*, 13(11), pp. 633–642. doi: 10.1038/nrgastro.2016.142.

Jacob, E., Baker, S. J. and Swaminathan, S. P. (1987) '"M" cells in the follicle-associated epithelium of the human colon.', *Histopathology*, 11(9), pp. 941–52. doi: 10.1111/j.1365-2559.1987.tb01900.x.

Jakab, R. L., Collaco, A. M. and Ameen, N. A. (2011) 'Physiological relevance of cell-specific distribution patterns of CFTR, NKCC1, NBCe1, and NHE3 along the crypt-villus axis in the intestine', *American Journal of Physiology-Gastrointestinal and Liver Physiology*, 300(1), pp. G82–G98. doi: 10.1152/ajpgi.00245.2010.

Jenny, M. *et al.* (2002) 'Neurogenin3 is differentially required for endocrine cell fate specification in the intestinal and gastric epithelium', *EMBO Journal*, 21(23), pp. 6338–6347. doi: 10.1093/emboj/cdf649.

Johansson, M. E. V. and Hansson, G. C. (2016) 'Immunological aspects of intestinal mucus and mucins', *Nature Reviews Immunology*, 16(10), pp. 639–649. doi: 10.1038/nri.2016.88.

Johansson, M. E. V *et al.* (2011) 'Composition and functional role of the mucus layers in the intestine', *Cellular and Molecular Life Sciences*, 68(22), pp. 3635–3641. doi: 10.1007/s00018-011-0822-3.

Jones-Hall, Y. L. and Nakatsu, C. H. (2016) 'The intersection of TNF, IBD and the microbiome', *Gut Microbes*, 7(1), pp. 58–62. doi: 10.1080/19490976.2015.1121364.

Junker, Y. *et al.* (2012) 'Wheat amylase trypsin inhibitors drive intestinal inflammation via activation of toll-like receptor 4', *The Journal of Experimental Medicine*, 209(13), pp. 2395–2408. doi: 10.1084/jem.20102660.

Kanaya, T. *et al.* (2012) 'The Ets transcription factor Spi-B is essential for the differentiation of intestinal microfold cells', *Nature Immunology*, 13(8), pp. 729–736. doi: 10.1038/ni.2352.

Kanaya, T. *et al.* (2018) 'Development of intestinal M cells and follicle-associated epithelium is regulated by TRAF6-mediated NF-κB signaling', *The Journal of Experimental Medicine*, 215(2), pp. 501–519. doi: 10.1084/jem.20160659.

Karpova, M. B. *et al.* (2005) 'Raji revisited: Cytogenetics of the original Burkitt's lymphoma cell line', *Leukemia*, 19(1), pp. 159–161. doi: 10.1038/sj.leu.2403534.

Karrer, U. *et al.* (2000) 'Immunodeficiency of alymphoplasia mice (aly/aly) in vivo: structural defect of secondary lymphoid organs and functional B cell defect.', *European Journal of Immunology*, 30(10), pp. 2799–807. doi: 10.1002/1521-4141(200010)30:10<2799::AID-IMMU2799>3.0.CO;2-2.

Kazanjian, A. *et al.* (2010) 'Atonal homolog 1 is required for growth and differentiation effects of notch/gamma-secretase inhibitors on normal and cancerous intestinal epithelial cells.', *Gastroenterology*, 139(3), pp. 918–28, 928.e1–6. doi: 10.1053/j.gastro.2010.05.081.

Keita, Å. *et al.* (2008) 'Increased uptake of non-pathogenic E. coli via the follicle-associated epithelium in longstanding ileal Crohn's disease', *The Journal of Pathology*, 215(2), pp. 135–144. doi: 10.1002/path.2337.

Kernéis, S. *et al.* (1997) 'Conversion by Peyer's patch lymphocytes of human enterocytes into M cells that transport bacteria.', *Science*, 277(5328), pp. 949–952. doi: 10.1126/science.277.5328.949.

Kim, S.-H. *et al.* (2010) 'The M cell-targeting ligand promotes antigen delivery and induces antigen-specific immune responses in mucosal vaccination', *The Journal of Immunology*, 185(10), pp. 5787–5795. doi: 10.4049/jimmunol.0903184.

Kim, S.-H. and Jang, Y.-S. (2014) 'Antigen targeting to M cells for enhancing the efficacy of

mucosal vaccines', *Experimental & Molecular Medicine*, 46(3), pp. e85–e85. doi: 10.1038/emm.2013.165.

Kim, S. A. *et al.* (2011) 'Calcium-dependent dynamics of cadherin interactions at cell-cell junctions', *Proceedings of the National Academy of Sciences*, 108(24), pp. 9857–9862. doi: 10.1073/pnas.1019003108.

Kim, Y. S. and Ho, S. B. (2010) 'Intestinal goblet cells and mucins in health and disease: Recent insights and progress', *Current Gastroenterology Reports*, 12(5), pp. 319–330. doi: 10.1007/s11894-010-0131-2.

Kimura, S. *et al.* (2015) 'Visualization of the entire differentiation process of murine M cells: suppression of their maturation in cecal patches', *Mucosal Immunology*, 8(3), pp. 650–660. doi: 10.1038/mi.2014.99.

Kimura, S. *et al.* (2019) 'Sox8 is essential for M cell maturation to accelerate IgA response at the early stage after weaning in mice', *Journal of Experimental Medicine*, 216(4), pp. 831–846. doi: https://doi.org/10.1084/jem.20181604.

Knoop, K. A. *et al.* (2009) 'RANKL is necessary and sufficient to initiate development of antigen-sampling M cells in the intestinal epithelium', *The Journal of Immunology*, 183(9), pp. 5738–5747. doi: 10.4049/jimmunol.0901563.

Knoop, K. A., Miller, M. J. and Newberry, R. D. (2013) 'Transepithelial antigen delivery in the small intestine: different paths, different outcomes.', *Current Opinion in Gastroenterology*, 29(2), pp. 112–8. doi: 10.1097/MOG.0b013e32835cf1cd.

Kobayashi, A. *et al.* (2012) 'Identification of novel genes selectively expressed in the follicle-associated epithelium from the meta-analysis of transcriptomics data from multiple mouse cell and tissue populations', *DNA Research*, 19(5), pp. 407–422. doi: 10.1093/dnares/dss022.

Kong, Y. Y. *et al.* (1999) 'OPGL is a key regulator of osteoclastogenesis, lymphocyte development and lymph-node organogenesis.', *Nature*, 397(6717), pp. 315–23. doi: 10.1038/16852.

König, J. *et al.* (2016) 'Human intestinal barrier function in health and disease', *Clinical and Translational Gastroenterology*, 7(10), pp. e196–e196. doi: 10.1038/ctg.2016.54.

Korinek, V. *et al.* (1998) 'Depletion of epithelial stem-cell compartments in the small intestine of mice lacking Tcf-4', *Nature Genetics*, 19(4), pp. 379–383. doi: 10.1038/1270.

Kraiczy, J. *et al.* (2017) 'DNA methylation defines regional identity of human intestinal epithelial organoids and undergoes dynamic changes during development.', *Gut*, p. gutjnl-2017-314817. doi: 10.1136/gutjnl-2017-314817.

Lahar, N. *et al.* (2011) 'Intestinal subepithelial myofibroblasts support in vitro and in vivo growth of human small intestinal epithelium', *PLoS ONE*, 6(11), p. e26898. doi: 10.1371/journal.pone.0026898.

Lammers, K. M. *et al.* (2008) 'Gliadin Induces an Increase in Intestinal Permeability and Zonulin Release by Binding to the Chemokine Receptor CXCR3', *Gastroenterology*, 135(1), pp. 194–204. doi: 10.1053/j.gastro.2008.03.023.

Lancaster, M. A. *et al.* (2013) 'Cerebral organoids model human brain development and microcephaly', *Nature*, 501(7467), pp. 373–379. doi: 10.1038/nature12517.

de Lau, W. *et al.* (2012) 'Peyer's patch M cells derived from Lgr5+ stem cells require SpiB and are induced by RankL in cultured "miniguts"', *Molecular and Cellular Biology*, 32(18), pp. 3639–3647. doi: 10.1128/MCB.00434-12.

Leffler, D. A., Green, P. H. R. and Fasano, A. (2015) 'Extraintestinal manifestations of coeliac disease', *Nature Reviews Gastroenterology & Hepatology*, 12(10), pp. 561–571. doi: 10.1038/nrgastro.2015.131.

Lelouard, H. *et al.* (2012) 'Peyer's patch dendritic cells sample antigens by extending dendrites through M cell-specific transcellular pores.', *Gastroenterology*, 142(3), pp. 592-601.e3. doi: 10.1053/j.gastro.2011.11.039.

Lencer, W. I. and Tsai, B. (2003) 'The intracellular voyage of cholera toxin: going retro.', *Trends in Biochemical Sciences*, 28(12), pp. 639–45. doi: 10.1016/j.tibs.2003.10.002.

Leslie, J. L. *et al.* (2015) 'Persistence and toxin production by Clostridium difficile within human intestinal organoids result in disruption of epithelial paracellular barrier function.', *Infection and Immunity*, 83(1), pp. 138–45. doi: 10.1128/IAI.02561-14.

Leslie, J. L. and Young, V. B. (2016) 'A whole new ball game: Stem cell-derived epithelia in the study of host–microbe interactions', *Anaerobe*, 37, pp. 25–28. doi: 10.1016/j.anaerobe.2015.10.016.

Lesuffleur, T. *et al.* (1990) 'Growth adaptation to methotrexate of HT-29 human colon carcinoma cells is associated with their ability to differentiate into columnar absorptive and mucus-secreting cells.', *Cancer research*, 50(19), pp. 6334–43. Available at: http://www.ncbi.nlm.nih.gov/pubmed/2205381.

Liu, J. *et al.* (2015) 'Defective goblet cell exocytosis contributes to murine cystic fibrosis'associated intestinal disease', *Journal of Clinical Investigation*, 125(3), pp. 1056–1068. doi: 10.1172/JCI73193.

Lo, D. *et al.* (2004) 'Cell culture modeling of specialized tissue: Identification of genes expressed specifically by follicle-associated epithelium of Peyer's patch by expression profiling of Caco-2/Raji co-cultures', *International Immunology*, 16(1), pp. 91–99. doi: 10.1093/intimm/dxh011.

Loehry, C. a and Parrish, D. (1970) 'Small bowel permeability in animals and man.', *Gut*, 11(12), p. 1059. Available at: http://www.ncbi.nlm.nih.gov/pubmed/5511795.

López-Díaz, L. *et al.* (2007) 'Intestinal Neurogenin 3 directs differentiation of a bipotential secretory progenitor to endocrine cell rather than goblet cell fate', *Developmental Biology*, 309(2), pp. 298–305. doi: 10.1016/j.ydbio.2007.07.015.

Lügering, A. *et al.* (2005) 'Absence of CCR6 inhibits CD4+ regulatory T-cell development and M-cell formation inside Peyer's patches', *The American Journal of Pathology*, 166(6), pp. 1647–1654. doi: 10.1016/S0002-9440(10)62475-3.

Ma, T., Vetrivel, L., *et al.* (2002) 'High-affinity activators of cystic fibrosis transmembrane conductance regulator (CFTR) chloride conductance identified by high-throughput screening.', *The Journal of Biological Chemistry*, 277(40), pp. 37235–41. doi: 10.1074/jbc.M205932200.

Ma, T., Thiagarajah, J. R., *et al.* (2002) 'Thiazolidinone CFTR inhibitor identified by high-throughput screening blocks cholera toxin–induced intestinal fluid secretion', *Journal of Clinical Investigation*, 110(11), pp. 1651–1658. doi: 10.1172/JCI16112.

Ma, T. Y. *et al.* (2004) 'TNF-α-induced increase in intestinal epithelial tight junction permeability requires NF-κB activation', *American Journal of Physiology-Gastrointestinal and Liver Physiology*, 286(3), pp. G367–G376. doi: 10.1152/ajpgi.00173.2003.

Mabbott, N. A. *et al.* (2013) 'Microfold (M) cells: important immunosurveillance posts in the intestinal epithelium', *Mucosal Immunology*, 6(4), pp. 666–677. doi: 10.1038/mi.2013.30.

Maiuri, L. *et al.* (2003) 'Association between innate response to gliadin and activation of pathogenic T cells in coeliac disease', *Lancet*, 362(9377), pp. 30–37. doi: 10.1016/S0140-6736(03)13803-2.

Major, G. *et al.* (2017) 'Colon hypersensitivity to distension, rather than excessive gas production, produces carbohydrate-related symptoms in individuals with irritable bowel syndrome.', *Gastroenterology*, 152(1), pp. 124-133.e2. doi: 10.1053/j.gastro.2016.09.062.

Man, A. L. *et al.* (2008) 'Macrophage migration inhibitory factor plays a role in the regulation of microfold (M) cell-mediated transport in the gut.', *Journal of Immunology*, 181(8), pp. 5673–80. doi: 10.4049/jimmunol.181.8.5673.

Mantis, N. J. *et al.* (2002) 'Selective adherence of IgA to murine Peyer's patch M cells: evidence for a novel IgA receptor', *The Journal of Immunology*, 169(4), pp. 1844–1851. doi: 10.4049/jimmunol.169.4.1844.

Mantis, N. J., Rol, N. and Corthésy, B. (2011) 'Secretory IgA's complex roles in immunity and mucosal homeostasis in the gut', *Mucosal Immunology*, 4(6), pp. 603–611. doi: 10.1038/mi.2011.41.

Martinez-Argudo, I., Sands, C. and Jepson, M. A. (2007) 'Translocation of enteropathogenic Escherichia coli across an in vitro M cell model is regulated by its type III secretion system', *Cellular Microbiology*, 9(6), pp. 1538–1546. doi: 10.1111/j.1462-5822.2007.00891.x.

Masuda, K., Kajikawa, A. and Igimi, S. (2011) 'Establishment and evaluation of an in vitro M cell model using C2BBe1 cells and Raji cells.', *Bioscience and Microflora*, 30(2), pp. 37–44. doi: 10.12938/bifidus.30.37.

Matysiak-Budnik, T. *et al.* (2008) 'Secretory IgA mediates retrotranscytosis of intact gliadin peptides via the transferrin receptor in celiac disease', *The Journal of Experimental Medicine*, 205(1), pp. 143–154. doi: 10.1084/jem.20071204.

Mazumdar, K. *et al.* (2010) 'Visualization of transepithelial passage of the immunogenic 33-residue peptide from α-2 gliadin in gluten-sensitive macaques', *PLoS ONE*, 5(4). doi: 10.1371/journal.pone.0010228.

McAllister, B. P., Williams, E. and Clarke, K. (2018) 'A comprehensive review of celiac disease/gluten-sensitive enteropathies', *Clinical Reviews in Allergy & Immunology*. doi: 10.1007/s12016-018-8691-2.

McCall, M. N. *et al.* (2014) 'On non-detects in qPCR data', *Bioinformatics*, 30(16), pp. 2310–2316. doi: 10.1093/bioinformatics/btu239.

McDole, J. R. *et al.* (2012) 'Goblet cells deliver luminal antigen to CD103+ dendritic cells in the small intestine', *Nature*, 483(7389), pp. 345–349. doi: 10.1038/nature10863.

Ménard, S. *et al.* (2012) 'Paracellular versus transcellular intestinal permeability to gliadin peptides in active celiac disease', *American Journal of Pathology*, 180(2), pp. 608–615. doi:

10.1016/j.ajpath.2011.10.019.

Ménard, S., Cerf-Bensussan, N. and Heyman, M. (2010) 'Multiple facets of intestinal permeability and epithelial handling of dietary antigens', *Mucosal Immunology*, 3(3), pp. 247–259. doi: 10.1038/mi.2010.5.

Meresse, B., Malamut, G. and Cerf-Bensussan, N. (2012) 'Celiac Disease: an immunological jigsaw', *Immunity*, 36(6), pp. 907–919. doi: 10.1016/j.immuni.2012.06.006.

Mesin, L., Sollid, L. M. and Niro, R. Di (2012) 'The intestinal B-cell response in celiac disease', *Frontiers in Immunology*, 3(October), p. 313. doi: 10.3389/fimmu.2012.00313.

Middelhoff, M. *et al.* (2017) 'Dclk1-expressing tuft cells: critical modulators of the intestinal niche?', *American Journal of Physiology-Gastrointestinal and Liver Physiology*, 313(4), pp. G285–G299. doi: 10.1152/ajpgi.00073.2017.

Middendorp, S. *et al.* (2014) 'Adult stem cells in the small intestine are intrinsically programmed with their location-specific function', *Stem Cells*, 32(5), pp. 1083–1091. doi: 10.1002/stem.1655.

Milano, J. *et al.* (2004) 'Modulation of Notch processing by γ-secretase inhibitors causes intestinal goblet cell metaplasia and induction of genes known to specify gut secretory lineage Differentiation', *Toxicological Sciences*, 82(1), pp. 341–358. doi: 10.1093/toxsci/kfh254.

Miller, H. (2007) 'Intestinal M cells: The fallible sentinels?', *World Journal of Gastroenterology*, 13(10), p. 1477. doi: 10.3748/wjg.v13.i10.1477.

Miyazawa, K. *et al.* (2010) 'Transcytosis of murine-adapted bovine spongiform encephalopathy agents in an in vitro bovine M cell model', *Journal of Virology*, 84(23), pp. 12285–12291. doi: 10.1128/JVI.00969-10.

Miyoshi, H. and Stappenbeck, T. S. (2013) 'In vitro expansion and genetic modification of gastrointestinal stem cells in spheroid culture', *Nature Protocols*, 8(12), pp. 2471–2482. doi: 10.1038/nprot.2013.153.

von Moltke, J. *et al.* (2015) 'Tuft-cell-derived IL-25 regulates an intestinal ILC2–epithelial response circuit', *Nature*, 529(7585), pp. 221–225. doi: 10.1038/nature16161.

Moon, C. *et al.* (2014) 'Development of a primary mouse intestinal epithelial cell monolayer culture system to evaluate factors that modulate IgA transcytosis', *Mucosal Immunology*, 7(4), pp. 818–828. doi: 10.1038/mi.2013.98.

Moon, C. *et al.* (2015) 'Drug-induced secretory diarrhea: A role for CFTR', *Pharmacological Research*, 102, pp. 107–112. doi: 10.1016/j.phrs.2015.08.024.

Moor, K. *et al.* (2017) 'High-avidity IgA protects the intestine by enchaining growing bacteria', *Nature*, 544(7651), pp. 498–502. doi: 10.1038/nature22058.

Moran, O. (2017) 'The gating of the CFTR channel', *Cellular and Molecular Life Sciences*, 74(1), pp. 85–92. doi: 10.1007/s00018-016-2390-z.

Moreno, M. D. L. *et al.* (2017) 'Detection of gluten immunogenic peptides in the urine of patients with coeliac disease reveals transgressions in the gluten-free diet and incomplete mucosal healing', *Gut*, 66(2), pp. 250–257. doi: 10.1136/gutjnl-2015-310148.

Murray, J. A., Frey, M. R. and Oliva-Hemker, M. (2018) 'Celiac Disease', *Gastroenterology*,

154(8), pp. 2005–2008. doi: 10.1053/j.gastro.2017.12.026.

Mustata, R. C. *et al.* (2011) 'Lgr4 is required for Paneth cell differentiation and maintenance of intestinal stem cells ex vivo', *EMBO Reports*, 12(6), pp. 558–564. doi: 10.1038/embor.2011.52.

Mutch, D. M. *et al.* (2004) 'Regional variations in ABC transporter expression along the mouse intestinal tract', *Physiological Genomics*, 17(1), pp. 11–20. doi: 10.1152/physiolgenomics.00150.2003.

Mutoh, M. *et al.* (2016) 'RANKL regulates differentiation of microfold cells in mouse nasopharynx-associated lymphoid tissue (NALT)', *Cell and Tissue Research*, 364(1), pp. 175–184. doi: 10.1007/s00441-015-2309-2.

Nagashima, K., Sawa, S., Nitta, T., Tsutsumi, M., *et al.* (2017) 'Identification of subepithelial mesenchymal cells that induce IgA and diversify gut microbiota', *Nature Immunology*, 18(6), pp. 675–682. doi: 10.1038/ni.3732.

Nagashima, K., Sawa, S., Nitta, T., Prados, A., *et al.* (2017) 'Targeted deletion of RANKL in M cell inducer cells by the Col6a1-Cre driver', *Biochemical and Biophysical Research Communications*, 493(1), pp. 437–443. doi: 10.1016/j.bbrc.2017.09.004.

Nagy, V. and Penninger, J. M. (2015) 'The RANKL-RANK Story', *Gerontology*, 61(6), pp. 534–542. doi: 10.1159/000371845.

Nair, V. R. *et al.* (2016) 'Microfold cells actively translocate Mycobacterium tuberculosis to initiate infection', *Cell Reports*, 16(5), pp. 1253–1258. doi: 10.1016/j.celrep.2016.06.080.

Nakagawa, N. *et al.* (1998) 'RANK is the essential signaling receptor for osteoclast differentiation factor in osteoclastogenesis', *Biochemical and Biophysical Research Communications*, 253(2), pp. 395–400. doi: 10.1006/bbrc.1998.9788.

Nakamura, T. (2018) 'Recent progress in organoid culture to model intestinal epithelial barrier functions', *International Immunology*, 67(10), pp. 1905–1906. doi: 10.1093/intimm/dxy065.

Nakato, G. *et al.* (2012) 'Cutting edge: Brucella abortus exploits a cellular prion protein on intestinal M cells as an invasive receptor', *The Journal of Immunology*, 189(4), pp. 1540–1544. doi: 10.4049/jimmunol.1103332.

Neutra, M. R. *et al.* (1987) 'Transport of membrane-bound macromolecules by M cells in follicle-associated epithelium of rabbit Peyer's patch', *Cell and Tissue Research*, 247(3), pp. 537–546. doi: 10.1007/BF00215747.

Neutra, M. R., Mantis, N. J. and Kraehenbuhl, J. P. (2001) 'Collaboration of epithelial cells with organized mucosal lymphoid tissues', *Nature Immunology*, 2(11), pp. 1004–1009. doi: 10.1038/ni1101-1004.

Nguyen, T. L. A. *et al.* (2015) 'How informative is the mouse for human gut microbiota research?', *Disease Models & Mechanisms*, 8(1), pp. 1–16. doi: 10.1242/dmm.017400.

Niess, J. H. *et al.* (2005) 'CX3CR1-mediated dendritic cell access to the intestinal lumen and bacterial clearance.', *Science*, 307(5707), pp. 254–258. doi: 10.1126/science.1102901.

Noah, T. K. *et al.* (2010) 'SAM pointed domain ETS factor (SPDEF) regulates terminal differentiation and maturation of intestinal goblet cells', *Experimental Cell Research*, 316(3), pp. 452–465. doi: 10.1016/j.yexcr.2009.09.020.

Noah, T. K., Donahue, B. and Shroyer, N. F. (2011) 'Intestinal development and differentiation', *Experimental Cell Research*, 317(19), pp. 2702–2710. doi: 10.1016/j.yexcr.2011.09.006.

Nochi, T. *et al.* (2007) 'A novel M cell-specific carbohydrate-targeted mucosal vaccine effectively induces antigen-specific immune responses.', *The Journal of Experimental Medicine*, 204(12), pp. 2789–96. doi: 10.1084/jem.20070607.

Noel, G. *et al.* (2017) 'A primary human macrophage-enteroid co-culture model to investigate mucosal gut physiology and host-pathogen interactions', *Scientific Reports*, 7(1), p. 45270. doi: 10.1038/srep45270.

Nozaki, K. *et al.* (2016) 'Co-culture with intestinal epithelial organoids allows efficient expansion and motility analysis of intraepithelial lymphocytes', *Journal of Gastroenterology*, 51(3), pp. 206–213. doi: 10.1007/s00535-016-1170-8.

Odenwald, M. A. and Turner, J. R. (2013) 'Intestinal Permeability Defects: Is It Time to Treat?', *Clinical Gastroenterology and Hepatology*, 11(9), pp. 1075–1083. doi: 10.1016/j.cgh.2013.07.001.

Odenwald, M. A. and Turner, J. R. (2016) 'The intestinal epithelial barrier: a therapeutic target?', *Nature Reviews Gastroenterology & Hepatology*, 14(1), pp. 9–21. doi: 10.1038/nrgastro.2016.169.

Ohno, H. (2016) 'Intestinal M cells', *Journal of Biochemistry*, 159(2), pp. 151–160. doi: 10.1093/jb/mvv121.

Ohno, H. and Hase, K. (2010) 'Glycoprotein 2 (GP2)', *Gut Microbes*, 1(6), pp. 407–410. doi: 10.4161/gmic.1.6.14078.

Owen, R. L. and Jones, A. L. (1974) 'Epithelial cell specialization within human Peyer's patches: an ultrastructural study of intestinal lymphoid follicles.', *Gastroenterology*, 66(2), pp. 189–203. Available at: http://www.ncbi.nlm.nih.gov/pubmed/4810912.

Pelaseyed, T. *et al.* (2014) 'The mucus and mucins of the goblet cells and enterocytes provide the first defense line of the gastrointestinal tract and interact with the immune system', *Immunological Reviews*, 260(1), pp. 8–20. doi: 10.1111/imr.12182.

Pellegrinet, L. *et al.* (2011) 'Dll1- and Dll4-mediated Notch signaling are required for homeostasis of intestinal stem cells', *Gastroenterology*, 140(4), pp. 1230-1240.e7. doi: 10.1053/j.gastro.2011.01.005.

Pinto-Sánchez, M. I. and Verdú, E. F. (2016) 'Non-coeliac gluten sensitivity: are we closer to separating the wheat from the chaff?', *Gut*, 65(12), pp. 1921–1922. doi: 10.1136/gutjnl-2016-312471.

Ponnusamy, D. *et al.* (2013) 'Mycobacterium avium subsp. paratuberculosis invades through M cells and enterocytes across ileal and jejunal mucosa of lambs', *Research in Veterinary Science*, 94(2), pp. 306–312. doi: 10.1016/j.rvsc.2012.09.023.

Pott, J., Kabat, A. M. and Maloy, K. J. (2018) 'Intestinal epithelial cell autophagy is required to protect against TNF-induced apoptosis during chronic colitis in mice', *Cell Host & Microbe*, 23(2), pp. 191-202.e4. doi: 10.1016/j.chom.2017.12.017.

Potten, C. S., Owen, G. and Booth, D. (2002) 'Intestinal stem cells protect their genome by selective segregation of template DNA strands.', *Journal of Cell Science*, 115(Pt 11), pp. 2381–

8. Available at: http://www.ncbi.nlm.nih.gov/pubmed/12006622.

De Re, V. *et al.* (2013) 'The versatile role of gliadin peptides in celiac disease', *Clinical Biochemistry*, 46(6), pp. 552–560. doi: 10.1016/j.clinbiochem.2012.10.038.

Reboul, E. and Borel, P. (2011) 'Proteins involved in uptake, intracellular transport and basolateral secretion of fat-soluble vitamins and carotenoids by mammalian enterocytes', *Progress in Lipid Research*, 50(4), pp. 388–402. doi: 10.1016/j.plipres.2011.07.001.

Rej, A., Aziz, I. and Sanders, D. S. (2019) 'Breaking bread!', *Proceedings of the Nutrition Society*, 78(1), pp. 118–125. doi: 10.1017/S0029665118002549.

Rescigno, M. *et al.* (2001) 'Dendritic cells express tight junction proteins and penetrate gut epithelial monolayers to sample bacteria', *Nature Immunology*, 2(4), pp. 361–367. doi: 10.1038/86373.

Riccio, O. *et al.* (2008) 'Loss of intestinal crypt progenitor cells owing to inactivation of both Notch1 and Notch2 is accompanied by derepression of CDK inhibitors p27Kip1 and p57Kip2', *EMBO Reports*, 9(4), pp. 377–383. doi: 10.1038/embor.2008.7.

des Rieux, A. *et al.* (2005) 'Transport of nanoparticles across an in vitro model of the human intestinal follicle associated epithelium', *European Journal of Pharmaceutical Sciences*, 25(4–5), pp. 455–465. doi: 10.1016/j.ejps.2005.04.015.

des Rieux, A. *et al.* (2007) 'An improved in vitro model of human intestinal follicle-associated epithelium to study nanoparticle transport by M cells', *European Journal of Pharmaceutical Sciences*, 30(5), pp. 380–391. doi: 10.1016/j.ejps.2006.12.006.

Rios, D. *et al.* (2016) 'Antigen sampling by intestinal M cells is the principal pathway initiating mucosal IgA production to commensal enteric bacteria.', *Mucosal Immunology*, 9(4), pp. 907–16. doi: 10.1038/mi.2015.121.

Roberts, C. L. *et al.* (2010) 'Translocation of Crohn's disease Escherichia coli across M-cells: contrasting effects of soluble plant fibres and emulsifiers.', *Gut*, 59, pp. 1331–1339. doi: 10.1136/gut.2009.195370.

Roberts, C. L. *et al.* (2013) 'Soluble plantain fibre blocks adhesion and M-cell translocation of intestinal pathogens', *The Journal of Nutritional Biochemistry*, 24(1), pp. 97–103. doi: 10.1016/j.jnutbio.2012.02.013.

Rochereau, N. *et al.* (2013) 'Dectin-1 is essential for reverse transcytosis of glycosylated SIgA-antigen complexes by intestinal M cells.', *PLoS Biology*, 11(9), p. e1001658. doi: 10.1371/journal.pbio.1001658.

Ross, A., Rubin, A. W. and Deren, J. J. (1972) 'Differential permeability of the proximal and distal rabbit small bowel', *Journal of Clinical Investigation*, 51(9), pp. 2414–2419. doi: 10.1172/JCI107054.

Rouch, J. D. *et al.* (2016) 'Development of functional microfold (M) cells from intestinal stem cells in primary human enteroids', *PLoS ONE*, 11(1), p. e0148216. doi: 10.1371/journal.pone.0148216.

Round, J. L. and Mazmanian, S. K. (2009) 'The gut microbiota shapes intestinal immune responses during health and disease', *Nature Reviews Immunology*, 9(8), pp. 600–600. doi: 10.1038/nri2614.

Di Sabatino, A. *et al.* (2012) 'The function of tissue transglutaminase in celiac disease', *Autoimmunity Reviews*, 11(10), pp. 746–753. doi: 10.1016/j.autrev.2012.01.007.

Said, H. M. (2011) 'Intestinal absorption of water-soluble vitamins in health and disease', *Biochemical Journal*, 437(3), pp. 357–372. doi: 10.1042/BJ20110326.

Saint-Criq, V. and Gray, M. A. (2017) 'Role of CFTR in epithelial physiology', *Cellular and Molecular Life Sciences*, 74(1), pp. 93–115. doi: 10.1007/s00018-016-2391-y.

Sakhon, O. S. *et al.* (2015) 'M cell-derived vesicles suggest a unique pathway for trans-epithelial antigen delivery', *Tissue Barriers*, 3(1–2), p. e1004975. doi: 10.1080/21688370.2015.1004975.

Sambuy, Y. *et al.* (2005) 'The Caco-2 cell line as a model of the intestinal barrier: influence of cell and culture-related factors on Caco-2 cell functional characteristics', *Cell Biology and Toxicology*, 21(1), pp. 1–26. doi: 10.1007/s10565-005-0085-6.

Sato, S. *et al.* (2013) 'Transcription factor Spi-B–dependent and –independent pathways for the development of Peyer's patch M cells', *Mucosal Immunology*, 6(4), pp. 838–846. doi: 10.1038/mi.2012.122.

Sato, T. *et al.* (2009) 'Single Lgr5 stem cells build crypt-villus structures in vitro without a mesenchymal niche.', *Nature*, 459(7244), pp. 262–265. doi: 10.1038/nature07935.

Sato, T., Stange, D. E., *et al.* (2011) 'Long-term expansion of epithelial organoids from human colon, adenoma, adenocarcinoma, and Barrett's epithelium', *Gastroenterology*, 141(5), pp. 1762–1772. doi: 10.1053/j.gastro.2011.07.050.

Sato, T., van Es, J. H., *et al.* (2011) 'Paneth cells constitute the niche for Lgr5 stem cells in intestinal crypts.', *Nature*, 469(7330), pp. 415–418. doi: 10.1038/nature09637.

Sato, T. and Clevers, H. (2013) 'Growing self-organizing mini-guts from a single intestinal stem cell: mechanism and applications', *Science*, 340(6137), pp. 1190–1194. doi: 10.1126/science.1234852.

Schimpel, C. *et al.* (2014) 'Development of an advanced intestinal in vitro triple culture permeability model to study transport of nanoparticles', *Molecular Pharmaceutics*, 11(3), pp. 808–818. doi: 10.1021/mp400507g.

Schmittgen, T. D. and Livak, K. J. (2008) 'Analyzing real-time PCR data by the comparative CT method', *Nature Protocols*, 3(6), pp. 1101–1108. doi: 10.1038/nprot.2008.73.

Schneider, C. A., Rasband, W. S. and Eliceiri, K. W. (2012) 'NIH Image to ImageJ: 25 years of image analysis', *Nature Methods*, 9(7), pp. 671–675. doi: 10.1038/nmeth.2089.

Schulte, R. *et al.* (2000) 'Translocation of Yersinia enterocolitica across reconstituted intestinal epithelial monolayers is triggered by Yersinia invasin binding to beta1 integrins apically expressed on M-like cells', *Cellular Microbiology*, 2(2), pp. 173–185. doi: 10.1046/j.1462-5822.2000.00047.x.

Schulz, O. and Pabst, O. (2013) 'Antigen sampling in the small intestine', *Trends in Immunology*, 34(4), pp. 155–161. doi: 10.1016/j.it.2012.09.006.

Schumann, M. *et al.* (2008) 'Mechanisms of epithelial translocation of the alpha(2)-gliadin-33mer in coeliac sprue.', *Gut*, 57(6), pp. 747–54. doi: 10.1136/gut.2007.136366.

Schumann, M. *et al.* (2017) 'Celiac disease: role of the epithelial barrier', *Cellular and Molecular Gastroenterology and Hepatology*, 3(2), pp. 150–162. doi: 10.1016/j.jcmgh.2016.12.006.

Schuppan, D. *et al.* (2015) 'Non-celiac wheat sensitivity: Differential diagnosis, triggers and implications', *Best Practice and Research: Clinical Gastroenterology*, 29(3), pp. 469–476. doi: 10.1016/j.bpg.2015.04.002.

Schuppan, D., Junker, Y. and Barisani, D. (2009) 'Celiac disease: from pathogenesis to novel therapies', *Gastroenterology*, 137(6), pp. 1912–1933. doi: 10.1053/j.gastro.2009.09.008.

Schuppan, D. and Zimmer, K.-P. (2013) 'The diagnosis and treatment of Celiac disease', *Deutsches Aerzteblatt Online*, 110(49), pp. 835–46. doi: 10.3238/arztebl.2013.0835.

Schwank, G. *et al.* (2013) 'Functional repair of CFTR by CRISPR/Cas9 in intestinal stem cell organoids of cystic fibrosis patients', *Cell Stem Cell*, 13(6), pp. 653–658. doi: 10.1016/j.stem.2013.11.002.

Scott, A. *et al.* (2016) 'Long-term renewable human intestinal epithelial stem cells as monolayers: A potential for clinical use', *Journal of Pediatric Surgery*, 51(6), pp. 995–1000. doi: 10.1016/j.jpedsurg.2016.02.074.

Sehgal, A. *et al.* (2017) 'c-Rel is dispensable for the differentiation and functional maturation of M cells in the follicle-associated epithelium', *Immunobiology*, 222(2), pp. 316–326. doi: 10.1016/j.imbio.2016.09.008.

Sekirov, I., Russell, S. and Antunes, L. (2010) 'Gut microbiota in health and disease', *Physiological Reviews*, 90(3), pp. 859–904. doi: 10.1152/physrev.00045.2009.

Shan, L. (2002) 'Structural basis for gluten intolerance in celiac sprue', *Science*, 297(5590), pp. 2275–2279. doi: 10.1126/science.1074129.

Shen, L. *et al.* (2011) 'Tight junction pore and leak pathways: a dynamic duo', *Annual Review of Physiology*, 73(1), pp. 283–309. doi: 10.1146/annurev-physiol-012110-142150.

Shima, H. *et al.* (2014) 'A novel mucosal vaccine targeting Peyer's patch M cells induces protective antigen-specific IgA responses', *International Immunology*, 26(11), pp. 619–625. doi: 10.1093/intimm/dxu061.

Shinkura, R. *et al.* (1999) 'Alymphoplasia is caused by a point mutation in the mouse gene encoding NF-κB-inducing kinase', *Nature Genetics*, 22(1), pp. 74–77. doi: 10.1038/8780.

Shorning, B. Y. *et al.* (2009) 'Lkb1 deficiency alters goblet and paneth cell differentiation in the small intestine', *PLoS ONE*, 4(1), pp. 1–8. doi: 10.1371/journal.pone.0004264.

Shroyer, N. F. *et al.* (2005) 'Gfi1 functions downstream of Math1 to control intestinal secretory cell subtype allocation and differentiation', *Genes and Development*, 19(20), pp. 2412–2417. doi: 10.1101/gad.1353905.

Spence, J. R. *et al.* (2011) 'Directed differentiation of human pluripotent stem cells into intestinal tissue in vitro', *Nature*, 470(7332), pp. 105–109. doi: 10.1038/nature09691.

Stanger, B. Z. *et al.* (2005) 'Direct regulation of intestinal fate by Notch', *Proceedings of the National Academy of Sciences*, 102(35), pp. 12443–12448. doi: 10.1073/pnas.0505690102.

Strugnell, R. A. and Wijburg, O. L. C. (2010) 'The role of secretory antibodies in infection

immunity', *Nature Reviews Microbiology*, 8(9), pp. 656–667. doi: 10.1038/nrmicro2384.

Sun, S.-C. (2011) 'Non-canonical NF-κB signaling pathway', *Cell Research*, 21(1), pp. 71–85. doi: 10.1038/cr.2010.177.

Tahoun, A. *et al.* (2011) 'Comparative analysis of EspF variants in inhibition of Escherichia coli phagocytosis by macrophages and inhibition of E. coli translocation through human- and bovine-derived M cells', *Infection and Immunity*, 79(11), pp. 4716–4729. doi: 10.1128/IAI.00023-11.

Tahoun, A. *et al.* (2012) 'Salmonella transforms follicle-associated epithelial cells into M cells to promote intestinal invasion', *Cell Host & Microbe*, 12(5), pp. 645–656. doi: 10.1016/j.chom.2012.10.009.

Taniguchi, K. and Karin, M. (2018) 'NF-κB, inflammation, immunity and cancer: coming of age', *Nature Reviews Immunology*, 18(5), pp. 309–324. doi: 10.1038/nri.2017.142.

Taylor, R. T. *et al.* (2007) 'Lymphotoxin-independent expression of TNF-related activation-induced cytokine by stromal cells in cryptopatches, isolated lymphoid follicles, and Peyer's patches', *The Journal of Immunology*, 178(9), pp. 5659–5667. doi: 10.4049/jimmunol.178.9.5659.

Terahara, K. *et al.* (2008) 'Comprehensive gene expression profiling of Peyer's Patch M cells, villous M-like cells, and intestinal epithelial cells', *The Journal of Immunology*, 180(12), pp. 7840–7846. doi: 10.4049/jimmunol.180.12.7840.

Thiagarajah, J. R. *et al.* (2004) 'A small molecule CFTR inhibitor produces cystic fibrosis-like submucosal gland fluid secretions in normal airways.', *FASEB Journal*, 18(7), pp. 875–7. doi: 10.1096/fj.03-1248fje.

Thiagarajah, J. R., Donowitz, M. and Verkman, A. S. (2015) 'Secretory diarrhoea: mechanisms and emerging therapies', *Nature Reviews Gastroenterology & Hepatology*, 12(8), pp. 446–457. doi: 10.1038/nrgastro.2015.111.

Thompson, C. A. *et al.* (2017) 'GATA4 is sufficient to establish jejunal versus ileal identity in the small intestine', *Cellular and Molecular Gastroenterology and Hepatology*, 3(3), pp. 422–446. doi: 10.1016/j.jcmgh.2016.12.009.

Thompson, C. A., DeLaForest, A. and Battle, M. A. (2018) 'Patterning the gastrointestinal epithelium to confer regional-specific functions.', *Developmental Biology*, 435(2), pp. 97–108. doi: 10.1016/j.ydbio.2018.01.006.

Tucková, L. *et al.* (2002) 'Activation of macrophages by gliadin fragments: isolation and characterization of active peptide.', *Journal of Leukocyte Biology*, 71(4), pp. 625–31. Available at: http://www.ncbi.nlm.nih.gov/pubmed/11927649.

Tyrer, P. *et al.* (2002) 'Validation and quantitation of an in vitro M-cell model', *Biochemical and Biophysical Research Communications*, 299(3), pp. 377–383. doi: 10.1016/S0006-291X(02)02631-1.

Tyrer, P. *et al.* (2006) 'Microbial pattern recognition receptors mediate M-cell uptake of a gram-negative bacterium', *Infection and Immunity*, 74(1), pp. 625–631. doi: 10.1128/IAI.74.1.625-631.2006.

Ulluwishewa, D. *et al.* (2011) 'Regulation of tight junction permeability by intestinal bacteria

and dietary components', *The Journal of Nutrition*, 141(5), pp. 769–776. doi: 10.3945/jn.110.135657.

Vallabhapurapu, S. and Karin, M. (2009) 'Regulation and function of NF-κB transcription factors in the immune system', *Annual Review of Immunology*, 27(1), pp. 693–733. doi: 10.1146/annurev.immunol.021908.132641.

VanDussen, K. L. *et al.* (2012) 'Notch signaling modulates proliferation and differentiation of intestinal crypt base columnar stem cells', *Development*, 139(3), pp. 488–497. doi: 10.1242/dev.070763.

VanDussen, K. L. *et al.* (2015) 'Development of an enhanced human gastrointestinal epithelial culture system to facilitate patient-based assays', *Gut*, 64(6), pp. 911–920. doi: 10.1136/gutjnl-2013-306651.

VanDussen, K. L. and Samuelson, L. C. (2010) 'Mouse atonal homolog 1 directs intestinal progenitors to secretory cell rather than absorptive cell fate', *Developmental Biology*, 346(2), pp. 215–223. doi: 10.1016/j.ydbio.2010.07.026.

Vazeille, E. *et al.* (2016) 'GipA factor supports colonization of Peyer's patches by Crohn's disease-associated Escherichia coli', *Inflammatory Bowel Diseases*, 22(1), pp. 68–81. doi: 10.1097/MIB.0000000000000609.

Vazquez-Roque, M. I. *et al.* (2013) 'A controlled trial of gluten-free diet in patients with irritable bowel syndrome-diarrhea: effects on bowel frequency and intestinal function', *Gastroenterology*, 144(5), pp. 903-911.e3. doi: 10.1053/j.gastro.2013.01.049.

Verbrugghe, P. *et al.* (2006) 'Murine M cells express annexin V specifically', *Journal of Pathology*, 209(2), pp. 240–249. doi: 10.1002/path.1970.

Verbrugghe, P. *et al.* (2008) 'Clusterin in human gut-associated lymphoid tissue, tonsils, and adenoids: Localization to M cells and follicular dendritic cells', *Histochemistry and Cell Biology*, 129(3), pp. 311–320. doi: 10.1007/s00418-007-0369-4.

Villella, V. R. *et al.* (2019) 'A pathogenic role for cystic fibrosis transmembrane conductance regulator in celiac disease', *The EMBO Journal*, 38(2), p. e100101. doi: 10.15252/embj.2018100101.

Volta, U. *et al.* (2015) 'Non-celiac gluten sensitivity: A work-in-progress entity in the spectrum of wheat-related disorders', *Best Practice and Research: Clinical Gastroenterology*, 29(3), pp. 477–491. doi: 10.1016/j.bpg.2015.04.006.

Wald, A. (2012) 'Irritable bowel syndrome-Diarrhoea', *Best Practice and Research: Clinical Gastroenterology*, 26(5), pp. 573–580. doi: 10.1016/j.bpg.2012.11.002.

Walker, E. M. *et al.* (2014) 'Characterization of the developing small intestine in the absence of either GATA4 or GATA6', *BMC Research Notes*, 7(1), p. 902. doi: 10.1186/1756-0500-7-902.

Walker, E. M., Thompson, C. A. and Battle, M. A. (2014) 'GATA4 and GATA6 regulate intestinal epithelial cytodifferentiation during development.', *Developmental biology*, 392(2), pp. 283–94. doi: 10.1016/j.ydbio.2014.05.017.

Wang, J. *et al.* (2009) 'TNFR and LTβR agonists induce follicle-associated epithelium and M cell specific genes in rat and human intestinal epithelial cells', *Cytokine*, 47(1), pp. 69–76. doi: 10.1016/j.cyto.2009.05.001.

Wang, J. *et al.* (2011) 'Convergent and divergent development among M cell lineages in mouse mucosal epithelium', *The Journal of Immunology*, 187(10), pp. 5277–5285. doi: 10.4049/jimmunol.1102077.

Weih, F. *et al.* (1995) 'Multiorgan inflammation and hematopoietic abnormalities in mice with a targeted disruption of RelB, a member of the NF-kappa B/Rel family.', *Cell*, 80(2), pp. 331–40. doi: 10.1016/0092-8674(95)90416-6.

van Wering, H. M. *et al.* (2004) 'Complex regulation of the lactase-phlorizin hydrolase promoter by GATA-4', *American Journal of Physiology-Gastrointestinal and Liver Physiology*, 287(4), pp. G899–G909. doi: 10.1152/ajpgi.00150.2004.

Westphal, S. *et al.* (2008) 'Resistance of chemokine receptor 6-deficient mice to Yersinia enterocolitica infection', *The American Journal of Pathology*, 172(3), pp. 671–680. doi: 10.2353/ajpath.2008.070393.

Wieser, H. (2007) 'Chemistry of gluten proteins', *Food Microbiology*, 24(2), pp. 115–119. doi: 10.1016/j.fm.2006.07.004.

Williams, J. M. *et al.* (2013) 'A mouse model of pathological small intestinal epithelial cell apoptosis and shedding induced by systemic administration of lipopolysaccharide.', *Disease Models & Mechanisms*, 6(6), pp. 1388–99. doi: 10.1242/dmm.013284.

Williams, J. M. *et al.* (2016) 'Intestinal preparation techniques for histological analysis in the mouse', in *Current Protocols in Mouse Biology*, pp. 148–168. doi: 10.1002/cpmo.2.

Wilson, S. S. *et al.* (2015) 'A small intestinal organoid model of non-invasive enteric pathogen–epithelial cell interactions', *Mucosal Immunology*, 8(2), pp. 352–361. doi: 10.1038/mi.2014.72.

Wong, B. R. *et al.* (1997) 'TRANCE is a novel ligand of the tumor necrosis factor receptor family that activates c-Jun N-terminal kinase in T cells', *Journal of Biological Chemistry*, 272(40), pp. 25190–25194. doi: 10.1074/jbc.272.40.25190.

Wong, B. R. *et al.* (1998) 'The TRAF family of signal transducers mediates NF-κB activation by the TRANCE receptor', *Journal of Biological Chemistry*, 273(43), pp. 28355–28359. doi: 10.1074/jbc.273.43.28355.

Wood, M. B., Rios, D. and Williams, I. R. (2016) 'TNF-α augments RANKL-dependent intestinal M cell differentiation in enteroid cultures', *American Journal of Physiology-Cell Physiology*, 311(3), pp. C498–C507. doi: 10.1152/ajpcell.00108.2016.

Worthington, J. J., Reimann, F. and Gribble, F. M. (2017) 'Enteroendocrine cells-sensory sentinels of the intestinal environment and orchestrators of mucosal immunity', *Mucosal Immunology*, 11(1), pp. 3–20. doi: 10.1038/mi.2017.73.

Yang, Q. (2001) 'Requirement of Math1 for secretory cell lineage commitment in the mouse intestine', *Science*, 294(5549), pp. 2155–2158. doi: 10.1126/science.1065718.

Yilmaz, Z. B. (2003) 'RelB is required for Peyer's patch development: differential regulation of p52-RelB by lymphotoxin and TNF', *EMBO Journal*, 22(1), pp. 121–130. doi: 10.1093/emboj/cdg004.

Yui, S. *et al.* (2012) 'Functional engraftment of colon epithelium expanded in vitro from a single adult Lgr5+ stem cell', *Nature Medicine*, 18(4), pp. 618–623. doi: 10.1038/nm.2695.

Yui, S. *et al.* (2018) 'YAP/TAZ-dependent reprogramming of colonic epithelium links ECM remodeling to tissue regeneration', *Cell Stem Cell*, 22(1), pp. 35-49.e7. doi: 10.1016/j.stem.2017.11.001.

Zecchini, V. (2005) 'Notch signaling regulates the differentiation of post-mitotic intestinal epithelial cells', *Genes & Development*, 19(14), pp. 1686–1691. doi: 10.1101/gad.341705.

Zhang, Y.-G. *et al.* (2014) 'Salmonella-infected crypt-derived intestinal organoid culture system for host-bacterial interactions', *Physiological Reports*, 2(9), pp. e12147–e12147. doi: 10.14814/phy2.12147.

Zihni, C. *et al.* (2016) 'Tight junctions: from simple barriers to multifunctional molecular gates', *Nature Reviews Molecular Cell Biology*, 17(9), pp. 564–580. doi: 10.1038/nrm.2016.80.

Zimmer, K. P. *et al.* (2010) 'Endocytotic segregation of gliadin peptide 31-49 in enterocytes', *Gut*, 59(3), pp. 300–310. doi: 10.1136/gut.2008.169656.

Zimmermann, C. *et al.* (2014) 'Epithelial transport of immunogenic and toxic gliadin peptides in vitro', *PLoS ONE*, 9(11), pp. 1–17. doi: 10.1371/journal.pone.0113932.

Appendices

APPENDIX 1 – Buffers and solutions

Lysogeny broth

10 g Tryptone

5 g Yeast extract

5 g NaCl

1 L ddH_2O

Lysogeny broth agar

10 g Tryptone

5 g Yeast extract

5 g NaCl

15 g Agar

1 L ddH_2O

Phosphate buffered saline

8 g NaCl

0.2 g KCl

1.44 g Na_2HPO_4

0.24 g KH_2PO_4

1 L ddH_2O

Adjusted to pH 7.4

0.1 M phosphate buffer, pH 7.4

40.5 mL 0.2 M Na_2HPO_4

9.5 mL 0.2 M NaH_2PO_4

Lead aspartate

0.066 g Lead nitrate

10 mL 0.03 M aspartic acid

Adjusted to pH 5.5

1X TAE buffer

4.84 g Tris-base

1.14 mL Glacial acetic acid

2 mL 0.5 M EDTA

1 L ddH_2O

5X SDS-PAGE sample buffer

1 mL 0.5 M Tris-HCl

0.8 mL Glycerol

1.6 mL 10% SDS

0.4 mL Beta-mercaptoethanol

0.2 mL 0.05% (w/v) bromophenol blue

4 mL ddH_2O

1X SDS-PAGE running buffer

14.4 g Glycine

3.03 g Tris-base

1 g Sodium dodecyl sulphate

1 L ddH_2O

APPENDIX 2 – Plasmid sequences (as determined by Sanger sequencing)

Key:

GST sequence

LpfA sequence

mCherry sequence

Restriction sites

GST-LpfA-mCherry – pGEX Fwd:

TACANTGNCNNGGCTGCACCCGTTTGGTGGTGGCGACCATCCTCCAAATCGGATCTGGTTCCGCGTGG
ATCCGCTGAATCTGGTGACGGCACCATTAAATTCACCGGTGAAATCGTTGACGCGCCATGCGTCGTTTC
TACTGACTCCCAGAACCAGGAAGTTGTGCTGGGTCAGGTTAAGAAAAATATCTTCAAAGCCATTGGCG
ACAAGTCTTCTTCTAAGCCTTTCCAGATCAAACTGGAAGACTGTGACATCACCTCTAATACCAAAGTTAA
CGTAAGCTTCAATGGCGTTGGTGATACAGACGATGCGACACTGGTTTCTGTTAACACTGAAGCAGGTG
CGGCAACTGGCGTGGGCATCGGTATCTACGACAACGCTAACAAGCTTGTTGAAATGAACACCGGTAAA
TCCACCACTACGTTGGCTGCTGGTCAGACCGTGCTGTACTACACCGCTAACTACGTTGCAACAAAAGAT
ACTGTAACCACTGGTTACGGTAACGCAGAAGTGGACTTCAACCTGTCCTACGAATAATCGAATTTTCGT
TAATACAGACAATCATAATGGCAACGGAAATCCCGTTGCCATTTTTTCCAGCGGAGGCTCAGGAAGAG
AATCTCTAGAATGGCAAGCAAGGGCGAGGAGGATAACATGGCCATCATCAAGGAGTTCATGCGCTTCA
AGGTGCACATGGAGGGCTCCGTGAACGGCCACGAGTTCGAGATCGAGGGCGAGGGCGAGGGCCGCC
CCTACGAGGGCACCCAGACCGCCAAGCTGAAGGTGACCAAGGGTGGCCCCCTGCCCTTCGCCTGGGAC
ATCCTGTCCCCTCAGTTCATGTACGGCTCCAAGGCCTACGTGAAGCACCCCGCCGACATCCCCGACTACT
TGAAGCTGTCCTTCCCCGAGGGCTTCAAGTGGGAGCGCGTGATGAACTTCAAGGACGGCGGCGTGGT
GACCGTGACCCAGGACTCCTCCCTGCAGGACGGCCAGTTCATCTACAAGGTGAAGCTGCGCGGCACCA
ACTTCCCCTCCAACGGCCCCGTAATGCAAAAAAAAAACATGGGCTGGGAGGCCTCTTCCGAGGGAAGT
ACCCCAAGGACGGGCCCCTGAAGGGCAGATCAACCAAAGGCTGAAGCTGAAGANCGNNGCCCCTNCA
ACCTTGNGGTCAAGACCCCCTCAAGGGCAAAAAAGCCGGGGAGTGCCCGGGNCCAAAACNTCAACTN
NGGTGGGANNCCCNNCCCANNGGGGANANCCCATCGGGGAAAGNTAAANGGCCGNNGGGGCCCCC
CTCC

GST-LpfA-mCherry – pGEX Rev (reverse complement):

GGGGCCCCNNNNTTTAAAAAAAAAAAAATTTTTTTTTTTNAAAAAANNCCCCCTTTGGGGGGCNAAAA
AATTTTTTTTTTTTTTTAAAACCCCCTTTTCCCCAAATTNNAAANNCTGGGGAAAGGGGNTGGGGNCNC
CCCCCCCCTTTTAAATCCCCAAAAGTTTAAANNNTAANNTTTTCCAAAAGGGGGGNTTNGNNTAAACN
NANGGGNGTTGGGNNCCCNTTGNTTTTTTTTTTTAAANNCTTNAAAACCAGGGGGGGGGCAAAATTT
TGGGGGGGGGCANTCGGGTTTTTTTTGGAAAAACNNTTAACCAAAGCTTTGTTGAAAATGGAACCCCC
GGTAAATTCCCCCCCCTTACCGTTGGGTTTCTTGGTTCAANACCCGGGGNNNTTTTTCCACCCGCTAAAT
TACGGTTGCAACAAAAAGATACTGTAACCCCCTGGTTTACGGTAACGCCAGAAAGTGGACTTTCAACCC
TTTCCTTACGAATAATTGAATTTTCGTTTAATACAGACAATCATAATGGCAACGGAAATCCCCGTTGCCA
TTTTTTCCAGCGGAGGGTTCAGGAAGAGAATCTCTAGAATGGCAAGCAAGGGCGAGGAGGATAACAT
GGCCATCATCAAGGAGTTCATGCGCTTCAAGGTGCACATGGAGGGCTCCGTGAACGGCCACGAGTTCG
AGATCGAGGGCGAGGGCGAGGGCCGCCCCTACGAGGGCACCCAGACCGCCAAGCTGAAGGTGACCA
AGGGTGGCCCCCTGCCCTTCGCCTGGGACATCCTGTCCCCTCAGTTCATGTACGGCTCCAAGGCCTACG
TGAAGCACCCCGCCGACATCCCCGACTACTTGAAGCTGTCCTTCCCCGAGGGCTTCAAGTGGGAGCGC
GTGATGAACTTCGAGGACGGCGGCGTGGTGACCGTGACCCAGGACTCCTCCCTGCAGGACGGCGAGT
TCATCTACAAGGTGAAGCTGCGCGGCACCAACTTCCCCTCCGACGGCCCCGTAATGCAGAAGAAGACC
ATGGGCTGGGAGGCCTCCTCCGAGCGGATGTACCCCGAGGACGGCGCCCTGAAGGGCGAGATCAAGC
AGAGGCTGAAGCTGAAGGACGGCGGCCACTACGACGCTGAGGTCAAGACCACCTACAAGGCCAAGAA
GCCCGTGCAGCTGCCCGGCGCCTACAACGTCAACATCAAGTTGGACATCACCTCCCACAACGAGGACTA
CACCATCGTGGAACAGTACGAACGCGCCGAGGGCCGCCACTCCACCGGCGGCATGGACGAGCTGTAC
AAGTCTTGAATTCCCGGGTCGACTCGAGCGGCCGCATCGTGACTGACTGACGATCTGCCTCGCGNTTCG
GAGTAAGAGGAAATTTCAGNTTATNTNNAAAGA

GST-mCherry – pGEX Fwd:

CCNATCGGCGTNCTANNGATTTANCGGGCNGCACCCGTTTTNGGGTGGCGACCATCCTCCAAATCGGA
TCTGGTTCCGCGTGGATCCATGGCAAGCAAGGGCGAGGAGGATAACATGGCCATCATCAAGGAGTTCA
TGCGCTTCAAGGTGCACATGGAGGGCTCCGTGAACGGCCACGAGTTCGAGATCGAGGGCGAGGGCGA
GGGCCGCCCCTACGAGGGCACCCAGACCGCCAAGCTGAAGGTGACCAAGGGTGGCCCCCTGCCCTTCG
CCTGGGACATCCTGTCCCCTCAGTTCATGTACGGCTCCAAGGCCTACGTGAAGCACCCCGCCGACATCC
CCGACTACTTGAAGCTGTCCTTCCCCGAGGGCTTCAAGTGGGAGCGCGTGATGAACTTCGAGGACGGC
GGCGTGGTGACCGTGACCCAGGACTCCTCCCTGCAGGACGGCGAGTTCATCTACAAGGTGAAGCTGCG
CGGCACCAACTTCCCCTCCGACGGCCCCGTAATGCAGAAGAAGACCATGGGCTGGGAGGCCTCCTCCG
AGCGGATGTACCCCGAGGACGGCGCCCTGAAGGGCGAGATCAAGCAGAGGCTGAAGCTGAAGGACG
GCGGCCACTACGACGCTGAGGTCAAGACCACCTACAAGGCCAAGAAGCCCGTGCAGCTGCCCGGCGC
CTACAACGTCAACATCAAGTTGGACATCACCTCCCACAACGAGGACTACACCATCGTGGAACAGTACGA
ACGCGCCGAGGGCCGCCACTCCACCGGCGGCATGGACGAGCTGTACAAGTCTTGAATTCCCGGGTCGA
CTCGAGCGGCCGCATCGTGACTGACTGACGATCTGCCTCGCGCGTTTCGGTGATGACGGTGAAAACCT
CTGACACATGCAGCTCCCGGAAGACGGTCACAGCTTGTCTGTAAGCGGATGCCGGGAACAAAACAAGC
CCGTCAGGGCGCGTCACCGGGGGTTGGCGGGTGGTCGGGGGCGCACCCATGACCCAGTCACGTAGCG
ATAGCGGAAGNGTATAATTCTTGAAAAANAAAAGGGCCCCCGGGATACCCCCTATTTTTTAAAGGGTA
AAGGGCCAGGAAAAAAAAGGGGTTTCTTAAAANNCCCGGGGGGGCCCTTTTTCGGGGAAAATGGGG
GCGGGAAACCCCCAATTNGGTTTAATTTTTTCAAAAAAANNTNCCAAAAATTGTTTCCCCCCCCCAGGA
AAAAAAAACCCCTGNAAAAAGGGCTTNNAATAATTTTTGNAAAAGGGGAAAAAATTNGNAAATTTCN
AAAATTTCCCGGGGGGCCCCCCTTTTTCCCCTTTTTTTGGGGGGAAATTTGGGCCNTTCCNNNTTTTTTN
NCCCCCCCCCCAAAAAAACCCGGGGGGGAAAAAAAAAAAAAAAGGGGGGAAAAAAANNTTTGGGGGG
GGGCCCAAAGGGGGGGGTTTAACCCCCAAAAGGGGGTTTTTCCCCNCCCCGGGGGAAAAAAACCCTTT
GGAAAATTTTTTTCCCCCCCCCNAAAAAGGTTTTTTT

GST-mCherry – pGEX Rev (reverse complement):

TACCCTTCGCCTGGGACATCCTGTCCCCTCAGTTCATGTACGGCTCCAAGGCCTACGTGAAGCACCCCGC
CGACATCCCCGACTACTTGAAGCTGTCCTTCCCCGAGGGCTTCAAGTGGGAGCGCGTGATGAACTTCGA
GGACGGCGGCGTGGTGACCGTGACCCAGGACTCCTCCCTGCAGGACGGCGAGTTCATCTACAAGGTG
AAGCTGCGCGGCACCAACTTCCCCTCCGACGGCCCCGTAATGCAGAAGAAGACCATGGGCTGGGAGG
CCTCCTCCGAGCGGATGTACCCCGAGGACGGCGCCCTGAAGGGCGAGATCAAGCAGAGGCTGAAGCT
GAAGGACGGCGGCCACTACGACGCTGAGGTCAAGACCACCTACAAGGCCAAGAAGCCCGTGCAGCTG
CCCGGCGCCTACAACGTCAACATCAAGTTGGACATCACCTCCCACAACGAGGACTACACCATCGTGGAA
CAGTACGAACGCGCCGAGGGCCGCCACTCCACCGGCGGCATGGACGAGCTGTACAAGTCTTGAATTCC
CGGGTCGACTCGAGCGGCCGCATCGTGACTGACTGACGATCTGCNTCGCGCGTTCGGGGAAGGTTTCC
TNANGGTAGTCTANC